# *Mini-TORBED Technology for Carbon Capture Adsorbent Screening*

A thesis submitted to Newcastle University in partial fulfilment of the requirement for the degree of Doctor of Philosophy in the Faculty of Science, Agriculture and Engineering

**Rouzbeh Jamei**

B.Eng. Chemical Engineering

MSc. Chemical Engineering

School of Engineering Newcastle University

Newcastle upon Tyne

United Kingdom

June 2024

## Abstract

Carbon capture (CC) via fluidized bed reactors presents a promising avenue for mitigating $CO_2$ emissions across the energy, industrial, and transportation sectors. This research focuses on developing and evaluating a small-scale and efficient $CO_2$ capture screening platform employing a 3D-printed toroidal fluidized bed (TORBED) reactor. A commercial sorbent, based on branched polyethyleneimine (BPEI), was screened for capturing $CO_2$ from artificial flue gas streams under a range of conditions. The adsorption screening experiments involved the introduction of various $N_2$/ $CO_2$ ratios into the TORBED reactor, and breakthrough curves were collected under different operating conditions, including $CO_2$ volume fractions, BPEI bed loads, gas flow rates, and temperatures.

In the hydrodynamic study, three potential industrial materials (RTI, Sasol, and Casale materials) were screened for compatibility with the TORBED reactor. The 'desirable flow regime' was quantified through methods such as visual observations, pressure drop analysis, and standard deviation analysis of pressure drop measurements, which provided insights into particle formations, flow stability, and uniform fluidization. Key results indicated that the RTI material exhibited optimal flow regimes with minimal pressure drop and high stability, making it the most suitable candidate for further adsorption and desorption studies. This comprehensive approach ensured the selection of an effective sorbent and optimal operating conditions for the TORBED reactor, contributing to advancements in carbon capture technology.

In adsorption screening experiments, artificial flue gas streams comprising various $N_2/CO_2$ ratios were introduced into the TORBED reactor. Breakthrough curves were collected under different operating conditions, including $CO_2$ volume fractions (ranging from 2 to 20 vol%), BPEI bed loads (1–2.5 g), gas flow rates (20–35 L/min), and temperatures (40–70 °C). The breakthrough curves provided insights into the sorption behaviour of BPEI under different conditions, facilitating the characterization of its adsorption capacity and kinetics. A maximum sorbent capacity of 2.64 ± 0.06 mmol/g was measured within experiment durations lasting no longer than 10 seconds. This rapid data collection rate highlights the potential for high throughput screening. Moreover, precise temperature control within the TORBED effectively minimized the influence of heat of adsorption on kinetics.

Desorption, a critical aspect of CC, was then studied given its importance in the overall process and lack of relative attention compared to adsorption in the wider literature. The desorption characteristics of the commercial BPEI adsorbent were also investigated using breakthrough experiments, with a focus on studying the influence of heat transfer effects. Experimental results revealed that higher desorption temperature (110 °C), shorter preheating time (achieved with a gas flow rate of 25 L/min), and elevated $CO_2$ concentrations during adsorption (20 vol%) improved the desorption efficiency significantly (defined as $CO_2$ desorbed compared to the adsorbed amount). Kinetic modelling plays a crucial role in understanding and optimizing adsorption and desorption processes. Upon analysis of the cumulative uptake curves extracted from the breakthrough data, it was found that the fractional order kinetic model best matches the behaviour of the BPEI adsorbent compared to the pseudo-1$^{st}$ order and pseudo-2$^{nd}$ order models. This implies that both physisorption and chemisorption processes are responsible for the binding of the $CO_2$ with the BPEI surface.

This work reinforced by two published papers in the Chemical Engineering Journal—provides fundamental insights and practical solutions that directly contribute to more efficient,

flexible, and economically viable CCS processes. 1. Jamei et al. (2023, Chem. Eng. J. 451:138405) demonstrated rapid and intensified screening of a branched polyethyleneimine (BPEI) adsorbent, achieving breakthrough measurements in a matter of seconds. This unprecedented speed of data collection allows for the rapid assessment of multiple sorbents and conditions, ultimately reducing the time and resources required for sorbent selection and optimization.

2. Jamei et al. (2024, Chem. Eng. J., 1385894724070591) addressed challenges related to small-scale Temperature Swing Adsorption (TSA) in CCS. The study showed that by tuning temperature profiles and flow regimes within the TORBED reactor, it is possible to enhance sorbent regeneration efficiency.

In summary, this research highlights the potential use of small-scale TORBED technology for screening CC materials to advance carbon capture more generally. By investigating adsorption and desorption characteristics and employing kinetic modelling, this study offers valuable insights for example optimising desirable flow regime to uniform fluidisation of sorbents in entire bed area for enhancing the efficiency of $CO_2$ capture and mitigating industrial emissions.

**Keywords:** TORBED, Adsorption, swirling, carbon capture, Fluidisation, BPEI

## Acknowledgements

First and foremost, I extend my deepest gratitude to my beloved wife, whose unwavering support, understanding, and encouragement sustained me throughout this challenging journey. I am profoundly grateful for your presence by my side.

I am immensely indebted to my esteemed supervisors Vladimir Zivkovic and Jonathan McDonough for their invaluable guidance, mentorship, and expertise throughout the entirety of my doctoral research. Their insightful advice, constructive criticism, and unwavering support have been instrumental in shaping my academic and personal growth. I am truly fortunate to have had the opportunity to work under their mentorship.

I extend my sincere appreciation to Newcastle University Overseas Research Scholarships (NUORS) for their funding, which enabled me to pursue and complete this PhD project. Their support has been crucial in facilitating the realization of my research aspirations.

Special thanks are also due to Torftech Ltd. for their invaluable assistance in designing and operating the reactor. Their expertise and guidance were indispensable in navigating the complexities of my research endeavour. Additionally, I express my gratitude to RTI International for providing the essential adsorbent, which significantly contributed to the successful execution of my project.

# Table of Contents


**1. INTRODUCTION ..... 6**

1.1 BACKGROUND ..... 6
1.2 PROPOSED SOLUTION ..... 7
1.3 CHALLENGES OF THE STUDY ..... 8
1.4 OBJECTIVES OF THE STUDY ..... 10

**2. LITERATURE REVIEW ..... 11**

2.1 CARBON CAPTURE IMPORTANCE ..... 11
*2.1.1 Challenges of shifting from fossil fuel to renewable energy ..... 12*
2.2 CARBON CAPTURE APPROACHES ..... 13
2.3 POST-COMBUSTION CARBON CAPTURE AS A KEY MITIGATION STRATEGY ..... 14
2.4 ADSORPTION TECHNOLOGY: A SUSTAINABLE SOLUTION ..... 15
*2.4.1 Sorbent Development: The Heart of Adsorption Technology ..... 16*
*2.4.2 Sorbent Regeneration: as a supplementary criterion ..... 18*
*2.4.3 Reactor Technology: Optimising Adsorption Processes ..... 20*
*2.4.4 Conventional Fluidized Bed Reactor Technology ..... 23*
2.5 PROCESS INTENSIFICATION BY FLUIDISED BED REACTOR ..... 26
*2.5.1 Micro Fluidised Bed ..... 26*
*2.5.2 Centrifugal Fluidized Bed ..... 27*
*2.5.3 Circulating Fluidised Bed ..... 29*
*2.5.4 Vortex Fluidized Bed (VFB) ..... 30*
*2.5.5 Rotating Distributor Fluidized Bed (RDFB) ..... 31*
*2.5.6 Bubbling Fluidized Bed Reactors (BFBR) ..... 33*
*2.5.7 Swirling Fluidized Bed Reactor (SFBRs) ..... 34*
2.6 TOROIDAL FLUIDIZED BED (TORBED) ..... 35
*2.6.1 TORBED Technology Description ..... 36*
*2.6.2 Swirling Technology vs Rotating Fluidised bed ..... 42*
*2.6.3 TORBED Technology Design ..... 44*
*2.6.4 Distributors Design ..... 45*
*2.6.5 TORBED and Carbon Capture ..... 49*
*2.6.6 TORBED and Desorption Technology ..... 51*
*2.7 Summary ..... 54*

**3. METHODOLOGY ..... 55**

3.1 CHAPTER OVERVIEW ..... 55
3.2 SORBENT SPECIFICATION ..... 55
3.3 TORBED DESIGN AND ADDITIVE MANUFACTURING ..... 58
3.4 EQUIPMENT FLOWSHEET ..... 64
3.5 HYDRODYNAMIC EXPERIMENT METHODOLOGY ..... 67
3.6 BREAKTHROUGH AND ADSORPTION METHODOLOGY ..... 70
3.7 DESORPTION BREAKTHROUGH SETUP AND METHOD ..... 74
*3.7.1 Pre-treatment ..... 78*
*3.7.2 Conditions Adjustment ..... 79*
*3.7.3 Adsorption ..... 79*
*3.7.4 Preheating ..... 79*
*3.7.5 Desorption ..... 79*
*3.8 Conclusion ..... 80*

**4. SORBENT HYDRODYNAMIC CHARACTERISTICS ..... 82**

4.1 INTRODUCTION ..... 82
4.2 VISUAL OBSERVATION OF TORBED REGIMES ..... 83
4.3 PRESSURE DROP ANALYSIS ..... 85
4.4 STANDARD DEVIATION ANALYSIS ..... 96
4.5 CONCLUSION ..... 99

**5. ADSORPTION RESULTS & DISCUSSION ..... 100**

5.1 OVERVIEW OF $CO_2$ BREAKTHROUGH ..... 100
*5.1.1 Effect of Feed $CO_2$ Concentration ..... 101*
*5.1.2 Effect of Bed Loading ..... 106*
*5.1.3 Effect of Gas Flowrate ..... 106*
*5.1.4 Effect of Temperature and Heat Transfer in the TORBED ..... 110*
5.2 KINETIC MODELLING ..... 115
5.3 CONCLUSION ..... 119

**6. DESORPTION RESULTS & DISCUSSION ..... 121**

6.1 INTRODUCTION ..... 121
6.2 DESORPTION RESULTS ..... 122
*6.2.1 Effect of Temperature on Adsorption and Desorption Capacities ..... 125*
*6.2.2 Effect of Temperature on Desorption Rate ..... 128*
*6.2.3 Effect of Pre-Heating Rate on Desorption process ..... 131*
*6.2.4 Effect of $CO_2$ Concentration on Adsorption and Desorption ..... 135*
*6.2.5 Effect of Gas Flow Rate on Adsorption and Desorption ..... 137*
6.3 CYCLIC MEASUREMENTS ..... 138
6.4 DESORPTION KINETIC MODELLING ..... 140
6.5 CONCLUSION ..... 145

**7. CONCLUSIONS AND RECOMMENDATIONS ..... 147**

7.1 SUMMARY OF HYDRODYNAMIC FINDINGS ..... 147
7.2 SUMMARY OF ADSORPTION FINDINGS ..... 148
7.3 SUMMARY OF DESORPTION FINDINGS ..... 149
7.4 RECOMMENDATIONS FOR FUTURE WORK ..... 150

## List of Figures

Figure 2.1 Different regimes in a conventional fluidized bed in order of increasing velocities[63].....24
Figure 2.2 Example of a fully-assembled 3D-printed reactor[65].....27
Figure 2.3 Centrifugal fluidised bed with static geometry showing tangential inlets [71].....28
Figure 2.4Circulating fluidised Bed[74].....30
*Figure 2.5 The Schematic diagram of vortex chamber fluidized bed with two solid inlet [76]* .....31
*Figure 2.6 Rotating Distributor Fluidized Bed [64]* .....32
*Figure 2.7 Bubbling fluidized bed Reactor [90]*.....33
*Figure 2.8 Torodial fluidized bed (TORBED) Process gas flow through fixed blades gives toroidal particle motion [8]* .....35
*Figure 2.9 Spiral distributor schematic & Bed behaviour at the spiral distributor [86]*.....38
*Figure 2.10 Configuration of a toroidal fluidized bed reactor [57]* .....39
*Figure 2.11 Schematic diagram of the 'cold' model of a conical SFBC [17]*.....40
*Figure 2.12 Principle of particle movement in a toroidal fluidized bed reactor [68]*.....44
*Figure 2.13 mesh-coupled annular distributor [18]* .....46
*Figure 2.14 schematic of Spiral Distributor with different inclination angle [93]* .....46
*Figure 2.15 plenum design with Conical and cylindrical shape [87]* .....47
*Figure 2.16. 3-D printed TORBED Reactor[94]*.....48
*Figure 2.17 Swirling Reactor with Inclined Hole Distributor [89]*.....48
*Figure 3.1. Diagram of the Geldart classification of particles [44]* .....57
Figure 3.2, a. Images of different 3 distinct types of particles: branched polyethyleneimine (BPEI), b. Hydrotalcite powder, c. Casale Pellets in TORBED reactor.....58
Figure 3.3 (a) Form2 SLA 3D printer with example of printed parts, (b) which are then washed in ultrasonic bath (FormWash) (c) and dried by compressed air to remove the remaining material, (d) and cured by UV light in (FormCure),(e) Assembled reactor .....60
Figure 3.4. CAD models and corresponding photos of the 3D-printed Mini-TORBED; (a) bed chamber/freeboard region, (b) central cone, (c) distributor, (d) plenum chamber. .....63
Figure 3.5. Schematic of CO2 breakthrough for assessing adsorption kinetics. .....64
Figure 3.6. Image of CO2 adsorption kinetics screening rig (note, the TORBED is wrapped in wool insulation during the experiments to improve the temperature stability) .....66
Figure 3.7. Thermocouple location inside freeboard region for detection of heat of adsorption (the square patch of wire mesh for minimizing loss of fines is also visible).....67
Figure 3.8. Schematic of Hydrodynamic experiment .....68
Figure 3.9. Image of Hydrodynamic rig .....68
Figure 3.10. (a) Normalised breakthrough curves for ID4 (with deadtime removed); (b) $CO_2$ uptake curve for ID4; (c) cumulative $CO_2$ uptake curve for ID4 and comparison to simple kinetic models .....72
Figure 3.11. Schematic of $CO_2$ breakthrough for assessing adsorption/desorption kinetics...75
Figure 3.12. (a) 3D-printed mini-TORBED, (b) Full experiment rig.....76
Figure 3.13.Normalised desorption breakthrough curves and Bed temperature profile during TSA cycles with pure heated $N_2$ .....78
Figure 4.1. Examples of different particle formations observed in the 3D-printed mini-TORBED for BPEI; fluidising gas = N2, bed loading = 2 g, pressure = 1 bar.g, temperature = ambient; (a) un-swirled, 5–10 L/min, (b) collapsed, 15 L/min, (c) maldistributed, 20 L/min, (d) uniformly swirled, 25–35 L/min, (e) over-aired, 40–45 L/min, (f) entrained, 50–60 L/min...85

Figure 4.2. BPEI related Pressure drop (in kPa) as a function of gas flow rate and bed loading .....88
Figure 4.3. Hydrotalcite related Pressure drop (in kPa) as a function of gas flow rate and bed loading.....92
Figure 4.4. Examples of different particle formations observed in the 3D-printed mini-TORBED with Hydrotalcite; fluidising gas = N2, bed loading = 2 g, pressure = 1 bar.g, temperature = ambient; (a) Un-Swirled, 5–20 L/min, (b) Collapsed & Maldistributed, 20-40 L/min, (c) Over Aired, 40-50 L/min, (d) Entrained, 55-65 L/min.....92
Figure 4.5. Casale related Pressure drop (in kPa) as a function of gas flow rate and bed loading .....95
Figure 4.6. Examples of different particle formations observed in the 3D-printed mini-TORBED with Casale; fluidising gas = N2, bed loading = 2 g, pressure = 1 bar.g, temperature = ambient; (a) Un-Swirled, 5–40 L/min, (b) Collapsed & Maldistributed, 45-85 L/min, (c) Over Aired 85-100 Lit/min .....95
Figure 4.7. BPEI sorbent related Standard deviation of Pressure drop (in Pa) as a function of gas flow rate for 2 g of bed loading .....97
*Figure 4.8. Hydrotalcite Sorbent related Standard deviation of Pressure drop (in Pa) as a function of gas flow rate for 2 g of bed loading*.....98
Figure 4.9. Casale Sorbent related Standard deviation of Pressure drop (in Pa) as a function of gas flow rate for 2 g of bed loading .....99
*Figure 5.1. Normalised breakthrough curves as a function of: (a) $CO_2$ concentration (ID 1–4), (b) bed loading (ID 5–8), (c) gas flow rate (ID 9–12), (c) gas temperature (ID 13–16)* .....102
Figure 5.2. $CO_2$ uptake curves recorded at different $CO_2$ concentrations; (a) 2 vol%, (b) 8 vol%, (c) 14 vol%, and (d) 20 vol% (note, the capacities shown in this figure correspond to a single run, whereas the capacities shown in Table 5.3 are the mean values .....104
Figure 5.3. Trend of $q_e$ (equilibrium uptake) and $\Delta\tau$ (saturation time) as a function of: (a) $CO_2$ concentration (ID 1–4), (b) bed loading (ID 5–8), (c) gas flow rate (ID 9–12), (c) gas temperature (ID 13–16).....105
Figure 5.4. Temperature increase as a function of: (a) $CO_2$ concentration (ID 1–4), (b) bed loading (ID 5–8), (c) gas flow rate (ID 9–12), (c) gas temperature (ID 13–16).....112
Figure 5.5. Comparison of the experimentally measured cumulative $CO_2$ uptake curves in the TORBED against the pseudo first-order, pseudo second-order, and fractional-order models at different conditions; (a) ID4, (b) ID5, (c) ID9, (d) ID14.....116
Figure 6.1. Normalised adsorption and desorption breakthrough curves and bed temperature profiles measured during a single TSA cycle; (a) T_ads=T_des¬ at different temperatures (40°C, 80°C & 110°C), and (b) T_des>T_ads at different gas flow rates (20 L/min) .....124
Figure 6.2 Desorption efficiency as a function of desorption temperature (error bars omitted for clarity; see Table 3).....127
Figure 6.3 Relationship between the measured ‘desorbed capacity’ and measured adsorbed capacity at all experiment conditions.....128
*Figure 6.4 Cumulative percentage of CO2 desorbed and $CO_2$ desorption rates over time as a function of temperature (gas flow rate = 25 L/min, $CO_2$ concentration = 20 vol%); solid lines represent desorption%, dashed lines represent desorption rate* .....129
Figure 6.5(a) Effect of temperature on the breakthrough time (tb) and desorption time (t95) for the $T_{ads}$=$T_{des}$ configuration; and (b) Desorption time (t95) for the $T_{des}$>$T_{ads}$ configuration gas flow rate = 25 L/min, $CO_2$ concentration = 20 vol%.....131
Figure 6.6 Effect of pre-heating rate on the (a) average desorption rate, and (b) desorption efficiency.....132
Figure 6.7Pre-Heating Rate as a function of (a) gas flow rate, and (b) feed $CO_2$ concentration used during adsorption.....133

Figure 6.8 Effect of $CO_2$ concentration used during adsorption and pre-heating on the desorption efficiency.....134
*Figure 6.9 Desorption capacity as a function of adsorption capacity categorised by $CO_2$ concentration and adsorption temperature; the black dotted line indicates complete desorption ($qdes = qads$)*.....136
Figure 6.10 (a) Desorption capacity as a function of adsorption capacity categorised by gas flow rate, and (b) desorption efficiency as a function of gas flow rate at fixed $CO_2$ concentration of 20 vol%.....138
Figure 6.11 Adsorption index (AI%) and regeneration index (RI%) as a function of cycle number; AI% is based on an adsorption capacity of 2.56 mmol/g for n = 1; RI% is based on a desorbed amount of 2.13 mmol/g for n = 1 .....139
Figure 6.12 Comparison of kinetic models against experimental cumulative desorption curves, (a) $T_{ads}$ = 40 °C & $T_{des}$ = 80 °C, (b) $T_{ads}$ = 80 °C & $T_{des}$ = 100 °C, (c) (a) $T_{ads}$ = 40 °C & $T_{des}$ = 110 °C .....142
Figure 6.13 Fractional order rate constant plotted as a function of (a) amount of adsorbed $CO_2$ (no correlation), and (b) amount of desorbed $CO_2$ (positive correlation).....145

## List of Tables

Table 2.1 Significant swirling bed reactor results .....40
Table 3.1 Summary of adsorption experiment conditions.....71
Table 3.2. Summary of desorption experiment conditions.....77
Table 4.1. Summary of experiment conditions and accuracy.....83
Table 4.2. Pressure drop (in kPa) and observed flow regimes within the TORBED reactor for BPEI under different operating conditions. .....87
Table 4.3. Pressure drop (in kPa) and observed flow regimes within the TORBED reactor for Hydrotalcite under different operating conditions. .....91
Table 4.4. Pressure drop (in kPa) and observed flow regimes within the TORBED reactor for Casale under different operating conditions. .....94
Table 5.1. Process parameters determined from the adsorption breakthrough experiments .108
Table 5.2. Comparison of $CO_2$ adsorbent performance and reactor technologies for $CO_2$ capture .....109
Table 6.1. Key Performance Metric Definitions.....122
Table 6.2 Summary of Breakthrough Experiments Results .....125
Table 6.3 Comparison of average desorption rates with reported data in the literature .....130
Table 6.4 Models for describing the desorption kinetics.....141
Table 6.5 Kinetic parameters fitted from desorption experiments .....143

## Abbreviations

| | |
|---|---|
| $CC$ | Carbon Capture |
| $CO_2$ | Carbon Dioxide |
| $BPEI$ | Branched Polyethyleneimine |
| $SFB$ | Swirling Fluidized Bed |
| $TORBED$ | Toroidal Fluidized Bed |
| $TSA$ | Temperature Swing Adsorption |
| $PSA$ | Pressure Swing Adsorption |
| $VSA$ | Vacuum Swing Adsorption |
| $CBR$ | Compact Bed Reactor |
| $EBR$ | Expanded Bed Reactor |
| $CCS$ | Carbon Capture and Storage |
| $CCU$ | Carbon Capture and Utilisation |
| $MFBs$ | Micro-fluidized beds |
| $VFB$ | Vortexing fluidized bed |
| $CAD$ | Computer-Aided Design |
| $SLA$ | Stereolithography |

## Nomenclature

| | |
|---|---|
| $C$ | $CO_2$ concentration in the effluent gas (vol%) |
| $C_0$ | $CO_2$ concentration in the inlet gas (vol%) |
| $k_1$ | Pseudo first-order rate constant ($s^{-1}$) |
| $k_2$ | Pseudo second-order rate constant ($s^{-1}$) |
| $k_f$ | Fractional-order rate constant ($s^{-1}$) |
| $m$ | Empirical coefficient |
| $n$ | Empirical coefficient |
| $q_e$ | Equilibrium $CO_2$ uptake (mmol) |
| $q_t$ | $CO_2$ uptake at time $t$ (mmol) |

| | |
|---|---|
| $q_{ads}$ | Amount of $CO_2$ adsorbed per gram of material (mmol/g) |
| $q_{des}$ | Amount of $CO_2$ desorbed/released per gram of material (mmol/g) |
| $\varepsilon_{des}$ | Desorption Efficiency $(q_{des}/q_{ads}) \times 100$ (%) |
| $Q$ | Volumetric gas flow rate (L/min) |
| $\dot{Q}$ | Pre-Heating Rate $(T_{des} - T_{ads})/t$, (°C/s) |
| $R^2$ | Coefficient of determination |
| $t$ | Time (s) |
| $T$ | Temperature recorded in the freeboard region (see Figure 4) (°C) |
| $T_{max}$ | Maximum recorded temperature (°C) |
| $\Delta\tau$ | Saturation time $(= \tau_{95} - \tau)$ (s) |
| $\tau$ | Breakthrough time (time for $C$ to reach 5% of equilibrium value) (s) |
| $\tau_{95}$ | Time for $C$ to reach 95% of final equilibrium value (s) |

# 1. Introduction

## 1.1 Background

The escalating global demand for energy, primarily driven by industries heavily reliant on fossil fuels, continues to contribute significantly to the alarming rise in carbon dioxide ($CO_2$) emissions. In 2024, the atmospheric concentration of $CO_2$ reached a record high of 423 ppm ± 0.1 ppm, reflecting a concerning trend of accelerated growth compared to the 1960s, with an increase of 2.27 ± 0.1 ppm per year in 2020 [1]. This surge in atmospheric $CO_2$ levels has manifested in profound climate system alterations, underscoring the urgent need for robust climate action [2].

Recognizing the gravity of the situation, international agreements such as the Paris Agreement and initiatives like the European Green Deal have been established to mitigate the impact of climate change. The Paris Agreement specifically targets limiting the global average temperature increase to well below 2°C, with efforts to further restrict it to 1.5°C by offsetting greenhouse gas emissions. The European Green Deal, introduced in September 2020, aims to reduce 2030 greenhouse gas emissions to at least 55% of the 1990 levels [3]. As industrialized nations strive to meet these ambitious targets, innovative and effective solutions are imperative.

To address the urgent need for greenhouse gas reduction, various strategies have been proposed, including transitioning to renewable energy sources, enhancing energy efficiency in existing processes, and actively reducing emissions of greenhouse gases, particularly $CO_2$ [4]. Achieving net-zero emissions, where the quantity of greenhouse gas emissions produced is equalled or surpassed by the amount removed from the atmosphere, is a critical objective. While alternative energy sources and process modifications offer potential solutions, the reluctance of industries to shift away from fossil fuels due to issues of availability and suitability necessitates immediate, practical, and cost-effective solutions.

Carbon capture (CC) emerges as a pragmatic and accessible short-term solution to mitigate $CO_2$ emissions [5]. While conventional methods like chemical absorption, physical adsorption, membrane separation, and cryogenic distillation have been proposed for CC from flue gas, each method has its limitations. Chemical absorption, the prevalent commercial method, faces challenges such as sorbent degradation, expensive solvent regeneration, and equipment corrosion.

Additionally, emerging technologies like the combination of membrane and adsorption with innovative fillers such as metal-organic frameworks (MOFs) show promise but remain in the early stages of investigation [5].

Solid sorbent adsorption, however, presents a compelling alternative, contingent on the development of highly specific materials tailored at the molecular scale and improved gas-solid contact efficiency at the process scale [6]. While these methods hold promise, there is a critical need for advancements to reduce costs, energy consumption, and enhance efficiency, particularly in treating large flue gas streams from fossil fuel-fired plants. Researchers are actively focusing on developing innovative, efficient, and cost-effective techniques to propel carbon capture technologies forward. This study aligns with this ongoing effort by investigating the feasibility of sorbent screening via a mini–Toroidal Fluidised Bed (TORBED) reactor, aiming to contribute valuable insights towards the realization of effective and scalable carbon capture solutions.

### 1.2 Proposed Solution

Out of the numerous proposed carbon capture solutions, adsorption is a promising option because of its relative simplicity and low cost. However, a successful adsorption process depends on both the development of specific sorbents and the improvement of gas–solid contact efficiency, which must be achieved in parallel to maximise competitiveness. The swirling fluidized bed, exemplified by the TORBED reactor, offers a compelling alternative for intensifying gas-solid fluidization, and addresses the drawbacks associated with conventional methods discussed earlier [7]. Notably, the distributor design of TORBED, utilizing inclined blades to create toroidal motion, minimizes axial momentum while enhancing radial and tangential momentum. This innovative approach facilitates improved flow distribution and enables the effective processing of a wide range of particle sizes [8].

The swirling motion, generated by the inclined blades, reduces pressure drop and particle scattering, primarily dissipating gas stream momentum at the base of the bed in the tangential direction. Moreover, the increased turbulence leads to a decrease in the boundary layer thickness around particles, thereby enhancing heat and mass transfer rates. The proposed benefits directly align with the project's goals, encompassing better process control, adsorption intensification, improved contact mixing, higher heat/mass transfer rates, fluidization of a wide range of particle sizes, higher bed loading capacity, accurate temperature control, lower energy consumption (lower pressure drop), reduced wastage/recycling, and a smaller plant volume.

The TORBED reactor comes in two distinct types: the Compact Bed Reactor (CBR) and the Expanded Bed Reactor (EBR). The literature review indicates that the CBR, employing an annular distributor for toroidal motion, is more common. It is suitable for suspending a low-height bed of varying particle sizes. Although this design decreases the residence time due to the smaller bed weight.

### 1.3 Challenges of the Study

Researchers have consistently sought methods to enhance the adsorption process, particularly in the field of carbon capture, with a focus on cost reduction and improved yield [5]. Recently, the exploration of $CO_2$ molecule adsorption through dry regenerable sorbents has emerged as a promising alternative. However, traditional adsorption processes face challenges such as slow kinetics, handling large volumes of adsorbent, particle attrition, agglomeration, and difficulties in heat control for large-scale adsorber vessels, leading to the release of sorbents into the air [9].

To address these problems, it is crucial to recognize that the efficiency of adsorption is not only based on the development of highly specific materials, but also on improving gas-solid contact mixing. Various technologies have been developed to facilitate intimate interactions between solid particles and fluids, such as fluid bed reactors, fixed bed reactors, and fluidized bed reactors. Among these, fluidized beds stand out as a promising solution due to their ability to intensify processes through increased mass and heat transfer rates, providing advantages like high removal efficiency and low pressure drop [10].

In the context of carbon capture, where heat transfer is crucial to prevent hot spots during exothermic reactions, the application of fluidized beds becomes particularly important. Girimonte et al. [2017] compared fluidized bed and packed bed reactors for $CO_2$ removal [11], revealing that fluidized beds positively impact efficiency and exhibit a considerable increase in breakthrough time. Despite these advantages, conventional fluidized bed reactors encounter challenges in handling fine-sized particles and large particles, leading to issues like maldistribution of flow and increased pressure drop [12].

In response to these limitations, researchers have explored new fluidization methods with a focus on achieving low pressure drop and accommodating a wider range of particle sizes. Among these innovations, the SFB, also known as the toroidal fluidized bed, has gained attention. The SFB aims to overcome the shortcomings of conventional fluidized beds by enabling the fluidization of tiny particles without agglomeration issues (13-18).

Commercial models, such as TORBED, have been developed and utilized in various chemical and mechanical processes, offering a potential solution to enhance the efficiency and applicability of fluidized bed systems [8]. Despite these advancements, there remains a research gap in understanding the intricacies of the swirling fluidized bed, its performance in diverse applications, and its potential for optimizing carbon capture processes. This study seeks to bridge this gap by investigating the sorbent screening via a mini TORBED reactor, incorporating swirling fluidized bed principles to contribute valuable insights into the development of efficient and scalable carbon capture solutions.

The existing body of research on the desorption kinetics and cyclability of sorbents in fluidized bed reactors using the TSA method is limited. In the context of substantial exhaust gas flows and elevated $CO_2$ concentrations, the saturation time for sorbents is brief. Efficient regeneration of sorbents is imperative to enhance performance and reduce the capital costs associated with carbon capture processes. The desorption performance plays a pivotal role in $CO_2$ separation, typically occurring after the adsorption phase, enabling sorbent reuse and regeneration.

There is a pressing need to develop technology that ensures efficient contact mixing between gas and solid, minimizing bypassing and hot spot zones during the desorption process. Additionally, in continuous long-term carbon capture operations, sorbent deactivation during multi-cycle adsorption-desorption poses a significant challenge. The regeneration and cyclability of sorbents emerge as critical factors influencing the economic viability of potential carbon capture processes. Various desorption techniques have been reported, including TSA, PSA, VSA, Microwaves, or combinations thereof. Effective desorption methods must facilitate complete recovery of adsorption capacity, necessitate low energy consumption, and short regeneration time, and avoid significant alterations to the adsorbent's properties (19, 20).

TSA, relying on the binding strength differential between $CO_2$ molecules and the adsorbent at different temperatures, is a widely used method with the TORBED reactor platform. The TORBED's high heat convective transfer rates, in conjunction with conductive heating, prove instrumental in regenerating the sorbent. Practical implementation involves adjusting the inlet gas temperature while maintaining a desirable flow regime.

Despite TSA's simplicity, it comes with drawbacks such as long desorption time, high energy consumption, potential changes to the adsorbent's physical and chemical properties, and heat loss. However, the TORBED reactor addresses some of these challenges by achieving efficient

heat transfer rates and providing a platform for conductive heating to optimize sorbent regeneration.

## 1.4 Objectives of the Study

The primary aim of this thesis is to explore the efficacy of sorbent screening using a mini TORBED reactor for carbon capture applications. The specific objectives are as follows:

- To assess the performance of sorbent materials in a simulated carbon capture environment within the mini TORBED reactor.
- To identify key factors influencing sorbent performance, including adsorption capacity, kinetics, and thermal stability.
- To investigate the hydrodynamics of different sorbent types in the mini TORBED reactor.
- To identify acceptable conditions for achieving the desired flow regime and pressure drop in the TORBED reactor.
- To evaluate sorbent performance in both adsorption and desorption processes within the mini TORBED reactor.
- To contribute insights into the optimization of sorbent-based systems for enhanced carbon capture efficiency.
- To address challenges and limitations associated with existing carbon capture technologies and propose potential solutions through sorbent screening.

By accomplishing these objectives, this research aims to make meaningful contributions to the development of advanced and efficient carbon capture technologies, aligning with global efforts to combat climate change and achieve sustainable energy solutions.

# 2. Literature review

## 2.1 Carbon Capture Importance

The 21st century presents humanity with a formidable challenge - mitigating the adverse effects of anthropogenic climate change. One of the primary contributors to this global crisis is the excessive release of carbon dioxide ($CO_2$) into the atmosphere, primarily from the combustion of fossil fuels for energy generation, industrial processes, and transportation. Elevated levels of $CO_2$ in the atmosphere are known to trap heat, resulting in a rise in global temperatures, a phenomenon commonly referred to as global warming [21]. The consequences of global warming include more frequent and severe weather events, rising sea levels, disruption of ecosystems, and a host of socio-economic challenges [2].

Addressing the climate crisis requires a multifaceted approach, and one crucial strategy is Carbon Capture and Storage (CCS) or Carbon Capture and Utilisation (CCU). These technologies aim to capture $CO_2$ emissions from various sources, prevent their release into the atmosphere, and either store them underground or utilise them in a manner that does not contribute to global warming. Reducing $CO_2$ emissions is essential to stabilise the Earth's climate [22]. Carbon capture technologies can help industries and power plants significantly cut their emissions, enabling a smoother transition to a low-carbon or carbon-neutral energy system. This is particularly important as the world seeks to limit global warming to well below 2 °C, as stipulated in the Paris Agreement [23].

There is no single global regulation that forces countries to address carbon capture and storage (CCS) or carbon capture and utilisation (CCU) issues. However, there are several international agreements, organisations, and initiatives that encourage and support countries in taking action to reduce carbon emissions and promote CCUS technologies [3]. The latest agreement is about Glasgow conference which most of countries agreed on a roadmap for the global energy sectors to reach net zero by 2050 and limiting the rise in global temperatures to 1.5 °C [4]. Generally, a new milestone to carbon capture, usage, and storage was announced by countries, cities, businesses, and other institutions are pledging to achieve net-zero emissions [2]. Around 76% of global emissions are covered by countries with net-zero targets, including China, the United States, and the European Union [3].

The Science-Based Targets Initiative is working with more than 3,000 businesses and financial institutions to reduce their emissions. And more than 1000 cities, over 1000 educational

institutions, and over 400 financial institutions have joined the Race to Zero, pledging to take rigorous, immediate action to halve global emissions by 2030 [24]. However, there is no force on countries to meet this milestone and they can postpone it as long as it does not have a negative effect on their economy. For example, in 2023, the UK government has vowed to "max out" North Sea oil and gas by issuing hundreds of new development licences. So, it is obvious that governments all over the world will not get rid of fossil fuels easily in the short term [25]. They believed that the technology aims to capture carbon released by burning fossil fuels and store it in a way that does not affect the environment. As a result, industries and governments all over the world are not willing to switch to renewable energy as soon as possible, and they will use the technology as an excuse to do so [2].

### 2.1.1 Challenges of shifting from fossil fuel to renewable energy

Governments and industries both face economic and practical hurdles when trying to shift rapidly from fossil fuels to renewable energy sources [26]. Several factors contribute to this. First, in terms of Economic Considerations, fossil fuels have been the backbone of many economies for decades, providing stable jobs and revenue streams. Transitioning away from them can be disruptive and costly, which can lead governments and industries to seek ways to continue their use, at least in the short term [27]. Secondly, in terms of Energy Security, fossil fuels can provide a security because they are often domestically produced. Countries may be reluctant to give up this security in favour of more variable renewable energy sources. Also, Infrastructure and Investment is another challenge [26]. There's a substantial existing infrastructure for fossil fuel extraction, transportation, and utilisation. Shifting to renewable energy requires significant investments in new infrastructure, which takes time and resources. The last one is Political and Lobbying Influence. The fossil fuel industry often wields significant political influence, which can slow down the transition to renewables [28].

Transitioning to renewable energy and reducing carbon emissions is a complex process. It requires advances in energy storage, grid management, and other technologies that aren't fully matured yet. Carbon capture and storage (CCS) and carbon capture and utilisation (CCU) can serve as important tools in mitigating climate change in the short term, particularly in sectors where rapid decarbonization is challenging, such as heavy industry and certain types of transportation [5]. These technologies can help reduce emissions and provide a bridge to a cleaner energy future. However, it's important to emphasise that CCS and CCU should not be seen as a long-term solution or an excuse to delay the transition to renewable energy. They should complement broader efforts to reduce carbon emissions and must be part of a

comprehensive strategy that includes aggressive efforts to increase renewable energy use, energy efficiency, and other emissions-reduction measures.

## 2.2 Carbon Capture Approaches

Carbon emissions sources can vary depending on the combustion or emission control method being used. Post-combustion, pre-combustion, and oxyfuel combustion are different approaches to managing carbon emissions in various industrial processes, especially in power generation and fuel production context. The key carbon emission sources for each of these approaches is discussed below [4].

In post-combustion capture, carbon emissions primarily originate from the flue gas of fuel combustion processes. These emissions contain various pollutants, including carbon dioxide ($CO_2$), which is the primary target for capture. Besides $CO_2$, flue gases can contain trace amounts of other carbon-containing compounds, such as carbon monoxide (CO), methane ($CH_4$), and volatile organic compounds (VOCs). These may also be sources of emissions, especially if not adequately captured and treated [22]. It's important to note that for tackling the global challenges each of them should be considered, which is not the only solution. It should be part of a broader strategy that includes a transition to cleaner and more sustainable energy sources, energy efficiency improvements, and changes in lifestyle and consumption patterns. Additionally, carbon capture technologies must be implemented with proper monitoring and regulations to ensure safe and effective management of captured $CO_2$ [5].

In pre-combustion capture, the primary goal is to capture carbon dioxide ($CO_2$) before the combustion of carbon-rich feedstocks, like coal or biomass, takes place. During the gasification process, these feedstocks are converted into synthesis gas (syngas), primarily composed of carbon monoxide (CO) and hydrogen ($H_2$). While combustion of syngas would result in $CO_2$ emissions, an additional aspect involves implementing the gas-shift reaction ($CO + H_2O \rightleftharpoons CO_2 + H2$). This reaction is crucial in transforming CO into $CO_2$ and generating hydrogen.

The strategic use of this gas-shift reaction allows for the production of a syngas stream with high concentrations of $CO_2$, making it easier to capture. The ultimate objective is to remove $CO_2$ from the syngas, especially as it is usually present in concentrated forms. This process results in the production of hydrogen-rich fuel. It's important to highlight that syngas, enriched with hydrogen, can be employed as fuel with minimal adjustments. However, the overarching idea is to produce hydrogen fuel, often referred to as "blue hydrogen," which may require additional adjustments and considerations for optimal efficiency in the overall process [29].

Oxyfuel combustion uses pure oxygen for combustion instead of air. To produce pure oxygen, energy is required, and this process may generate additional carbon emissions, particularly if fossil fuels are used for oxygen production. Oxyfuel combustion directly produces carbon emissions in the form of $CO_2$ when burning fossil fuels. However, because of the absence of nitrogen in the combustion process, the flue gas is nearly pure $CO_2$, making it more suitable for capture [30].

### 2.3 Post-Combustion Carbon Capture as a Key Mitigation Strategy

One pivotal strategy in addressing the carbon emission challenge is the implementation of post-combustion carbon capture technologies. Unlike pre-combustion and oxy-fuel combustion capture methods, which modify the combustion process itself, post-combustion carbon capture technologies focus on capturing $CO_2$ emissions after combustion has occurred [9]. Post-combustion carbon capture is considered a key solution in the context of reducing carbon emissions for several reasons which summarised in below:

1- Retrofitting Existing Infrastructure: Post-combustion carbon capture can be applied to existing power plants and industrial facilities without significant modifications to their core combustion processes. This is particularly important because a large portion of the world's energy infrastructure relies on fossil fuels, and replacing or upgrading this infrastructure is often expensive and time-consuming [31].

2- Flexibility and Versatility: Post-combustion capture technology is versatile and can be used with a variety of fuels and processes. It is not limited to specific fuel types or industries, making it applicable to a wide range of sectors, including electricity generation, cement production, and steel manufacturing [30].

3- Transition to Low Carbon: Post-combustion capture can facilitate the transition to a low-carbon energy system. By retrofitting existing power plants with carbon capture technology, it is possible to continue using fossil fuels while significantly reducing $CO_2$ emissions, thus helping to bridge the gap between current energy needs and a cleaner, more sustainable future [24].

4- Reducing Emissions from Hard-to-Decarbonize Sectors: In certain sectors, such as cement and petrochemicals, emissions are challenging to eliminate entirely due to the nature of the industrial processes. Post-combustion capture provides a viable means of capturing and reducing emissions in these industries [3].

5- Research and Development: Over the years, significant research and development efforts have been devoted to improving post-combustion carbon capture technologies.

This has led to advancements in capture efficiency, cost reduction, and energy requirements, making it more viable and cost-effective [29].

6- Carbon Management: Post-combustion capture provides a way to manage $CO_2$ emissions effectively. Captured $CO_2$ can be stored underground (carbon storage) or used in various applications, including enhanced oil recovery (EOR), carbon utilisation, and the production of synthetic fuels and chemicals [3].

## 2.4 Adsorption Technology: A Sustainable Solution

Adsorption technology is based on the principle of selectively capturing $CO_2$ molecules from flue gases or gas mixtures onto solid materials known as sorbents [36]. These sorbents possess the remarkable ability to adsorb $CO_2$ molecules onto their surfaces while allowing other gases to pass through, offering a sustainable and efficient means of separating and concentrating $CO_2$ for subsequent storage, utilisation, or sequestration [36].

The choice of the "best" carbon capture technology depends on various factors, including the specific application, the characteristics of the emission source, and economic considerations [34]. Adsorption is one of several carbon capture technologies, and it may be considered a favourable option in certain situations for the following reasons:

- Adsorption processes can be highly selective, which means they can effectively capture $CO_2$ from flue gas or other gas streams without capturing other gases. This selectivity reduces the energy and cost required for separation [37].
- Adsorption systems can be designed to be regenerable, which means that once the adsorbent material is saturated with $CO_2$, it can be regenerated by releasing the captured $CO_2$ and then reused. This regeneration capability can improve the overall cost-effectiveness of the technology [37].
- Adsorption can be an energy-efficient carbon capture method, especially in cases where the temperature and pressure conditions are favourable for adsorption-desorption cycles. This can result in lower operational costs compared to some other capture technologies [38].
- Adsorption technologies can be adapted to a range of applications, from large-scale industrial processes to smaller, decentralised systems. This adaptability makes them suitable for various industries and emissions sources.
- Adsorption systems are often scalable, allowing them to be adjusted in size and capacity to meet the specific needs of different installations.

- There is a variety of sorbent materials available for adsorption, and ongoing research and development are leading to the discovery of new and more efficient adsorbents. This offers flexibility in choosing the right material for a given application.
- Adsorption technologies can have a lower environmental impact compared to some other carbon capture methods, particularly in terms of the chemicals and waste generated in the capture process [1].

Despite these advantages, it's important to note that adsorption may not be the best solution in all circumstances. The choice of carbon capture technology should take into account factors such as the concentration of $CO_2$ in the emissions source, the space available for capture equipment, the costs of the adsorbent material, and the local infrastructure for waste handling or $CO_2$ utilisation. Ultimately, the success of adsorption as a carbon capture solution hinges on advancements in sorbent development and innovations in process technology. The development of efficient adsorbent materials for capturing carbon dioxide must indeed occur in conjunction with advancements in gas-solid contacting technology. These two aspects are interlinked and mutually influential in optimising the performance of adsorption-based carbon capture systems. Additionally, the successful regeneration of sorbents is a critical element in the success of adsorption-based carbon capture solutions. It ensures the continuous and efficient operation of these systems, optimises resource utilisation, reduces environmental impacts, and enhances the economic viability of carbon capture. Therefore, advancements in sorbent regeneration, in parallel with sorbent development and process technology, are pivotal for realising the full potential of carbon capture in mitigating greenhouse gas emissions and addressing climate change.

Collaborations between researchers, engineers, and industries are essential to bring effective and economically viable adsorption systems to the forefront of carbon capture efforts [11]. Continuous research and development in both these areas are critical to improving the efficiency and feasibility of adsorption as a carbon capture solution [38].

### 2.4.1 Sorbent Development: The Heart of Adsorption Technology

The effectiveness of adsorption technology is pivotal in the quest for efficient carbon capture, with the development and optimization of sorbent materials standing at its forefront.
[19]. While various sorbent materials, such as activated carbons, zeolites, and metal-organic frameworks (MOFs) [39], offer notable advantages, the focus has shifted toward polyethyleneimine (PEI)-based materials due to their unique properties. PEI-based sorbents

exhibit exceptional $CO_2$ selectivity and strong sorbent-$CO_2$ interactions, making them promising candidates for carbon capture applications. Recent strides in sorbent design have concentrated on enhancing the performance of PEI-based materials. Customizing the surface chemistry and pore structure of these sorbents has demonstrated potential in augmenting $CO_2$ adsorption capacity and selectivity. Moreover, the utilization of PEI-based sorbents aligns with the broader goal of developing sustainable materials for carbon capture, as they can be synthesized from abundant and low-cost feedstocks, thereby reducing the environmental footprint associated with the technology. This strategic choice emphasize a concerted effort toward environmental stewardship while advancing the efficiency of carbon capture processes [40].

For solid sorbents to become competitive, further research is needed since solid sorbents have difficulty in low pressure and high temperature environments. Furthermore, the development of promising adsorbent materials that can capture carbon dioxide efficiently with minimal regeneration energy/cost penalties must occur in parallel with the development of the gas-solid contacting technology. This will maximize the competitiveness of carbon capture (CCS) in various applications, specifically in high pollutant industries like cement and iron/steel which produce huge amount of $CO_2$ content (25–30%) from their flue gas stacks [41].

Numerous studies have been reported in the literature (9, 41-44) for the development of suitable sorbents that can capture carbon at low cost and with high efficiency. These include activated carbons, pillared clays, metal oxides, polyethylenimine (PEI), and zeolites. Typically, $CO_2$ sorbents are categorized based on their working temperatures as such: low-temperature (<200 °C), intermediate-temperature (200–400 °C), and high-temperature (>400 °C). Additionally, the adsorption capacity, adsorption kinetics, recycling/regeneration stability and cost should be carefully considered when evaluating a sorbent [45]. To avoid the aforementioned problems linked to aqueous amines, some solid amine adsorbents loaded with different support materials have been investigated [43]. The silica-supported polyethylenimine (PEI) sorbents are a particularly promising material, consisting of repeating units containing one amine group and two carbon aliphatic spacers [40]. Because PEI has multiple reaction sites, it can theoretically adsorb substantial amounts of $CO_2$ per unit weight. Additionally, it is relatively inexpensive and has low volatility, making it an attractive $CO_2$ absorbent.

The first PEI-based sorbents were fabricated by binding PEI onto the surface of silica gel by Tsuda et al. [46]. PEI sorbents can also be prepared by impregnating linear or branched PEI

onto porous surfaces including silica [47] , nanotubes (48, 49), metal–organic frameworks (MOFs) [49], glass fibres [50], membranes [51], carbons [52], or polymers [53]. As a result of the noticeably enlarged surface area, $CO_2$ and PEI interact more readily which maximizes $CO_2$ adsorption. Generally, $CO_2$ uptake is in the range of 100–200 milligrams of $CO_2$ per gram of the sorbent [41].

Siriwardane et al. [54] reported that the adsorption capacity of amine sorbent for $CO_2$ was improved with zeolite 13X, where an adsorption capacity of 8.5 mmol/g was reported at 25 °C and 1 atm. Tejavath et al. [55] showed that the adsorption capacity for $CO_2$ adsorption was improved with amine at a constant loading percentage of 40wt % over 13X-DETA-40, showing an adsorption capacity of 1.054 mmol/g in 20 min. In the first two minutes of their experiment, approximately 0.8 mmol/g was adsorbed by the initial time of adsorption process. In addition to materials development, technology development to ensure good contact mixing between gases and solids is essential for achieving a suitable solid-based carbon capture solution. In this regard, there are several studies by many researchers (9, 42, 46).

In summary, the development of promising adsorbent materials that can capture carbon dioxide efficiently with minimal regeneration energy/cost penalties must occur in parallel with the development of the gas-solid contacting technology. This will maximise the competitiveness of carbon capture (CCS) in various applications, specifically in high pollutant industries like cement and iron/steel which produce huge amounts of $CO_2$ content (25–30%) from their flue gas stacks. Another factor to consider is the process conditions which differ by industry, which means each process condition requires a different sorbent and technology [53].

### 2.4.2 Sorbent Regeneration: as a supplementary criterion

Sorbent regeneration is a crucial aspect of carbon capture processes, playing a pivotal role in the efficiency, cost-effectiveness, and sustainability of these technologies. While many studies focus on the adsorption process itself, few delve into the desorption kinetics and cyclability of sorbents. Due to the significant exhaust gas flows and high $CO_2$ concentrations, sorbent saturation time are short, necessitating efficient regeneration for enhanced performance and reduced capital costs in carbon capture processes.

Sorbent regeneration, within the context of carbon capture, involves the controlled release of captured carbon dioxide ($CO_2$) and other contaminants from the sorbent material. This process allows for the systematic reuse of the sorbent in subsequent cycles of $CO_2$ capture. The

significance of sorbent regeneration cannot be overstated, as it directly impacts the continuous operation of carbon capture systems and contributes to the reduction of $CO_2$ emissions.

During the capture phase, the sorbent adsorbs $CO_2$ from flue gas or other emission sources. Once saturated, the sorbent loses its ability to capture additional $CO_2$ effectively. Sorbent regeneration reactivates the material, enabling its repeated use in a continuous cycle. Accumulation of non-desorbed particles can lead to decreased working capacity and a shorter life cycle for the sorbent.

The regeneration step significantly influences the economic viability of carbon capture processes. Regeneration typically requires the input of energy to release $CO_2$ from the sorbent. Efficient regeneration processes minimise the energy and cost penalties associated with carbon capture, making the technology more cost-effective. Lower operational costs are a key factor in the adoption and scalability of carbon capture systems [56]. Furthermore, sorbents are valuable resources, and their efficient use is essential for sustainability. By regenerating and reusing sorbent materials, the need for frequent replacement is reduced, leading to resource conservation and a decrease in waste generation. This optimization of resources is vital for long-term environmental and economic sustainability.

Carbon capture processes, including regeneration, can also have environmental consequences such as waste generation or emissions [11]. Efficient regeneration methods are designed to minimise these impacts. When the regeneration step is executed with environmental considerations in mind, it reduces the overall ecological footprint of carbon capture systems (including sourcing and disposal of the adsorbent materials). Also, the efficient regeneration of sorbents is a key factor in scaling up carbon capture systems for industrial applications. Large-scale operations require reliable and efficient regeneration techniques to be practical and economically viable. Unreliable regeneration can lead to operational downtime, increased maintenance requirements, and decreased system performance.

In addressing sorbent deactivation during multi-cycle adsorption-desorption, effective desorption techniques are essential. Various methods, such as Temperature Swing Adsorption (TSA), Pressure Swing Adsorption (PSA), Vacuum Swing Adsorption (VSA), Microwaves, or combinations thereof, have been explored. The gas-solid contacting technology faces specific challenges that require desorption techniques allowing complete recovery of adsorption capacity, low energy consumption, short regeneration time, and minimal impact on the adsorbent.

Temperature Swing Adsorption relies on the temperature differential between low and high temperatures to drive desorption, often using hot purge/sweep gas, steam, or in-line heaters. Pressure Swing Adsorption involves preferential adsorption at high pressure and subsequent desorption by lowering the pressure. Developing regenerable sorbents with high selectivity and adsorption capacity is critical for successful PSA processes. Microwave-assisted vacuum desorption has been explored as a means of rapidly regenerating sorbents with wet feed gases. This technique, as studied by Webley et al. [109], directs thermal energy to the sorbent surface, liberating water and $CO_2$. The addition of microwave radiation improves $CO_2$ desorption, enhancing captured $CO_2$ purity. Such innovative approaches contribute to the ongoing efforts to optimize sorbent regeneration processes in carbon capture technologies.

### 2.4.3 Reactor Technology: Optimising Adsorption Processes

In conjunction with sorbent development, reactor technology plays a pivotal role in adsorption-based carbon capture. Reactors are responsible for the cyclic process of adsorption and desorption, ensuring the efficient and continuous operation of the carbon capture system. The design and operation of these reactors are critical in achieving high capture efficiency and minimising energy consumption [18]. Various reactor configurations are employed in adsorption technology, such as fluidized-bed, and packed-bed reactors. Each configuration offers distinct advantages and challenges in terms of sorbent performance, pressure drop, and heat management. The choice of reactor design depends on specific application requirements [57].

Adsorption reactors play a vital role in carbon capture processes, managing adsorption, desorption, and regeneration cycles. Precise control of these cycles is essential to capture $CO_2$ efficiently while using minimal energy. By optimizing energy balance, including heat management and integrating waste heat, energy consumption can be reduced for desorption and sorbent regeneration, making the process more economically viable and sustainable.

Energy efficiency is crucial in carbon capture, and innovative reactor designs aim to minimize energy requirements through strategies like utilizing waste heat or leveraging exothermic reactions for desorption. This optimization not only enhances economic viability but also promotes environmental sustainability.

Reactor design is central to carbon capture systems, impacting overall efficiency and feasibility. Therefore, understanding and optimizing reactor designs are crucial for advancing carbon capture technology. Ongoing efforts focus on developing various reactor technologies to meet

stringent carbon capture requirements, emphasizing performance and sustainability enhancements.

These technologies encompass a spectrum of designs, each with distinct features, advantages, and limitations. Notable examples include:

- **Packed Bed Reactors**: Packed Bed Reactors consist of a column filled with solid sorbent materials either packed randomly or structured. Their simplicity allows for easy scalability, making them applicable to various settings. One key advantage lies in their efficient heat management, contributing to the overall energy balance of the carbon capture system. Their robust nature and straightforward operation make them suitable for diverse applications, ensuring reliability and adaptability [58].
- **Moving Bed Reactors**: Moving Bed Reactors offer a dynamic approach where sorbent particles move through different zones for adsorption and regeneration. This design brings flexibility to the process, allowing for tailored control over heat integration strategies. The ability to alternate between adsorption and regeneration zones enhances the system's efficiency. This adaptability, combined with effective heat management, positions Moving Bed Reactors as versatile solutions for optimizing energy consumption in carbon capture processes [59].
- **Rotary Kilns**: Rotary Kilns present a distinctive design with a rotating cylindrical vessel for the sorbent material. Noteworthy for their proficiency in high-temperature processes, they excel in applications demanding rapid heat transfer. This design feature enhances the overall energy efficiency of the system, particularly in scenarios where high temperatures are involved. The rotating motion contributes to uniform heat distribution, making Rotary Kilns well-suited for processes requiring intense thermal conditions [60].
- **Fluidized Bed Reactors**: Fluidized bed reactors stand out due to their distinctive ability to create a dynamic suspension of sorbent particles within the reactor vessel [40]. This fluidized state enables efficient gas-solid contact, resulting in high mass transfer rates and enhanced sorbent performance [54]. Fluidized bed reactors have garnered considerable attention and investment in recent years due to their notable advantages in the context of carbon capture:
    - Enhanced Mass Transfer: The dynamic nature of fluidized beds ensures efficient gas-solid contact, leading to rapid $CO_2$ capture and desorption [61]. This feature results in high capture efficiency and shorter contact time.

- Improved Heat Transfer: Fluidization facilitates excellent heat transfer between the gas phase and solid sorbents, reducing the energy requirements for sorbent regeneration and lowering overall operational costs [62].
- Scalability: Fluidized bed systems are adaptable to a wide range of sizes, making them suitable for both small-scale and large-scale carbon capture applications [62].
- Flexibility: Fluidized bed reactors can accommodate a variety of sorbent materials, offering flexibility in selecting sorbents with superior $CO_2$ capture properties.

Various technologies aim to enhance the interaction between solid particles, such as catalysts or reactants, and fluids, either gases or liquids. Reactors like Continuous Stirred Tank Reactors, Fluidized Bed Reactors, and Fixed Bed Reactors have been employed for this purpose. However, fluidized bed reactors stand out as a promising solution due to their capacity for high mass and heat transfer rates [2].

The choice of the fluidized bed over a packed bed is particularly advantageous in carbon capture processes. It ensures high mass and heat transfer rates while maintaining low pressure drop, a critical factor for efficient removal of $CO_2$. In the context of carbon capture, managing heat transfer is crucial to prevent the formation of hot spots during the highly exothermic carbonation reaction [61].

A study by Girimonte [23] compared the performance of fluidized bed and packed bed reactors in $CO_2$ removal. The research investigated the impact of $CO_2$ concentration, gas velocity, and particle size on both types of reactors. In the fluidized bed, the exothermic nature of the process resulted in a smaller temperature effect, controllable by adjusting the superficial gas velocity. In contrast, the packed bed showed the presence of hot spot zones. Girimonte concluded that the fluidized bed significantly improved efficiency, leading to a considerable increase in breakthrough time.

Fluidized bed reactors play a pivotal role in carbon capture processes due to their exceptional performance in critical areas such as superior mixing, extensive catalytic surface areas, and efficient heat transfer, surpassing other conventional reactor technologies [62]. Their unique strengths are particularly advantageous in applications where these characteristics are crucial for effective carbon capture. Despite these advantages, the selection of the most suitable reactor technology should be driven by process-specific requirements and economic considerations. While fluidized bed reactors are an attractive prospect for carbon capture scenarios, conventional systems like packed bed reactors and fixed-bed reactors may still find relevance

in certain applications, depending on specific conditions and desired outcomes. Fluidized bed reactors offer distinct advantages and tailored benefits, especially in the context of chemical, catalytic, and gas-solid or liquid-solid processes integral to carbon capture (63, 64).

### 2.4.4 Conventional Fluidized Bed Reactor Technology

Fluidized bed reactors (FBRs) are a diverse category of reactors, each offering unique advantages. The foundational work of Warren K. Lewis and Edwin R. Gilliland in the 1940s pioneered the concept of fluidized bed reactors—a dynamic system where solid particles emulate fluid behaviour upon exposure to fluidizing gas. This innovation has permeated various industrial processes, including those pivotal to carbon capture and sequestration (CCS) (65, 66).

In the realm of conventional fluidized bed reactors, where distributors facilitate fluidization, the landscape is rich with possibilities. These reactors play pivotal roles in gas adsorption, coating applications, and chemical reactions. However, their utility comes with intrinsic challenges. High pressure drops in comparison of conventional fluidized bed type, maldistribution leading to undesired flow regimes, suboptimal contact mixing, limited bed loading efficiency, and the intricacies of handling varied particle sizes and shapes pose substantial hurdles (11, 23, 25, 62).

A critical parameter in this context is the minimum fluidized velocity ($U_{mf}$), a key metric determining the smallest gas or liquid flow velocity required to loosen a packed bed and initiate fluidization. A nuanced understanding of $U_{mf}$ becomes imperative for steering optimal reactor performance through a spectrum of industrial applications (25, 46, 54, 67).

In fluidized beds, energy consumption is considerable due to the pumping of the gas as well as elutriation of finer particles are unavoidable [16]. Therefore, there is a limitation on particle size range in the bed and operating velocity regime that can be utilized. Immersed surfaces can be severely eroded and ‘defluidised’ depending on the reaction and the materials used (15, 16). There are different types of flow regime in fluidized bed. When increasing gas velocity through a bed of granular solids, the following changes in the contacting mode of the gas-solid occur, summarised in figure 2.1 [63]:

- Packed Bed/ Fixed Bed regime
- Minimum fluidization point

- Fluidized Bed
- Bubbling Bed
- Slugging Bed
- Turbulent Bed

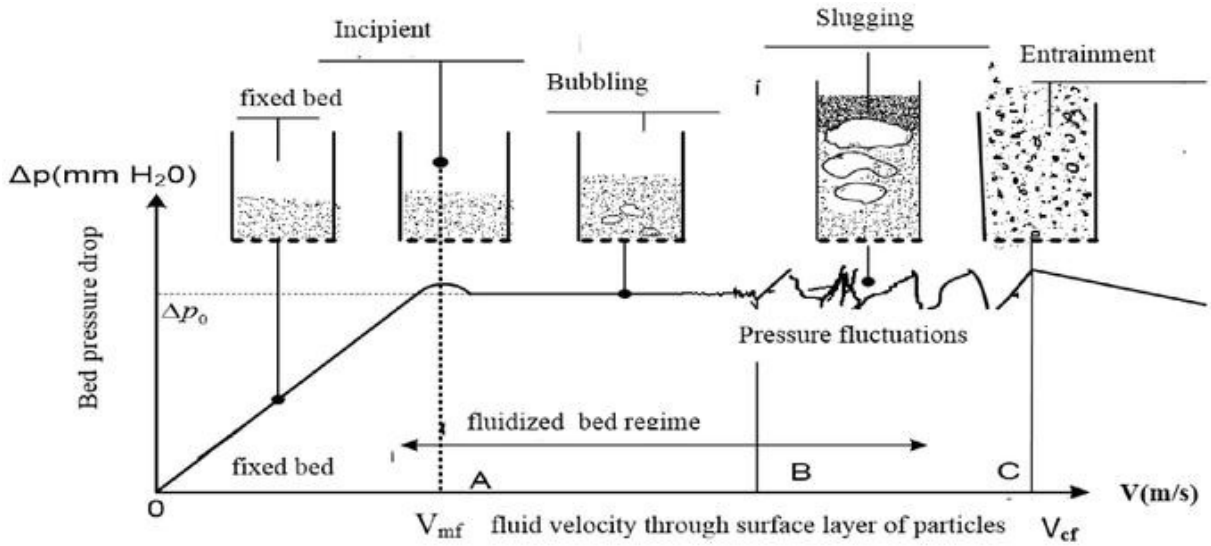


*Figure 2.1 Different regimes in a conventional fluidized bed in order of increasing velocities[63]*

According to the previous studies on different types of fluidized bed reactor, some advantages have been reported. The most salient of these are described here:

Under isothermal conditions, fluidized beds provide excellent mixing and facilitate high transfer rates. For large-scale operations involving heat-sensitive reactions, fluidized beds are ideal. Because of its fluid-like behaviour, it facilitates free flow of the bed between adjacent reactors. Because there are no moving parts and small bed is needed, the costs are reduced. A continuous process coupled with high throughput is possible even without a skilled operator. Multistage operations can convert a batch fluidized bed reactor into a continuous reactor, achieving the desired residence time. This property makes it possible for the bed to flow freely between adjacent reactors because it resembles a fluid [64]. In a summary the advantage of fluidised bed reactor categorised in below:

- Fluidized bed reactors provide outstanding mixing between the solid catalyst or sorbent and the fluid phase, ensuring even contact and improved mass and heat transfer. This is particularly advantageous for processes that require efficient mixing, such as gas-solid reactions or catalytic reactions [16].

- The large surface area of the fluidized solid particles allows for more efficient contact with the reacting fluid, leading to enhanced reaction rates and higher catalytic activity [22].
- Fluidized beds offer efficient heat transfer due to the intimate contact between the solid particles and the fluid. This is especially beneficial for endothermic and exothermic reactions, where heat management is crucial.
- Fluidized beds generally exhibit lower pressure drops compared to packed beds, making them more energy-efficient and reducing the need for high-pressure pumps [65].
- Fluidized beds can be easily scaled up or down to meet the requirements of different processes, allowing for flexibility in reactor size and capacity.
- They are versatile and applicable to a range of processes, including gas-solid reactions, catalysis, drying, combustion, and gasification [65].

Despite the advantages offered by fluidized bed reactors, challenges persist, particularly with fine-sized particles falling under Geldart Classes C and D. Geldart classification is a categorization system based on the fluidization behaviour of particles, and Classes C and D encompass particles that are cohesive (C) and tend to form aggregates, or particles that spout with minimal mixing (D). These both pose difficulties in fluidization, often resulting in maldistribution issues such as slugging and channelling. While fluidized beds excel in heat and mass transfer compared to packed bed reactors, these challenges persist (34, 67).

The hydrodynamics of fluidized beds present modelling and scaling challenges, necessitating modifications to reactor geometry. Undesirable effects like turbulent mixing, segregation, interactions at the distributor, and agglomeration can hamper efficiency [72]. Key disadvantages include the complex design and operational requirements leading to elevated capital and operational costs. Continuous particle movement may cause abrasion and attrition, impacting catalyst or sorbent longevity. Higher energy requirements for maintaining fluidization can result in increased operational costs. Fluidized beds may also face limitations in applications involving a liquid phase due to potential particle entrainment issues [17].

## 2.5 Process intensification by Fluidised Bed Reactor

The definition of PI can be divided into two categories: (a) process-intensifying equipment; and (b) process-intensifying methodologies. The equipment consists of different types of functional reactors (e.g. oscillatory baffled reactors, spinning disc reactors, rotating packed bed reactors, membrane reactors, etc.) and various other unit operations such as static mixers, compact heat exchangers, centrifugal adsorbers, etc [68]. For intensified processing, PI methods may also utilize multifunctional reactors or external energy sources such as microwave heating and ultrasonic waves. A fluidized bed reactor is another type of reactor that has been widely used in chemical and process industries because of its excellent multi-phase contact, low diffusion resistance, and good heat and mass transfer properties. For the purpose of improving control and the quality of the mixture in a fluidized bed, significant modifications were made to the design of conventional fluidized beds, resulting in improved dynamic stability, as well as improved fluid/solid contact efficiency.

### 2.5.1 Micro Fluidised Bed

Micro-fluidized beds (MFBs) are indeed gaining popularity in various fields, including process intensification (PI) and the screening of solid processes and bioprocesses. MFBs provide a platform for conducting experiments on a small scale [69]. This is particularly valuable in the early stages of process development when limited quantities of materials or samples are available. Due to their small size, MFBs require less material and energy, which can result in cost savings, especially when working with expensive or limited resources. MFBs can facilitate high-throughput screening of various process conditions and parameters. Researchers can quickly test multiple variables, leading to more efficient process optimization. In addition to promoting the solid-fluid contact intensity, the miniaturization of fluidized beds will also increase fluid and solid mixing, which is extremely important for industrial production. MFBs allow researchers to rapidly assess the performance of different solid processes and bioprocesses under real-World conditions, which is essential for evaluating potential applications and scalability. Micro-fluidized beds have found applications in various industries, including pharmaceuticals, petrochemicals, and environmental engineering (24, 65, 70). They play a significant role in the development of novel processes, optimization of existing ones, and the exploration of new technologies. Their growing popularity in process intensification is a testament to their potential for accelerating research and development while minimizing costs and resource consumption.

The definition of a Miniature Fluidized Bed (MFB) varies across studies, with criteria based on factors such as hydraulic diameter, inner diameter, and static bed height. For instance, it may have a hydraulic diameter of less than 500 mm [70] or a few centimetres. Xu et al. [70] specified an MFB with an inner diameter of 21 mm and a static bed height ranging from 20 to 50 mm. The Process Intensification Group at Newcastle University [65] utilized three 3D-printed MFBRs with bed diameters (Dt) of 10–15 mm and various bed heights (Hs/Dt = 1–3), successfully fluidizing cohesive Geldart C powder. An example of a 3D-printed MFBR with a bed diameter of 10 mm and a height of 150 mm is illustrated in Figure 2.2. Other studies employed fluidized beds with a 50 mm inner diameter (ID) and particle sizes of 2–3 mm (75, 76). These miniature fluidized bed systems offer several advantages, making them attractive for research and development purposes.

*Figure 2.2 Example of a fully-assembled 3D-printed reactor[65]*

### 2.5.2 Centrifugal Fluidized Bed

The concept of a centrifugal bed is an innovative approach designed to address some of the challenges associated with conventional fluidized beds, such as particle maldistribution and poor contact mixing, which can lead to the formation of large bubbles. In a centrifugal bed, the operating principle involves using centrifugal forces to create a more controlled and efficient fluidized bed system. The core principle of a centrifugal bed is the use of centrifugal force to distribute and fluidize particles within the bed. By rapidly rotating the bed and higher gas flow

rate consumption, particles are subjected to centrifugal forces that help achieve more uniform distribution and mixing.

The primary component of a fluidized centrifugal bed is a cylindrical vessel or column. This vessel is designed to rotate around its central axis, creating a centrifugal force that pushes particles towards the outer wall of the column. as shown in figure 2.3 [71]. The two important parameters in centrifugal reactors are rotation speed and radius of the bed. The combination of centrifugal forces and aeration ensures thorough mixing and contact between the fluidized particles. This can be advantageous for various processes that require uniform particle distribution or enhanced heat and mass transfer.

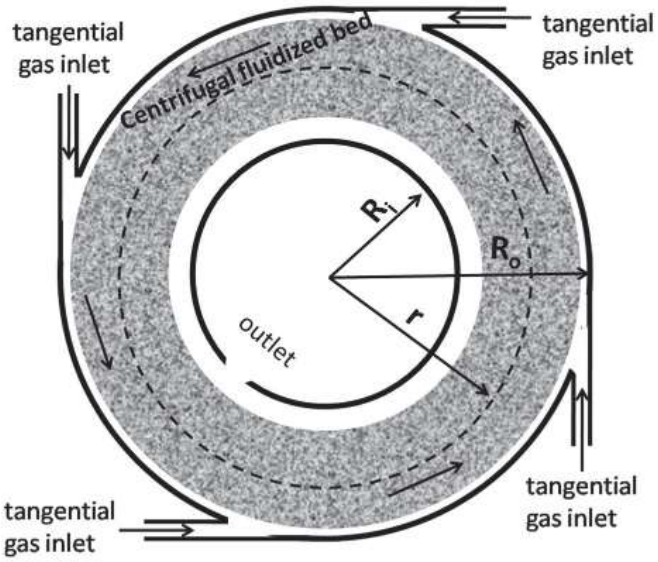


*Figure 2.3 Centrifugal fluidised bed with static geometry showing tangential inlets [71]*

Using both experimental and theoretical techniques, Takahashi et al. [27] evaluated centrifugal reactors with different particle sizes and densities. In centrifugal reactors, pressure drop is strongly influenced by rotational speed. Moreover, as gas velocity increases, the bed pressure drop tends to decrease as it reaches its maximum value at the minimum fluidizing velocity. The presence of many components, moving parts, and mechanical links can make the equipment more challenging to design, manufacture, and maintain. Also, the presence of numerous moving parts and mechanical links can lead to reduced efficiency and increased maintenance requirements. The need for regular maintenance and potential mechanical failures can result in higher operating costs. In addition, at very high rotating speeds, there is a possibility of particles massing toward the wall of the cylindrical vessel due to increasing

centrifugal forces. This can create uneven particle distribution, which may not be desirable for certain processes. while fluidized centrifugal beds offer advantages in terms of improved mixing and contact of fluidized particles, they come with significant complexities and potential challenges related to construction, maintenance, and operation. The decision to use such equipment should take into account the specific process requirements, cost considerations, and the trade-offs between the benefits and drawbacks associated with fluidized centrifugal beds [71].

### 2.5.3 Circulating Fluidised Bed

In circulating fluidized bed reactors, solid particles are entrained and circulated with the gas stream, leaving the main bed. These particles are then separated, cooled, and recirculated. CFBRs are used in combustion processes, gasification of coal or biomass, and some chemical reactions requiring high temperatures and efficient gas-solid contact. They provide excellent heat transfer, high solids residence time, and the ability to handle a wide range of feedstocks. One the challenge of the conventional fluidized bed is maldistribution flow regime with increases in the air flow rate beyond the minimum fluidization value causing bubbling and large pressure fluctuations [72].

Circulating Fluidized Bed (CFB) technology is indeed highly regarded in various industries due to several advantageous properties and features that make it a promising choice for a wide range of applications. [73]. CFBs are known for maintaining a high degree of temperature uniformity throughout the bed. This property is especially valuable in processes where consistent and controlled temperatures are critical. CFBs facilitate efficient mixing of solid particles with gases or liquids, ensuring that reactants are in close contact. This is essential for processes such as combustion, gasification, and chemical reactions. The design and operation of CFBs allow for excellent heat transfer rates between the walls of the bed and the interior. This feature is vital in applications where heat exchange is a primary concern, such as in power generation and fluid catalytic cracking. The CFB consists of a cylinder in which a gas-solid suspension is transported upward. The two-phase gas-solid mixture is separated at the top and solids are recycled to the bottom after being filtered through a cyclone. A schematic representation of circulating fluidized bed is shown in Figures 2.4 [74].

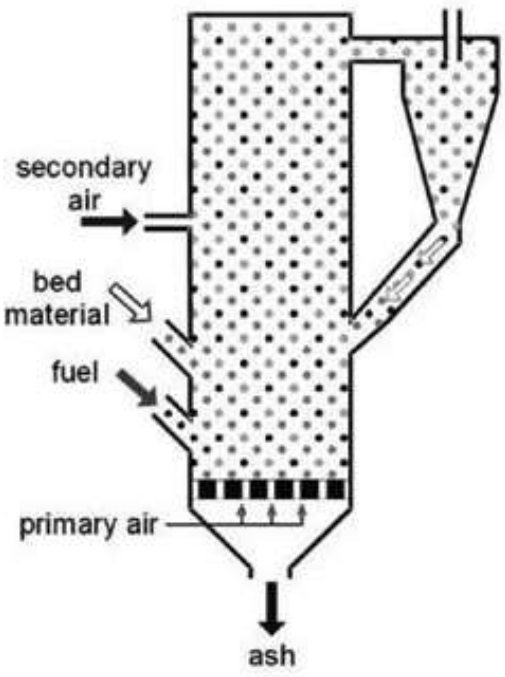


*Figure 2.4Circulating fluidised Bed[74]*

### 2.5.4 Vortex Fluidized Bed (VFB)

A Vortexing fluidized bed likely describes a fluidized bed in which there is a strong swirling or vortex-like motion of the fluid (typically a gas or liquid) and the solid particles within the bed. Vortexing fluidized beds are known for their distinct hydrodynamic behaviour, which includes the formation of vortices and increased mixing and contact between particles and the fluid. The schematic diagram of vortex chamber fluidized bed is shown Figure 2.5. The Vortexing fluidized bed (VFB) was patented by Sowards [75]. With the VFB, particle resistance time is increased, particle separation is improved, heat and mass transport are improved. There are, however, some disadvantages. [75].

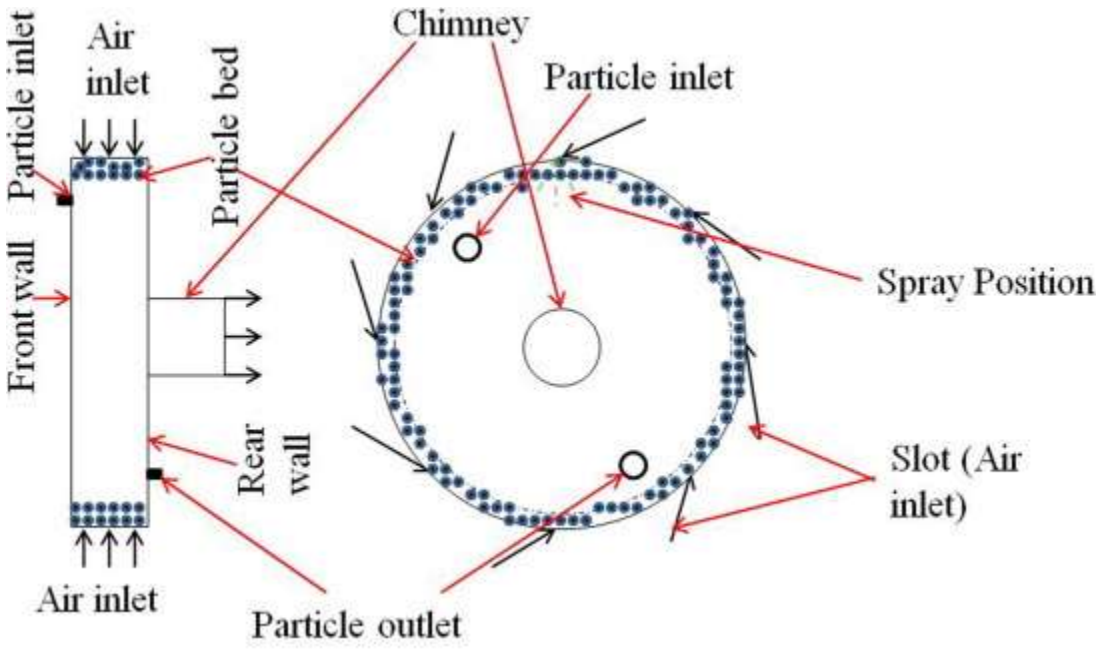


*Figure 2.5 The Schematic diagram of vortex chamber fluidized bed with two solid inlet [76]*

### 2.5.5 Rotating Distributor Fluidized Bed (RDFB)

A Rotating Distributor Fluidized Bed (RDFB) (Figures. 2.6) was proposed by Sobrino et al. [64]. This is a type of fluidized bed reactor or vessel used in various industrial processes for mixing, chemical reactions, and other applications (9, 56). The key feature of an RDFB is the use of a rotating distributor or agitator at the base of the fluidized bed. This rotating distributor serves to improve the distribution and mixing of solid particles within the bed. The rotating distributor at the base of the bed helps to create a more uniform distribution of solid particles. It promotes thorough mixing and contact between the particles, which is often crucial in processes such as chemical reactions, drying, and heat transfer. By breaking up stagnant regions and promoting circulation, RDFBs can help prevent channelling, which is the uneven flow of gas or liquid through the bed. This ensures consistent contact between reactants and minimizes local variations in temperature and composition. Furthermore, RDFBs often exhibit enhanced heat transfer rates due to the improved mixing and contact between solid particles and the surrounding fluid. This can be beneficial in processes involving heat-sensitive materials. While RDFBs offer advantages in terms of improved mixing and heat transfer, it's important to note that their design and operation may require more complex equipment and controls compared to traditional fluidized beds. Additionally, considerations such as equipment maintenance and power consumption should be taken into account when using RDFBs in industrial processes.

As a result of its high mass transfer performance, the rotating packed bed (RPB) is the most suitable PI technology to intensify carbon capture, according to Wang et al. [6] Other mass transfer devices include spinning disc reactors, static mixers, loop reactors, etc. According to Ma and Chen [77], in a centrifugal pump rotating at less than 1800 rpm, $CO_2$ removal efficiency increased with centrifugal acceleration. However, as gas flow rate increased, efficiency decreased. Additionally, they require less investment, have 15 less equipment footprint and can handle highly concentrated amine-based solvents more efficiently [78]. Furthermore, Yu and Tan [79] demonstrated that RPBs have a greater gas-liquid contact area and are better at capturing $CO_2$. A comparison of rotating packed beds with conventional columns showed that rotating packed beds are more efficient, save space, and reduce absorb size. (Jassim et al. [20]).

The potential risk of mechanical failure due to bed particles getting stuck between the rotating distributor and static support is worth mentioning, however. It is possible that the rotational motion of the distributor may be obstructed if the particles get crushed. In addition, this concept requires a lot of power to rotate the distributor, and it requires a lot of maintenance [20].

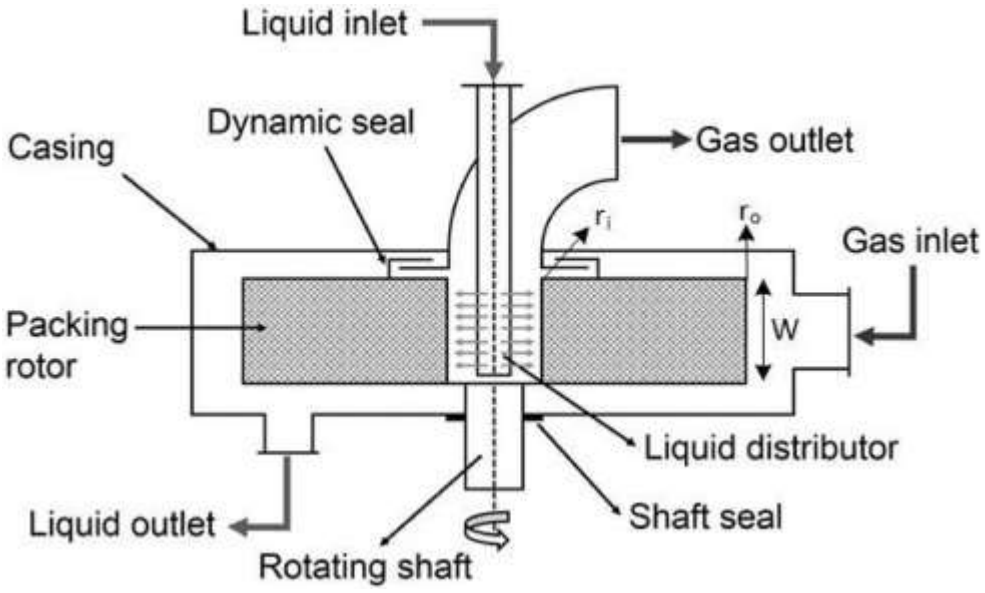


*Figure 2.6 Rotating Distributor Fluidized Bed [64]*

### 2.5.6 Bubbling Fluidized Bed Reactors (BFBR)

A bubbling fluidized bed reactor is a type of fluidized bed reactor as shown in Figure 2.7 used in various industrial processes, including chemical and petrochemical processes, as well as in environmental and energy-related applications. In this type of reactor, a gas (usually a fluidizing gas such as air or steam) is forced upward through a bed of solid particles. The velocity of the gas is adjusted to create a fluidized state, where the particles are suspended and remain in constant motion within the reactor vessel [80]. The solid particles in the bed are fluidized, meaning they behave like a fluid when the gas velocity is sufficient to overcome the force of gravity. This creates a dynamic mixture of solid particles and gas.

As the name suggests, the gas flow creates bubbles within the bed of solid particles. These bubbles rise and burst, causing the solid particles to move and mix. The bubbling action enhances the contact between the gas and the solid particles, which is crucial for various chemical reactions or heat transfer processes. In addition, the high degree of mixing in a bubbling fluidized bed reactor promotes efficient heat transfer between the gas and solid particles. This makes it useful for processes that require precise temperature control. Yi et al. (12, 80) have shown Flow rates and reaction characteristics of $CO_2$ between a bubbling fluidized-bed reactor and a bubbler fluidized-bed regenerator using dry sorbent in the continuous solid circulating mode. In the fast fluidized reactor, the Sorb NX30 sorbent captured all of the 10 % $CO_2$ within 3 seconds, demonstrating fast kinetics.

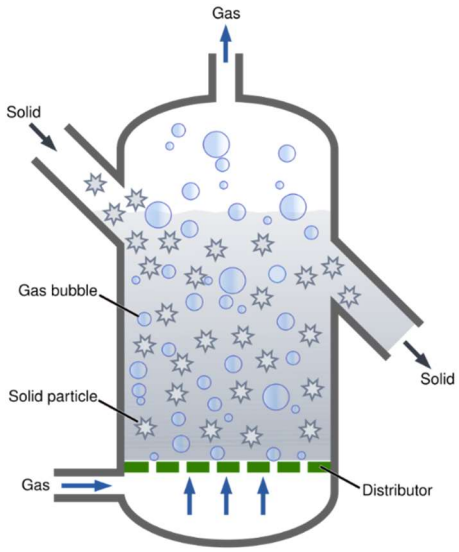


*Figure 2.7 Bubbling fluidized bed Reactor [90]*

### 2.5.7 Swirling Fluidized Bed Reactor (SFBRs)

Swirling Fluidized Bed Reactors (SFBRs) represent a specialised category within the broader realm of fluidized bed reactors. They are distinguished by the deliberate introduction of tangential swirling motion to the fluidized bed, creating a vortex-like flow pattern within the reactor. Swirling Fluidized Beds (SFBs) are another recent technique developed by researchers to overcome the drawbacks of conventional fluidized beds. The fluid (usually a gas) enters the SFB at an angle through the inclined opening of the annular distributor resulting in two components of velocity: (i) the vertical component causes fluidization and (ii) the horizontal component causes swirling motion. The Swirling Fluidized Beds (SFBs) has many considerable advantages over the other intensified fluidized bed concepts: no limitation for fine and light particles, good heat and mass transfer, no moving mechanical parts, uniform mixing, better quality of fluidization and lower distributor pressure drop, hence lower pumping power [81].

This swirling motion profoundly impacts the hydrodynamics and performance of the fluidized bed, making SFBRs particularly suited for a range of applications. Key Characteristics of SFBRs are listed below ((Shu et al. [57]), (Raghavan et al. [7]), (Eslami et al. [82]), (Jamei et al. [16]), (Mohideen et al. [83]):

- **Enhanced Mixing**: The swirling motion induced in SFBRs results in superior mixing of solid particles, gases, and reactants. This enhanced mixing contributes to improved mass transfer, making SFBRs suitable for reactions requiring rapid and uniform contact between phases.
- **Heat Transfer Efficiency**: The vortex-like flow in SFBRs enhances heat transfer rates, crucial for endothermic or exothermic reactions. This characteristic can lead to higher reaction efficiencies and reduced energy consumption.
- **Scalability**: SFBRs are scalable and adaptable to various sizes, making them suitable for both laboratory-scale research and industrial-scale applications.
- **Versatility**: SFBRs find applications in a wide range of processes, including combustion, gasification, catalytic reactions, drying, and particle coating.

## 2.6 Toroidal Fluidized Bed (TORBED)

A commercial Swirling Fluidized bed, called the toroidal fluidized bed (or TORBED) (16, 68), is already widely established throughout industry for a wide range of chemical and mechanical processes. For the first time this technology has been launched by Torftech company to provide novel, cost effective means for processing many different materials [8]. By using these technologies, processes involving gas-solid contact can be controlled accurately and quickly, often at higher temperatures than those experienced with conventional equipment.

In these reactor designs, inclined blades are used to introduce tangential motion to the fluidizing gas as shown in figure 2.8. This tangential motion imparts a swirling effect to the gas-solid mixture within the reactor. While the tangential motion contributes to swirling, the vertical velocity component is responsible for fluidization. The upward flow of gas suspends the solid particles within the reactor. The design minimizes entrainment of solid particles in the gas stream. This is achieved by dissipating the majority of the gas momentum at the base of the bed in radial and tangential directions [7]. The central cone within the reactor results in an increasing cross-sectional area as one moves away from the distributor. This design feature allows smaller particle sizes to be effectively fluidized compared to conventional fluidized beds.

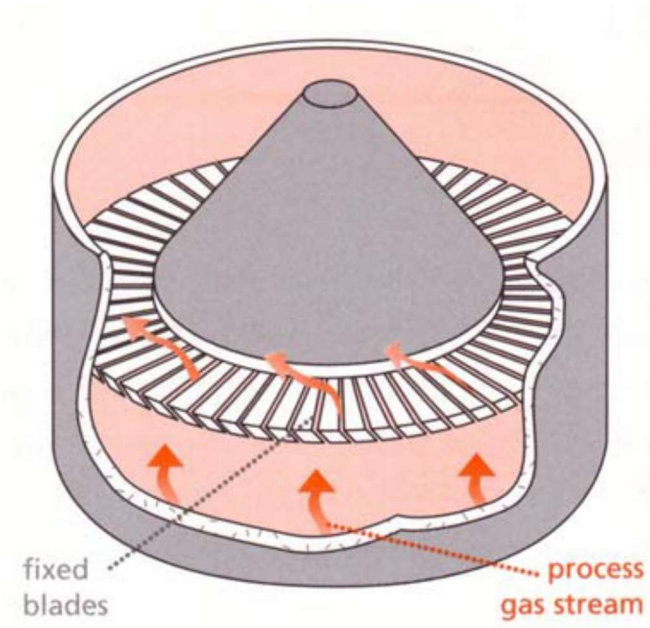


*Figure 2.8 Torodial fluidized bed (TORBED) Process gas flow through fixed blades gives toroidal particle motion [8]*

Smaller particles have several advantages, including reduced thermal mass, enabling faster heating and cooling, and shorter internal diffusion path lengths, which intensify mass transfer. the energy dissipated by the distributor and the resulting gas flow turbulence within the bed lead to several benefits like Thinning of Boundary Layers. The turbulence in the bed causes the thinning of boundary layers around the solid particles. This promotes efficient heat and mass transfer by reducing the resistance to mass and heat transfer (68, 77, 84).

Overall, TORBED and similar technologies provide a versatile and efficient means of handling gas-solid processes. They are particularly well-suited for industries where precise control, rapid reactions, and high-temperature operations are essential. The ability to operate at higher temperatures, while maintaining control and efficiency, makes these systems valuable in a wide range of industrial applications. TORBED technology is often more compact compared to conventional equipment, which can result in cost savings, especially in terms of capital and operational expenses. The ability to handle smaller scales is advantageous for niche or specialized applications.

### 2.6.1 TORBED Technology Description

In 1986, the first commercial prototypes were installed. There are now over 100 TORBED reactors in commercial use in Europe, North America, South Africa, New Zealand, Australia, China, India and Japan for applications as diverse as fat free "frying" of foods, toxic waste destruction and materials recycling. The Principle of Toroidal Fluidized Bed technology was proposed and patented by Dodson [85]. It features a unique reactor design characterized by a toroidal or doughnut-shaped bed. An essential component of this reactor is the gas distributor at the bottom of the annular bed.

The distributors in fluidized beds serve a comprehensive set of functions beyond the mere introduction of fluidizing media. They are integral to the overall performance and quality of fluidization by ensuring proper mixing, uniformity, and bed support. Selecting the appropriate distributor type is a crucial consideration in designing and operating fluidized bed systems in various industrial applications. There are several features which could describe a desirable distributor. They are essential for ensuring the efficient and effective operation of fluidized beds. Here is a summary of these desirable characteristics [65]:

- Uniform and Stable Fluidization: A good gas distributor should induce and maintain uniform and stable fluidization across the entire cross-section of the bed. This ensures that all particles experience consistent conditions.
- Prevent Non-Fluidized Regions: It should prevent the formation of non-fluidized regions on the grid, as such regions can disrupt the fluidization process and reduce efficiency.
- Longevity: The distributor should be designed to operate for an extended period without breaking or requiring frequent maintenance or replacement.
- Solids Leakage Prevention: It should minimize the leakage of solid particles into the plenum chamber, which can be undesirable and affect the overall process.
- Maldistribution Mitigation: The distributor should minimize maldistribution of bed particles, ensuring even distribution of fluid and particles throughout the bed.
- Structural Strength: It should have sufficient structural strength to resist failure during operation, which is crucial for the safety and reliability of the fluidized bed system.
- Support for Static Bed Weight: The distributor should be able to support the weight of the static bed, which is important during startup, shutdown, or when the bed is in a non-fluidized state.
- Low Pressure Drop: A good distributor should have a low pressure drop, minimizing the power consumed by the system. High-pressure drops can be energy-intensive and increase operational costs.

The study by Ouyang et al. which proposed a spiral distributor for swirl motion as shown in Figure 2.9, is an important contribution to the field of fluidized bed reactor design and gas-solid mixing. The use of a spiral distributor is aimed at achieving controlled swirl or rotational motion within the reactor, which can have several benefits in terms of mixing and mass transfer. Their study compared the characteristics of this distributor with those of sintered-plate distributors, including pressure drop, fluidization quality, and heat transfer coefficient.

The TORBED reactor's unique combination of the toroidal bed and the gas distributor with angled blades offers improved control, mixing, and heat transfer compared to traditional fluidized bed reactors. The design of the spiral distributor as described, with overlapping blades shaped as sectors of a circle and an opening between the blades, is a specific configuration aimed at achieving the desired swirling or tangential motion of the gas as it enters the fluidized bed reactor. This configuration is designed to enhance the fluidization and mixing of solid

particles within the bed. The overlapping blades, which are shaped as sectors of a circle, are a critical component of the spiral distributor. These blades are strategically arranged at the bottom of the reactor to direct the incoming gas flow in a controlled manner. Also, the design of the spiral distributor is intended to create a tangential airflow at the opening between the blades. When the gas exits through this gap, it imparts a swirling or tangential motion to the solid particles within the bed. Furthermore, the tangential airflow induced by the spiral distributor results in a swirl motion within the reactor. This swirling motion enhances the mixing of the gas and solid particles, promoting uniform distribution and contact between the two phases.

Overall, the design of the spiral distributor with overlapping blades and a tangential gas flow is a practical approach for achieving the benefits of swirl motion in fluidized bed reactors. It improves mixing, mass transfer, and temperature control, making it valuable for various industrial processes that rely on fluidized bed technology.

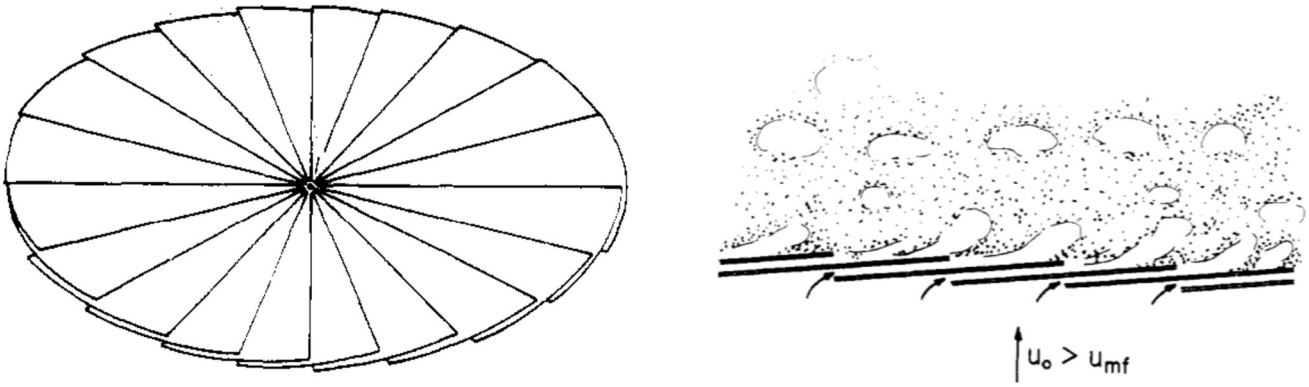


*Figure 2.9 Spiral distributor schematic & Bed behaviour at the spiral distributor [86]*

The study conducted by Shu et al. that investigated the hydrodynamics of a toroidal fluidized bed (TORBED) with fine particles and compared it to the performance of a conventional bed is of significant interest in the field of fluidized bed technology. This type of research can provide valuable insights into the behaviour and efficiency of TORBED technology in handling fine particles as compared to conventional fluidized beds. The study focused on the behavior of fine particles within the TORBED as shown in Figure 2.10 Fine particles can present unique challenges in fluidized bed systems due to their cohesive and agglomeration tendencies. Understanding how TORBED technology handles fine particles is crucial for applications in various industries, including pharmaceuticals, chemicals, and materials processing. To assess

the advantages of TORBED technology, the study compared the performance of the TORBED with fine particles to that of a conventional fluidized bed. This comparative analysis likely involved factors such as particle mixing efficiency, residence time, heat and mass transfer, and overall process performance [86].

The development of a new version of swirling fluidized bed called the "conical swirling fluidized bed," as undertaken by Kaewklum et al. [17], represents an innovative approach in the field of fluidized bed technology. This modified design likely offers distinct features and advantages compared to traditional fluidized beds. While the specific details of the design and its applications would be found in the research conducted by Kaewklum and colleagues. The use of the term "conical" indicates that the bed likely has a conical or tapered shape. This geometry can influence the behavior of the fluidized particles and the gas flow within the bed. Swirling fluidized beds are known for their efficiency in mixing solid particles and gases. The conical design may further optimize this mixing process, making it suitable for applications where thorough mixing is essential as shown in Figure 2.11.

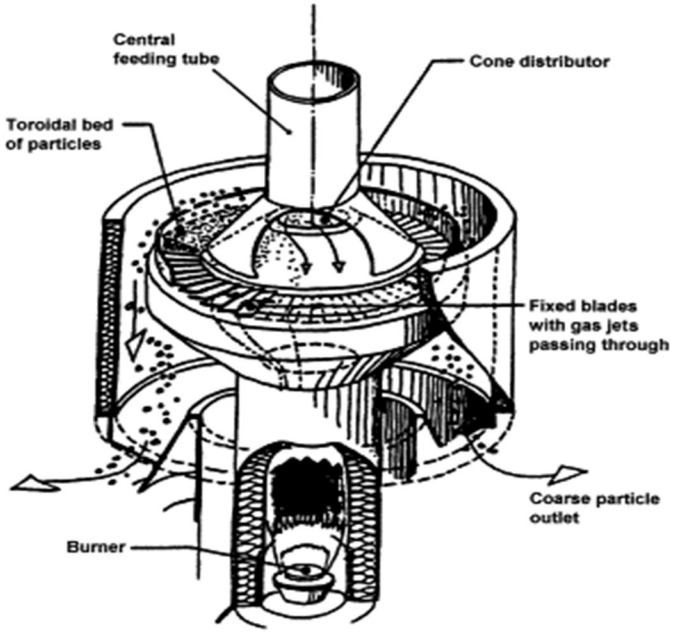


*Figure 2.10 Configuration of a toroidal fluidized bed reactor [57]*

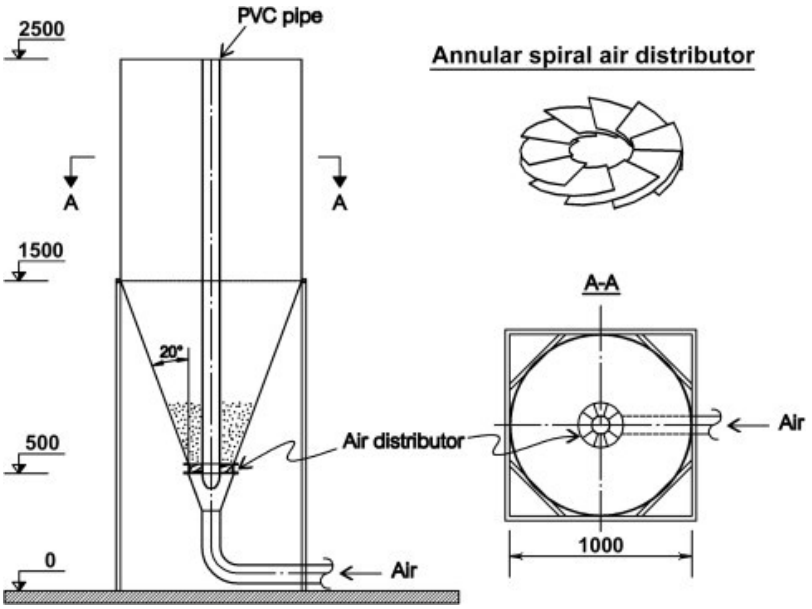


*Figure 2.11 Schematic diagram of the 'cold' model of a conical SFBC [17]*

In the table 2.1 summarizes some other findings of swirling fluidization behavior observed in the literature:

*Table 2.1 Significant swirling bed reactor results*

| Reference | Distributor Type | Parameters | Results |
|---|---|---|---|
| **Shukrullah,2020 [18]** | Mesh-coupled annular | Blade distributor, Bed weight, superficial velocity, blade angle, pressure drop, bed velocity | The proposed hybrid design can effectively minimize the required pressure drop for uniform fluidization of materials. This design stops the smaller particles from falling through the gaps between the blades without increasing the pressure drop. |
| **Lutfi, 2020 [84]** | Spiral Blade Distributor | Pitch Length, Blade Inclination Angle | The pitch length and inclination angle increases, the velocity distribution also increase. This current design will promote vigorous mixing, but the pressure drop for this type is high. Further, it would result more power usage to run this model, as this will increase the cost of energy consumption. |

| | | | |
|---|---|---|---|
| **Tawfik 2020 [87]** | Annular Distributor | Number of blades, Velocity, bed hight, plenum effect | Utilization of central bodies either conical or cylindrical shapes resulted in a negative effect due to increasing the distributor and bed pressure drops and decreasing the heat transfer coefficient |
| **McDonough et al, 2020 [88]** | Annular Distributor | Bed loading, gas volumetric flow rate, gas temperature and gas humidity | The desirable uniformly packed state occurred at bed loadings of ms ≥ 1200mg and gas flow rates of Q ≥ 35.5 L/min. Humidity and air temperature had minimal influence over the flow patterns |
| **Yudin, 2016 [19]** | Inclined slotted | Particulate mixing and uniform fluidization | Swirling motion resulted in uniform mixing of particles. The swirling flow pattern was obvious for shallow beds while two-layers motion was observed in case of deep beds. |
| **Shukrullah, 2019[62]** | Mesh-coupled annular blade | Bed weights, blade inclination angles, Bed Hight and superficial air velocities. | Overall, the bed velocity was found to be maximum when the bed weight was minimum, this design stops the smaller particles from falling through the gaps between the blades without increasing the pressure drop. For low-cost fluidization operations, lower Umf values are favourable, Although Umf decreased as the inclination angle increased |
| **Rees, 2006 [89]** | Perforated Plate | Superficial air velocity, pressure drop | Voids or bubble streams were observed even at U < Um. Dead zones were formed between the orifices of distributor. Jet length was increased with an increase in U/Um ratio |
| **Naz et al. 2017 [62]** | Annular distributor | Pressure drops, blade fin angle, superficial velocity, blade angle | Bed velocity exhibited Gaussian distribution on radial line. The optimized superficial velocity was 2.3 m/s. No bubbles were found in the bed due to swirling motion. Fall back of particles into the plenum chamber was a major drawback of the setup |
| **Kumar and Murthy 2010 [7]** | Swirled fluidized bed | The inlet diameter, number of inlets, settled bed height, diameter of column, properties of bed material | A swirl flow in bed material was achieved by the tangential flow of air via multiple fluid inlets, located at the base of bed column. The minimum swirl velocities were measured about 1.2–1.3 time the Um of conventional fluidized beds. The pressure drop across the bed decreased due to larger opening areas between the blades. |

| | | | |
|---|---|---|---|
| **Kumar , 2011 [90]** | Inclined blades in a single row, (ii) perforatedplate with inclined holes and (iii) inclined blades inthree rows. | weights of the bed material. Bed height, different distributor, superficial velocity | Perforated plate with inclined hole type distributor had very high pressure drop compared to the other two distributors. Thus, it is concluded that the inclined-blade three-row blade type distributor is superior to both inclined-blade single-row type and the perforated plate |
| **Batcha and Hafiz, 2011 [15]** | Annular distributor | Number of blades, blade angle, bed velocity, pressure drop | An annular assembly of 30 blades with inclination angle of 10◦ was found as an optimum configuration. Variations in pressure drop were nominal. |
| **Bakhurji, 2018 (90, 91)** | inclined hole distributors | Different orifice inclinations (30◦, 45◦, and 90◦), bed depth, velocity | Bed pressure drop increased with the inclined-hole distributors and with static bed height, in a shallow bed, the inclined-hole distributor led to less expansion compared with that of the 90◦-hole distributor. The minimum fluidization velocity was found to change with static bed height for the inclined-hole distributors and was also higher for steeper angles. |
| **Al-Hafiz Mohd Naw, 2013 [15]** | Annular distributor | Plenum Chamber Depth, number of inlets | It can be concluded that number of inlets has stronger influence on velocity distribution and distributor pressure drop in comparison to plenum chamber depth. |
| **Halim et al 2020 [90]** | perforated distributor, followed by a 45° swirling distributor, and 67° swirling distributor | Moisture content in 3 different distributors | From the three types of distributors tested, it was found that 67° swirling distributor has the best drying performance, where it managed to reduce the moisture content of raw pot-pollen sample. drying rate can be improved by using swirling distributor in the fluidized bed dryer |

### 2.6.2 Swirling Technology vs Rotating Fluidised bed

The contrast between rotating fluidized beds in a static geometry and swirling fluidized bed technology is an important point to consider when discussing fluidized bed systems. Both technologies have their unique features and advantages, and a comparison can help highlight their differences. Both technologies are used for gas-solid mixing and fluidization, but they differ in their approach and the benefits they offer.

The contrast between rotating fluidized beds in a static geometry and TORBED (or toroidal fluidized bed) technology can now be discussed. Distributor plates in rotating fluidized beds have multiple inlet slots through which fluidization gas is injected tangentially. This results in a rotating gas flow (a "tornado") that suspends the particles, known as the "tornado effect". TORBEDs fluidize rotating particle beds by forcing fluidization gas to enter via the distributor plate into the fluidization chamber (15, 92). The gas-solid drag force acts vertically upward to balance gravity. Since the TORBED does not have radial fluidization of the particles in the centrifugal field or the centrifugal force is not used to balance the radial gas-solid drag force, the TORBED is not a true rotating fluidized bed.

Here are the key differences between these two technologies: rotating fluidized beds are characterized by a rotating vessel or drum in which solid particles are suspended and fluidized by the rotation of the vessel. The rotational motion imparts a centrifugal force on the particles, which can promote mixing and segregation. The vessel housing the rotating fluidized bed remains stationary, and it's the bed itself that rotates. This means that the geometry of the vessel is typically static. Rotating fluidized beds are often used in applications that require controlled segregation of particles based on size or density, as the centrifugal force can lead to stratification [16].

Rotary packed bed systems may not be as suitable for uniform mixing and gas-solid contact, making them less suitable for applications where thorough mixing or heat transfer is essential. It is important to mention the possibility of mechanical failure caused by bed particles getting stuck between the rotating distributor and static support. Crushed particles may block the distributor's rotational motion. In addition, this concept requires a high amount of power for the distributor to rotate and requires high maintenance.

Whereas, the distinguishing feature of the TORBED technology is the toroidal or doughnut-shaped bed. The bed is designed to promote efficient gas-solid mixing and fluidization. TORBED technology often utilizes a spiral distributor to create tangential and swirl motion within the bed. This motion enhances gas-solid mixing and heat transfer. Additionally, the design of the TORBED bed is conducive to uniform mixing and heat transfer, making it suitable for a wide range of applications where uniformity is crucial. Also, TORBED technology can operate at a wide range of temperatures, including very high temperatures (up to 1,600°C or more) (8, 15), making it versatile for various industrial processes. The last but not least,

TORBED technology is adaptable to handling different shapes and sizes of feed solids, including fine particles and sludges [92].

### 2.6.3 TORBED Technology Design

In 2020 a miniature TORBED was developed by the Process Intensification Group at Newcastle University to investigate the hydrodynamic characteristics of this technique. A miniature version [68] presents the opportunity to reduce the cost and amount of sorbent needed for materials screening and development, where the resulting data could be used to inform larger scale designs and predict feasibility according to the existing industrial infrastructure.

TORBED technology categorized in 3 different designs: 'TORBED Compact Bed reactors ('CBR')', TORBED Expanded Bed reactors ('EBR') and TORBED Transport Bed reactors ('TBR'). In the CBR, jets of process gas suspend the layer of moving particles to be processed. Jets are formed by passing a process gas stream through slots between stationary angled "blades". The high velocity energy generated as the process gas passes through these slots dissipates on a shallow bed of particles at the base. As the high velocity jets impact the bed's base, a highly turbulent area is created, imparting both vertical lift and horizontal motion. (See Fig. 2.12)

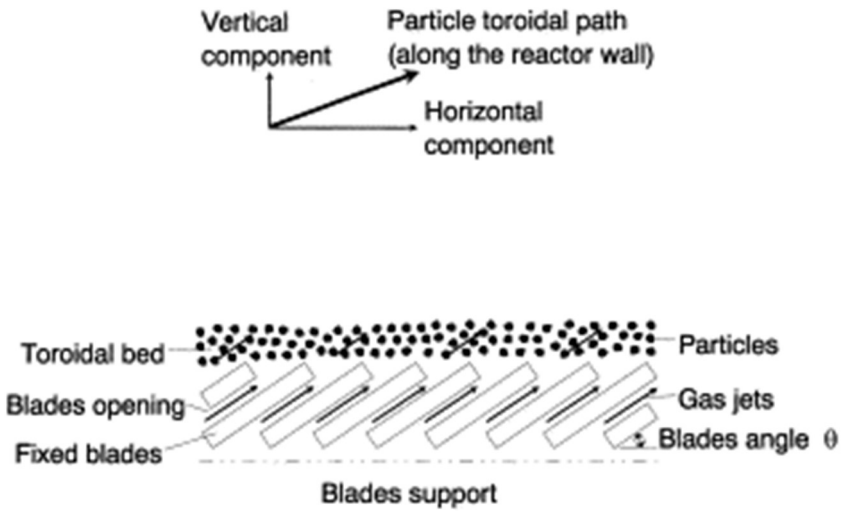


*Figure 2.12 Principle of particle movement in a toroidal fluidized bed reactor [68]*

In this type of reactor, the bed mass can be supported either by a large mass flow of process gas at low velocity or by a smaller mass flow of process gas at higher velocity. This flexibility in choosing the mass flow rates of the process gas allows for optimization of the reactor's operation for different industrial processes and applications. The Compact TORBED reactor

provides the ability to control the mass flow of process gas to support the bed of material. This control can be tailored to the specific requirements of the process, such as the desired level of fluidization and mixing. The flexibility to choose between a large mass flow at low velocity and a smaller mass flow at higher velocity means that the reactor can be optimized for different process conditions. For instance, it can be adjusted to maximize mixing, heat transfer, or other parameters that are essential for a particular application. The annular shape of the reactor creates a circulation pattern described as a "Toroidal BED" (TORBED) circulation pattern above the blades. This pattern likely involves a swirling motion within the reactor, which is advantageous for promoting mixing and improving contact between the gas and solid particles. The motion and circulation pattern generated by the Compact TORBED reactor have led to the creation of the "TORBED Process Reactor" trademark. This indicates that the TORBED technology is a proprietary and innovative approach to fluidized bed technology [16].

### 2.6.4 Distributors Design

The efficiency and performance of TORBED reactor is highly related to distributor design so it is the most essential part of the reactor and several studies had been conducted to modify design of distributors and reactor bed hydrodynamic. Various configurations are available exhibiting different bed geometries, center bodies, fractional open areas, gas flow rates, *etc.*

Other swirling modifications to fluidized beds have also been considered by various researchers to overcome conventional fluidized bed problems, achieve better contact between gas and solid phases such that the transfer rates are improved and purposed a generating swirl flow in a bed of solids.

Shukrullah et al. [18] designed a mesh-coupled annular distributor for producing swirling motion in the bed as shown in figure 2.13. The proposed hybrid design can effectively minimize the required pressure drop for uniform fluidization of materials. This design stops the fine particles from falling through the gaps between the blades without increasing the pressure drop.

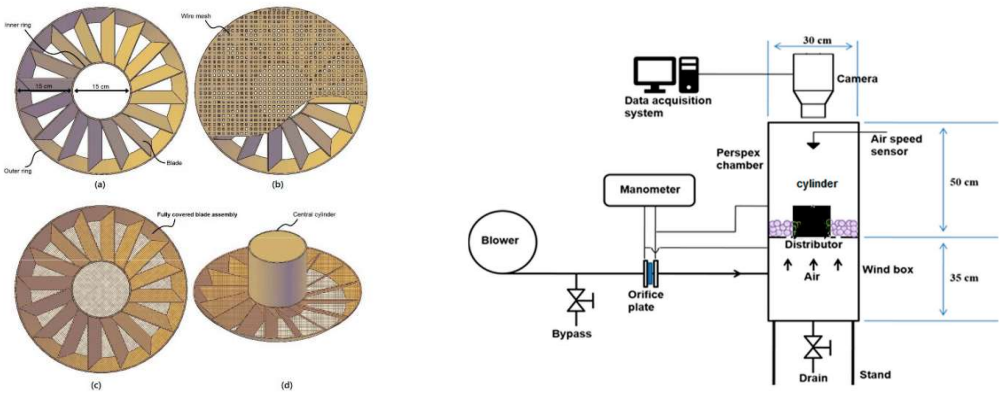


*Figure 2.13 mesh-coupled annular distributor [18]*

Muhammad Lutfi [93] investigated the effect of spiral blade distributor with variation of pitch length and blade inclination of angle on performance of SFB as shown in figure 2.14. They found that with increasing the pitch length and inclination angle, the velocity distribution also increased. This current design promoted vigorous mixing, but the pressure drop for this type was high so the cost of energy consumption will increase.

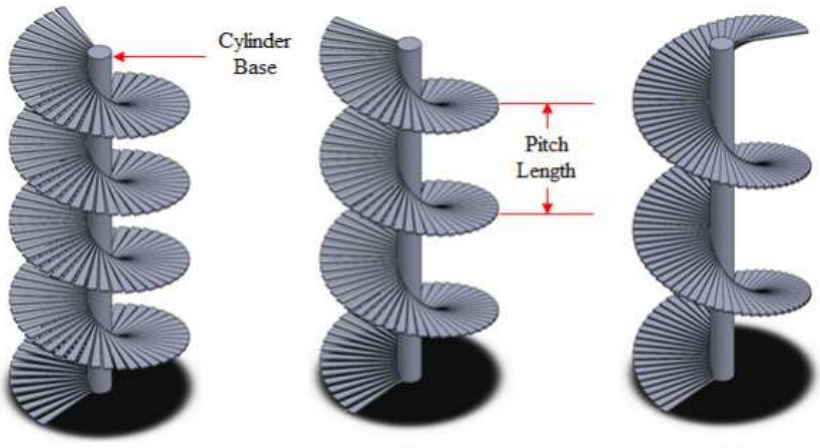


*Figure 2.14 schematic of Spiral Distributor with different inclination angle [93]*

Tawfik [87] designed an annular distributor with various sample inlets for investigating the effect of number of blades, velocity, bed height, plenum on heat transfer and bed hydrodynamic. Utilization of central bodies either conical or cylindrical shapes resulted in a negative effect due to increasing the distributor and bed pressure drops and decreasing the heat transfer coefficient as shown in figure 2.15. According to this study, using a higher number of blades allowed for a reduction in the fractional open area of the blades that meant less momentum was transferred to the bed, which resultantly decreased the bed pressure drop and

increased heat transfer coefficient (HTC). Also, they showed that using plenum resulted in reducing pressure drop and HTC.

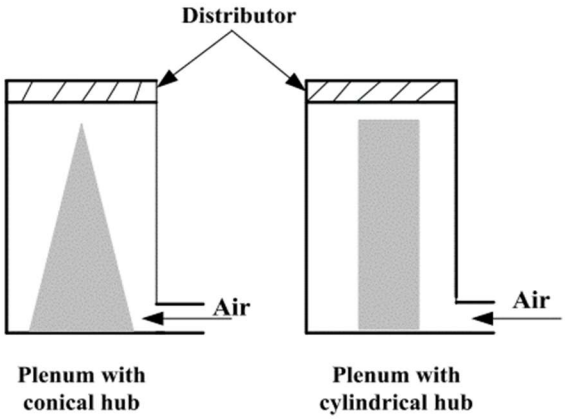


*Figure 2.15 plenum design with Conical and cylindrical shape [87]*

McDonough [94] studied the effects of bed loading, gas volumetric flow rate, gas temperature and gas humidity on flow regime with an annular distributor in 3D-printing a miniaturised TORBED (figure 2.16). They indicated that humidity and air temperature had minimal influence over the flow patterns. They also recommended higher bed loadings to maximize the potential adsorption capacity and found that a higher gas volumetric flow rate produced desirable uniform packing behavior. Authors used the stereolithography printing technique to fabricate a toroidal fluidised bed(TORBED) at the smallest scale ever achieved (50 mm diameter with 10 mm annular width) . In toroidal fluidisation, most of the kinetic energy of the fluidising gas is used to induce swirling of the particle bed meaning higher gas velocities can be used without entrainment.

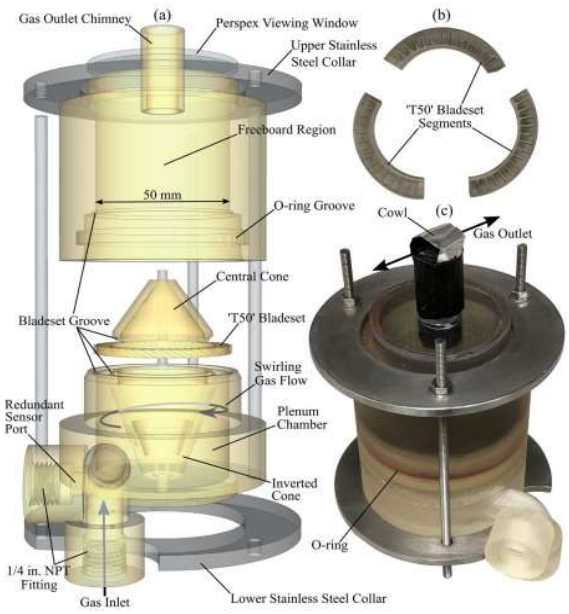


*Figure 2.16. 3-D printed TORBED Reactor[94]*

Bakhurji [91] tested inclined-hole distributor with various orifice inclinations, bed depth and velocity. They found that using the inclined-hole distributors caused bed pressure drops to increase. Investigation of bed expansion showed that, in a shallow bed, the inclined-hole distributor led to less expansion. However, in a deep bed, the orifice angle had negligible influence on bed expansion.

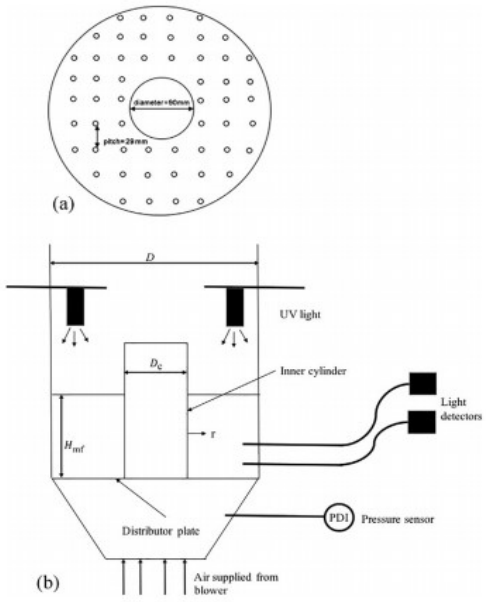


*Figure 2.17 Swirling Reactor with Inclined Hole Distributor [89]*

L A Halim et al [96] compared the effect of moisture content in 3 different distributors: a perforated distributor, and swirling annular distributors with two different angles of 45° and 67° swirling angles. It was found that the 67° swirling distributor had the highest efficiency in terms of particle drying. They stated that for heat sensitive food material such as stingless bee pot-pollen, drying rate can be improved by using swirling distributor in the fluidized bed dryer.

Kumar and Murthy [97] tested a Swirled fluidized bed via an annular distributor with multiple fluid inlets. The pressure drops of bed decreased due to larger opening areas between the blades. Ojeleye [98] used an annular distributor fabricated by 3D-printing. They showed that swirling motion has a significant effect on particle radial velocities.

### 2.6.5 TORBED and Carbon Capture

The efficiency of carbon dioxide ($CO_2$) capture processes is greatly influenced by the choice of the contacting system, which is responsible for facilitating the interaction between the sorbent and the $CO_2$-containing gas. This interaction impacts several critical factors, including process efficiency, the physical space required (footprint), and the overall cost of the capture process. It is essential to closely align material development with the selected reactor configuration and the chosen regeneration mode. Various types of reactors have been employed for adsorption-based $CO_2$capture, each with its own advantages and characteristics[16].

TORBED technology's capabilities in enhancing mixing and heat transfer make it a valuable tool for improving the efficiency of carbon capture processes. By optimizing the gas-solid contact and offering precise temperature control, TORBED technology can contribute to the reduction of $CO_2$ emissions from various industrial sources, aligning with efforts to combat climate change and reduce the environmental impact of industrial processes. In power plants and industrial processes, one of the most common methods of carbon capture is post-combustion capture, which involves capturing carbon dioxide ($CO_2$) from flue gases after combustion. In post-combustion carbon capture, solid sorbents are often used to capture $CO_2$ from flue gases. TORBED reactors can be designed to efficiently contact these sorbents with flue gases, leading to effective $CO_2$capture. After capturing $CO_2$, the sorbents need to be regenerated for the release of $CO_2$ and reuse. TORBED technology's ability to provide efficient heat transfer can be utilized to enhance the sorbent regeneration process. Furthermore, TORBED reactors can be tailored to meet specific requirements and industrial conditions. They

can be scaled up or down to accommodate various plant sizes and process volumes, making them adaptable to different carbon capture applications.

TORBED technology has been the subject of various research studies and applications across a range of industrial processes like Chemical Reactions and Catalysis, Materials Processing and Drying, Pharmaceuticals and Food Processing and so on. This study is the first time that TORBED technology has been used in carbon capture in a miniature version as part of process intensification. The total cost of implementing adsorptive $CO_2$ capture is influenced by both the system size and the operating cost. These factors are interrelated, and they play a critical role in determining the overall economic feasibility of a $CO_2$ capture system. In summary, the cost-effectiveness of implementing adsorptive $CO_2$ capture depends on finding a balance between system size and operating costs.

The size of the adsorber is determined based on the cycle time and the desired $CO_2$ capture duty, which is in turn influenced by the choice of sorbent material and the design of the adsorber. Effective optimization of these factors is essential for achieving efficient and economically viable $CO_2$ capture systems.

MacDowell et al. [99] reviewed the carbon capture technology and they clearly stated that the challenges associated with carbon capture technology for industrial adsorption in the context of carbon capture are critical considerations for the development and implementation of effective $CO_2$ capture systems. One of the primary challenges is the decrease in cyclic capacity over time. This decline in capacity can be caused by several factors, including sintering (particle coalescence), attrition (particle breakage), and chemical deactivation of the sorbent material. These issues can reduce the sorbent's ability to capture $CO_2$ effectively, which impacts the efficiency of the capture process. Furthermore, the operating cost of a carbon capture system is significantly affected by the energy required for the regeneration process. Effective regeneration is essential for releasing captured $CO_2$ from the sorbent and preparing it for the next cycle. The energy demand for regeneration is a key factor in determining the overall operational cost of the capture system. Addressing these challenges is crucial for developing economically viable and efficient carbon capture systems.

An intensified adsorber system should be designed to be easily retrofitted into existing industrial processes without requiring substantial alterations. Retrofitting should be a practical and cost-effective option for industries seeking to reduce $CO_2$ emissions. A number of laboratory scale applications of swirling fluidized beds have also been reported by Kuprianov

et al. [13], Zhu and Lee [100], McQueen [101], Sundaram and Sudhakar [102], Aworinde et al. [14] and McDonough et al. [22]. The characteristics of swirling fluidized bed reactors, as observed in industrial case studies compiled by Groszek and Laughlin [8], offer several advantages that are highly relevant to carbon capture applications. These characteristics contribute to the efficiency and effectiveness of carbon capture processes:

- Low specific energy consumption means they are energy-efficient and can help reduce the energy cost of carbon capture processes.
- Precise temperature control minimizes energy losses, which is essential for optimizing carbon capture reactions.
- The reactors can operate isothermally, maintaining a constant temperature throughout the process. This is advantageous for ensuring consistent and efficient $CO_2$ capture.
- Rapid heat and mass transfer rates enable efficient capture and release of $CO_2$ from sorbent materials.
- Their compact design is advantageous where space constraints may exist.
- Low pressure drop reduces the energy required for gas flow and enhances process efficiency.
- The reactors are effective at preventing particle elutriation, meaning that solid particles are well-contained and do not escape into the gas stream.
- They can handle a wide range of particle sizes, making them adaptable to various feed stream requirements.
- The ability to independently control gas and solid residence time allows for flexibility in the capture and release of $CO_2$ and other gases.
- Maintaining uniform particle residence time is essential for consistent and efficient carbon capture, as it ensures that all particles have an equal opportunity to interact with the gas phase.

These characteristics make swirling fluidized bed reactors, such as those based on TORBED technology, well-suited for carbon capture applications. They offer a combination of energy efficiency, control, and adaptability, which is crucial in optimizing the capture of $CO_2$ from industrial processes while minimizing energy consumption and overall costs.

### 2.6.6 TORBED and Desorption Technology

Temperature Swing Adsorption is a typical way for removal of trace components from a gas mixture like flue gas. In this process adsorbate that has to be removed, create a strong bound

with molecules of adsorbent [27]. For regeneration process, a hot gas is used to heat the sorbent for releasing the adsorbate. Several researchers showed that regeneration conditions and heating method can negatively impact the solid sorbent. Thermal conduction, hot gas purging, and steam heating outside of the adsorption reactor are usual methods used to regenerate sorbents. These methods, which remove saturated sorbent from the reactor and place it in another module for regeneration (named as an extractive methods), have some disadvantages, such as long desorption periods, high energy consumption, potential changes to the adsorbent's physical and chemical properties, and heat loss (to the surrounding equipment, gas stream and cooled saturated sorbent).

Gray et al. [10] investigated the performance of immobilized tertiary amine solid sorbents for adsorption/desorption of $CO_2$. The solid sorbents prepared in this study exhibited acceptable $CO_2$ capture capacities of 3.0 mol $CO_2$/kg sorbent at 298 K; however, at the critical operational temperature of 338 K, the capacity was reduced to 2.3 mol/kg sorbent. The TSA method regenerated sorbents with acceptable stability over the adsorption/desorption temperature range of 298–360 K.

The pressure swing adsorption (PSA) process involves preferentially adsorbing the gas ($CO_2$) on a solid sorbent at high pressure [10]. Gas is desorbed from porous sorbent when pressure is decreased, and the sorbent can be reused for subsequent adsorption [5]. It is critical to develop a regenerable sorbents that have high selectivity for $CO_2$ and high adsorption capacity for $CO_2$ for the success of the PSA process. During the regeneration step, the pressure difference required for PSA can either be achieved by compressing the feed or using a vacuum. For carbon capture processes, a vacuum during regeneration is usually more suitable than compression of feed because of the large volumes that need to be treated and the expensive and energy-consuming compression equipment. Vacuum swing adsorption (VSA) is the process of applying a vacuum for regeneration. Wang et al. [52] studied two vacuum swing adsorption (VSA) units, using 13XAPG as the adsorbent. The first unit was designed for $CO_2$ recovery and the second one was used for purification of the $CO_2$ gas. One VPSA unit was unable to achieve both high purity and high recovery of $CO_2$ from flue gases at atmospheric pressure. In order to further concentrate $CO_2$ stream from one (VSA) unit to above 95% purity, a one-column VPSA experiment was conducted.

Krishnamurthy et al. [103] examined a pilot plant study based on a basic 4-step (VSA) process with using zeolite 13X as a sorbent. This pilot plant concentrated $CO_2$ to 95.9 % and recovered

86.4 %. Four beds were used in the process to improve the performance of the process. As a result of 4 cycles, 94.8 % purity and 89.7 % recovery were achieved. In the literature review, there are several studies that show that PSA/VSA technology is not cost effective in the industrial scale due to the energy consumption which is mainly the power consumption of the vacuum pump, and the compressor was found so huge. Also, an evacuation pressure like 50 mbar is not technical feasible at industrial scale.

Microwave regeneration is an interesting approach. One of the advantages of the TORBED observed in our study was the elimination of any mass transfer zone, the entire bed simultaneously adsorbs $CO_2$ and also compatibility of the TORBED with different technology like microwave. Torftech and the University of Nottingham, have developed a new system which is the combination of TORBED technology and microwave technology to intensify the drying process and can be deployed across the process applications, including in regeneration and manufacture of catalysts. The 'TORWAVE' reactor [104] exploits the rapid and uniform heating of microwaves with the good mixing of the TORBED to enable rapid particle processing. Thus, applying microwaves for regeneration in small-scale beds means one could theoretically study the desorption kinetics in addition to the cyclability. Microwave technology enables fast, uniform heating throughout the entire bed as well as selective heating of one material within another. Though there are two disadvantages to this approach. Material's microwave transparency, such as high temperature 3D-printing resin is unknown, so probably alternative manufacturing approaches should be adapted which would restrict design freedom. Additionally, the microwave distributor would need to be engineered to ensure homogeneous irradiation of the shallow bed in order to avoid hot spots.

Liu et al. [105] examined the use of microwave assisted vacuum as a means of rapidly regenerating sorbents in wet feed gases. Thermal energy applied to the adsorbent surface can liberate water and $CO_2$. They used a small transparent adsorption column of 13X zeolite pre-saturated with a 12 % $CO_2$ in $N_2$ gas mixture for the small-scale processing of flue gas. The result shows that a microwave assisted vacuum could improve $CO_2$ desorption and column regeneration when using wet feed gas due to the desorption of water (a strong microwave absorber). As a result of adding microwave radiation to the desorption process, $CO_2$ desorption was improved, and the integrated $CO_2$ purity was improved from 60% to 80%.

McGurk et al. [106] present the feasibility of regenerating the spent amine solution with microwave irradiation. Their results show that microwaves can regenerate spent aqueous

monoethanolamine solutions quickly and at low temperatures (70–90 °C), potentially reducing overall process costs. There is a consistent and favourable cyclic stability across multiple microwave regeneration cycles.

Whichever regeneration technology is used, it should allow for complete recovery of adsorption capacity, require low energy consumption and short regeneration time, should not negatively affect adsorbate properties, nor cause changes to the adsorbent. In comparison between aforementioned methods, a combination of conductive heating for regenerating and TORBED technology is probably the simplest and most practical method to implement in a small-scale experiment platform because since the inlet gas temperature can be easily controlled via inline gas heater. Since the capacity of most adsorbents decreases at higher temperatures, cyclability of the adsorption kinetics could be studied in a small-scale TORBED by rapidly switching between 40 °C and up to 238 °C (based on the heat deflection point of the printed high temperature polymer). However, even with the superior heat transfer rates observed in the TORBED, this approach would lead to a significant deadtime in the experiments due to the high thermal inertia of the polymer structure; the majority of the experiment would consist of waiting for the bed to heat or cool. This would also prevent study of the desorption kinetics.

## 2.7 Summary

Chapter 2 provides a comprehensive review of carbon capture technologies and their importance in mitigating climate change. It explores key strategies such as post-combustion, pre-combustion, and oxyfuel combustion, with a focus on the challenges and opportunities in post-combustion carbon capture. Various approaches, including chemical absorption, membrane separation, cryogenic separation, and adsorption, are evaluated, highlighting adsorption technology as a sustainable solution due to its efficiency, scalability, and environmental benefits. The chapter emphasizes the critical role of sorbent development, reactor technologies, and sorbent regeneration in optimizing carbon capture processes. Innovative fluidized bed reactors, especially swirling fluidized beds like the TORBED reactor, are identified as transformative due to their enhanced gas-solid interactions, superior heat and mass transfer, and ability to handle diverse sorbent materials. By addressing gaps in reactor performance and sorbent efficiency, this literature review lays the groundwork for advancing adsorption-based carbon capture systems.

# 3. Methodology

## 3.1 Chapter Overview

This chapter provides a comprehensive description on the process of designing and fabricating the experimental setup, focusing on the TORBED design and fabrication, sorbent properties, hydrodynamic study, and the methodology employed in the adsorption and desorption experiments. The initial phase involved 3D modelling of the Mini TORBED reactor design using Google Sketchup software, specifically tailored for 3D printing. It is pertinent to note that the supervisory team had previously developed a miniature version of the TORBED reactor, forming the basis for further enhancements [68]. To ascertain the optimal flow conditions and particle size for the study, a hydrodynamic sorption investigation was conducted using three distinct sorbent types. This critical step aimed to identify the most suitable sorbent for subsequent monitoring in the adsorption and desorption studies. For this purpose, different experimental rigs were designed to accommodate the diverse requirements of hydrodynamic, adsorption, and desorption studies.

Furthermore, the chapter delves into the methodology employed to achieve the overarching objectives of the study. It sheds light on the instrumentation and technology harnessed to measure various parameters throughout the investigation. The detailed discussion encapsulates the iterative process of design considerations, reflecting the commitment to optimizing the experimental setup for precise and insightful exploration of adsorption and desorption phenomena.

## 3.2 Sorbent specification

To assess the viability of the mini-TORBED platform for expeditious adsorbent screening, three different commercial sorbents underwent testing within a TORBED reactor. Consequently, a hydrodynamic study was initiated to discern the optimal sorbent particles suitable for TORBED reactor technology, accounting for considerations such as size, type, and flow regime. This hydrodynamic investigation placed specific emphasis on particles categorized into Geldart groups A, C, and D. These classifications are rooted in the fluidization behaviour of particles, with each group exhibiting distinctive characteristics related to their fluidization properties.

Geldart Group C particles are characterized as fine, cohesive powders, Geldart Group A particles display a wide range of particle sizes, and Geldart Group D particles are identified by larger, non-cohesive particles. Through the careful selection of particles representative of Geldart groups A, C, and D, a comparative analysis of their fluidization behaviour within a TORBED reactor can be conducted. This approach enables the systematic evaluation of particle performance, facilitating the identification of the most promising candidates for subsequent in-depth investigations into adsorption and desorption behaviours. Additionally, this methodology affords valuable insights into the nuanced influence of diverse particle types and sizes on the hydrodynamics of the TORBED system.

The first group, representing Geldart group A, consists of commercial branched polyethyleneimine (BPEI) provided by RTI International (image given in Figure 3.2a). This sorbent comprises a blend of branched polyethyleneimine (BPEI), ethylenediamine, and silica gel. Notably, it manifests as a spherical white powder, with an average particle size of 75 μm and a bulk particle density of 1.4 g/cm³ [16].

The second group, embodying Geldart group C attributes, is represented by commercial hydrotalcite powder (PURAL MG70 supplied by Sasol) [65], as shown in Figure 3.2b. This sorbent, characterized as fine and cohesive, adds another dimension to the sorbent spectrum under investigation. As supplied, the powder looked like talc and had a density of 1.6 g/cm3 with sizes of <25 μm (45.9%), <45 μm (76.4%), <90 μm (99.6%). Due to the raw powder's 'stickiness' and cohesion, a sieve method was used to improve fluidization quality. Powder was sieved using a basic sieve shaker (Retsch Gmbh, MESH S-STEEL) using several tray filters (sizes of 32, 45, 53, 63 and 75 mm). Consequently, powder with particle diameters ranging from 45 to 63 microns was extracted. This size of Geldart C material has been successfully fluidized in 3D-printed MFBRs in the past [65].

Finally, the third group, representing Geldart group D, is constituted by pellets supplied from Casale (shown in Figure 3.2c). This sorbent category is characterized by larger, non-cohesive particles, contributing a unique set of properties to the comparative study. The mean pellet size was Dm = 1.70 ± 0.47 mm. The measured tapped bulk density was 0.58 g/cm3, which placed the particles on the boundary between Geldart D (spouting).

In Figure 3.1, Geldart classification has been shown and these 3 particles regions are shown based on their average particle size and density in below graph.

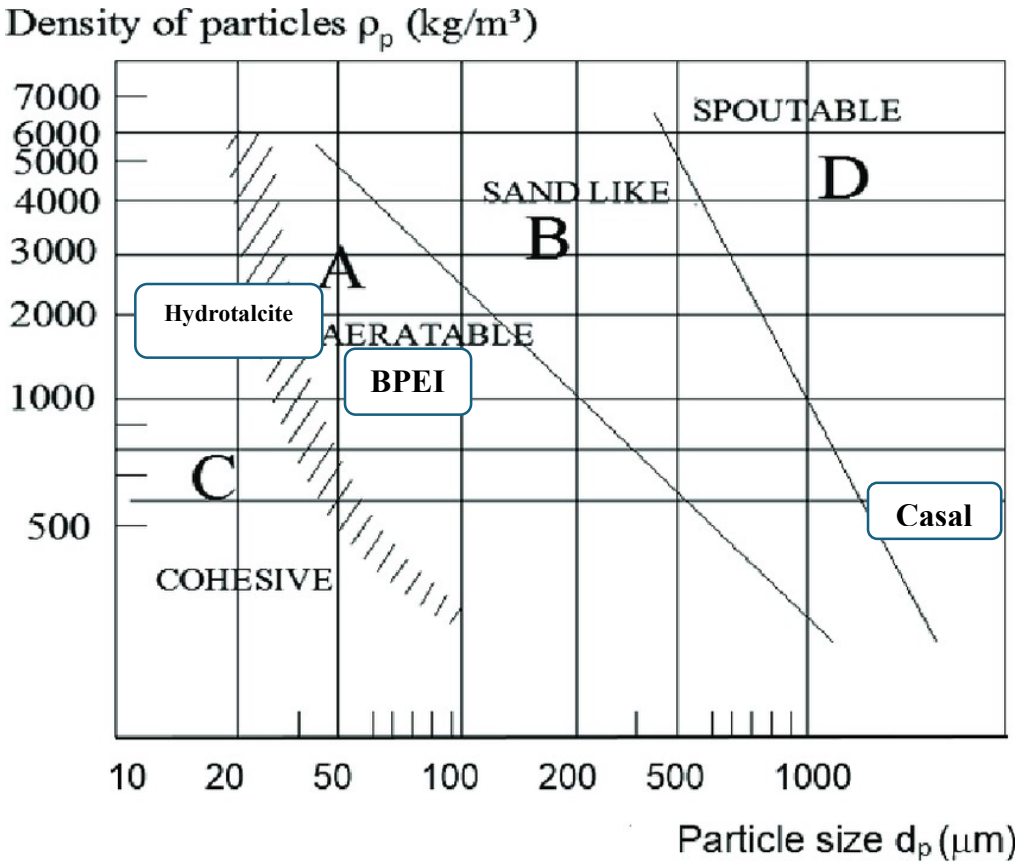


*Figure 3.1. Diagram of the Geldart classification of particles [44]*

Note, information such as heat of adsorption and specific heat capacity are commercially sensitive. By categorizing sorbents into these distinct groups, a methodical exploration of their characteristics can be conducted, setting the stage for a nuanced understanding of their respective roles in the adsorption and desorption processes. It is important to note that while the Geldart classification primarily pertains to fluidization characteristics, the fluidization behaviour of sorbents can significantly influence their performance in adsorption and desorption processes. Therefore, the categorization based on Geldart classification indirectly becomes relevant to the study, as it provides insights into how the fluidization properties of sorbents may impact their behaviour during these key processes. This connection underscores the multifaceted nature of sorbent characterization, where fluidization characteristics intertwine with adsorption and desorption dynamics, contributing to a comprehensive analysis of their behaviour in various applications.

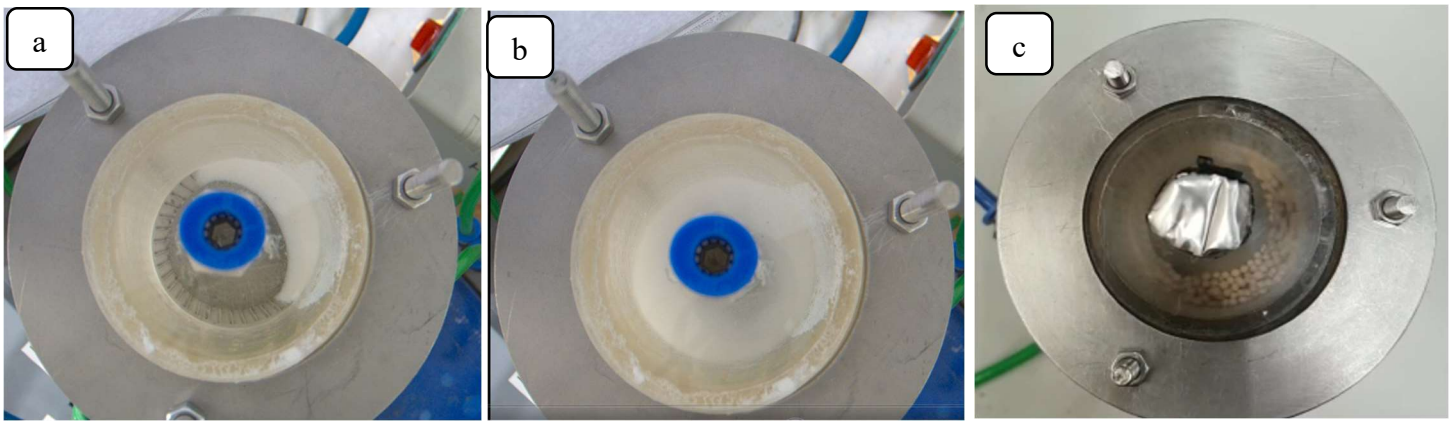


*Figure 3.2, a. Images of different 3 distinct types of particles: branched polyethyleneimine (BPEI), b. Hydrotalcite powder, c. Casale Pellets in TORBED reactor*

### 3.3 TORBED design and additive manufacturing

All experimental procedures were conducted within a mini-scale TORBED reactor with a 50 mm diameter, as originally developed by McDonough et al. [68] and with Torftech license under NDA. The reactor was subsequently modelled and manufactured through the utilization of 3D printing technology. Figure 3.3 & 3.4 provides a visual comparison between the Computer-Aided Design (CAD) representations of the reactor's key components and their corresponding 3D-printed counterparts. The fabrication process involved the use of a Form2 Stereolithography (SLA) printer, employing FormLabs' proprietary High Temperature V2 resin, High Temp Resin has a heat deflection temperature (HDT) of 238 °C @ 0.45 MPa.

Stereolithography (SLA) is a 3D printing technology that involves the layer-by-layer construction of parts through the photopolymerization of a resin [68]. In below, an overview of the technology and materials used in the stereolithography process.

- **UV Laser Details:** Wavelength: 405 nm
- **Laser Spot Size:** 140 µm
- **Laser Power:** 250 mW
- **Resin Composition (FLGPCL02):** Methyl Acrylate Monomer: 55-75% w/w**,** Methyl Acrylate Oligomers: 35-40% w/w**,** Photo-initiator Additives: 10-15% w/w
- **Resin Characteristics:** Translucent & Proprietary formulation

The use of a UV laser to selectively cure a resin layer by layer allows for the creation of and detailed 3D printed parts. The composition of the resin, with its mix of monomers, oligomers, and photo-initiators, is crucial for the curing process and the final properties of the printed object. In order to build each layer, a laser scanner scanned through the resin tank quickly according to the shape defined by the corresponding slice through the geometry, followed by the build platform being raised according to the Z-axis resolution specified by the user. In order to develop a prototype model, several details, such as workflow, equipment, and parameters must be followed when using the Form2 SLA 3D printer.

The initial phase of the process commences with the creation of a 3D Computer-Aided Design (CAD) model using Google SketchUp. Subsequently, this CAD model undergoes transformation into a triangular mesh model saved in the .stl file format, a widely used format in the realm of 3D printing. Prior to printing, the model undergoes meshing and slicing, breaking it down into distinct layers. These layers are then converted into tool paths through the utilization of the PreForm software. The printing process is executed via the Form2 Stereolithography (SLA) 3D printer. During this stage, it is imperative to define the resolution settings. The printer allows for a maximum XY resolution of 140 μm and offers Z-axis resolutions spanning 25–100 μm.

An essential consideration in the printing process is the orientation of the model; parts are printed at an approximate angle of 60° from the horizontal in both the X and Y directions. This strategic orientation serves to enhance resin drainage, thereby improving part stability and overall print quality. Post-printing processes comprise several crucial steps. First, the printed parts undergo cleaning in an isopropyl alcohol (IPA) ultrasonic bath (FormWash) to eliminate excess and uncured resin (refer to Figure 3.3b). Subsequently, the parts are dried using compressed air, as depicted in Figure 3.3c. Curing is the next stage, conducted at 60°C for 30–60 minutes in 405 nm UV light using the FormCure apparatus (Figure 3.3d). Finally, Figure 3.3e illustrates the assembled reactor, constructed from six separate printed parts, culminating in the completion of the entire fabrication process.

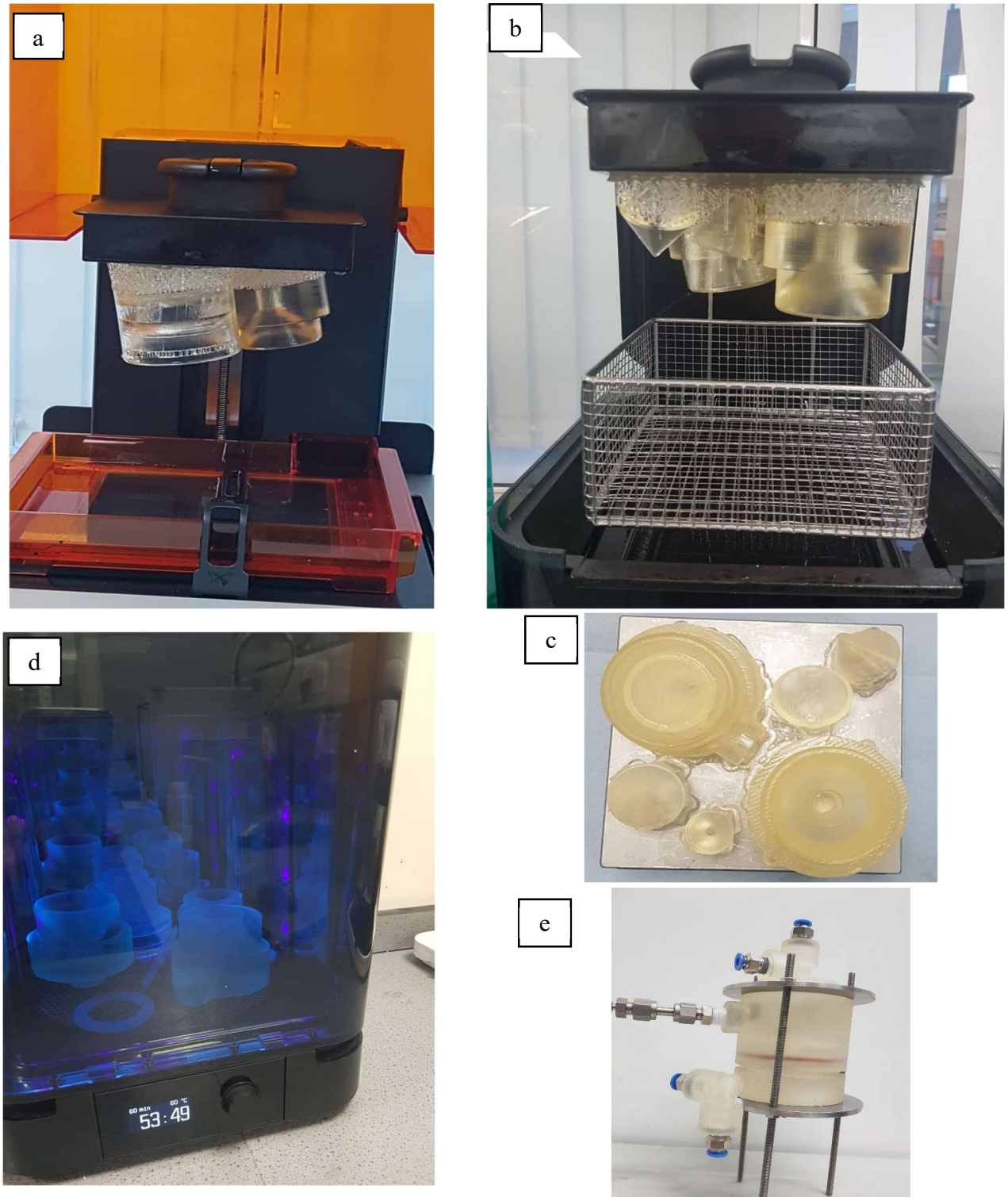


*Figure 3.3 (a) Form2 SLA 3D printer with example of printed parts, (b) which are then washed in ultrasonic bath (FormWash) (c) and dried by compressed air to remove the remaining material, (d) and cured by UV light in (FormCure),(e) Assembled reactor*

The segmentation of the TORBED reactor into discrete components for 3D printing and subsequent assembly represents a prevalent strategy in additive manufacturing, particularly in the context of expansive or complicated structures. This methodological approach affords several advantages, including enhanced manageability in the printing of individual components and the potential to employ distinct materials or settings for specific parts. Breaking down the TORBED reactor into components designed for separate printing and subsequent assembly introduces a level of adaptability, simplifying the manufacturing process and enabling the optimization of each part for printing and post-processing.

Furthermore, this modular approach not only streamlines the transportation of individual components but also provides practical advantages regarding the possibility of material substitutions or adjustments in printing parameters for specific elements. The inherent flexibility in this segmented manufacturing approach extends to the optimization of each component's design and characteristics, thereby enhancing overall efficiency and performance. It is noteworthy to mention that this approach proves particularly beneficial in the printing of TORBED parts, such as the distributor, which consists of fine and delicate components. The segmentation allows for more precise control over the printing process, mitigating challenges associated with complex designs. This adaptability has proven instrumental in overcoming issues of model failure during printing, as adjustments to printer specifications can be made iteratively to achieve a successful and accurate representation of the intended model. Furthermore, the modularity introduced by dividing the TORBED reactor into printable and assembleable components contributes to the ease of maintenance. In the event of specific parts requiring replacement or upgrades, the modular design simplifies the task, offering a streamlined and cost-effective solution. This forward-looking aspect of the approach enhances the reactor's overall lifecycle management, aligning with the principles of sustainability and adaptability in advanced manufacturing practices.

The TORBED reactor featured a plenum chamber (refer to Fig. 3.4d) equipped with an offset inlet connection port and an inverted cone designed to induce swirling in the fluidizing flue gas stream. This swirling stream entered a bladed distributor (Fig. 3.4c), comprising 40 equally spaced slots measuring 0.9 × 10 mm each, angled at approximately 10 degrees. The vertical velocity component of the flue gas facilitated fluidization of the bed, while the horizontal velocity component imparted a swirling motion. This unique design allowed for the utilization of very high gas velocities without entrainment, thereby significantly enhancing heat and mass transfer rates at the base of the bed [22].

Above the distributor, a cone (Fig. 3.4b) was positioned to create an annular flow path for the particle bed. The fluidized bed materials were contained in a 50 mm diameter and 65 mm tall freeboard region (depicted in Fig. 3.4a). The reactor's inlet and outlet were equipped with dual push-fit 1/4 in NPT connections, one for tubing attachment and the other for connecting a pressure transducer to monitor the total pressure drop across the bed.

To prevent gas leakage around the blade set, a piston-type O-ring seal was employed. Utilizing a standard size 228 silicone O-ring (AS 568 A 228) based on the 50 mm diameter of the T50 ring proved effective. A groove in the inner wall of the upper freeboard section accommodated the O-ring, and the joint was lubricated with high-vacuum silicone grease applied to the O-ring. Additionally, two stainless steel collars, secured with three sets of M4 studding, were strategically employed to prevent the TORBED from inadvertently opening under pressure, ensuring the integrity and safety of the system.

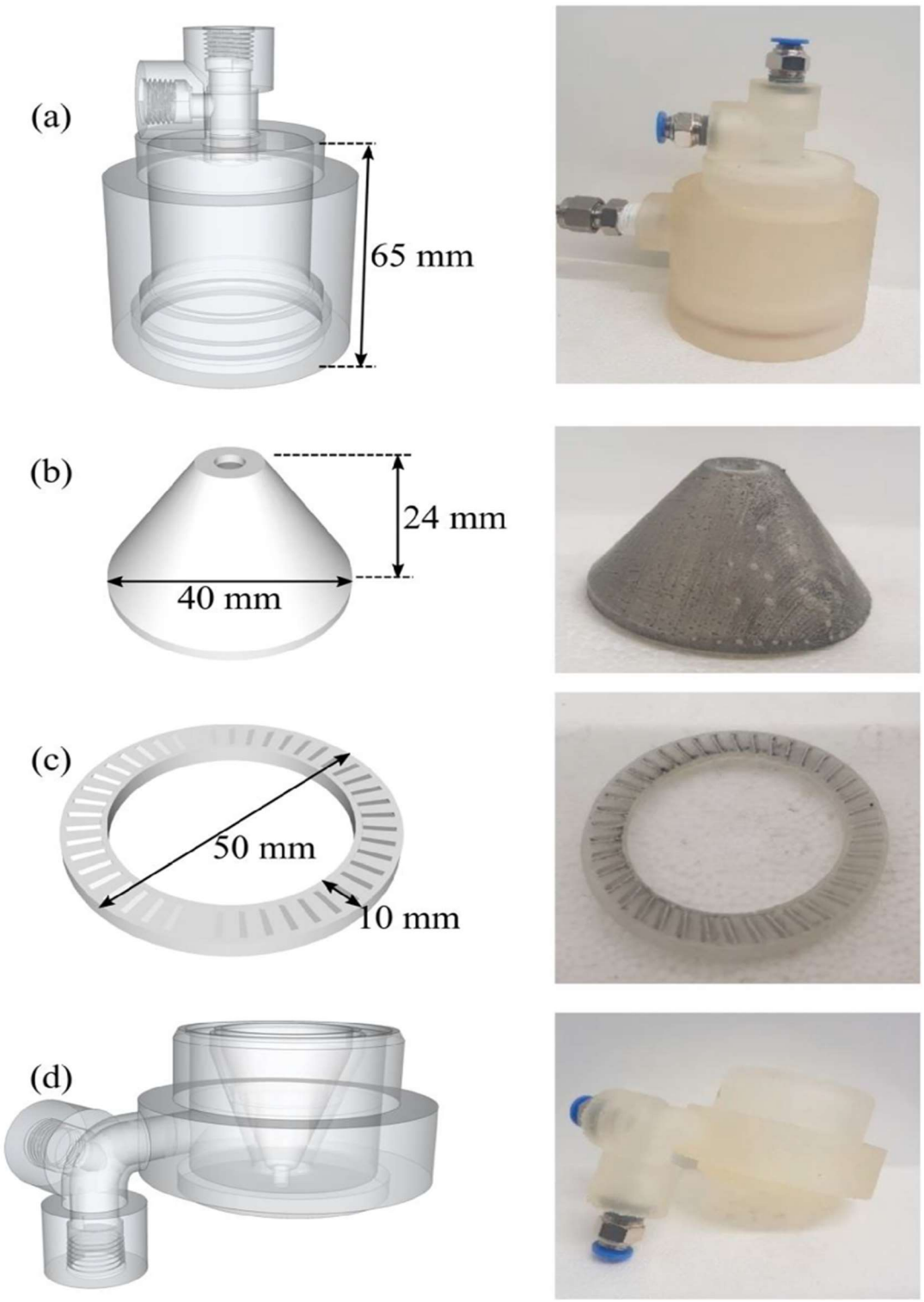


*Figure 3.4. CAD models and corresponding photos of the 3D-printed Mini-TORBED; (a) bed chamber/freeboard region, (b) central cone, (c) distributor, (d) plenum chamber.*

### 3.4 Equipment Flowsheet

Figure 3.5 provides a comprehensive schematic representation of the experiment flowsheet, illustrating the details of the experimental setup. In addition, Figure 3.6 offers a labelled photo of the almost entire experimental arrangement. It is noteworthy that the experimental rig has undergone modifications tailored to the specific objectives of each experiment. In the context of the adsorption experiment, as exemplified in Figure 3.5, an artificial flue gas mixture, ranging from 0% to 20% vol $CO_2$ in $N_2$, was carefully generated. This was achieved by blending pure $CO_2$ (99.8%) and Nitrogen (99.9%) sourced from standard 34 kg and 9.8 m3 cylinders, respectively, both obtained from BOC.

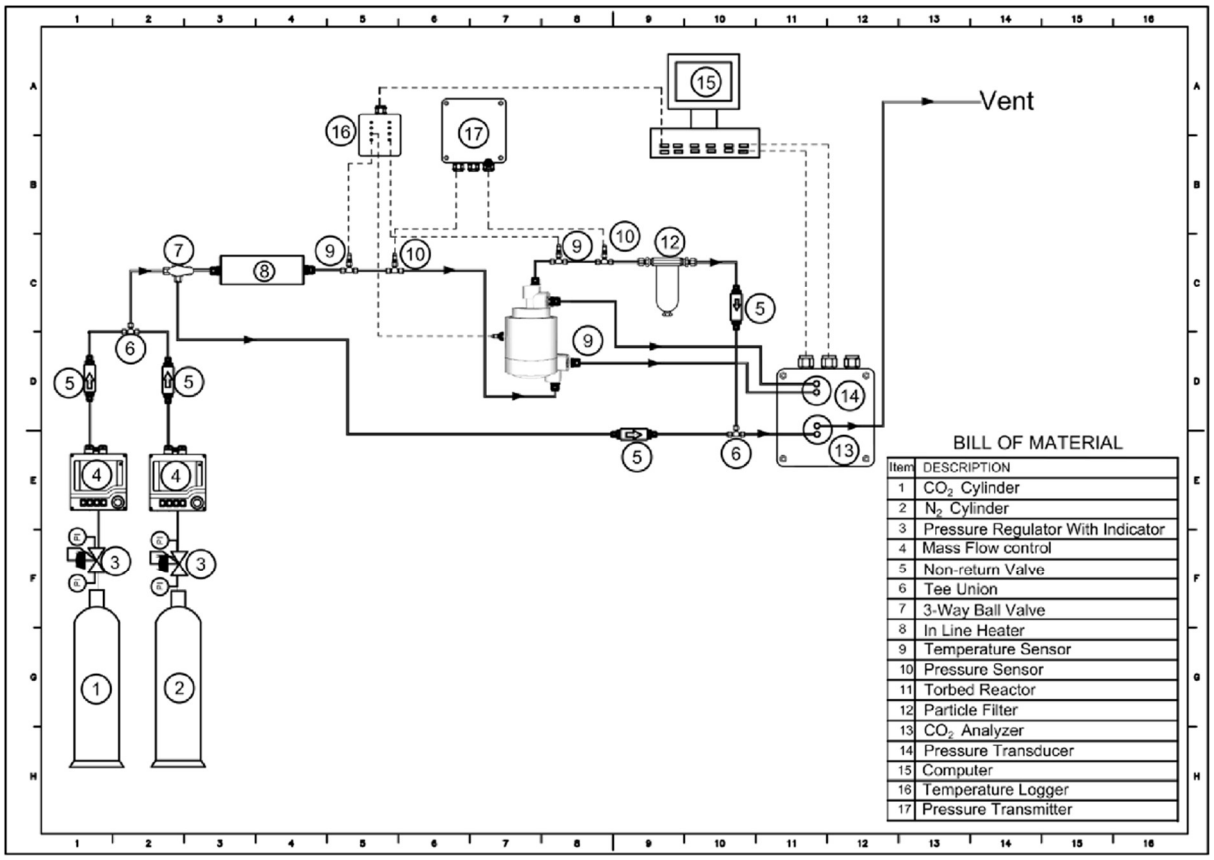


*Figure 3.5. Schematic of CO2 breakthrough for assessing adsorption kinetics.*

To maintain precise control over the pressure within the cylinders, dedicated dual-stage pressure regulators were employed. For $CO_2$, the BOC Series 8500 Carbon Dioxide ($CO_2$) Multi-Stage Regulator was utilized, while the BOC Series 8500 Inert Inline regulator multi-stage 0-4 bar (Nitrogen) was employed for Nitrogen. These regulators featured inlet pressure indicators calibrated up to 250 barg and outlet pressure indicators ranging from 0 to 10 barg, ensuring accurate pressure regulation throughout the experimental procedures.

The systematic control of gas composition and pressure is critical for achieving reproducibility and reliability in the experimental outcomes. In this setup, the control of the volumetric flow of $CO_2$ and Nitrogen was achieved through the utilization of two mass flow controllers (EL-flow Bronkhorst, with a range of 0–100 L/min). The Bronkhorst digital instruments were managed and monitored using two distinct software applications, namely flowPlot and flowView provided by Bronkhorst, allowing for the real-time adjustment of flow rates and servicing requirements. Additionally, a rotameter (Brooks, with a range of 0–100 L/min) was employed for visual observation and measurement of the volumetric flow rate of the mixed gas.

To prevent back-mixing into the cylinders, non-return valves (Swagelok; cracking pressure of 3–50 psi) were integrated into the system. The gas temperature was subsequently controlled within a range of 40˚C to 120˚C using an in-line heater 200W (Omega, AHP-3742). The control thermocouple (RS PRO, Type K) was strategically positioned directly at the reactor inlet for precise temperature regulation. Furthermore, a thermocouple immersed in the freeboard region (refer to Fig. 3.6) continuously monitored the bed temperature, providing insight into the heat of adsorption and desorption processes. To maintain the gas temperature consistently from the heater to the reactor bed, an electrical heated trace (RS PRO, 15W/m, 240V ac, -60 → +200 °C ) with insulation around the ¼’’ tube was employed.

The total pressure drop across the bed was measured using a differential pressure transducer (Sensirion, SDP800, Digital DP sensor (±125 Pa, Accuracy: 0.08 Pa), manifold connection). This transducer was strategically positioned at the inlet and outlet of the reactor, as illustrated in Figure 3.5, enabling the accurate quantification of the pressure drop across the entire bed. These precise control and monitoring mechanisms are integral to ensuring precise experimental conditions and reliable data collection throughout the adsorption processes in the TORBED reactor.

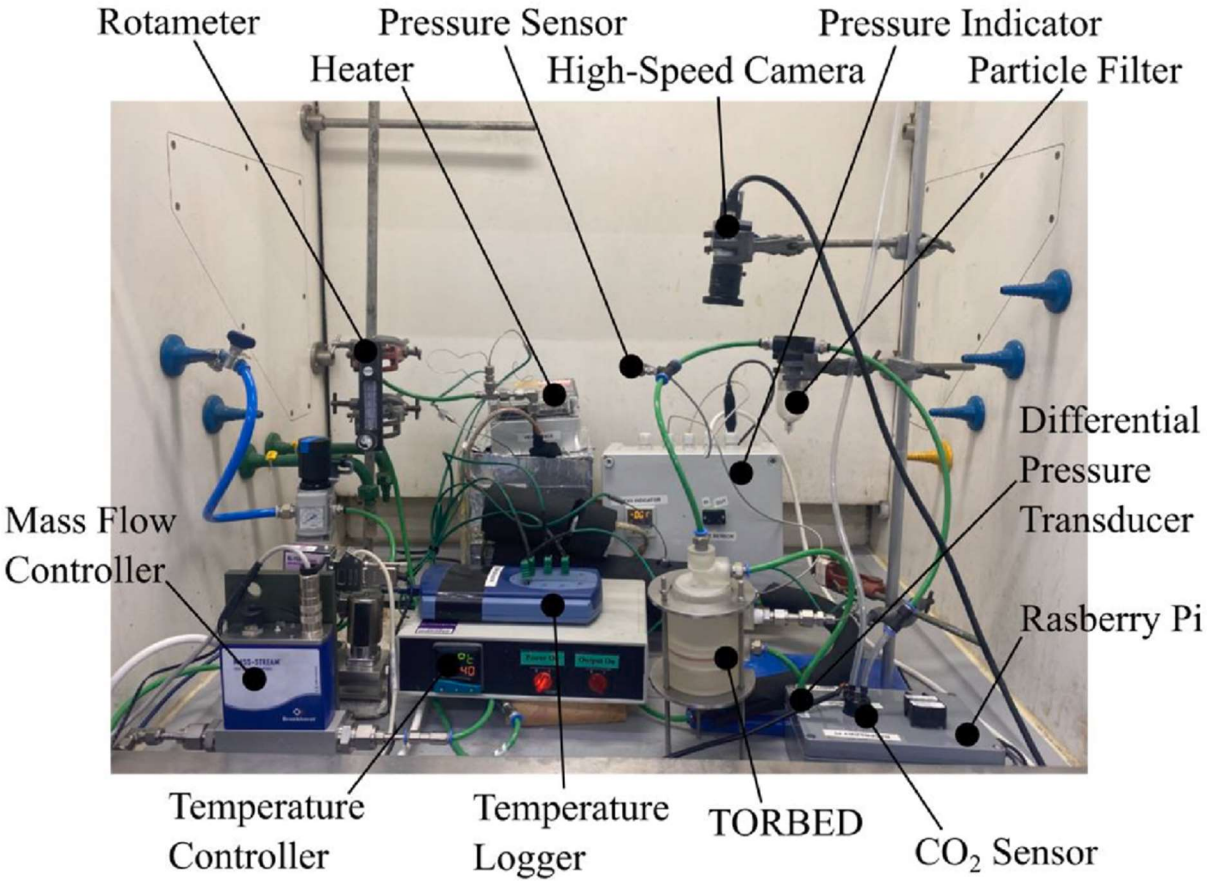


*Figure 3.6. Image of CO2 adsorption kinetics screening rig (note, the TORBED is wrapped in wool insulation during the experiments to improve the temperature stability)*

The analogue signal derived from the pressure transducer was subjected to conversion and digital adjustment, with subsequent monitoring and logging facilitated by a Node-Red program running on a Raspberry Pi-3 module. As depicted in Figure 3.7, the interior outlet of the freeboard was strategically covered with a woven wire mesh (50 µm in size) to prevent the loss of sorbent material from the bed. Furthermore, the outlet from the TORBED passed through a 40 µm universal particle filter (Norgren, F07) before being directed into the gas analyzer (GSS, SprintIR). This gas analyzer effectively recorded concentrations within the range of 0–20,000 ppm with accuracy of ±300 ppm at a 20 Hz sampling frequency.

For a comprehensive understanding of the bed flow regime, a high-speed camera was positioned at top the bed. A prototype of an individual capsule, printed on the roof of the reactor for hydrodynamic purposes, was employed for monitoring. The Perspex viewing window and freeboard were securely bonded using epoxy. High-speed videos capturing the dynamics of the fluidized beds were recorded using a Basler A1440 camera (169 fps, 1.3 MP) equipped with a COSMICAR Television lens (12.5 mm, 1:14).

The entire process was efficiently monitored through the Pylon Viewer software (Basler), providing valuable insights into the fluidized bed behaviour during the experiments.

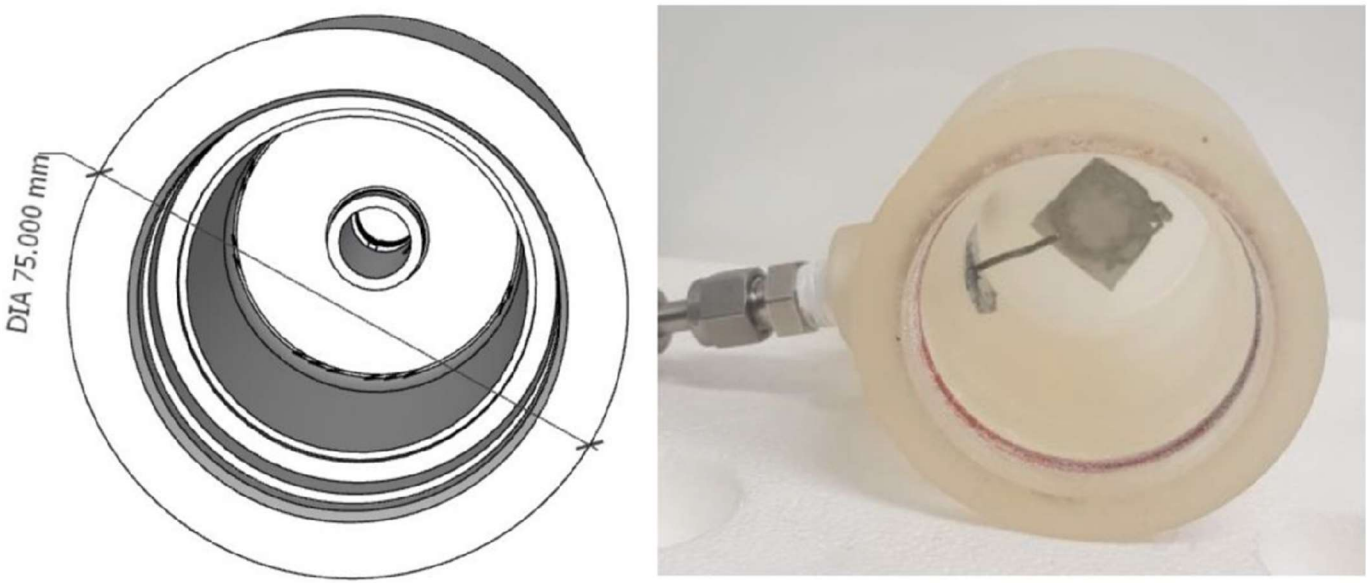


*Figure 3.7. Thermocouple location inside freeboard region for detection of heat of adsorption (the square patch of wire mesh for minimizing loss of fines is also visible).*

### 3.5 Hydrodynamic Experiment Methodology

Prior to embarking on the adsorption/desorption kinetic screening experiments, it was imperative to characterize the fluidization behaviour of each sorbent type. This preliminary step aimed to inform the selection of appropriate operating conditions and identify the optimum sorbent material for further investigation. Two key variables, namely flow rate and bed loading, were employed to determine the optimal conditions for achieving the desired flow regime and bed pressure drop. These established conditions were then utilized in subsequent adsorption and desorption experiments.

These tests were conducted at a temperature of 20 ºC and a pressure of 1 bar.g, utilizing nitrogen/air as the fluidizing gas. Figure 3.8 depicted schematic drawing of hydrodynamic rig and in figure 3.9, photo of rig has been shown. The pressure drops across the bed were quantified by measuring the pressure at the inlet and outlet of the reactor using a pressure transducer, while the flow rate was precisely measured by a mass flow controller. This enabled accurate control of the volumetric flow rate within the range of 5–100 l/min.

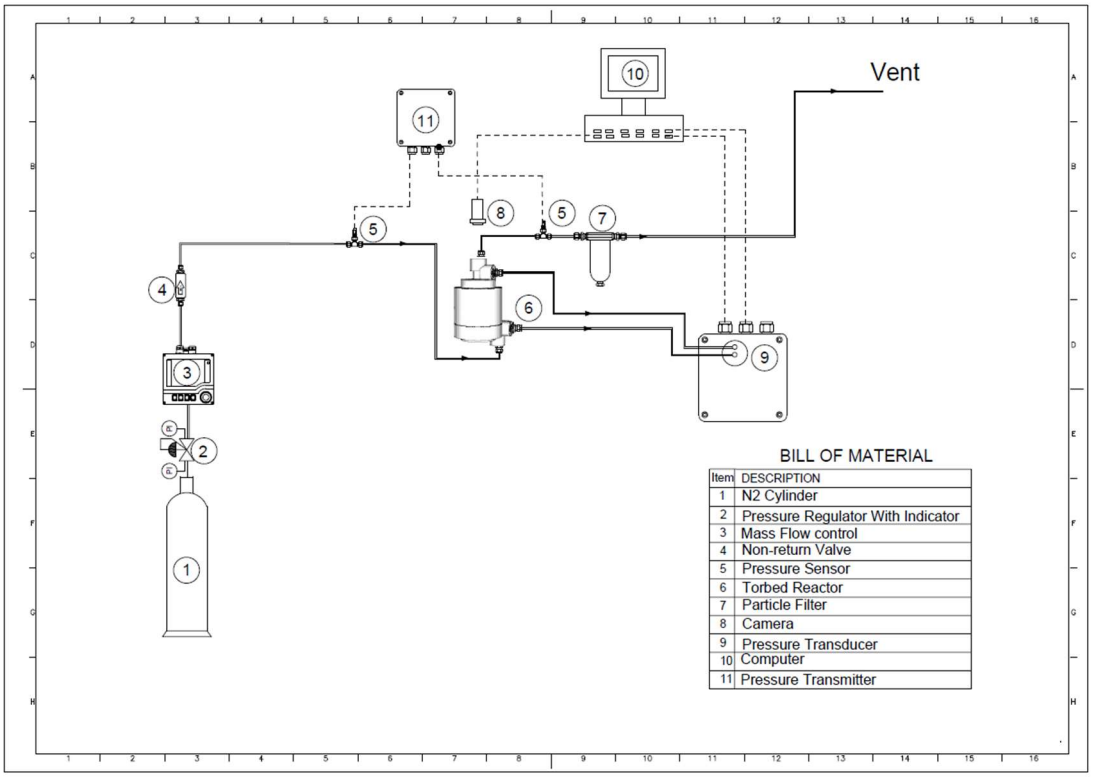


*Figure 3.8. Schematic of Hydrodynamic experiment*

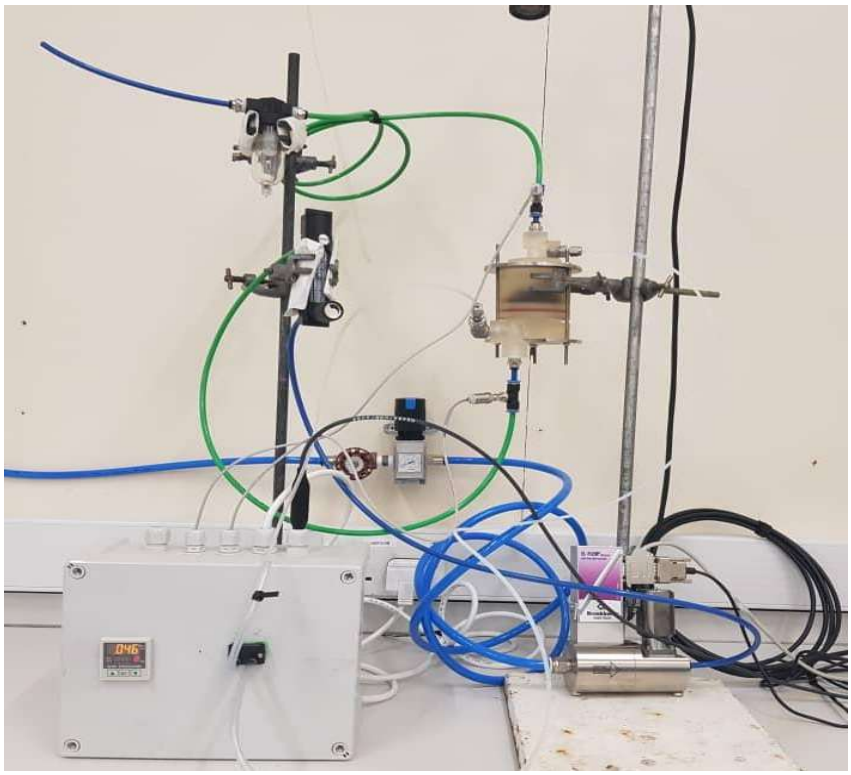

*Figure 3.9. Image of Hydrodynamic rig*

Additionally, a high-speed camera (Basler, A1440) was strategically positioned directly above the TORBED. This camera could be modified with a Perspex window for monitoring and recording the formations within the bed. The systematic measurement and monitoring of bed pressure drop, and flow regime were crucial for determining the optimum conditions of the TORBED reactor and identifying the desirable flow regimes for each specific sorbent material. These detailed characterizations provided valuable insights that guided subsequent experimental procedures. It is essential to note that the reported pressure drops were calculated by subtracting the pressure drop measured across the empty bed from the pressure drop measured with a loaded bed for all gas flow rates. This approach ensures that the pressure drop corresponds specifically to the swirling particles and remains independent of the experiment platform. The experimental procedure involved two main steps for each flow rate set point ranging from 5-100 l/min.

In the first step, empty bed pressure drops were measured. In the second step, the bed was filled with one of the three particle grades based on the bed loading amount. To validate the starting weight, the particles were emptied from the bed and weighed. Subsequently, pressure drop data and high-speed videos were recorded for both increasing and decreasing air flow rates to capture any hysteresis effects. During fluidization experiments where the gas flow rate was incrementally increased, 30 seconds of pressure drop data were recorded for each particle-condition arrangement. This was followed by 'defluidization' experiments where the flow rate was incrementally decreased. Before recording data, the bed was allowed to stabilize for a few minutes at each flow rate. The diverse bed formations were captured by a high-speed camera positioned directly above the TORBED, as depicted in Figure 3.8. The Photron FASTCAM Viewer (PFV) software facilitated image capture at 1000 frames per second for 10 seconds (limited by the camera's RAM), and these images were subsequently transferred to an external hard drive for later transfer to a larger storage server. Finally, the data for pressure drop and bed formation videos were used to categorize the various flow regimes and specify desirable regimes and optimum variable ranges. This detailed analysis contributed to a comprehensive understanding of the fluidization behaviour under different conditions.

## 3.6 Breakthrough and Adsorption Methodology

Standard breakthrough experiments were conducted to investigate the $CO_2$ capacity and kinetic performance of the sorbent within the TORBED platform. The experimental design considered various process conditions, as summarized in Table 3.1. The effects of $CO_2$ concentration (ranging from 2% to 20% vol), bed loading (varying from 1 to 2.5 g), gas flow rate (ranging from 20 to 35 L/min), and gas temperature (between 40 and 70 °C) were systematically examined.

The selection of these specific ranges for bed loadings and gas flow rates was informed by the optimal conditions identified in the hydrodynamics characterization experiments. Parameters falling outside the determined optimal range were also included in the trials to assess the potential negative impact on the $CO_2$ capture behaviour of the sorbent.

An adsorption temperature of 40 °C was recommended by the sorbent provider (RTI). Lower temperatures were excluded from consideration due to the occurrence of water condensate in real flue gases below 40 °C [16]. Consequently, several higher temperatures were employed for benchmarking purposes. The chosen $CO_2$ concentrations covered the full working range of the $CO_2$ analyzer (GSS, SprintIR). To ensure robust characterization and reliability of results, each set of conditions was run in triplicate, providing a basis for understanding experimental variability and characterizing potential errors.

All experiments were conducted at a pressure of 1 bar.g due to limitations imposed by the pressure drop in the experimental rig. The mass flow controller faced challenges in delivering the desired flow rate at 1 bar.a (atmospheric pressure), necessitating an increase in the inlet gas pressure to compensate. For ease of replication and to avoid the complexities associated with precisely regulating pressure for each individual run, experiments were standardized at 1 bar.g.

The breakthrough experiments followed a systematic procedure. Initially, the designated amount of sorbent was placed in the reactor and fluidized in pure $N_2$ at 120 °C for 10 minutes to condition the adsorbent. This step aimed to eliminate moisture and residual $CO_2$ and stabilize the flow regime to optimize gas–solid contact. Subsequently, the temperature was adjusted to the desired value for the specific run, and the bed was allowed to stabilize for an additional 10 minutes, ensuring that the flow regime was fully established, and that the temperature had reached the desired setpoint.

*Table 3.1 Summary of adsorption experiment conditions*

| Parameter | ID | Bed Loading (g) | $CO_2$ Conc. (vol%) | Flowrate (L/min) | Adsorption Temp. (°C) | Pressure (bar.g) | No. Repeats |
|---|---|---|---|---|---|---|---|
| $CO_2$ Concentration | 1 | 2 | 2 | 25 | 40 | 1 | 3 |
| | 2 | 2 | 8 | 25 | 40 | 1 | 3 |
| | 3 | 2 | 14 | 25 | 40 | 1 | 3 |
| | 4 | 2 | 20 | 25 | 40 | 1 | 3 |
| Bed Loading | 5 | 1 | 14 | 25 | 40 | 1 | 3 |
| | 6 | 1.5 | 14 | 25 | 40 | 1 | 3 |
| | 7 | 2 | 14 | 25 | 40 | 1 | 3 |
| | 8 | 2.5 | 14 | 25 | 40 | 1 | 3 |
| Gas Flowrate | 9 | 2 | 14 | 20 | 40 | 1 | 3 |
| | 10 | 2 | 14 | 25 | 40 | 1 | 3 |
| | 11 | 2 | 14 | 30 | 40 | 1 | 3 |
| | 12 | 2 | 14 | 35 | 40 | 1 | 3 |
| Temperature | 13 | 2 | 14 | 25 | 40 | 1 | 3 |
| | 14 | 2 | 14 | 25 | 50 | 1 | 3 |
| | 15 | 2 | 14 | 25 | 60 | 1 | 3 |
| | 16 | 2 | 14 | 25 | 70 | 1 | 3 |

The mass flow controller setpoint for $CO_2$ was then configured (without activation), aiming to achieve the desired concentration at the given total gas flow rate for the experiment. The mass flow controller was then activated simultaneously with the initiation of data logging on the $CO_2$ analyser. This process recorded the $CO_2$ concentration, known as the breakthrough curve, at a sampling rate of 20 Hz. Concurrently, the pressure drop across the TORBED and temperatures throughout the system were recorded. An example of a breakthrough curve is illustrated in Fig. 8a, depicting the conditions at ID4. The breakthrough time ($\tau$) reported denote the time taken for the $CO_2$ concentration to reach 5% of the inlet concentration, as shown in Fig. 3.10a.

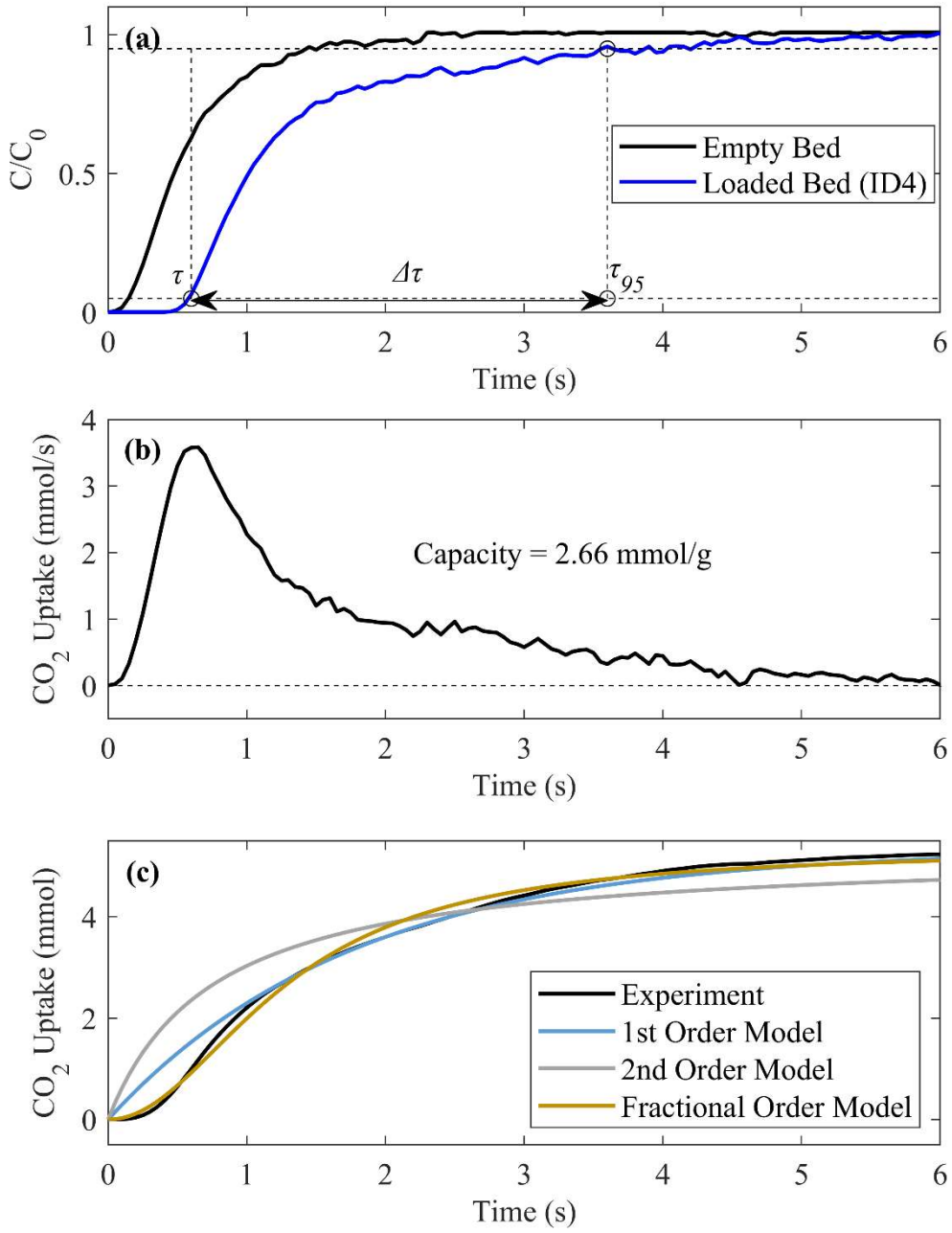


*Figure 3.10. (a) Normalised breakthrough curves for ID4 (with deadtime removed); (b) $CO_2$ uptake curve for ID4; (c) cumulative $CO_2$ uptake curve for ID4 and comparison to simple kinetic models*

To determine sorbent capacity, deconvolution of the breakthrough curve measured in the TORBED without material and the breakthrough curve of the specific experiment containing the adsorbent was performed. For kinetics evaluation, the empty bed signal was subtracted

from the signal recorded with the sorbent, effectively removing the effects of diffusion and dispersion between $CO_2$ and $N_2$ within the rig.

The resulting uptake curve retained two components: [1] the signal associated with mass transfer in the empty bed, and [2] the signal associated with adsorption into the particles. Importantly, in the TORBED, the subtracted signal likely corresponds almost entirely to the adsorption process alone due to the use of higher gas flow rates, eliminating external mass transfer resistances around the particles. This characteristic represents a potential major advantage of the TORBED platform, as depicted in the graphical photo shown in Figure 9a.

In Fig. 3.10b, the resulting deconvoluted instantaneous $CO_2$ uptake curves are presented, showcasing their dependence on $CO_2$ concentration. The area beneath these curves corresponds to the capacity, as labelled for reference. To further analyse adsorption kinetics, a saturation time, $\Delta\tau$, was defined. Specifically, $\Delta\tau$ was determined as $\Delta\tau = (\tau_{95} - \tau)$, where $\tau_{95}$ represents the time taken for the $CO_2$ concentration measured at the outlet to reach 95% of the final value, and $\tau$ is the standard breakthrough time (the time for the $CO_2$ concentration to reach 5% of the inlet concentration). The saturation time is also labelled in Fig. 3.10a. $\Delta\tau$ essentially corresponds to the slope of the breakthrough curve, with a smaller value indicating a steeper breakthrough curve and vice versa. Therefore, $\Delta\tau$ represents the time required for the bed to fully saturate, with a smaller value indicating a more rapid saturation process. This additional parameter provides insights into the kinetics of the adsorption process, enhancing the comprehensive analysis of the TORBED platform's performance.

To delve deeper into the kinetics of the adsorption process, with the aim of informing the design of a potential industrial-scale process, three typical adsorption kinetic models were fitted to the experimental data. The pseudo first-order model, pseudo second-order model, and fractional-order model (Eqs. [1], [2], and [3] respectively) were employed to describe the change in bulk concentration of $CO_2$, utilizing simple fitting parameters.

$$q_t = q_e(1 - e^{-k_1 t}) \qquad (1)$$

$$q_t = \left(\frac{{q_e}^2 k_2 t}{1 + q_e k_2 t}\right) \qquad (2)$$

$$q_t = q_e - \left( \frac{(n-1)k_f}{m} t^m + \left( \frac{1}{q_e^{n-1}} \right)^{\frac{1}{n-1}} \right)^{-1} \qquad (3)$$

Here, $q_t$ represents the $CO_2$ uptake at time $t$ (mmol), $q_e$ is the uptake of $CO_2$ once equilibrium is achieved (mmol), t is the time (s), $k_1$ is the pseudo first-order rate constant ($s^{-1}$), $k_2$ is the pseudo second-order rate constant ($g.mmol^{-1}.s^{-1}$), $k_f$ is the fractional-order rate constant ($s^{-1}$), and $n$ and $m$ are empirical coefficients used to refine the shape of the fractional-order model curve [107]. The $n$ coefficient characterizes the driving force, and $m$ represents the adsorption time. These models predict the cumulative uptake behaviour of $CO_2$ as it is adsorbed onto the material's surface. The experimental cumulative uptake curves were obtained by integrating the instantaneous uptake curves shown in Fig. 3.10b. An example is illustrated in Fig. 3.10c, along with the fitted models, providing a comparative assessment of the theoretical predictions against the experimental data. This fitting process enhances our understanding of the adsorption kinetics and aids in the extrapolation of findings to potential industrial applications.

### 3.7 Desorption Breakthrough Setup and Method

The schematic diagram for the desorption experiment flowsheet is depicted in Figure 3.11, providing a visual representation of the experimental setup. Additionally, Figure 3.11 presents a photo and an image of the printed TORBED reactor and the experimental rig, offering insights into the physical configuration of the apparatus. It is pertinent to highlight that the configuration of the desorption rig differs from that of the adsorption rig, even though a majority of the devices utilized are identical, varying only in their arrangement. The ensuing explanation provides a detailed account of how these devices are adapted and arranged differently to cater to the distinct requirements of the desorption process compared to the adsorption process. In the desorption experiments, an artificial flue gas, with a $CO_2$ concentration ranging from 0% to 20% vol in $N_2$, was generated by blending $CO_2$ (99.8%) and Nitrogen (99.9%) gases from gas cylinders (1 & 2 in P&ID) in Tee Union [6] by controlling specific flowrates using mass flow controllers [4]. This controlled mixture serves as a representative flue gas for conducting desorption studies within the TORBED reactor. The combination of visual representations and detailed diagrams contributes to a comprehensive understanding of the experimental setup and the key components involved in the desorption process.

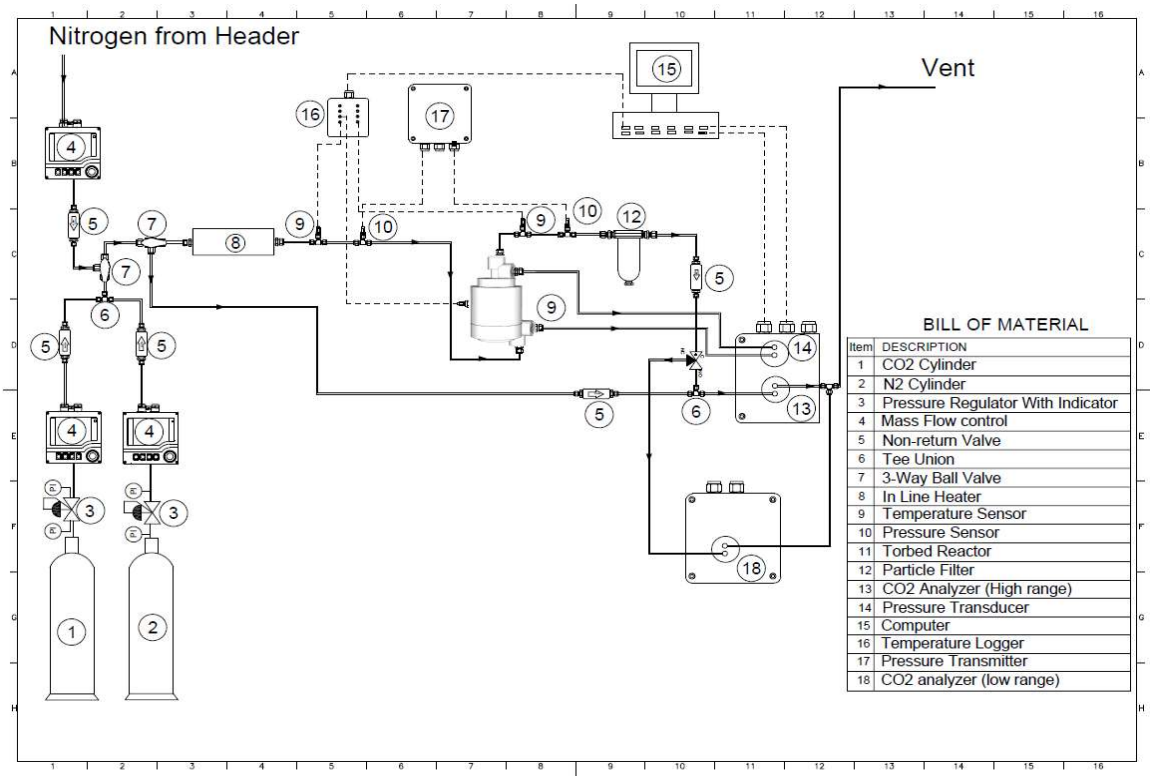


*Figure 3.11. Schematic of $CO_2$ breakthrough for assessing adsorption/desorption kinetics*

Cyclic adsorption and $CO_2$ adsorption/desorption breakthrough experiments were conducted in the TORBED reactor, aligning with the conditions elucidated from preceding hydrodynamics tests that established a desirable fully swirling flow regime. These conditions were characterized by inlet $CO_2$ concentrations ranging from 8% to 20% vol, temperatures spanning from 40°C to 110°C, and gas flow rates set between 20 and 30 L/min. The bed loading was maintained at a constant 2 g, a parameter optimized in hydrodynamic study.

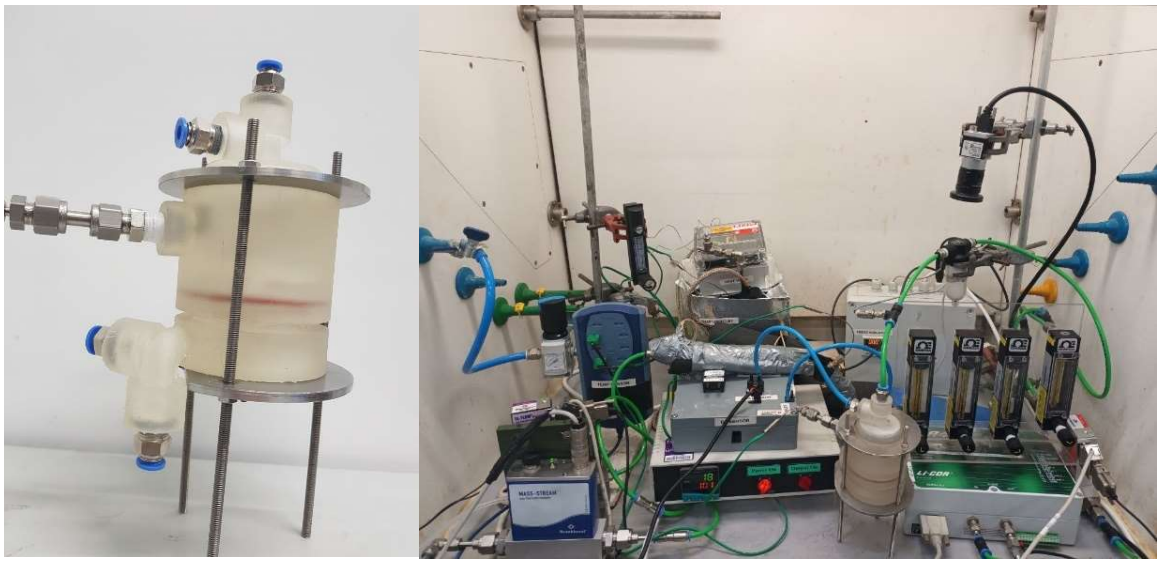

*Figure 3.12. (a) 3D-printed mini-TORBED, (b) Full experiment rig*

All these parameters were systematically studied at three levels within the specified ranges, with the mid-level positioned at or in close proximity to the midpoint of the range, as detailed in Table 3.2.

Throughout the adsorption and desorption breakthrough experiments, temperature measurements were recorded at the interior of the bed using a thermocouple. The inlet temperature was modulated by adjusting the power supplied to the inline heater, ensuring precise control over the experimental conditions. The methodical variation of these parameters allowed for a comprehensive exploration of the TORBED's performance under diverse operating conditions, essential for a thorough understanding of the adsorption and desorption processes.

*Table 3.2. Summary of desorption experiment conditions*

| ID | Parameter | Flow Rate (L/min) | $CO_2$ Concentration (vol%) | $T_{ads}$ (°C) | $T_{des}$ (°C) |
|---|---|---|---|---|---|
| 1 | Temperature $T_{ads} = T_{des}$ | 25 | 20 | 40 | 40 |
| 2 | | 25 | 20 | 80 | 80 |
| 3 | | 25 | 20 | 110 | 110 |
| 4 | Temperature ($T_{des} > T_{ads}$) & Gas Flow Rate | 20 | 20 | 40 | 80 |
| 5 | | 25 | 20 | 40 | 80 |
| 6 | | 30 | 20 | 40 | 80 |
| 7 | | 20 | 20 | 80 | 110 |
| 8 | | 25 | 20 | 80 | 110 |
| 9 | | 30 | 20 | 80 | 110 |
| 10 | | 20 | 20 | 40 | 110 |
| 11 | | 25 | 20 | 40 | 110 |
| 12 | | 30 | 20 | 40 | 110 |
| 13 | $CO_2$ Concentration | 25 | 8 | 40 | 110 |
| 14 | | 25 | 14 | 40 | 110 |
| 15 | | 25 | 20 | 40 | 110 |
| 16 | | 25 | 8 | 80 | 110 |
| 17 | | 25 | 14 | 80 | 110 |
| 18 | | 25 | 20 | 80 | 110 |

The experimental approach assumed that the adsorption of $N_2$ is negligible in the presence of $CO_2$. Consequently, the measured adsorption quantity in the $CO_2/N_2$ mixture was considered to represent the $CO_2$ adsorption capacity. Subsequent desorption experiments were conducted in situ inside the TORBED reactor, employing a pure stream of heated nitrogen. This methodology allowed for a more expeditious evaluation of cyclic stability compared to regenerating the material ex situ, for instance, using a vacuum oven. The in-situ desorption within the TORBED reactor facilitated a streamlined and efficient assessment of the material's cyclic performance, contributing to a more comprehensive understanding of its adsorption and desorption behaviour.

In this study, TORBED technology is used for desorption process means saturated sorbent will not be removed from the bed and use hot nitrogen gas instead of feed gas for regeneration of sorbent inside of reactor with toroidal motion called as in-situ method. Since our TORBED reactor is 3D printed, for TSA process the TORBED casing has been designed with an additional connection line for nitrogen stream which heated up via inline gas heater and pass through the reactor bed and create optimum flow regime as fully swirled. This would likely reduce the total experiment energy use, increase the concentration of the captured $CO_2$, and increase the preservation of the sorbent (since temperature cycling can lead to increased

degradation). However, while sorbent regeneration could be more rapidly via in situ method, and the bed would remain in a fluidised state with optimum flow regime. This would intensify the study of the desorption kinetics.

In-situ desorption experiments were conducted in the toroidal fluidizing bed unit (Fig. 3.12) using a gas mixture composed of 0-20% vol $CO_2$ in $N_2$, representative of flue gas. The experimental procedure consisted of five distinct steps: pre-treatment, conditions adjustment, adsorption, preheating, and desorption. Figure 3.13 serves as an illustrative example, specifically depicting ID1 to ID3 as outlined in Table 3.2. This graphical representation is intended to elucidate the diverse temporal phases of the desorption process, providing a visual reference to the distinct periods associated with each identified desorption instance.

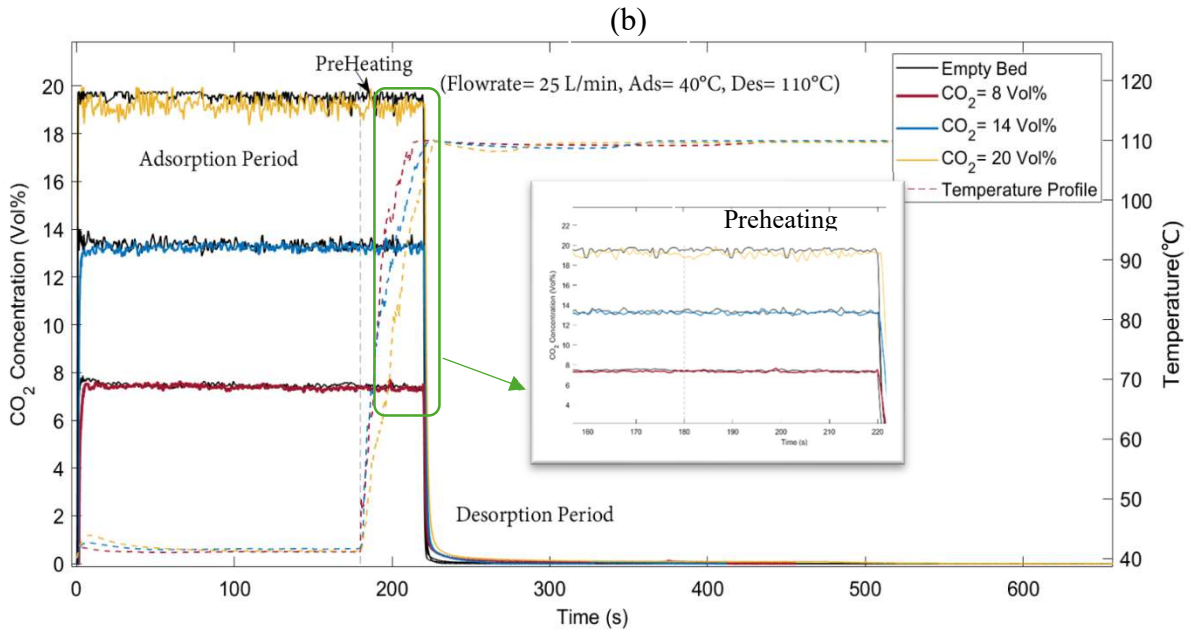


*Figure 3.13.Normalised desorption breakthrough curves and Bed temperature profile during TSA cycles with pure heated $N_2$*

### 3.7.1 Pre-treatment

2 g of the BPEI adsorbent was loaded into the TORBED reactor. Then, pure nitrogen gas, heated to 110 °C using an inline heater, was flowed into the bed for approximately 10 minutes to condition the adsorbent. This step aimed to remove moisture, establish the desirable swirling flow regime, and eliminate any residual $CO_2$. $CO_2$ sensors connected at the outlet were zeroed by nitrogen during pre-treatment to correct for any calibration deviations over time. As indicated in figure 3.13, temperature profile related to the bed inside thermocouple was

recorded with starting the adsorption process and record all period of adsorption, preheating and desorption process for monitoring.

### 3.7.2 Conditions Adjustment

Following pre-treatment, the bed was adjusted to the target adsorption temperature via inline heater and thermocouples inside of reactor. Gas flow rate was set based on the required artificial gas composition to ensure flow regime uniformity before initiating the adsorption process. This adjustment was performed at the end of the pre-treatment period.

### 3.7.3 Adsorption

The initiation of the adsorption process occurred upon achieving the targeted $CO_2$ concentration, as indicated in Table 3.2. This was achieved by activating the mass flow control on both the $N_2$ and $CO_2$ lines. Concurrently, the $CO_2$ sensor was closely monitored to verify that the specified concentration had been attained before proceeding further. $CO_2$ composition in the effluent gas was continuously monitored by a $CO_2$ analyser over time until the sorbent reached full saturation, indicated by constant baseline signals. The adsorption process typically took around 3±0.2 minutes. The temperature profile inside the bed, monitored by a thermocouple, was recorded throughout the adsorption, preheating, and desorption processes.

### 3.7.4 Preheating

After achieving sorbent saturation, the desorption process was initiated by a pre-heating period designed to establish the desorption temperature. This pre-heating phase, lasting between 15 seconds to 45 seconds depending on the experiment, occurred after the temperature was set and before discontinuing the $CO_2$ flow. This variation in pre-heating time accounted for differences in adsorption and desorption temperatures. Following sorbent saturation, the mixed gas flow was discontinued, and only $CO_2$ gas was allowed to flow at the specified rate. Subsequently, the preheater was set to the required temperature, and its monitoring was continued until it reached the specified temperature. Throughout the preheating stage, the $CO_2$ flow was sustained to minimize desorption and prevent any loss of $CO_2$ sorbent, ensuring the sorbent remained in a saturated state.

### 3.7.5 Desorption

The actual desorption process followed the pre-heating period. Different experimental conditions were designed to investigate the effects of desorption temperature on the sorbent, adjusting the pre-heating time to minimize the chances of $CO_2$ desorption during preheating.

The duration of pre-heating is crucial, and longer pre-heating time may increase the risk of desorption. Therefore, finding the appropriate pre-heating time is essential based on specific process conditions and the characteristics of the desorption system.

In the adsorption/desorption process, the outlet $CO_2$ concentration was continuously monitored using a $CO_2$ sensor (0–20 vol%) to observe the bulk desorption process. Separate baseline experiments were conducted for each experiment in Table 3.2 to provide blank data for benchmarking (see 'empty bed' data in Figure 3.13 in black line) and assessing desorbed capacity/kinetics After saturating the sorbent and adjusting the temperature setpoint to the target desorption temperature during the preheating period, the $CO_2$ feed was switched off, allowing only pure $N_2$ to flow into the bed. A complementary desorption breakthrough experiment was then performed, initiating the recording of bed temperature and outlet $CO_2$ concentration.

### 3.8 Conclusion

The desorption concentration profile shows a rapid decline to a minimum $CO_2$ outlet value (5% of the initial value) within relatively low desorption time (about 3-9 seconds) as shown in figure 3.13. This suggests that most of the adsorbed $CO_2$ is quickly removed from the samples during this fast stage. Subsequently, the curves exhibit a longer tail, indicating slower residual $CO_2$ desorption due to a reduction in desorption kinetics and the completion of the physisorption process. The slower stage involves chemisorption, where stronger chemical bonds between $CO_2$ and the amine groups on the porous material take longer to break, leading to a more gradual release of $CO_2$.

Transitioning from the adsorption phase to the desorption phase through TSA can be achieved using different approaches, including the preheating period. The inherent time lag between saturating the adsorbent with $CO_2$ and raising the temperature to the setpoint is a critical factor influencing desorption during preheating. Researchers may adopt various methodologies for preheating, such as conductive heating (20, 108), microwave heating (106, 109), or extracting the sorbent and heating it up in an oven (20, 41, 42). Convective heating involves rapidly increasing the temperature of the sorbed material through direct contact with a high-temperature fluid, gas, or a heating element.

In TORBED platform, the high flow rate and small reactor volume can accelerate the desorption process compared to preheating. In some cases, 90% of desorption may occur faster than preheating time due to desorption period is too short in comparison to heating period as

shown in figure 3.13. Therefore, careful control of temperature is crucial to achieving optimum desorption kinetics. Various experiments exploring different adsorption-desorption temperature configurations were conducted to understand their complementary and competing effects in the TORBED platform.

Experiment conditions ID1, 2 & 3 were designed with the same adsorption and desorption temperatures, eliminating the need for a preheating period. This allowed the immediate observation of the temperature effect on adsorption and desorption capacity, making desorption effects more apparent. In other experiment runs, desorption temperature was higher than adsorption temperature, causing a delay in the preheating period. By implementing these conditions and monitoring trends, the study aimed to quantify and understand potential $CO_2$ desorption during the preheating step of the sorbent using a pure stream of heated nitrogen.

This chapter provides a detailed overview of the process involved in designing and fabricating the experimental setup for the TORBED reactor, emphasizing aspects such as the reactor design, sorbent properties, hydrodynamic study, and the methodology applied in adsorption and desorption experiments. The initial phase involves 3D modelling of the Mini TORBED reactor using Google Sketchup software, specifically adapted for 3D printing. Notably, a prior version of the TORBED reactor had been developed by the supervisory team, forming the foundation for subsequent improvements.

The study includes a hydrodynamic sorption investigation using three distinct sorbent types to determine optimal flow conditions and particle size. This critical step aims to identify the most suitable sorbent for subsequent monitoring in adsorption and desorption studies. Different experimental rigs are designed to cater to the diverse requirements of hydrodynamic, adsorption, and desorption studies.

The chapter also delves into the methodology employed to achieve the study's overarching objectives. It discusses the instrumentation and technology used to measure various parameters throughout the investigation. The detailed exploration emphasizes the iterative nature of design considerations, reflecting a commitment to optimizing the experimental setup for precise and insightful exploration of adsorption and desorption phenomena.

# 4. Sorbent Hydrodynamic Characteristics

## 4.1 Introduction

To adequately evaluate adsorption kinetics in subsequent experiments, a comprehensive understanding of the hydrodynamic principles governing fluidized beds was essential. This initial step was crucial for guiding the selection of optimal operating conditions and identifying superior adsorbents for the TORBED reactor in the adsorption/desorption process [90]. Exploring hydrodynamic aspects was necessary due to their significant impact on mass transfer and adsorption processes within the bed. The state of fluidization directly influences the contact between adsorbent particles and the fluid, thus affecting the overall efficiency of the adsorption system [91].

This understanding is particularly vital for adsorption processes, where the effectiveness of adsorbent-adsorbate interactions relies heavily on the dynamic behaviour of the fluidized bed. Systematically characterizing hydrodynamics allows for optimizing operating conditions, thereby improving the TORBED reactor's performance in the adsorption/desorption process. The systematic characterization of the hydrodynamic behaviour of the system involved both visual experiments and pressure drop measurements at various flow rates and bed loading. These experiments were conducted at ambient temperature and 1 bar.g pressure, with inert nitrogen ($N_2$) used as the fluidizing gas.

Employing a high-speed camera (Basler, acA1440-220um) was pivotal in providing detailed visualizations of bed formations. This established methodology, as discussed in the methodology chapter, enabling the observation of fluidization phenomena. The integration of the high-speed camera facilitated the recording of dynamic events within the fluidized bed, offering invaluable insights into the temporal evolution of bed structures and fluidization patterns. The Perspex window modification ensured optical clarity and camera accessibility, enabling unobstructed observation and recording of the hydrodynamic behaviour of the TORBED system [90].

By employing this methodology, the research not only obtained a qualitative understanding of fluidization phenomena but also acquired quantitative data crucial for characterizing the complicated hydrodynamic interplay within the system [91]. Visualizing and quantifying flow regimes and bed pressure drop play a significant role in the systematic analysis of the TORBED reactor's performance and constitute a foundational aspect of the experimental approach used in this study [57].

## 4.2 Visual Observation of TORBED Regimes

A high-speed camera, strategically positioned directly above the TORBED and complemented by a Perspex window modification, was employed to accurately capture diverse bed formations of the adsorbents across a spectrum of conditions. The observed behaviours of the adsorbent manifested distinct regimes contingent upon the sorbent type, bed loading, and gas flow rate. A comprehensive overview of the experimental conditions is provided in Table 4.1.

*Table 4.1. Summary of experiment conditions and accuracy*

| Parameter | Conditions | Accuracy |
|---|---|---|
| Bed material | BPEI, Hydrotalcite, Casale | N/A |
| Sorbent size | 75 μm, 35 μm, 1.50 mm | ± 12 μm, ± 15μm, ± 0.47 mm |
| Bed loading (mg) | 500 - 2500 | ± 2 mg |
| Flow rate (L/min) | 5 - 100 | ± 1 % |
| Temperature (◦C) | 17-20 | N/A |

In the miniaturized TORBED design, the adsorbent forms a shallow bed near the blade distributor, restricting the formation of bubbling and slugging structures due to spatial constraints limiting their development. As a result, in comparison to conventional fluidized bed reactors, it becomes necessary to introduce distinct categories of flow regimes that better capture the unique hydrodynamic characteristics exhibited by the TORBED under these specific operating conditions. The limitations on bed depth and space for structural development necessitate a re-evaluation and classification of flow regimes to effectively characterize the fluidization behaviour in the miniaturized TORBED configuration.

The TORBED displayed different swirling bed states depending on the bed loading and gas flow rate. The unique characteristics of these swirling bed states offer valuable insights into the dynamic behaviour of the system under varying operational conditions. Analysing the interaction between bed loading and gas flow rate allows for a better understanding of swirling bed dynamics in the TORBED, contributing to a comprehensive understanding of its operational limitations. The observed swirling bed states in the miniaturized TORBED system are classified into distinct categories based on their hydrodynamic characteristics (7, 8, 68) which has been shown in figure 4.1 as an example:

**Un-swirled (Figure 4.1a):**

- Absence of any swirling motion within the bed.
- Resultant from either low gas flow rate ('under-airing') or high bed loading.

**Collapsed (Figure 4.1b):**

- Partial swirling of the sorbent, causing most particles to accumulate in one area above the distributor.
- Occurs during overloading of particles or insufficient gas flow rate.

**Maldistributed (Figure 4.1c):**

- All particles are in a state of swirling, but a slower-moving aggregated region forms, moving around the bed at a pace slower than the average velocity.
- Gas stream energy is inadequate to induce uniform swirling, leaving portions of the distributor uncovered.

**Uniformly Swirled (Figure 4.1d):**

- Desirable state where the entire bed exhibits uniform swirling motion.
- Distributor remains fully covered by particles, preventing gas bypassing.

**Over-Aired (Figure 4.1e):**

- Uniform swirling of particles, but parts of the distributor become uncovered due to either under-loading of the bed or excessive gas velocity.
- May lead to gas bypassing.

**Entrained (Figure 4.1f):**

- Particles are lifted away from the distributor and accumulate at the inner wall or outlet of the reactor.

Entire distributor remains uncovered, resulting in almost complete gas bypassing and a significant pressure drop.

This categorization provides a comprehensive framework for understanding and analysing the diverse hydrodynamic behaviours exhibited by the miniaturized TORBED under varying operational conditions [88].

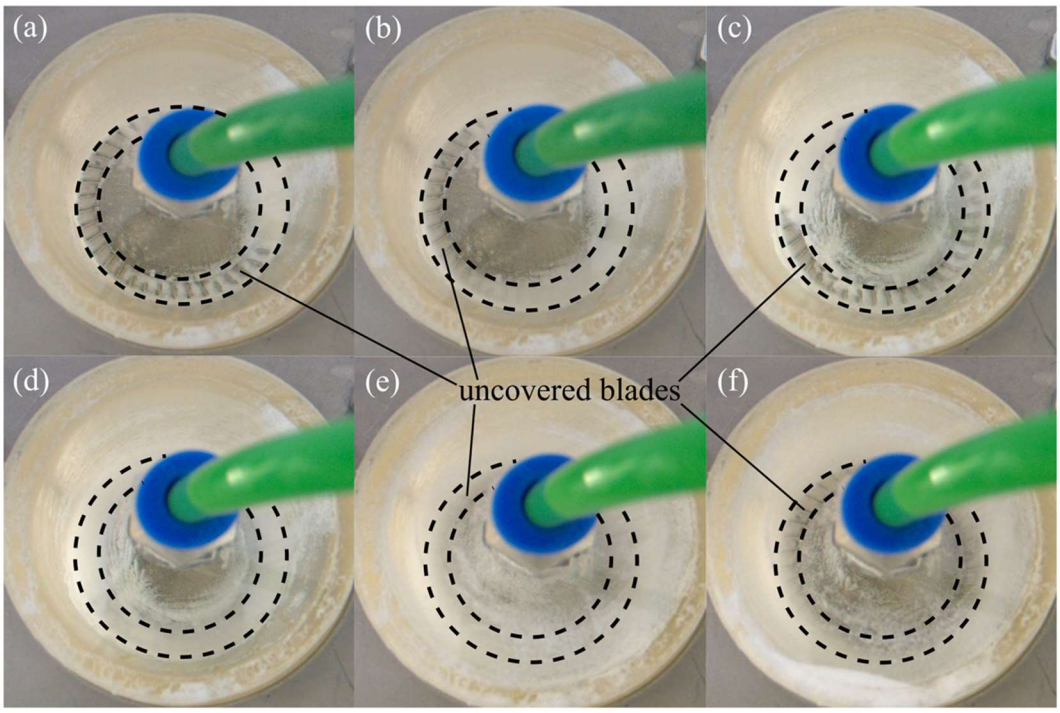


*Figure 4.1. Examples of different particle formations observed in the 3D-printed mini-TORBED for BPEI; fluidising gas = N2, bed loading = 2 g, pressure = 1 bar.g, temperature = ambient; (a) un-swirled, 5–10 L/min, (b) collapsed, 15 L/min, (c) maldistributed, 20 L/min, (d) uniformly swirled, 25–35 L/min, (e) over-aired, 40–45 L/min, (f) entrained, 50–60 L/min*

## 4.3 Pressure Drop Analysis

As detailed in the methodology chapter, the experimental setup comprised pressure transducer sensors (Sensirion, SDP800) generating an analogue signal. This signal was converted and digitally adjusted, with monitoring and logging conducted through a Node-Red program running on a Raspberry Pi-3 module, at both the reactor's inlet and outlet. This integrated instrumentation was designed to comprehensively record a diverse array of bed formations of the adsorbent and capture the entire bed pressure drop across a spectrum of conditions. The primary objective was to optimize operational conditions by pinpointing the ideal flow regimes [22].

This synergistic approach, combined visual data from the high-speed camera with real-time pressure measurements, provided a comprehensive overview of the system's dynamic response to changing conditions. Through systematic analysis of the recorded bed formations via visual observation and pressure drop profiles, the research aimed to identify and characterize flow regimes that are optimal for efficient adsorption processes within the TORBED. The integration of visual and pressure data contributes to a comprehensive strategy for condition optimization, providing a deeper insight into the dynamics of the miniaturized TORBED system.

To illustrate, consider the hydrodynamic outcomes for BPEI (polyethyleneimine) presented in Table 4.2 and figure 4.2, complemented by visual representations of distinct bed regimes in Figure 4.1. A parallel hydrodynamic study was conducted for two other sorbents, namely Hydrotalcite and Casale. The results for these sorbents are summarized in Tables 4.3 and 4.4, accompanied by photos depicting their respective bed regimes in Figures 4.4 and 4.5.

An important clarification concerns the methodology utilized to calculate the reported pressure drops in Tables 4.2, 4.3, and 4.4. These values were derived by subtracting the pressure drop measured across the empty bed from the pressure drop measured with a loaded bed across all gas flow rates. This calculation effectively isolates the pressure drop attributed solely to the swirling particles, thereby eliminating the influence of the experimental platform.

This deliberate separation from the experimental setup enhances the reliability and comparability of the findings, enabling meaningful analysis and interpretation of results across various experimental conditions.

In the pressure drop tables, the N/A entries denote instances where the uniformity regime or fluidization state lacks meaningful interpretation. This occurrence is observed, especially with particles such as BPEI and Hydrotalcite, owing to their fine particle size. The challenge arises when these particles adhere to the upper section of the visual screen and the outlet port, particularly in conditions of lower bed loading and higher flow rates.

In certain scenarios, these fine particles may surpass the filter mesh at the reactor outlet due to elevated pressure and high flow rates, leading to an undefined fluidization state. This phenomenon underscores the unique challenges posed by the specific characteristics of these particles during experimental observations. Hence, in cases where particles consistently result in N/A entries across all bed loadings, the experiment runs were halted upon reaching an increased flow rate. Notably, this decision was influenced by the observation that this phenomenon was absent for the Casale sorbent. The Casale sorbent exhibited a more extended range of flow rates compared to other sorbents, attributed to its larger particle size, which prevented the occurrence of this particular issue.

*Table 4.2. Pressure drop (in kPa) and observed flow regimes within the TORBED reactor for BPEI under different operating conditions.*

| **Flow Rate (L/min)** | **Empty Bed ΔP (kPa)** | **ΔP (kPa)at Different Bed Loadings** | | | | |
|---|---|---|---|---|---|---|
| | | **0.5g** | **1g** | **1.5g** | **2g** | **2.5 g** |
| 5 | 0.03 | 0.02 | 0.04 | 0.07 | 0.08 | 0.10 |
| 10 | 0.13 | 0.05 | 0.06 | 0.07 | 0.09 | 0.14 |
| 15 | 0.28 | 0.09 | 0.15 | 0.19 | 0.23 | 0.42 |
| 20 | 0.37 | 0.15 | 0.22 | 0.34 | 0.58 | 0.83 |
| 25 | 0.6 | 0.08 | 0.28 | 0.64 | 1.21 | 1.31 |
| 30 | 0.81 | 0.08 | 0.29 | 0.90 | 2.05 | 2.13 |
| 35 | 1.11 | 0.19 | 0.24 | 1.26 | 2.31 | 3.12 |
| 40 | 1.45 | 0.22 | 0.24 | 1.74 | 3.53 | 3.43 |
| 45 | 1.75 | 0.23 | 0.60 | 2.94 | 4.74 | 5.04 |
| 50 | 2.16 | 0.24 | 0.55 | 3.74 | 6.24 | 7.04 |
| 55 | 2.53 | 0.25 | 0.67 | 5.37 | 8.27 | 9.65 |
| 60 | 3.03 | N/A | 0.70 | 7.87 | 10.16 | 12.21 |
| 65 | 3.33 | N/A | N/A | N/A | 13.25 | 15.50 |
| 70 | 3.33 | N/A | N/A | N/A | N/A | N/A |

| | | | |
|---|---|---|---|
| **Un-Swirled**<br>- No swirling motion within the bed<br>-Due to low gas flow rate or high bed loading. | U | **Uniformly Swirled**<br>-Desirable state where the entire bed exhibits uniform swirling motion.<br>-Distributor remains fully covered by particles, preventing gas bypassing. | S |
| **Collapsed**<br>-Partial swirling<br>-Occurs during overloading of particles or insufficient gas flow rate | C | **Over Aired**<br>- Uniform swirling, but parts of the distributor are uncovered due to under-loading or excessive gas velocity. | O |
| **Maldistributed** | M | **Entrained** | E |

| | | | |
|---|---|---|---|
| - A slower-moving aggregated region swirls within the particles, moving below average velocity.<br><br>- Insufficient gas stream energy leaves parts of the distributor uncovered. | | -Particles lift from the distributor and accumulate at the inner wall or reactor outlet. | |

*Figure 4.2. BPEI related Pressure drop (in kPa) as a function of gas flow rate and bed loading*

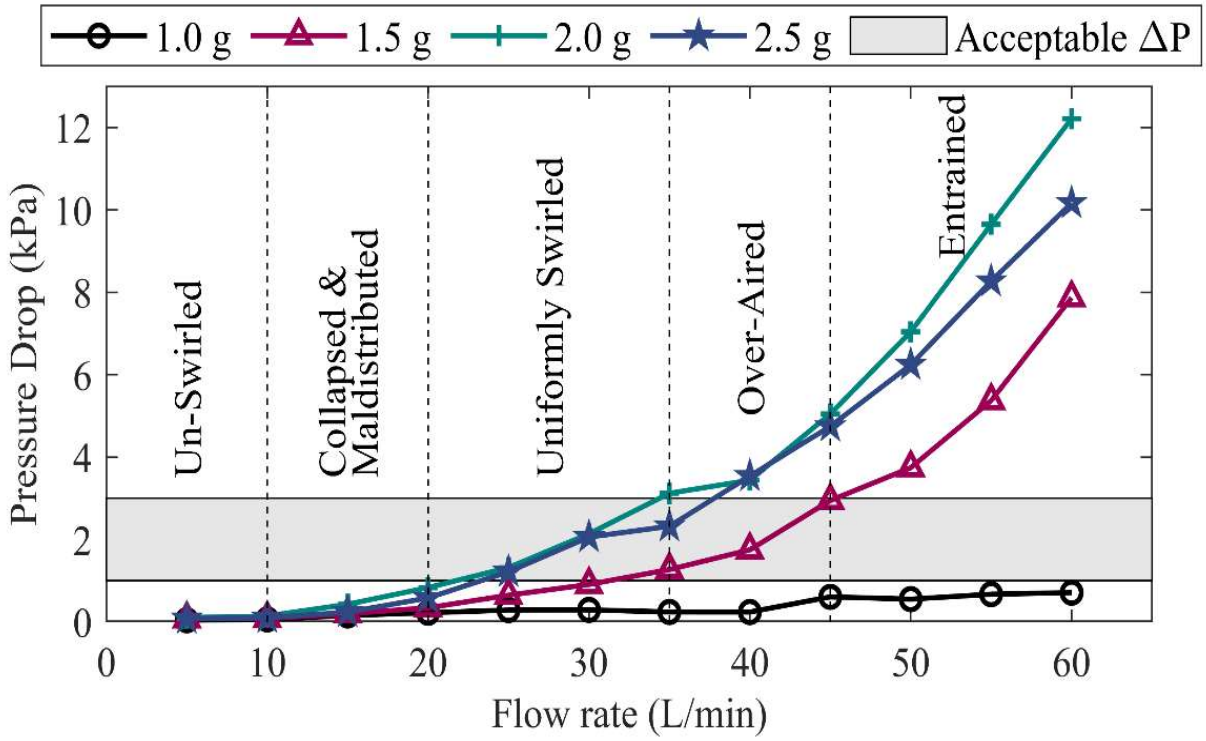


Figures 4.1 and 4.2 accompanied by Table 4.2 emphasize the significant impact of gas flow rate and bed loading on the development of distinct flow regimes of BPEI adsorbents within the TORBED system. Achieving optimal conditions for effective kinetic screening requires precise adjustments to attain the desirable uniformly swirled state. Our observations highlight instances of gas bypassing under conditions of low bed loading and low gas flow rates, where insufficient kinetic energy impedes swirling fluidization. Additionally, at very high gas flow rates, particles are forced toward the outer wall, resulting in an unacceptably high pressure drop.

In the specific case of the BPEI sorbent, the most favourable operating conditions for kinetic screening fall within the range of intermediate gas flow rates, specifically between 25–30 L/min. Under these conditions, the bed uniformly swirls without experiencing gas bypassing, as the distributor remains fully covered by the bed. This optimal state is versatile,

accommodating a wide range of bed loadings and enhancing the overall applicability of the TORBED system. At smaller bed loadings compared to higher bed loadings, the desired flow regime range is larger.

While smaller bed loadings struggle with higher momentum as the flow rate increases, leading to haphazard movement and over-airing of the bed and over range of flowrate, pressure drop significantly increased which cause pressure sensor goes out of range. On the other hand, higher bed loadings result in a higher bed pressure drop and loss in kinetic energy, causing an increased range of unswirled and maldistribution formation.

Moreover, in accordance with Torftech's observations [16] and design data, pressure drops ranging between 1 and 3 kPa for a TORBED of this scale are deemed acceptable. Table 4.2 illustrates that within this acceptable pressure drop range, the uniformly swirled state is achieved for bed loadings of 2.0 g and 2.5 g, reinforcing the suitability of these conditions for effective kinetic screening processes. This understanding of the complicated interplay between operational parameters and resulting flow regimes is indispensable for optimizing the TORBED system's performance, especially in the context of kinetic screening applications.

In the case of the Hydrotalcite sorbent, characterized as a Geldart C particle due to its diminutive size and adhesive nature, Table 4.3 and Figure 4.3 & 4.4 elucidate the flow regimes and pressure drop across different states. The majority of observed flow regimes are associated with the collapsed and maldistribution fields, stemming from a static collapsed state wherein an 'unswirled' region emerges at a fixed point on the blade distributor as shown in figure 4.3 and 4a, leading to a fixed near-zero velocity zone. This phenomenon arises due to the cohesive stickiness of Hydrotalcite, coupled with conditions of over-loading or 'under-airing,' where insufficient kinetic energy is imparted from the gas stream.

Another manifestation of the collapsed state is depicted in Figure 4.4b, showcasing a moving 'de-swirled' dune as pressure drop in figure 4.3 shows slightly increased but almost in acceptable range [16]. In this scenario, the collapsed region migrates in the opposite direction to the swirling particle motion. The swirling zone deposits particles at the leading edge of the collapsed zone, while particles on the opposite side of the collapsed zone become re-entrained. Consequently, the collapsed zone undergoes decay on one side and expansion on the other, resulting in the formation of the moving dune [68].

The maldistributed state (figure 4.3 and 4.4c) predominantly manifested at the lowest bed loadings. Despite the entire bed exhibiting swirling motion, there was incomplete coverage of the blades by the particles. A substantial portion of the particles fluidized outside the distributor area, resulting in an elevation of the bed height and a notable increase in pressure drop, as indicated in Table 4.3. The observed pressure drop in figure 4.3, in this region significantly surpassed that of the preceding two regimes, emphasizing the distinct and consequential hydrodynamic behaviour associated with the maldistributed state.

Figure 4.3d depicts the flow regime corresponding to the over-airing and entrained state. Over-airing of the bed amplified the centrifugal force, diminishing the coverage of the blades at the inner periphery. The conspicuous strong velocity profile resulted from a reduced particle density at the inner periphery, causing the particles to be pushed toward the wall and roof of the bed, leading to an elevated pressure drop. Consequently, unlike the over-airing state, the magnitude of pressure drop is an indicator of particle distribution in the entrained state.

In this scenario, the particle pressure drop significantly increased as shown in figure 4.3, reaching an unacceptable range. It is noteworthy that, for this sorbent type, a uniform flow regime was not observed under the described conditions.

At flow rates exceeding 65 L/min, no meaningful flow regime was discernible, and a significant portion of particles were expelled from the entire bed. These particles adhered to the wall and roof or passed through the filter mesh screen, with this phenomenon predominantly occurring at lower bed loadings. The absence of a discernible flow regime and the substantial particle removal underscore the critical influence of elevated flow rates on the dynamic behaviour and particle distribution within the TORBED system, particularly under conditions of lower bed loading. Based on the data presented in Table 4.3, it is evident that under various conditions, Hydrotalcite predominantly exhibited a non-fluidized regime at lower flow rates and a non-uniform swirling regime with significant pressure drop at higher flow rates.

This behaviour, characterized by significant gas bypassing through uncovered distributor areas, is deemed unacceptable for the sorbent screening stage across all conditions. Such bypassing substantially reduces the performance and efficiency of the adsorbents [57].

*Table 4.3. Pressure drop (in kPa) and observed flow regimes within the TORBED reactor for Hydrotalcite under different operating conditions.*

| Flow Rate (L/min) | Empty Bed Delta P (kPa) | Delta P (kPa)at Different Bed Loadings | | | | |
|---|---|---|---|---|---|---|
| | | 0.5g | 1g | 1.5g | 2g | 2.5 g |
| 5 | 0.03 | 0.14 | 0.29 | 0.32 | 0.45 | 2.12 |
| 10 | 0.13 | 0.58 | 0.75 | 0.89 | 1.16 | 3.72 |
| 15 | 0.28 | 0.77 | 0.98 | 1.58 | 3.79 | 9.33 |
| 20 | 0.37 | 1.89 | 3.85 | 5.67 | 14.35 | 14.27 |
| 25 | 0.6 | 2.58 | 6.58 | 10.68 | 21.25 | 23.06 |
| 30 | 0.81 | 4.68 | 10.25 | 14.65 | 24.61 | 31.1 |
| 35 | 1.11 | 8.98 | 12.68 | 16.85 | 29.04 | 38.07 |
| 40 | 1.45 | 10.35 | 13.57 | 18.98 | 35.00 | 62.19 |
| 45 | 1.75 | 14.35 | 16.68 | 19.58 | 45.34 | 71.57 |
| 50 | 2.16 | N/A | 19.78 | 25.69 | 51.86 | 77.57 |
| 55 | 2.53 | N/A | N/A | 38.25 | 67.97 | 85.51 |
| 60 | 3.03 | N/A | N/A | 42.21 | 74.14 | 93.09 |
| 65 | 3.1 | N/A | N/A | N/A | 77.55 | 101.11 |
| 70 | 3.15 | N/A | N/A | N/A | N/A | N/A |

| | | | |
|---|---|---|---|
| Un-Swirled | U | Uniformly Swirled | S |
| Collapsed | C | Over Aired | O |
| Maldistributed | M | Entrained | E |

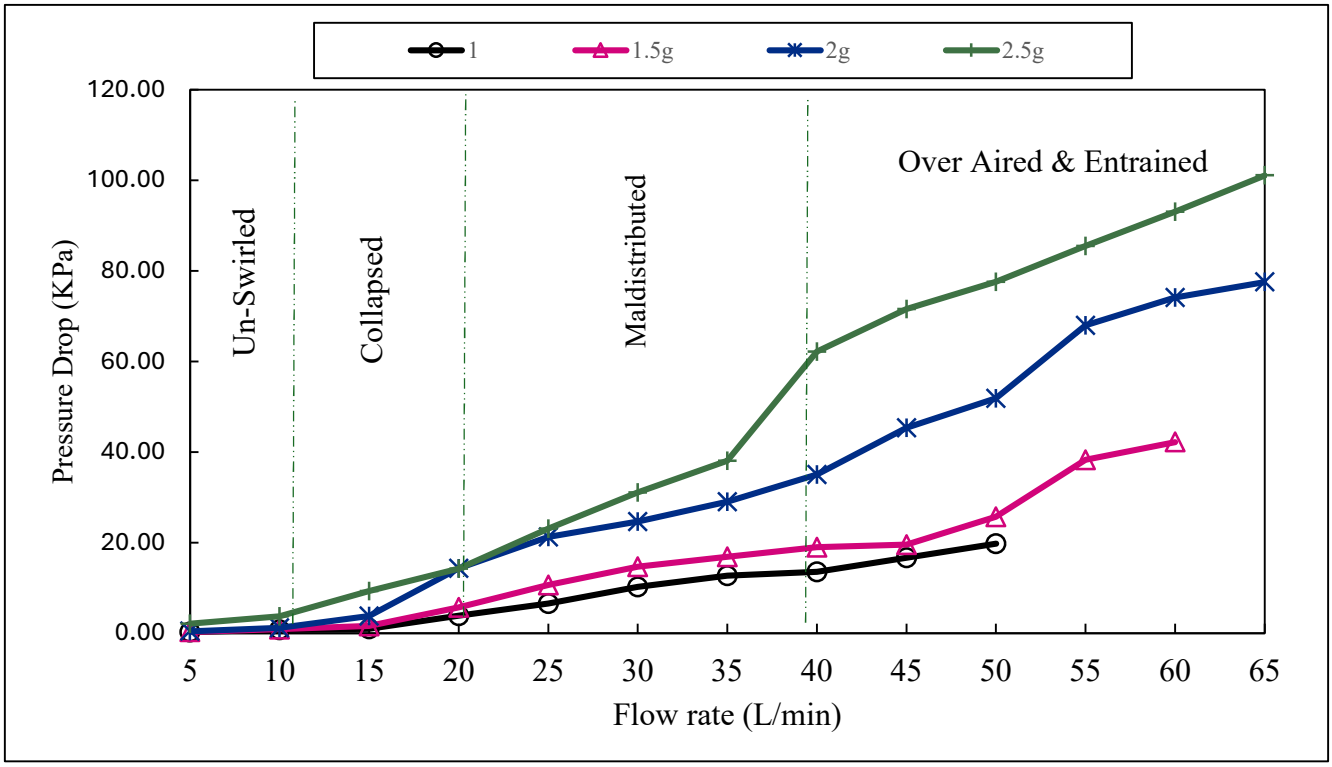


*Figure 4.3. Hydrotalcite related Pressure drop (in kPa) as a function of gas flow rate and bed loading*

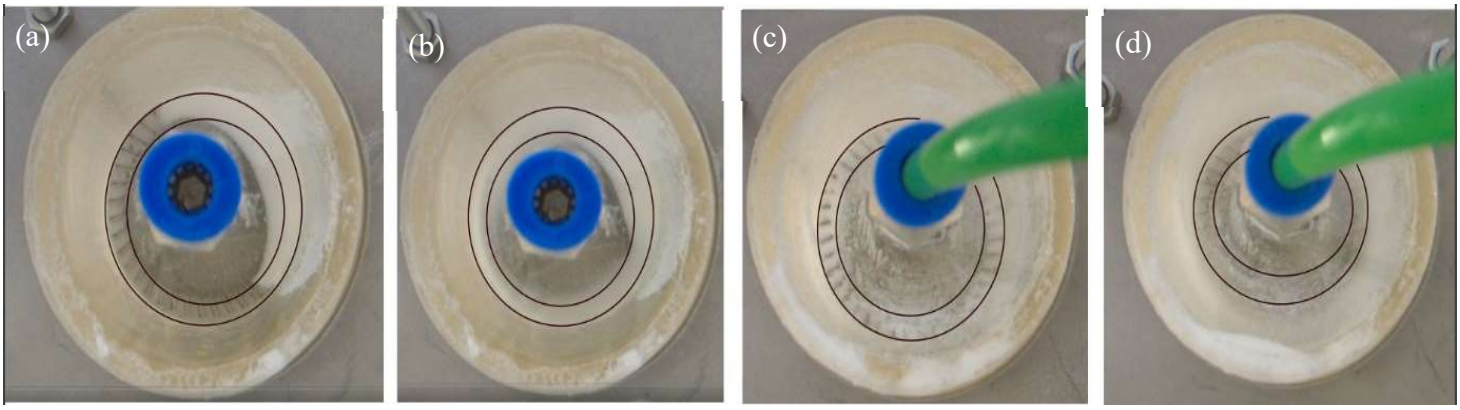


*Figure 4.4. Examples of different particle formations observed in the 3D-printed mini-TORBED with Hydrotalcite; fluidising gas = N2, bed loading = 2 g, pressure = 1 bar.g, temperature = ambient; (a) Un-Swirled, 5–20 L/min, (b) Collapsed & Maldistributed, 20-40 L/min, (c) Over Aired, 40-50 L/min, (d) Entrained, 55-65 L/min*

Table 4.4 and Figure 4.5 & 4.6 pertain to the Geldart D category, focusing on Casale sorbents characterized by larger particle size and spherical shape. The distinctive characteristics of this

sorbent type, such as its larger diameter and spoutable nature, pose challenges in achieving fluidization and swirling, especially under conditions of higher bed loading and lower flow rates. Table 4 illustrates that a higher flow rate is required for the initiation of fluidization in comparison to other sorbent groups. For instance, at a volume flow rate below 30 L/min, negligible movement is observed across all bed loading ranges (Figure 4.6a). In addition, figure 4.5 shows that pressure increases slightly with increasing the flow rate due to larger particles size, which require higher kinetic energy to fluidize.

Within the range of intermediate gas flow rates, specifically between 35–60 L/min, a collapsed regime is evident. Some sorbents initiate swirling around the bed, while the majority of particles remain stationary. An increase in flow rate intensifies the radial velocity of particles, enhancing their random motion throughout the entire bed height and leading to the manifestation of a maldistributed regime in range of 60-80 L/min for bed loading 2-2.5g, as depicted in Figure 4.5 & 4.6b.

During the transition from the maldistributed state to the over-aired state, no uniform flow regime is observed. The elevated flow rate, required to move the bulk of particles, induces arbitrary particle motion, resulting in the establishment of a uniform regime.

This dynamic behaviour further emphasizes the complicated challenges associated with achieving uniform fluidization and swirling for Geldart D group of particles under varying operational conditions.

It is noteworthy that, owing to the larger particle diameter of Casale sorbents, the associated pressure drop is considerably lower compared to other sorbent types. Even at the maximum flow rate, the pressure drop remains within the range of 3 Pa as shown in figure 4.5.

While this may be advantageous from the perspective of pressure drop considerations, it is crucial to acknowledge that this characteristic comes at the cost of a substantial increase in the kinetic energy required to fluidize the particles. The trade-off between reduced pressure drop and heightened energy requirements underline the importance of carefully balancing operational considerations when working with Geldart D (Casale) sorbents in the TORBED system.

*Table 4.4. Pressure drop (in kPa) and observed flow regimes within the TORBED reactor for Casale under different operating conditions.*

| Flow Rate (L/min) | Empty Bed ΔP (kPa) | ΔP (kPa)at Different Bed Loadings | | | | |
|---|---|---|---|---|---|---|
| | | 0.5g | 1g | 1.5g | 2g | 2.5 g |
| 5 | 0.03 | 0.03 | 0.05 | 0.08 | 0.11 | 0.13 |
| 10 | 0.13 | 0.04 | 0.09 | 0.15 | 0.22 | 0.25 |
| 15 | 0.28 | 0.08 | 0.09 | 0.24 | 0.46 | 0.48 |
| 20 | 0.37 | 0.10 | 0.19 | 0.39 | 0.65 | 0.70 |
| 25 | 0.6 | 0.22 | 0.35 | 0.55 | 0.91 | 0.99 |
| 30 | 0.81 | 0.39 | 0.49 | 0.89 | 1.22 | 1.35 |
| 35 | 1.11 | 0.43 | 0.52 | 1.18 | 1.57 | 1.75 |
| 40 | 1.45 | 0.52 | 0.62 | 1.2 | 1.71 | 1.84 |
| 45 | 1.75 | 0.58 | 0.69 | 1.4 | 1.94 | 2.02 |
| 50 | 2.16 | 0.62 | 0.72 | 1.57 | 2.1 | 2.18 |
| 55 | 2.53 | 0.67 | 0.79 | 1.68 | 2.28 | 2.36 |
| 60 | 3.03 | 0.71 | 0.85 | 1.75 | 2.37 | 2.38 |
| 65 | 3.1 | 0.74 | 0.89 | 1.87 | 2.47 | 2.54 |
| 70 | 3.15 | 0.80 | 0.92 | 1.92 | 2.51 | 2.68 |
| 75 | 3.21 | 0.81 | 0.95 | 1.98 | 2.47 | 2.75 |
| 80 | 3.35 | 0.85 | 0.98 | 2.01 | 2.47 | 2.86 |
| 85 | 3.37 | 0.87 | 1.02 | 2.05 | 2.60 | 2.93 |
| 90 | 3.41 | 0.89 | 1.05 | 2.12 | 2.84 | 3.12 |
| 95 | 3.46 | 0.89 | 1.12 | 2.15 | 2.86 | 3.14 |
| 100 | 3.51 | 0.89 | 1.15 | 2.21 | 2.82 | 3.25 |

| | | | |
|---|---|---|---|
| Un-Swirled | U | Uniformly Swirled | S |
| Collapsed | C | Over Aired | O |
| Maldistributed | M | Entrained | E |

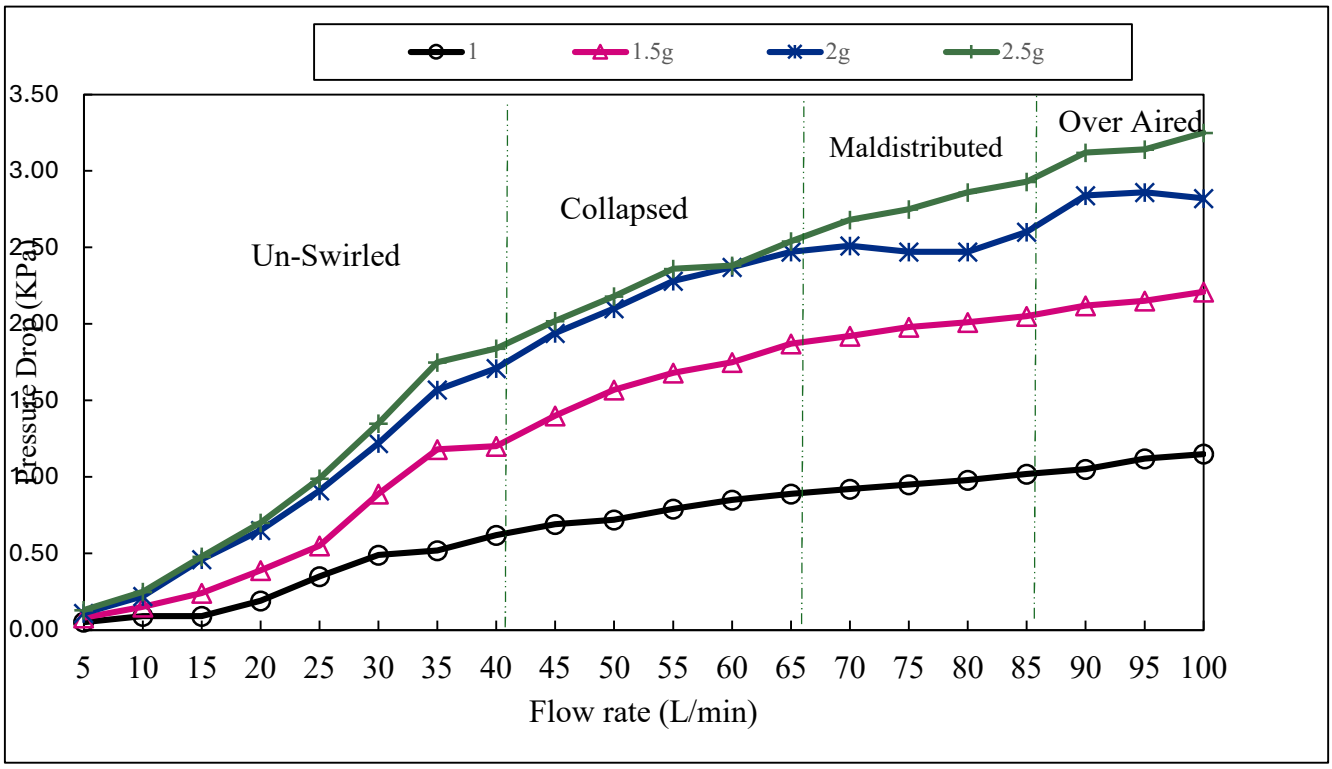


*Figure 4.5. Casale related Pressure drop (in kPa) as a function of gas flow rate and bed loading*

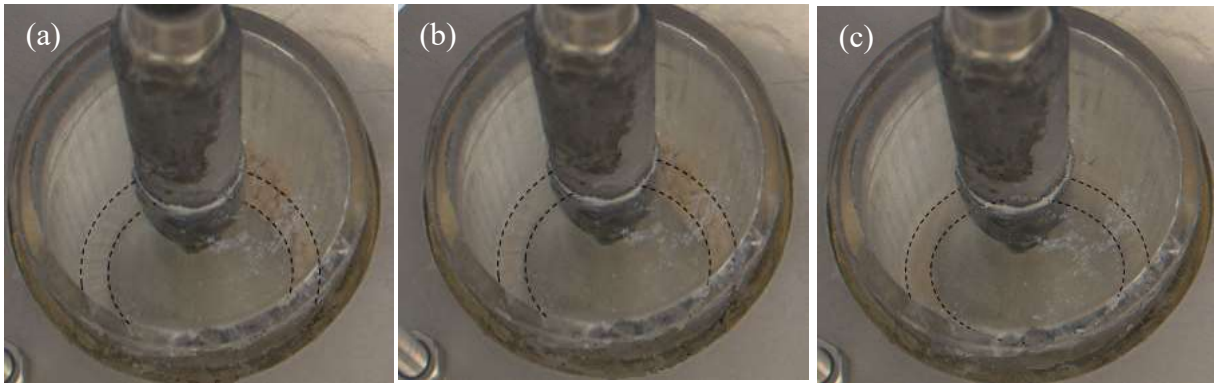


*Figure 4.6. Examples of different particle formations observed in the 3D-printed mini-TORBED with Casale; fluidising gas = N2, bed loading = 2 g, pressure = 1 bar.g, temperature = ambient; (a) Un-Swirled, 5–40 L/min, (b) Collapsed & Maldistributed, 45-85 L/min, (c) Over Aired 85-100 Lit/min*

Numerous researchers have extensively studied the variation of bed pressure drop concerning gas superficial velocity in 'conventional' fluidized beds (22, 57, 65, 88, 90, 91). In traditional fluidized beds, it is well-established that the particle pressure drop remains constant for all

superficial gas velocities exceeding the minimum fluidizing velocity, indicating the complete suspension of the buoyant weight of the particle bed in the gas phase.

However, the unique shallow particle bed configuration within the TORBED deviates from this conventional behaviour, as it lacks sufficient space for the development of bubbling or slugging phenomena (36, 82, 110). In contrast, TORBED illustrates a distinct pattern: the pressure drop for BPEI inside the bed increases with an escalation in gas flow rate as shown in figure 4.2. This phenomenon is attributed to the 'centrifugal mass' effect of the bed [82]. As particles rotate at higher speeds, they exert a greater apparent outward force, extracting energy from the fluidizing gas (57, 91). This distinction emphasizes the imperative of comprehending the hydrodynamic performance of each specific sorbent within the TORBED platform before initiating kinetic screening tests.

## 4.4 Standard Deviation Analysis

Utilizing the standard deviation of the pressure signal to distinguish flow regimes in gas-solid fluidized beds is a common and effective approach. In the context of a fluidized bed reactor, the behaviour of the standard deviation can provide insights into the prevailing flow regime.

In the packed bed regime, where particles are stationary, the standard deviation is typically close to zero due to the fixed nature of the particles [65]. As the fluidization process initiates and bubbles start to form, small pressure fluctuations corresponding to these bubbles become apparent. These fluctuations increase in intensity with higher gas velocities and larger bubble sizes [57].

Figures 4.7, 4.8, and 4.9 provide a comprehensive illustration of the standard deviation of pressure drop for each sorbent type BPEI, Hydrotalcite, and Casale across varying gas flow rates, specifically for a bed loading of 2 g. These figures provide a detailed insight into the dynamic behaviour and fluctuations in pressure drop, highlighting the unique responses of each sorbent type to variations in the gas flow rate and enabling us to discern transitions into different flow regimes within the TORBED system.

In a TORBED reactor, the standard deviation of the pressure signal is expected to exhibit distinctive characteristics across different flow regimes. Initially, in the unswirled regime, the standard deviation is minimal and near zero, reflecting the absence of particle movement and a bed appearance similar to a packed bed. As fluidization progresses, the emergence and growth of fluidization, along with particle motion, contribute to an increase in the standard deviation.

As illustrated in Figure 4.7 for BPEI sorbent, during the transition to the collapsed and maldistribution areas, the standard deviation experiences an increase due to the haphazard movement of particles around the bed. This results in significant fluctuations in bed pressure drop. In the subsequent flow regime, transitioning to uniformly swirled, where particles uniformly swirl around the bed at a lower bed height with reduced fluctuation, the standard deviation curve exhibits a flat period. This plateau could potentially be indicative of the desirable flow regime in the TORBED reactor, given that it was not observed for the other materials. Continuing with an increase in the flow rate of the feed gas, particularly in conditions of low bed loading and higher gas velocity, most particles undergo haphazard movement entire the bed, leading to an increase in bed height and a larger fluctuation in the standard deviation of pressure drop. As the gas flow further intensifies, causing most particles to adhere to the outflow, the pressure drop significantly increases. Finally, when particles are predominantly stuck to the bed wall, there is minimal fluctuation in pressure drop causing the standard deviation to drop to near zero.

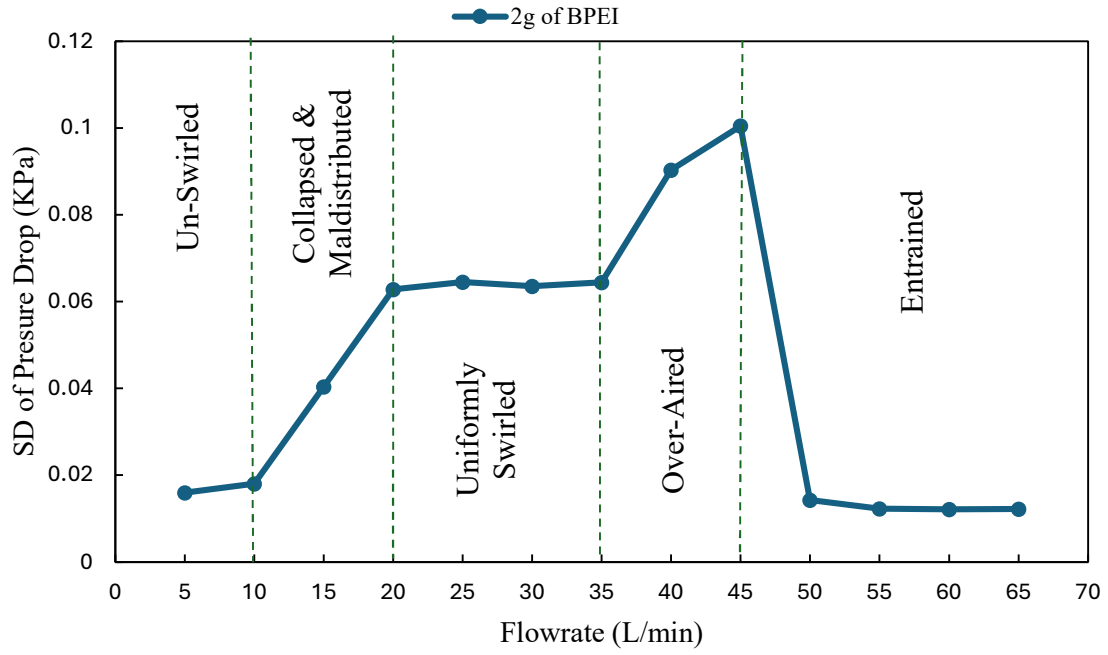


*Figure 4.7. BPEI sorbent related Standard deviation of Pressure drop (in Pa) as a function of gas flow rate for 2 g of bed loading*

Figure 4.8 presents the Standard Deviation of Pressure Drop (in kPa) for Hydrotalcite Sorbent as a function of gas flow rate, specifically for a bed loading of 2 g. The behaviour observed in the standard deviation graph for Hydrotalcite mirrors that of BPEI, highlighting similar trends

in the response to varying gas flow rates. Distinct flow regimes are discernible in the graph, analogous to those observed for BPEI. However, the uniformly swirled regime is not observed, and the expected plateau area in the standard deviation plot is notably absent.

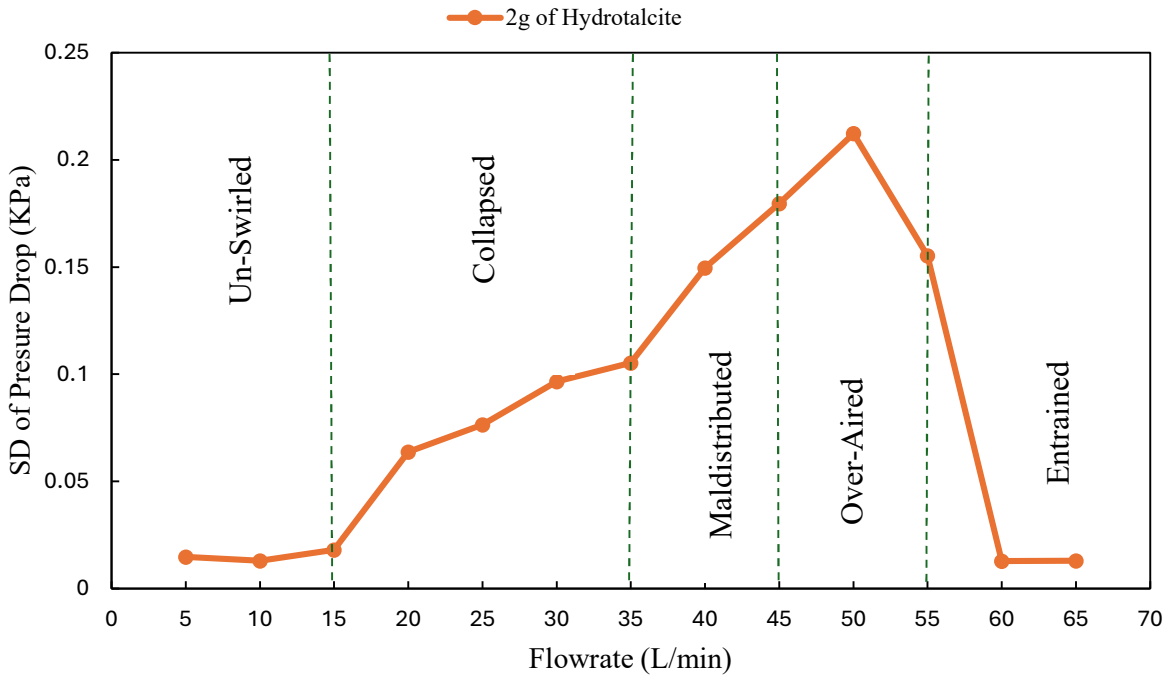


*Figure 4.8. Hydrotalcite Sorbent related Standard deviation of Pressure drop (in Pa) as a function of gas flow rate for 2 g of bed loading*

In Figure 4.7, the standard deviation behaviour for Casale Sorbent is depicted. Similar patterns are observed in different flow regimes, consistent with the behaviour observed in previous particles. However, notably, the uniformly swirled and entrained regimes, typical in other sorbent types, are not observed for Casale sorbents. Intriguingly, this distinct behaviour is also confirmed in the standard deviation plot. The absence of the uniformly swirled and entrained regimes in both the flow regime observations and the standard deviation plot emphasis on the unique characteristics and response of Casale Sorbent to varying gas flow rates.

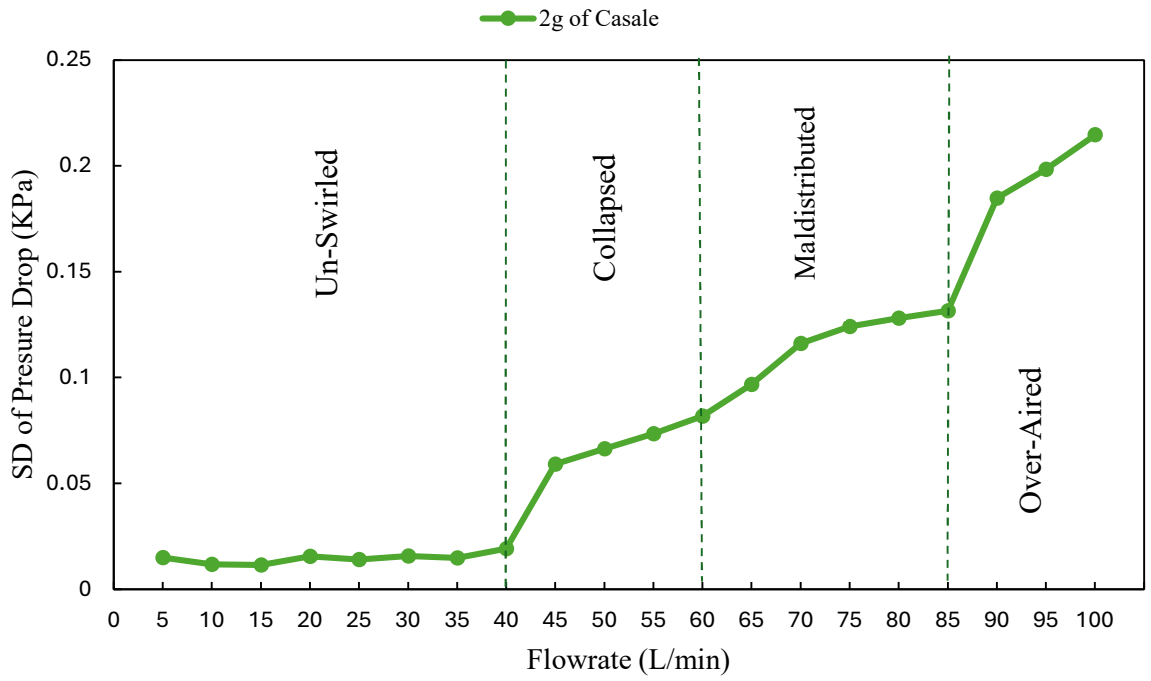


*Figure 4.9. Casale Sorbent related Standard deviation of Pressure drop (in Pa) as a function of gas flow rate for 2 g of bed loading*

## 4.5 Conclusion

In conclusion, based on the comprehensive hydrodynamic analysis encompassing high-speed camera observations, bed pressure drop measurements, and standard deviation analysis over a 2-minute period, BPEI particles emerge as the most suitable candidate for advancing to the next stage of sorbent screening in adsorption and desorption within the TORBED technology.

The hydrodynamic results indicate that BPEI particles exhibit an acceptable pressure drop across the bed and achieve the desirable flow regime characterized by uniform swirling motion. This is in stark contrast to Hydrotalcite and Casale particles, where uniform swirling motion was not observed. Hydrotalcite, characterized by its tiny size and sticky nature, induces a significant and impractical pressure drop across the bed. On the other hand, Casale particles, with their large particle size falling into Geldart group D, require substantial flow rates to initiate swirling motion, leading to considerable consumption of feed gas and energy for fluidization. In contrast, BPEI particles consistently demonstrate the desired flow regime within an acceptable range of pressure drop and flow rate, even across a wide range of bed loadings. Therefore, BPEI has been selected as the preferred sorbent for further testing in TORBED technology for adsorption and desorption processes, aligning with the favourable hydrodynamic study results.

# 5. Adsorption Results & Discussion

## 5.1 Overview of $CO_2$ Breakthrough

In this chapter, the focus is on the determination of sorbent capacity and the evaluation of adsorption kinetics, particularly within the context of breakthrough experiments conducted using the TORBED reactor. Breakthrough experiments offer valuable insights into the dynamic behaviours of adsorption systems and provide essential data for process optimization and scale-up.

One key parameter in evaluating the performance of sorbent materials is sorbent capacity, which quantifies the amount of $CO_2$ adsorbed per unit mass of sorbent. Determining sorbent capacity involves analysing breakthrough curves obtained from experimental setups. These breakthrough curves depict the concentration of $CO_2$ in the effluent gas stream over time, providing insights into the adsorption kinetics and behaviour of the sorbent material.

A common method for determining sorbent capacity involves deconvolution of breakthrough curves. This process entails comparing breakthrough curves obtained from the reactor containing the sorbent material with those obtained from an empty reactor. By subtracting the signal associated with the empty reactor from the signal obtained with the sorbent, the effects of diffusion and mixing between $CO_2$ and nitrogen ($N_2$) within the system can be mitigated. Additionally, deadtime associated with the transport of $CO_2$ from the mass flow controller to the detector is also accounted for in this analysis.

The resulting uptake curve obtained after deconvolution reflects two main components: the signal related to mass transfer within the bed and the signal associated with adsorption onto the sorbent particles. Notably, in certain reactor configurations such as the TORBED, characterized by high gas flow rates, external mass transfer resistances around the particles are minimized. Consequently, the subtracted signal predominantly represents the adsorption process, highlighting a potential advantage of such platforms in enhancing adsorption efficiency.

In this study, the primary focus is to investigate the influence of various factors, namely $CO_2$ concentration, bed loading, flow rate, and temperature, on the adsorption kinetics within the TORBED system. Here the performance of a commercial sorbent (based on branched polyethyleneimine, BPEI) was tested for capturing $CO_2$ from artificial flue gas streams comprised of different $N_2$/ $CO_2$ mixtures. Breakthrough curves were subsequently collected for a variety of $CO_2$ volume fractions (2–20 vol%), BPEI bed loads (1–2.5 g), gas flow rates (20–

35 L/min), and temperatures (40–70 °C). By systematically varying these parameters, the aim was to elucidate their individual and collective impacts on the adsorption process. The deepening of our understanding of how these factors interact and influence the efficiency and performance of $CO_2$ capture within the TORBED reactor is sought through comprehensive analysis of the resulting data.

In summary, the focus was on elucidating the sorbent capacity of adsorbent (BPEI) for $CO_2$ capture using breakthrough curve analysis. By examining the deconvoluted uptake curves, the aim was to gain insights into the adsorption kinetics and performance of sorbents. Furthermore, by fitting adsorption kinetic models to the experimental data, efforts are made to enhance our understanding of the underlying mechanisms governing $CO_2$ adsorption onto sorbent materials.

### 5.1.1 Effect of Feed $CO_2$ Concentration

To investigate the impact of $CO_2$ concentration on the adsorption kinetics within the TORBED, experiments were conducted at a temperature of 40°C, utilizing 2 grams of sorbent at a gas flow rate of 25 L/min, which was determined to be the optimal fluidization condition based on hydrodynamic tests results in previous chapter. The first four entries in Table 5.1, corresponding to ID1–4, summarize the effects of varying $CO_2$ concentration from 2% to 20% on sorbent capacity, breakthrough time ($\tau$), maximum temperature recorded during adsorption ($T_{max}$), and equilibrium $CO_2$ uptake ($q_e$). The corresponding breakthrough curves, uptake curves, and saturation time $\Delta\tau$ are illustrated in Figures 5.1a, 5.2, and 5.3a, respectively.

Figures 5.1a and 5.2 indicate that increasing $CO_2$ concentration from 2% to 20% results in a decrease in breakthrough time $\tau$ (from 4.25 ± 0.10 s to 0.55 ± 0.01s), accompanied by an increase in $CO_2$ capacity (from 1.98 ± 0.18 mmol/g to 2.64 ± 0.06 mmol/g). Furthermore, figure 5.3a demonstrates a general decrease in $\Delta\tau$ as $CO_2$ concentration rises, suggesting a more rapid saturation of the bed at higher $CO_2$ concentrations. These findings align with expectations, as the increase in concentration gradient between the gas and bulk solid enhances the diffusion coefficient, thereby increasing the internal mass transfer rate within the adsorbent. Additionally, slight tailing observed in Figures 5.1a and 5.2 at the highest concentration indicates a decrease in the mass transfer coefficient as the adsorbent approach saturation. This effect may contribute to the slight increase in $\Delta\tau$ observed at a $CO_2$ concentration of 20 vol%. Such an effect could be more pronounced at higher concentrations due to the elevated mass transfer coefficient, making any change more challenging to discern at lower concentrations.

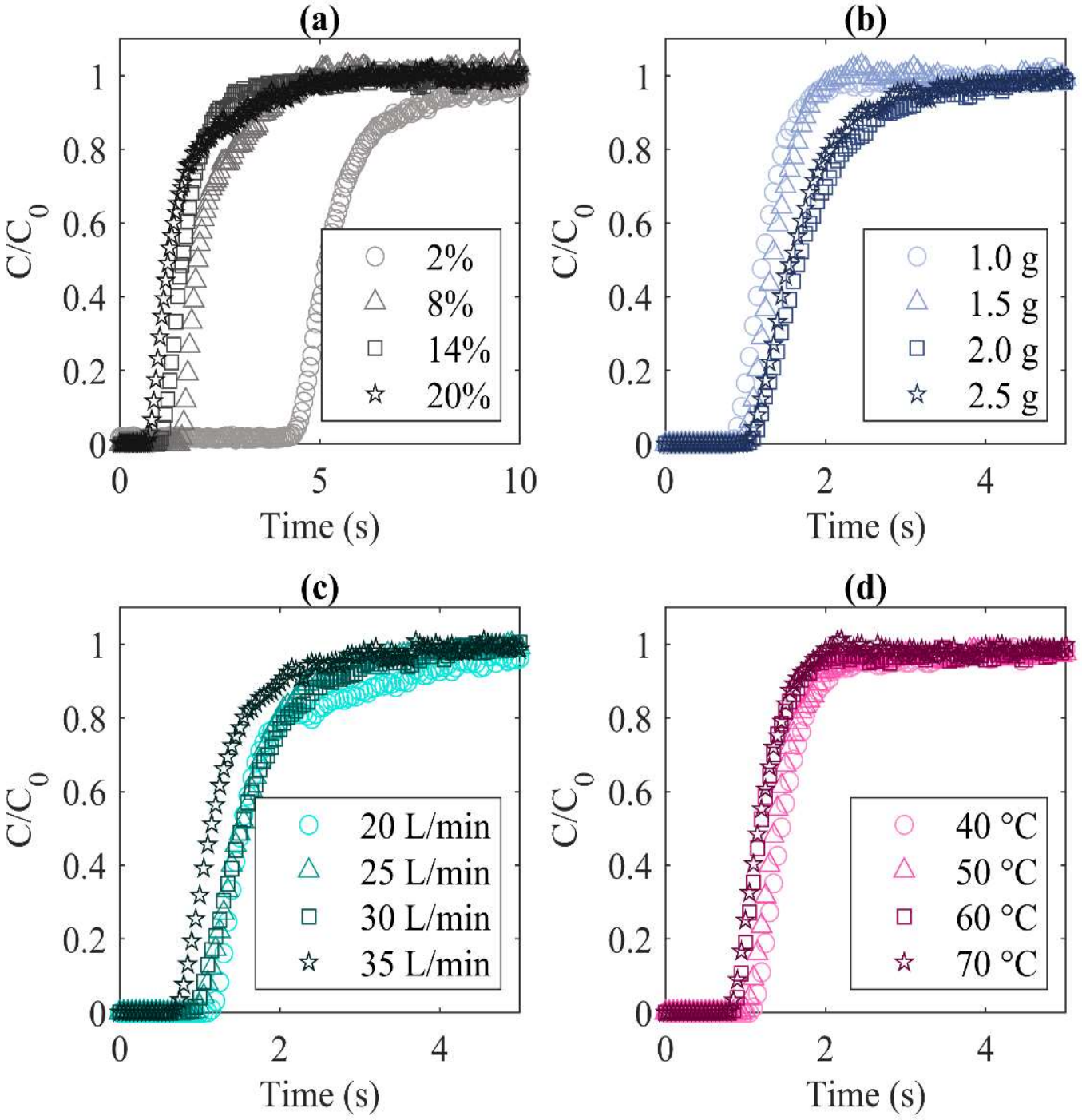


*Figure 5.1. Normalised breakthrough curves as a function of: (a) $CO_2$ concentration (ID 1–4), (b) bed loading (ID 5–8), (c) gas flow rate (ID 9–12), (c) gas temperature (ID 13–16)*

It is acknowledged that one potential limitation of the TORBED is the necessity for high gas flow rates to induce the desired swirling flow regime. This requirement underscores the need for a $CO_2$ sensor with both high sensitivity and rapid response rates to accurately capture the subtle adsorption kinetics. As a result, each experiment was conducted three time to ensure reliability, and the average values along with standard deviations were used to characterize each parameter of interest, as summarized in Table 5.1.

Variations observed between runs primarily stemmed from two sources. Firstly, the timing of $CO_2$ injection and the start of data collection needed to be as closely synchronized as possible to enable accurate subtraction of the empty bed signal from the adsorbent-filled bed. Secondly, slight fluctuations in the gas flow rate, particularly noticeable at $CO_2$ concentrations of 2 vol%, were observed from the mass flow controller, resulting in a standard deviation of ± 0.18 mmol/g. Nonetheless, the standard deviation remained within approximately 5% relative error for all conditions, indicating that the observed trends are genuine and not mere artifacts of noise. Furthermore, operating at higher $CO_2$ concentrations improved the signal-to-noise ratio of the measured signal, enhancing overall data quality and reliability.

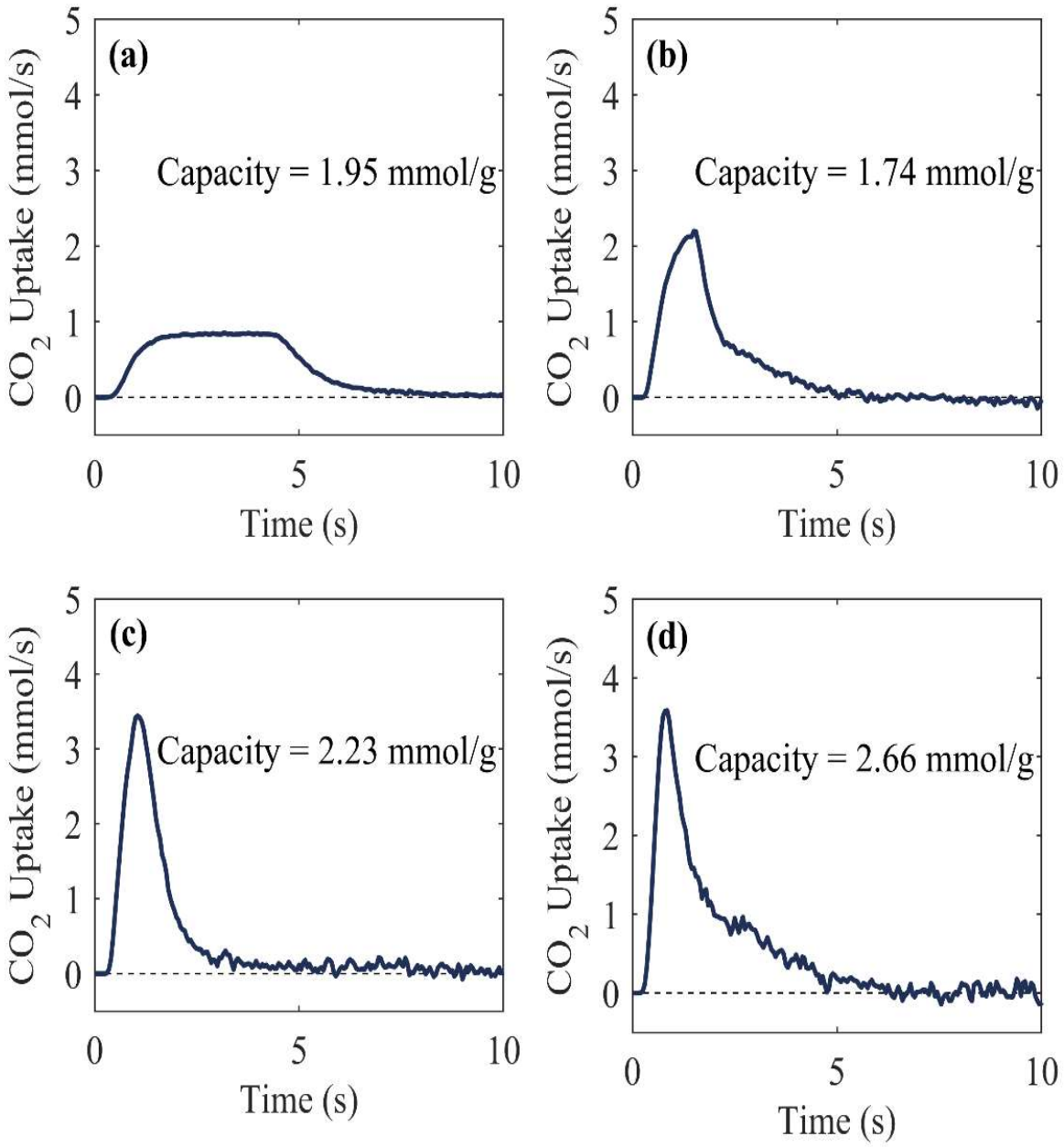


*Figure 5.2. $CO_2$ uptake curves recorded at different $CO_2$ concentrations; (a) 2 vol%, (b) 8 vol%, (c) 14 vol%, and (d) 20 vol% (note, the capacities shown in this figure correspond to a single run, whereas the capacities shown in Table 5.3 are the mean values*

`

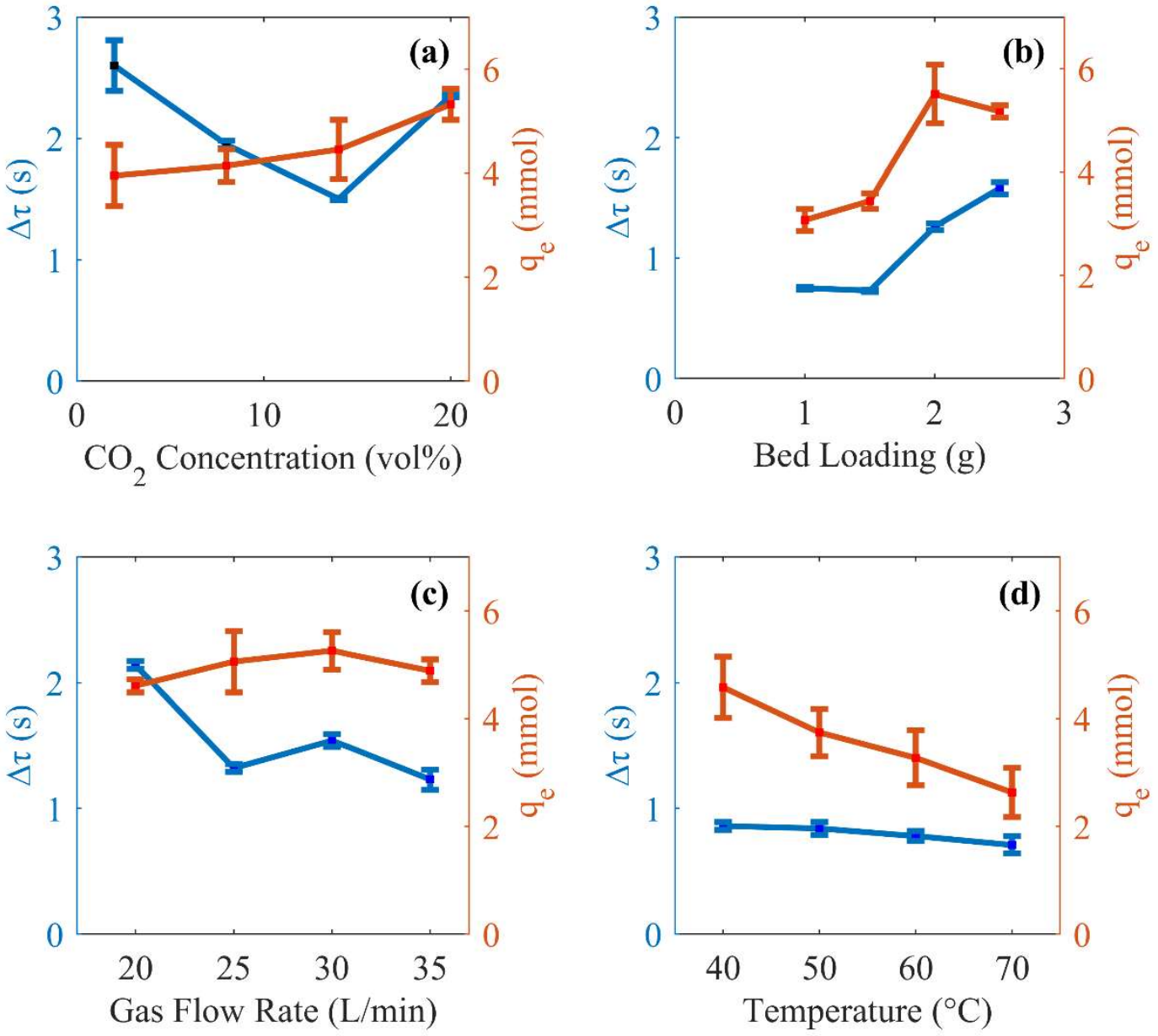


*Figure 5.3. Trend of $q_e$ (equilibrium uptake) and $\Delta\tau$ (saturation time) as a function of: (a) $CO_2$ concentration (ID 1–4), (b) bed loading (ID 5–8), (c) gas flow rate (ID 9–12), (c) gas temperature (ID 13–16)*

### 5.1.2 Effect of Bed Loading

The effect of bed loading on the TORBED platform is a crucial consideration in maintaining the desired swirling flow regime. As demonstrated in the hydrodynamics testing, both gas flow rate and bed loading significantly influence flow regime and pressure drop. To assess the impact of bed loading on kinetic behaviour, experiments were conducted at a gas flow rate of 25 L/min and 40°C, utilizing a 14 vol% $CO_2$ concentration. The resulting breakthrough curves are depicted in Figure 5.1b, with rows 5–8 in Table 5.1 (ID5–8) summarizing the kinetic parameters. Trends in equilibrium $CO_2$ uptake and $\Delta\tau$ are illustrated in Figure 5.3b.

Observations indicate that as bed loading increased from 1 to 2.5 g, sorbent capacity also increased (1.61 ± 0.02 mmol/g to 2.61 ± 0.10 mmol/g), suggesting enhanced $CO_2$ removal efficiency from the artificial flue gas. This trend aligns with findings reported in the literature [11]. The augmentation in bed loading within the TORBED improves distributor coverage, consequently reducing the likelihood of gas bypassing. Figure 5.3b further demonstrates that increased bed loading results in higher equilibrium $CO_2$ uptake and $\Delta\tau$.

Moreover, Table 5.1 reveals a slight decrease in reaction rate with increased bed loading. For instance, the fractional order rate constant $k_f$ decreased from 1.16 ± 0.15 $s^{-1}$ to 0.71 ± 0.11 $s^{-1}$. This reduction can be attributed to the increased number of active sites accompanying increased loading, without corresponding increments in driving force or temperature.

### 5.1.3 Effect of Gas Flowrate

Based on the insightful hydrodynamic test results, a discernible evolution of the flow regime is observed, transitioning from maldistributed to uniformly swirled, and eventually to entrainment as the gas flow rate escalates. This evolution precipitates a notable increase in bed height and pressure drop, underscoring the sensitivity of the system to gas flow rate variations. Consequently, it is posited that the sorbent capacity would exhibit a corresponding increase with the escalation of gas flow rate, initially transitioning from maldistributed to uniformly swirled, before potentially diminishing. Given the critical role of gas flow rate selection as a design parameter for the TORBED platform, a precise evaluation of its impact on kinetics and sorbent capacity was performed.

As shown in Figure 5.1c and expounded upon in Table 5.1 (ID9–12), the anticipated decrease in breakthrough time with increasing gas flow rate is decreased (from 1.01 ± 0.03 s to 0.57 ± 0.08 s with a 15 L/min increase). This reduction is paralleled by a corresponding decrease in $\Delta\tau$, decrease from 2.1 s to 1.2 s, signifying accelerated bed saturation at higher flow rates (refer to Figure 5.3c). Additionally, figure 5.3c illustrates a concurrent increase in equilibrium uptake (from 4.38 ± 0.12 mmol to 5.00 ± 0.16 mmol) as the gas flow rate increases from 20 to 25 L/min. This observed increase is likely attributable to the bed transitioning into the desirable uniformly swirled state, characterized by uniform velocity distribution and optimal particle packing above the distributor.

Further increase of the flow rate from 25 to 30 L/min maintains the flow in a uniformly swirled state, resulting in negligible alteration in capacity, remaining approximately at 5 mmol. However, a subsequent increase to 35 L/min induces a slight decrease in both uptake and capacity (4.89 ± 0.10 mmol and 2.42 ± 0.05 mmol/g respectively), confirming the initial hypothesis. At this elevated flow rate, particle entrainment intensifies due to marginal over-airing, leading to the uncovering of the distributor's inner periphery and consequent gas bypassing. Additionally, the heightened flow rate subtly diminishes the saturation time $\Delta\tau$, possibly due to an augmentation of the mass transfer coefficient.

*Table 5.1. Process parameters determined from the adsorption breakthrough experiments*

| Parameter | ID | Sorbent Capacity (mmol/g) | Breakthrough Time, $\tau$ (s) | $T_{Max}$ (°C) | $q_e$ (mmol) | 1st Order Model | | 2nd Order Model | | Fractional Order Model | | | |
|---|---|---|---|---|---|---|---|---|---|---|---|---|---|
| | | | | | | $k_1$ ($s^{-1}$) | $R^2$ (%) | $k_2$ (g. $mmol^{-1}.s^{-1}$) | $R^2$ (%) | $k_f$ ($s^{-1}$) | $n$ (-) | $m$ (-) | $R^2$ (%) |
| **$CO_2$ Concentration** | 1 | 1.98 ± 0.18 | 4.25 ± 0.10 | 40.6 ± 0.36 | 3.96 ± 0.36 | 0.32 ± 0.10 | 88.80 | 0.25 ± 0.09 | 42.02 | 0.12 ± 0.01 | 1.39 ± 0.55 | 1.24 ± 0.22 | 97.25 |
| | 2 | 2.10 ± 0.05 | 1.35 ± 0.03 | 41.4 ± 0.25 | 4.20 ± 0.10 | 0.68 ± 0.08 | 88.64 | 0.44 ± 0.04 | 47.48 | 0.67 ± 0.09 | 1.41 ± 0.55 | 1.69 ± 0.34 | 94.20 |
| | 3 | 2.32 ± 0.08 | 1.00 ± 0.01 | 42.1 ± 0.18 | 4.46 ± 0.16 | 0.72 ± 0.03 | 93.31 | 0.26 ± 0.03 | 63.91 | 1.05 ± 0.06 | 1.47 ± 1.04 | 2.24 ± 0.17 | 98.30 |
| | 4 | 2.64 ± 0.06 | 0.55 ± 0.01 | 43.7 ± 0.20 | 5.28 ± 0.12 | 0.96 ± 0.05 | 98.70 | 0.21 ± 0.07 | 60.05 | 1.29 ± 0.02 | 1.77 ± 0.51 | 2.16 ± 0.14 | 99.61 |
| **Bed Loading** | 5 | 1.61 ± 0.02 | 0.70 ± 0.01 | 41.2 ± 0.25 | 3.22 ± 0.05 | 1.22 ± 0.03 | 94.78 | 0.70 ± 0.08 | 63.01 | 0.86 ± 0.15 | 3.19 ± 0.95 | 3.00 ± 0.16 | 98.50 |
| | 6 | 1.79 ± 0.09 | 0.92 ± 0.01 | 41.7 ± 0.18 | 3.58 ± 0.18 | 1.23 ± 0.01 | 91.96 | 0.63 ± 0.05 | 58.88 | 0.95 ± 0.12 | 3.50 ± 0.65 | 3.22 ± 0.11 | 98.25 |
| | 7 | 2.30 ± 0.08 | 1.07 ± 0.03 | 42.4 ± 0.18 | 4.60 ± 0.16 | 0.87 ± 0.13 | 88.95 | 1.32 ± 0.12 | 01.77 | 0.86 ± 0.16 | 1.50 ± 1.04 | 2.19 ± 0.17 | 96.72 |
| | 8 | 2.61 ± 0.10 | 1.00 ± 0.05 | 42.0 ± 0.10 | 5.17 ± 0.15 | 0.80 ± 0.01 | 85.93 | 1.11 ± 0.11 | 02.00 | 0.71 ± 0.11 | 1.76 ± 0.45 | 2.41± 0.05 | 99.42 |
| **Gas Flow Rate** | 9 | 2.19 ± 0.08 | 1.01 ± 0.03 | 40.7 ± 0.40 | 4.38 ± 0.12 | 0.56 ± 0.03 | 97.10 | 0.26 ± 0.09 | 75.17 | 0.51 ± 0.05 | 1.52 ± 0.43 | 2.10 ± 0.02 | 99.57 |
| | 10 | 2.50 ± 0.08 | 0.93 ± 0.03 | 42.0 ± 0.18 | 5.00 ± 0.16 | 0.70 ± 0.05 | 93.60 | 0.14 ± 0.10 | 68.79 | 0.97 ± 0.16 | 1.59 ± 1.04 | 2.15 ± 0.17 | 99.95 |
| | 11 | 2.52 ± 0.07 | 0.91 ± 0.05 | 44.1 ± 0.33 | 5.04 ± 0.15 | 0.95 ± 0.08 | 93.19 | 0.19 ± 0.10 | 30.66 | 1.26 ± 0.09 | 2.08 ± 0.95 | 2.25 ± 0.10 | 98.72 |
| | 12 | 2.42 ± 0.05 | 0.57 ± 0.08 | 42.9 ± 0.32 | 4.89 ± 0.10 | 1.62 ± 0.05 | 97.00 | 0.28 ± 0.20 | 81.69 | 1.58 ± 0.10 | 2.48 ± 1.13 | 2.62 ± 0.12 | 99.54 |
| **Gas Temperature** | 13 | 2.32 ± 0.08 | 0.99 ± 0.03 | 42.2 ± 0.18 | 4.64 ± 0.16 | 0.80 ± 0.05 | 95.16 | 0.39 ± 0.13 | 72.19 | 0.78 ± 0.16 | 1.58 ± 1.04 | 2.18 ± 0.17 | 99.11 |
| | 14 | 1.85 ± 0.09 | 1.06 ± 0.05 | 52.3 ± 0.35 | 3.74 ± 0.18 | 0.89 ± 0.09 | 95.45 | 0.45 ± 0.02 | 75.87 | 0.82 ± 0.01 | 2.20 ± 2.55 | 2.14 ± 0.12 | 99.92 |
| | 15 | 1.75 ± 0.11 | 0.92 ± 0.04 | 62.0 ± 0.40 | 3.47 ± 0.25 | 0.93 ± 0.01 | 93.88 | 0.37 ± 0.18 | 91.23 | 0.96 ± 0.02 | 2.05 ± 0.93 | 1.98 ± 0.02 | 93.30 |
| | 16 | 1.58 ± 0.13 | 0.88 ± 0.07 | 71.7 ± 0.25 | 3.15 ± 0.26 | 1.02 ± 0.08 | 92.40 | 0.81 ± 0.14 | 64.81 | 1.01 ± 0.14 | 2.09 ± 0.44 | 2.14 ± 0.16 | 97.78 |

*Table 5.2. Comparison of $CO_2$ adsorbent performance and reactor technologies for $CO_2$ capture*

| Ref | Adsorption Technology | Sorbent | Capacity (mmol/g) | Breakthrough Time (s) | Geldart Category | Operating Temperature (°C) | Bed Loading (g) | Flow Regime |
|---|---|---|---|---|---|---|---|---|
| [8] | Confined Fluidised Bed | Pelletized 13X Zeolite | 1.56 | 136 | A & B | 25 | 100 | Expanded Bed & Fixed Bed |
| [41] | Fixed Bed | Mesoporous Carbon-supported MgO | 1.68 | - | - | 25 | 0.1 | Packed |
| [11] | Fixed Bed | Immobilized Zeolite (FAZ) | 0.76 | 600 | C | 20–80 | 2 | Packed |
| [42] | Fluidised Bed | Polyethyleneimine (PEI) | 1.8 | 200 | A | 40–90 | 2400 | - |
| [10] | Sound-Assisted Fluidisation | Activated Carbon | <0.5 | 120 | C | 25–850 | - | - |
| [19] | Packed Column | UiO-66 | 1.3 | 300 | - | 27 | 9.3 | - |
| [30] | Packed Bed | MLD-modified Zeolites | 1.62 | 42 | C | 25 | 0.065 | - |
| [20] | Packed Bed | FBNNSs/Zano | 1.78 | - | C | 0 | 0.3 | - |
| [33] | Packed Bed | Potassium-Promoted Hydrotalcite | - | 600 | D | 90 | 2,000 | Sorption Enhanced Water-Gas Shift (SEWGS) |
| [5] | Fluidised Bed | $Ca(OH)_2$ | 2.6 | 1200 | A & C | 25 | 3.45 | Bubble-Free Fluidisation |

### 5.1.4 Effect of Temperature and Heat Transfer in the TORBED

The effect of temperature and heat transfer within the TORBED system is a critical aspect to consider, particularly in the context of $CO_2$ adsorption, which is an exothermic reaction. It is well-established that increases in bed temperature can adversely impact adsorbent performance, as higher temperatures tend to drive off $CO_2$ from the sorbent. Therefore, monitoring of the bed temperature profile during experiments was essential to assess any correlation between capacity and maximum temperature. These findings are documented in Table 5.1 and visually depicted in Figure 5.4.

Additionally, the adsorbent provider, RTI, recommended an adsorption temperature of 40 °C based on their preliminary materials development. Hence, experiments at several other temperatures were conducted to evaluate potential impacts on kinetics. A consistent loading of 2 g and flow rate of 25 L/min were maintained, and a range of temperatures were explored while utilizing a 'middle' $CO_2$ concentration (14 vol%). Breakthrough curves recorded at temperatures ranging from 40 to 70 °C are illustrated in Figure 5.1d, while trends in $\Delta\tau$ and equilibrium $CO_2$ uptake ($q_e$) are elucidated in Figure 5.3d.

It is noteworthy that prior to adsorption experiments, the TORBED containing the BPEI adsorbent underwent a pre-heating and fluidization process in nitrogen gas for 10 minutes to condition the sorbent. This pre-treatment ensured that the particles and bed attained the correct setpoint temperature before the onset of adsorption experiments, thus ensuring the integrity and consistency of the experimental setup.

Given the highly exothermic nature of the carbon capture reaction within this adsorbent material, lower temperatures are thermodynamically favoured for achieving higher conversions. Analysis from Table 5.1 (ID13–16) and Figure 5.1d indeed confirms this, as higher temperatures are observed to decrease $CO_2$ capacity: from 2.32 ± 0.08 mmol/g at 40 °C to 1.58 ± 0.05 mmol/g at 70 °C. However, it's noteworthy that increasing the temperature also enhances the reaction rate. For instance, the fractional order rate $k_f$ increased from 0.78 ± 0.16 $s^{-1}$ to 1.01 ± 0.14 $s^{-1}$ for the same 40–70 °C temperature increase. Additionally, a marginal reduction in breakthrough time (refer to Table 5.1, ID13–16) and a slight decrease in $\Delta\tau$ (see Figure 5.3d) are observed with increasing temperature.

These observations can be attributed to the kinetic theory of gases: elevated temperatures result in more rapid movement of gas molecules, thereby intensifying mass transfer and augmenting the likelihood of collision with active sites within the sorbent. These trends align with findings reported in the literature as shown in table 4 [3, 9, 6, 11, 19, 42]. It's worth noting that the slightly larger error observed at higher temperatures (around ±0.13 mmol/g) stems from the response of the heater controller, which is based on the immersed thermocouple in the reactor.

While higher temperatures may be less effective for carbon capture applications, it's essential to acknowledge that flue gas streams often contain water, and the dew point of this water may vary depending on the application. In such scenarios, it's crucial to operate at temperatures above the dew point to prevent water condensation.

Another consequence of the exothermic nature of the $CO_2$ adsorption process is the imperative to precisely control bed temperature. Without proper control, reactors with inadequate heat transfer rates may develop hot spots, leading to significant localized temperature rises that adversely impact the sorbent's adsorption capacity. To address this, temperature monitoring during adsorption in the mini-TORBED was conducted using a thermocouple immersed within the freeboard region (as indicated in Figure 5.4).

As outlined in the methodology, beds were initially fluidized with nitrogen only until the target temperature and steady state were achieved. Figure 5.4 illustrates the measured temperature increases once $CO_2$ flow was activated, determined by subtracting the setpoint temperature from the measured temperature. Across all conditions, introduction of $CO_2$ to the bed resulted in a noticeable temperature rise in the freeboard region due to heat released during adsorption. Subsequently, as $CO_2$ uptake into the adsorbent reached saturation, temperatures gradually returned to the setpoint, typically within 20–30 seconds, owing to the enhanced heat transfer rates facilitated by the TORBED.

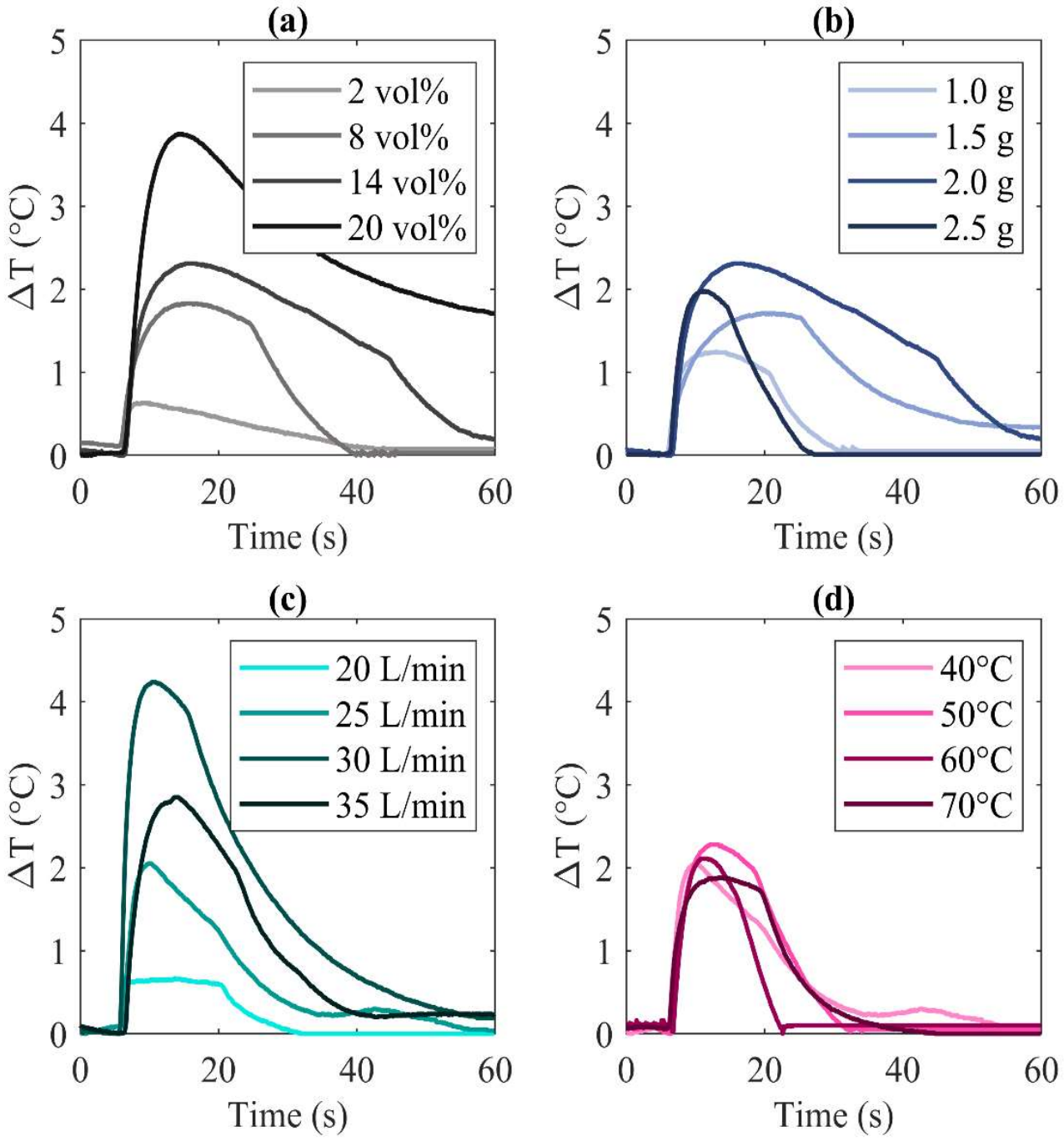


*Figure 5.4. Temperature increase as a function of: (a) $CO_2$ concentration (ID 1–4), (b) bed loading (ID 5–8), (c) gas flow rate (ID 9–12), (c) gas temperature (ID 13–16)*

Monazam et al. [111] conducted a comparative study involving a similar adsorbent, immobilized polyethyleneimine (PEI), in a packed bed, which provides a valuable benchmark for evaluating the performance of BPEI in the mini-TORBED. In their experiments, a bed depth of 25.4 cm containing 2.4 kg of PEI experienced temperature increases ranging from 10 to 15 °C at 16.7% $CO_2$ concentration (for a setpoint temperature of 40 °C) and from 15 to 20 °C at 33.3% $CO_2$ (for a setpoint temperature of 70 °C). The temperature gradually returned to the setpoint after 1800 s and 1000 s, respectively.

For a comparison with conventional fluidized beds, Girimonte et al. [11] provided insightful data. They investigated temperature variations in two distinct fluidization regimes (free bubbling and homogeneous expansion in a confined fluidized bed) using 100 g of zeolite 13X (710–800 μm). Employing a superficial gas velocity of 28.5 cm/s, an inlet $CO_2$ concentration of 10%, and a setpoint temperature of approximately 28 °C, they observed maximum temperatures of 53 °C and 39 °C in the two regimes, respectively, at breakthrough time of 14 s and 29 s. Subsequent to sorbent saturation, it took 240 s and 30 s for the beds to revert to temperatures of 40 °C and 30 °C, respectively. Remarkably, in the bubbling regime, the zeolite did not return to the setpoint temperature, indicating potential limitations of conventional fluidized bed systems in maintaining consistent operating conditions.

Figure 5.4a illustrates the impact of $CO_2$ concentration on temperature elevation within the bed. At the lowest $CO_2$ concentration (2 vol%, ID 1), a mere 0.6 °C temperature rise, equivalent to approximately 2% of the setpoint temperature, was observed. This minimal increase stemmed from the low adsorption rate, resulting in a gradual release of heat over an extended duration. As the feed $CO_2$ concentration escalated from 8 vol% to 20 vol%, the maximum recorded bed temperature also surged from 41.6 °C to 43.9 °C, representing approximately 5% and 10% increments from the 40 °C setpoint, respectively.

With increasing concentration, both the capacity and adsorption rate amplified due to the heightened driving force, consequently leading to a higher heat release. Additionally, it's noteworthy that the duration for the temperature to revert to the setpoint expanded as the concentration increased. This phenomenon can be attributed to the heightened adsorption reaction rate, resulting in more significant heat release, juxtaposed against a fixed heat transfer rate (as the gas flow rate remained constant).

Figure 5.4b depicts the relationship between the adsorbent loading and the maximum temperature within the bed. As the loading increased from 1.0 g to 2.0 g, there was a

corresponding rise in the maximum temperature. This phenomenon is elucidated in Section 3.3, where it was noted that the loading of 2.0 g facilitated the attainment of the desirable swirling state, effectively suppressing gas bypassing. Consequently, this enhanced both the reaction rate and capacity, leading to a higher amount of heat release. Conversely, when the bed was loaded with 2.5 g of material, there was a marginal decrease in the maximum temperature compared to the 2.0 g loading. This decrease can be attributed to the maldistribution that ensued as the flow regime changed. Consequently, this alteration resulted in a slightly prolonged duration for the bed temperature to return to the setpoint.

The normalized temperature profiles depicted in Figure 5.4c result from a combination of competing factors. A higher gas flow rate generates an increased swirling velocity, which effectively thins the boundary layer surrounding the adsorbent. This boundary layer typically acts as a thermal insulator. Consequently, one would anticipate an enhanced heat transfer rate, leading to a more rapid cooling effect. However, as discussed in Section 5.1.3, gas flow rates ranging from 25 to 30 L/min were identified as optimal, primarily to maximize the quality of swirling fluidization.

Interestingly, the highest temperature was observed at a gas flow rate of 30 L/min, despite the expected larger cooling rate due to the heightened heat transfer. This phenomenon arises because, at 30 L/min, the adsorption rate approached its kinetic limit, effectively preventing gas bypassing. In contrast, when the gas flow rate was increased to 35 L/min, gas bypassing occurred at the inner periphery of the bed. Consequently, this resulted in an apparent reduction in both capacity and adsorption rate, leading to a diminished release of adsorption heat. Consequently, the maximum temperature decreased from 44.1 °C to 42.9 °C (or from approximately a 10.5% increase down to a 7.5% increase, respectively).

Figure 5.4d illustrates the impact of operating temperature on the temperature profiles. Interestingly, the temperature rise exhibited a slight decrease at higher temperatures, while the time required to return to the setpoint remained comparable across all temperatures. This observation can be attributed to the slight decrease in reaction rate observed at elevated temperatures, as previously discussed.

Overall, the maximum recorded temperatures across all experiments conducted at 40°C exhibited slight variations, ranging from 40.2°C to 44.1°C. Notably, the temperature profiles generally returned to the setpoint within a timeframe of 20–30 seconds after saturation for most conditions. Considering that the corresponding breakthrough time were approximately 5 seconds, it suggests that the cooling heat transfer rate was significantly smaller than the heating heat transfer rate. This phenomenon can be attributed to the combined effects of the thermal inertia of the TORBED reactor, which has a wall thickness of 12 mm, the wool insulation surrounding the reactor (with a thickness of 50 mm), and the continuous heating of the fluidizing gas throughout the experiment. Consequently, the temperature driving force for cooling remained minimal.

Despite variations in temperature, the results affirm the TORBED platform's exceptional control over the exothermic reaction. This assurance allows us to attribute the adsorbent capacities reported in Table 5.3 primarily to other factors, such as the driving force ($CO_2$ concentration and bed loading) and contact time (gas flow rate). It is proposed that the TORBED's superior heat transfer capabilities mitigate the influence of the heat of adsorption on the observed kinetic results. By efficiently swirling the gas, the TORBED minimizes particle entrainment, ensuring optimal turbulence without suspending the bed. Consequently, the boundary layers around the particles are nearly eliminated, enhancing heat and mass transfer rates. Any temperature rise due to adsorption heat is swiftly dissipated by the excess thermal mass of the fluidizing gas, rapidly cooling the bed. This phenomenon aligns with findings by Girimonte et al. [11] on confined fluidized beds, where increasing gas velocity resulted in decreased maximum bed temperature due to enhanced heat transfer between particles and the bed wall.

## 5.2 Kinetic Modelling

Figure 5.5 compares the pseudo first-order, pseudo second-order, and fractional-order kinetic models with some of the experimentally measured cumulative $CO_2$ uptake curves (conditions ID4, 5, 9, and 14 in Table 5.1). Table 5.1 summarises the fitted parameters and corresponding $R^2$ values for all conditions.

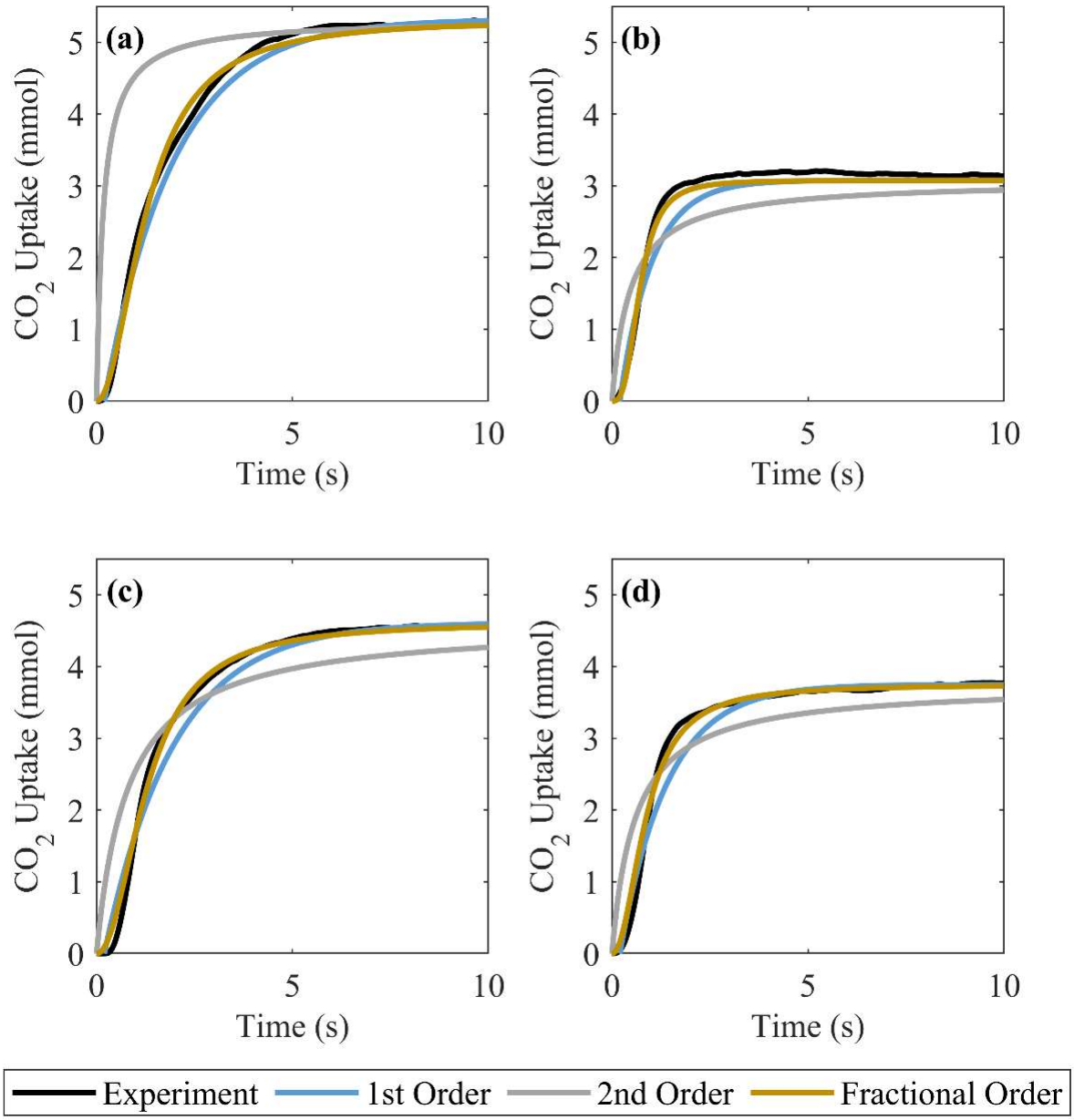


*Figure 5.5. Comparison of the experimentally measured cumulative $CO_2$ uptake curves in the TORBED against the pseudo first-order, pseudo second-order, and fractional-order models at different conditions; (a) ID4, (b) ID5, (c) ID9, (d) ID14*

In all tested conditions, the fractional order model exhibited the best fit to the experimental data, consistently yielding $R^2$ values exceeding 99%. Following closely, the pseudo first-order model also provided a good fit, with $R^2$ values ranging from 89% to 99%. Conversely, the pseudo second-order model performed poorly, with $R^2$ values ranging from just 2% to 91%. This discrepancy arises from the second-order model's inability to accurately describe both the final equilibrium uptake ($q_e$) and the uptake rate simultaneously. As illustrated in Figure 5.5,

the second-order model either matched the value of $q_e$ while overestimating the adsorption rate, or roughly matched the adsorption rate while undershooting $q_e$.

The process of $CO_2$ adsorption involves both physical and chemical mechanisms, known as physisorption and chemisorption, respectively. Physisorption entails the formation of physical bonds between the gas molecule and the adsorbent, such as Van der Waals interactions. On the other hand, chemisorption involves reactions between $CO_2$ and the active sites of sorbent molecules. Therefore, adsorption is typically controlled by either physisorption, chemisorption, or a combination of both. Additionally, the diffusion of $CO_2$ to the outer and inner surfaces of the sorbent through internal pores and channels can influence the shapes of the kinetic curves.

Figure 5.5 illustrates that the first-order model initially underestimates the uptake, followed by a gradual convergence to the observed equilibrium uptake as the adsorption process progresses. This behaviour is characteristic of a bulk diffusion process, which the first-order model describes, and is suitable for capturing the physisorption mechanism, particularly at low surface coverage [111] . Notably, the first-order model tends to provide a closer fit to the experimental data at higher $CO_2$ concentrations (as exemplified in Table 5.1 and Figure 5.5a), presumably due to the amplified driving force and faster diffusion rates.

Furthermore, the performance of the first-order model improved with increasing temperature, likely due to the reduction in surface coverage associated with the exothermic nature of the reaction. However, as the bed loading increased, the fit of the first-order model deteriorated, with the $R^2$ decreasing from approximately 95% to 85% as the loading increased from 1.0 to 2.5 g. This degradation in fit can be attributed to the improved flow regime quality and consequent enhancement in equilibrium uptake and capacity associated with higher loadings. Consequently, a higher coverage of active sites may have occurred, limiting the applicability of the first-order model.

The second-order model consistently exhibited the poorest performance among the three models, failing to accurately represent the uptake dynamics and equilibrium uptake values observed in the experiments. Typically, the second-order model is well-suited for systems governed by chemisorption mechanisms, where there is a strong chemical bond between the adsorbate and adsorbent. However, its inadequacy in capturing the experimental data suggests that physisorption mechanisms likely play a more significant role in the adsorption process of the BPEI material.

The fractional-order model, commonly utilized for describing complex adsorption processes combining physisorption and chemisorption mechanisms, offers a significantly closer fit to the experimental data, as evident in Figure 5. It effectively captures the characteristic 'S'-shaped uptake curve observed under most conditions, indicating a hybrid adsorption mechanism in the BPEI sample. This curve is characterized by three key features: midpoint, steepness, and tail.

The midpoint of the 'S' curve denotes a breakthrough time, influenced by operating conditions. For instance, higher temperatures decrease sorbent capacity, leading to shorter breakthrough time, while elevated $CO_2$ concentrations enhance the driving force, resulting in shorter breakthrough time at constant gas flow rates. The steepness of the curve is governed by the gas flow rate and $CO_2$ concentration, with higher values of both parameters intensifying the steepness and decreasing $\Delta\tau$.

The tail of the breakthrough curve reflects the process of equilibrium establishment. Higher $CO_2$ concentrations yield longer tails, indicating a prolonged time between the midpoint and equilibrium, likely due to a reduced driving force as the mass transfer coefficient decreases towards the end of the adsorption process. Minimizing tailing is crucial for reducing saturation time, ensuring an 'ideal' S-curve with minimal tailing.

In the fractional-order model (Eq. 3), the adsorption rate is further influenced by two empirical coefficients: n and m. The coefficient n serves as a measure of the driving force, akin to the number of active sites within the adsorbent core or the level of diffusion resistance. A higher n value indicates either a greater number of active sites or reduced internal resistance. As depicted in Table 5.1, n exhibits an expected increase with rising $CO_2$ concentration and gas flow rate, attributable to heightened driving forces. Conversely, increasing bed loading leads to a decrease in n, likely due to gas bypassing caused by changes in the flow regime. A marginal increase in temperature also tends to elevate n, potentially due to enhanced internal mass transfer resulting from faster molecular diffusion.

On the other hand, the coefficient m characterizes the speed of the adsorption process. It was observed that m escalates with higher gas flow rates and diminishes with increased loading, consistent with expectations. Higher flow rates expedite saturation, while higher loadings tend to slow down saturation rates, provided other variables remain constant.

## 5.3 Conclusion

In this study, the efficacy of a commercially available sorbent, based on branched polyethyleneimine (BPEI), was evaluated in capturing $CO_2$ from artificial flue gas streams composed of varying $N_2$/ $CO_2$ ratios. Breakthrough curves were subsequently generated across a range of $CO_2$ volume fractions (2–20 vol%), BPEI bed loads (1–2.5 g), gas flow rates (20–35 L/min), and temperatures (40–70 °C). Notably, our experiments in the TORBED yielded a high sorbent capacity of 2.64 ± 0.06 mmol/g, achieved within experiment durations lasting no longer than 10 seconds. This rapid data collection rate underlines the potential for high throughput screening. Additionally, by monitoring bed temperature throughout each experiment, it was observed that the high heat transfer rates within the mini-TORBED effectively minimized the influence of heat of adsorption on the kinetics.

The adsorption outcomes affirm the advantageous impact of the TORBED on enhancing the efficacy of the adsorption process. The highlighted results are as follows:

- Optimized $CO_2$ Capacity: Under optimal operational conditions characterized by uniformly swirled flow regimes, the TORBED showcased its prowess by achieving the highest recorded $CO_2$ capacity of 2.64 ± 0.06 mmol/g. This pinnacle performance was notably observed within specific ranges of bed loadings (1.5–2 g) and gas flow rates (25–30 L/min), tailored to the employed adsorbent. Conversely, deviations such as bed mal-distribution or entrainment led to diminished capacities, primarily attributed to gas bypassing.
- Flow Regime Dominance: Within the TORBED domain, the $CO_2$ adsorption capacity of BPEI demonstrated a significant correlation with prevailing flow regimes, overshadowing the influence exerted by variations in gas flow rates alone. This observation shows the TORBED's unique capability in modulating flow dynamics, thereby optimizing adsorption performance.
- Temperature Sensitivity: Operating temperature fluctuations wielded discernible impacts on adsorption capacities. Elevated temperatures induced reduced capacities due to the inherently exothermic nature of the carbon capture reaction. Conversely, lower temperatures favoured thermodynamically favourable adsorption. Notably, the TORBED exhibited adept temperature regulation capabilities, evidenced by minimal temperature escalations of merely 2 °C across all operational conditions. This accomplishment is attributed to its ability to accommodate higher gas velocities pre-

entrainment, thereby facilitating efficient heat dissipation and preserving adsorbent kinetics and capacity.

- Kinetic Modelling Insights: Kinetic modelling endeavours entailed fitting various models to cumulative $CO_2$ uptake curves. Among these models, the fractional-order model emerged as the closest approximation to experimental data, effectively encapsulating the characteristic 'S'-shaped uptake curve. This observation suggests the coexistence of physisorption and chemisorption mechanisms within the BPEI adsorbent under the study conditions, further validating the TORBED's efficacy in facilitating diverse adsorption phenomena.

# 6. Desorption Results & Discussion

## 6.1 Introduction

In adsorption chapter, the impressive adsorption capabilities of branched polyethylenimine (BPEI) within the confines of a small-scale swirling fluidized bed reactor was highlighted, achieving a notable working capacity of approximately 2.6 mmol/g at 40 °C and 2 bar. Also, Toroidal Fluidized Bed (TORBED) reactor platform offers efficient gas-solid interaction, effectively mitigating gas bypassing and hot spot formation through its superior convective heat transfer rates.

The objective of this chapter focuses on exploring the desorption behaviour of the same BPEI material, aiming to understand its kinetics and cyclic stability. While Temperature Swing Adsorption (TSA) presents a straightforward approach compatible with the TORBED reactor platform, its implementation encounters challenge due to the significant deadtime inherent in the system. This deadtime primarily stems from the 3D printed polymer reactor structure's high thermal inertia, leading to prolonged heating and cooling periods that impede the study of desorption kinetics. The majority of the experiment consist of waiting for the bed to heat or cool, which inhibits the study of the desorption kinetics.

Therefore, in the present chapter, the implementation of the TSA approach itself was studied to see how these impacts on the desorption behaviour (kinetics and cyclic stability) of the BPEI material. The principal challenge is the deadtime whilst the bed is heated from the ‘optimal’ adsorption temperature of 40 °C to the target 110 °C desorption temperature. Consequently, it can be seen how this deadtime influences the desorption process by comparing this preheating approach to one where desorption is performed at the same temperature as adsorption. Here the advantage of 3D printing has been taken to redesign the TORBED so that it can be introduced a secondary heated nitrogen gas stream. It should be emphasised that for adsorption to be successful in the $CO_2$ capture landscape, the sorbent material and technology must be developed in tandem; comment on this dual development from the perspective of desorption are presented throughout the present manuscript. Our experimental investigations unveil noteworthy insights:

Kinetic analyses reveal that the fractional-order kinetic model emerges as the optimal fit for characterizing the desorption behaviour of our PEI adsorbent. This finding stresses the multifaceted nature of the adsorption-desorption interplay, implicating the involvement of

concurrent molecular interactions, physisorption, and chemisorption processes. The inadequacy of simpler pseudo 1st or 2nd order models in capturing this complexity underscores the complicated nature of PEI adsorption mechanisms.

## 6.2 Desorption Results

In this chapter, the influence of temperature, gas flow rate, and $CO_2$ concentration on desorption processes have been investigated. Table 6.1 outlines the key performance metrics used in analysis, while Table 6.2 provides a summary of the corresponding results.

*Table 6.1. Key Performance Metric Definitions*

| Metric | Nomenclature | Units | Definition |
|---|---|---|---|
| Breakthrough Time | $t_b$ | s | Defined as time for $CO_2$ to change by more than 5% from the initial value |
| Desorption Time | $t_{95}$ | s | Defined as time for $CO_2$ concentration to reach 5% (or 95% of starting value) |
| Adsorbed Capacity | $q_{ads}$ | mmol/g | Amount of $CO_2$ adsorbed per gram of material |
| Amount Desorbed | $q_{des}$ | mmol/g | Amount of $CO_2$ desorbed/released per gram of material |
| Desorption Efficiency | $\varepsilon_{des}$ | % | $(q_{des}/q_{ads}) \times 100$ |
| Pre-Heating Rate | $\dot{Q}$ | °C/s | $(T_{des} - T_{ads})/t$ |

Precise temperature control emerged as a crucial factor in elucidating desorption kinetics across various applications. Prioritizing in situ desorption over ex situ regeneration methods, such as vacuum oven treatments, offers distinct advantages, particularly in evaluating cyclic stability (41, 42, 108) . To explore the effects of temperature configurations on desorption kinetics, comparative analyses of two different in-situ adsorption-desorption setups was conducted.

In the first group of experiments (ID1-3, Table 6.2), desorption occurred at the same temperature as adsorption, specifically at 40 °C, 80 °C, and 110 °C. While not strictly conforming to TSA, this approach eliminates preheating periods, enabling clearer observation

of temperature effects on desorption kinetics. However, it results in varying initial and equilibrium adsorbed $CO_2$ quantities at different temperatures. Subsequent experiments (ID3-18, Table 6.2) involved desorption at higher temperatures than adsorption, introducing a heating delay but ensuring complete desorption and consistent initial $CO_2$ adsorption quantities across different temperatures. Three temperature combinations low, medium, and high and varied preheating time from 15 s to 45 s has been explored, also maintaining $CO_2/N_2$ flow during preheating to maintain the adsorbent in the saturated state (ie prevent/minimize desorption during pre-heating period).

For both TSA configurations ($T_{ads}=T_{des}$ and $T_{des}>T_{ads}$), a reverse breakthrough technique during desorption employed, switching off $CO_2$ flow while fluidizing the bed with heated nitrogen gas. Outlet $CO_2$ concentration and bed temperature were monitored, comparing desorption curves with blank baselines recorded under each condition to assess desorbed capacity and kinetics.

Figure 6.1 illustrates adsorption and desorption breakthrough curves and bed temperature profiles for both TSA configurations. Notably, maintaining $CO_2/N_2$ flow during preheating ensured minimal differences between BPEI and blank breakthrough curves, with the calculated desorbed amount in order of ±0.001 mmol/g which can be consider as experimental noise.

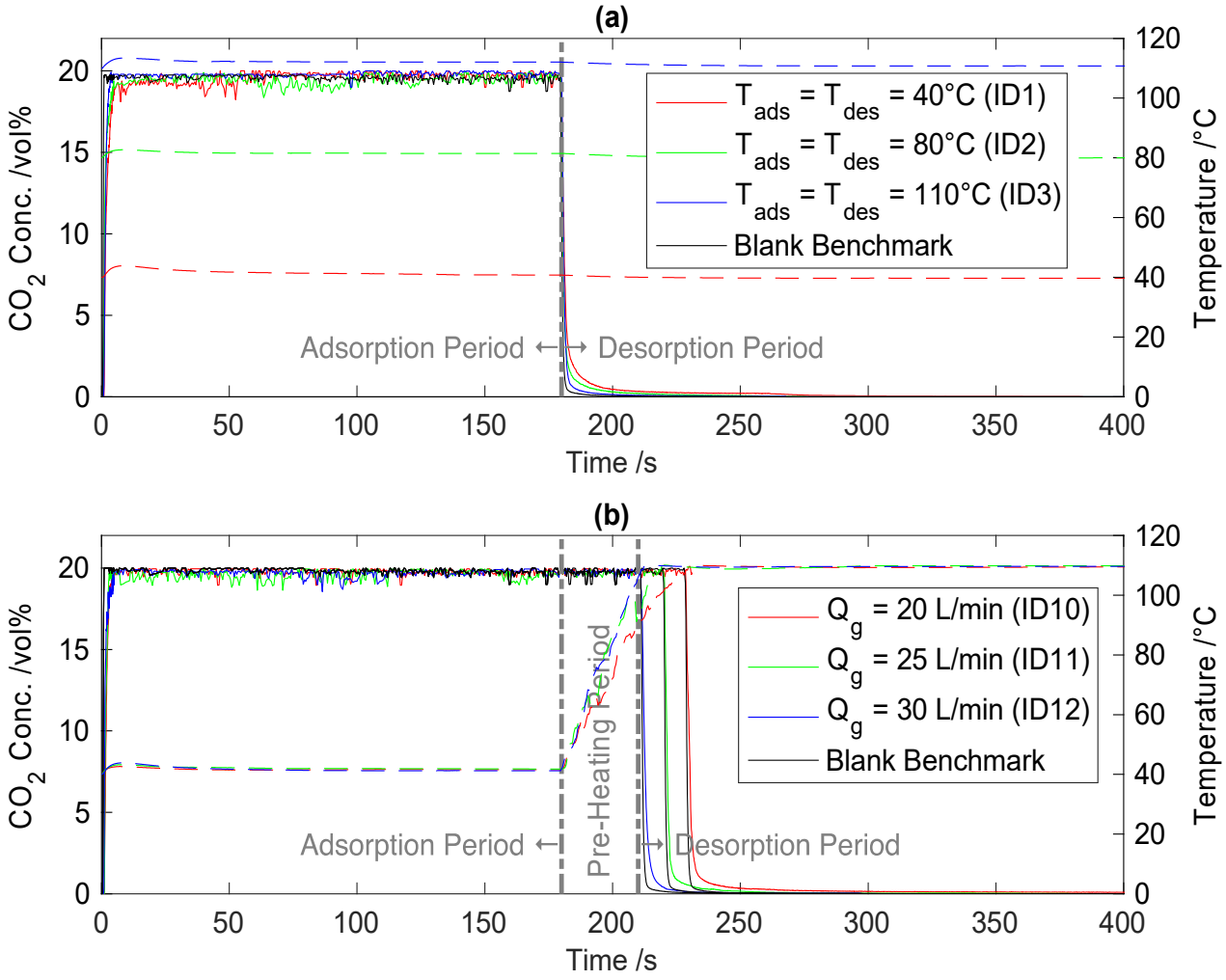


Figure 6.1. Normalised adsorption and desorption breakthrough curves and bed temperature profiles measured during a single TSA cycle; (a) T_ads=T_des¬ at different temperatures (40°C, 80°C & 110°C), and (b) T_des>T_ads at different gas flow rates (20 L/min)



(b)

*Table 6.2 Summary of Breakthrough Experiments Results*

| ID | $q_{ads}$ (mmol/g) | $q_{des}$ (mmol/g) | $t_b$ (s) | $t_{95}$ (s) | $\varepsilon_{des}$ (%) | $\dot{Q}$ (°C/s) |
|---|---|---|---|---|---|---|
| 1 | 2.44 ± 0.02 | 0.33 ± 0.06 | 1.11 ± 0.02 | 8.21 ± 0.12 | 13.52 | - |
| 2 | 2.16 ± 0.02 | 0.83 ± 0.02 | 0.91 ± 0.01 | 5.64 ± 0.10 | 41.60 | - |
| 3 | 1.46 ± 0.05 | 1.16 ± 0.09 | 0.62 ± 0.01 | 3.79 ± 0.09 | 79.45 | - |
| 4 | 2.33 ± 0.05 | 0.86 ± 0.02 | 1.20 ± 0.08 | 7.02 ± 0.09 | 36.90 | 1.34 |
| 5 | 2.46 ± 0.02 | 1.01 ± 0.08 | 1.09 ± 0.04 | 6.45 ± 0.06 | 41.46 | 1.73 |
| 6 | 2.55 ± 0.03 | 1.15 ± 0.04 | 0.82 ± 0.02 | 6.12 ± 0.08 | 45.09 | 2.42 |
| 7 | 1.85 ± 0.06 | 1.48 ± 0.10 | 1.19 ± 0.03 | 4.25 ± 0.06 | 80.25 | 1.35 |
| 8 | 2.15 ± 0.03 | 1.81 ± 0.04 | 1.05 ± 0.05 | 3.25 ± 0.05 | 84.41 | 1.76 |
| 9 | 2.33 ± 0.04 | 2.06 ± 0.05 | 0.74 ± 0.02 | 2.90 ± 0.06 | 88.41 | 2.40 |
| 10 | 2.30 ± 0.02 | 1.80 ± 0.01 | 1.25 ± 0.06 | 4.55 ± 0.08 | 78.26 | 1.34 |
| 11 | 2.48 ± 0.01 | 2.13 ± 0.01 | 1.12 ± 0.04 | 3.99 ± 0.09 | 85.88 | 1.75 |
| 12 | 2.53 ± 0.01 | 2.22 ± 0.05 | 0.84 ± 0.01 | 3.15 ± 0.06 | 87.74 | 2.50 |
| 13 | 1.99 ± 0.03 | 1.52 ± 0.01 | 1.55 ± 0.02 | 8.51 ± 0.14 | 76.38 | 1.83 |
| 14 | 2.24 ± 0.03 | 1.82 ± 0.06 | 1.32 ± 0.05 | 5.46 ± 0.10 | 81.25 | 1.79 |
| 15 | 2.50 ± 0.02 | 2.14 ± 0.16 | 1.11 ± 0.04 | 3.85 ± 0.08 | 85.87 | 1.75 |
| 16 | 1.69 ± 0.02 | 1.37 ± 0.02 | 1.79 ± 0.06 | 7.95 ± 0.12 | 81.06 | 1.89 |
| 17 | 1.88 ± 0.01 | 1.60 ± 0.04 | 1.52 ± 0.06 | 4.98 ± 0.10 | 85.10 | 1.81 |
| 18 | 2.11 ± 0.02 | 1.85 ± 0.05 | 1.05 ± 0.02 | 3.15 ± 0.08 | 88.00 | 1.76 |

### 6.2.1 Effect of Temperature on Adsorption and Desorption Capacities

The effect of temperature on adsorption is reported in previous chapter 5 sections. Briefly, the effect of temperature on adsorption is complex and depends on various factors, including the nature of the adsorbent and adsorbate, the strength of the adsorbate-adsorbent interaction, and the heat of adsorption. Adsorption of $CO_2$ onto the BPEI does not seem to be diffusion-limited in our case because increasing the temperature would be expected to improve the diffusion rate which would lead to an increased rather than decreased apparent adsorption capacity [20]. Whereas, the adsorption capacity amount decreased by 40% with increasing the temperature from 40 °C to 110 °C (see ID1-3 in Table 6.2).

Consequently, $CO_2$ adsorption into the BPEI adsorbent seems to be thermodynamically (equilibrium) and/or kinetically (rate)-limited. As other studies have shown (20, 54, 107), since the adsorption process is exothermic, any increase in temperature will generally shift the equilibrium towards one with a lower capacity. *Ergo*, increased temperature weakens the binding affinity of $CO_2$ to the surface (41, 108).

The effect of temperature on the desorption process is similarly influenced by the strength of the adsorbent-adsorbate bond, surface area of the adsorbent, type of adsorbate, *etc.* For weakly adsorbed molecules, lower temperatures may be sufficient to cause desorption, while strongly adsorbed molecules may require much higher temperatures. Additionally, adsorption and desorption are in equilibrium; changing the temperature can shift this equilibrium towards the adsorbed or desorbed state. According to Le Chatelier's principle, an increase in temperature favours the endothermic reaction, which in this case, corresponds to the desorption process [42]. Accordingly, temperature is a key design factor for the regeneration of the BPEI adsorbent due to the nature of the chemical interactions between $CO_2$ and surface. As the temperature increases, the $CO_2$ is expected to bind more weakly to the BPEI. Further, the BPEI polymer itself becomes more flexible at higher temperatures (111, 112), which improves the permeability of $CO_2$ in the pores, which can also further increase the apparent desorbed amount. However, desorption at very high temperatures can also potentially introduce thermal stress to the material, so careful consideration should be given to the sorbent's thermal properties and structural integrity [66].

There are several ways to quantify the influence of temperature on the desorption process. First, Figure 6.2 shows how the desorption efficiency is affected by the desorption temperature for both configurations of TSA across all experiment conditions. Clearly the desorption temperature has the strongest effect on the regeneration efficiency, since changes in $CO_2$ concentration and total gas flow rate produce little spread in the data at each temperature. The same trend is widely reported for desorption across various reactor types (54, 108). Additionally, the same regeneration efficiency is observed whether the adsorption and desorption temperatures were the same ($T_{ads} = T_{des}$), or when the desorption temperature was higher than adsorption ($T_{des} > T_{ads}$).

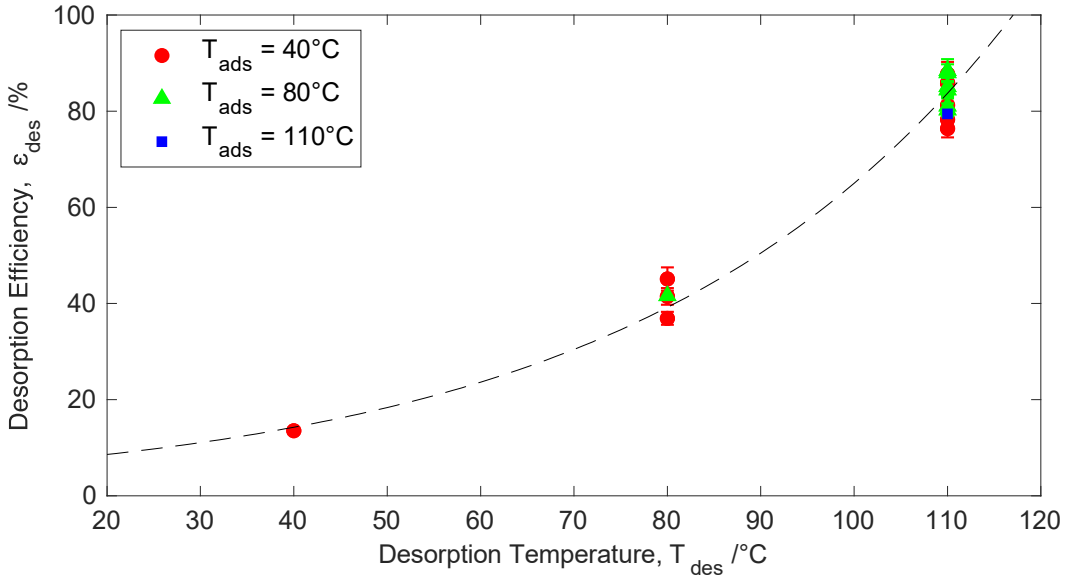


*Figure 6.2 Desorption efficiency as a function of desorption temperature (error bars omitted for clarity; see Table 3)*

To further understand the desorption efficiency results, the measured desorbed capacity can be plotted against the corresponding measured adsorbed capacity as shown in Figure 6.3. Unsurprisingly, the desorption capacity is highly correlated with the adsorbed amount for all experiment conditions (more $CO_2$ can be desorbed if more was adsorbed on the surface). Increasing the desorption temperature shifts the desorbed capacity to the theoretical maximum, defined by the adsorbed capacity (dotted line in Figure 6.3). Though as mentioned earlier, higher temperatures also risk enhanced material degradation due to thermally induced stresses.

The lowest desorption capacities at each desorption temperature correspond to the '$T_{ads} = T_{des}$' isothermal TSA configuration. Here, the highest adsorption capacity (2.44 mmol/g) and lowest desorption capacity (0.33 mmol/g) were obtained at 40 °C, while the lowest adsorption capacity (1.46 mmol/g) and highest desorbed capacity (1.16 mmol/g) were obtained at 110 °C. Therefore, by maintaining the same temperature for both adsorption and desorption, it is not possible to capture the optimal conditions for each process. Ultimately, it has been observed that the adsorption process indirectly influences the study of the desorption process, since the amount of adsorbed $CO_2$ is not a directly controlled variable; it depends on the adsorption conditions.

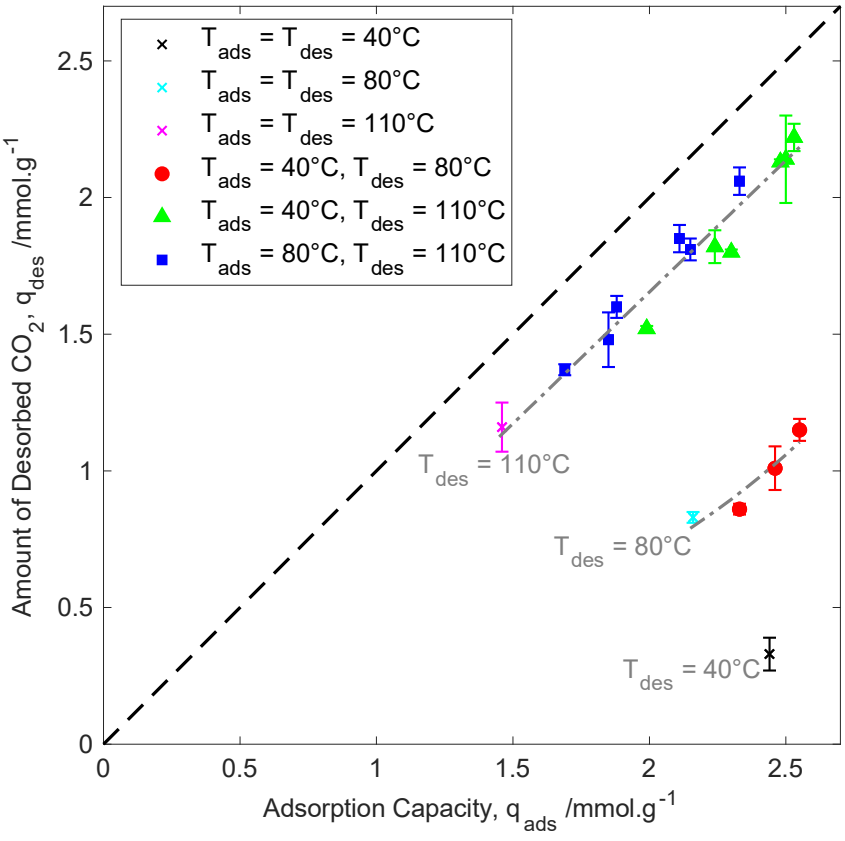


*Figure 6.3 Relationship between the measured 'desorbed capacity' and measured adsorbed capacity at all experiment conditions*

### 6.2.2 Effect of Temperature on Desorption Rate

Figure 6.4 shows the percentage of $CO_2$ desorbed and desorption rates measured over time. Across all experiments, 50% of the $CO_2$ was desorbed in less than 3 s, with the peak rate of desorption occurring in ~2 s. The desorption rate then rapidly fell to 0 $mmol.g^{-1}.s^{-1}$ for all conditions. The fastest desorption rate was achieved using an adsorption temperature of 40 °C and desorption temperature of 110 °C, followed by adsorption/desorption temperatures of 80/110 °C then finally 40/80 °C. The bonds between the adsorbed $CO_2$ molecules and surface are weakened at higher temperatures [5-7], meaning the desorption process is favored over adsorption and the overall rate of desorption increases at higher temperatures [31-32]. Ergo, a desorption temperature of 110 °C is beneficial for the BPEI material. The 40 °C adsorption temperature likely produced a higher desorption rate than the 80 °C adsorption temperature because more $CO_2$ was initially attached to the surface.

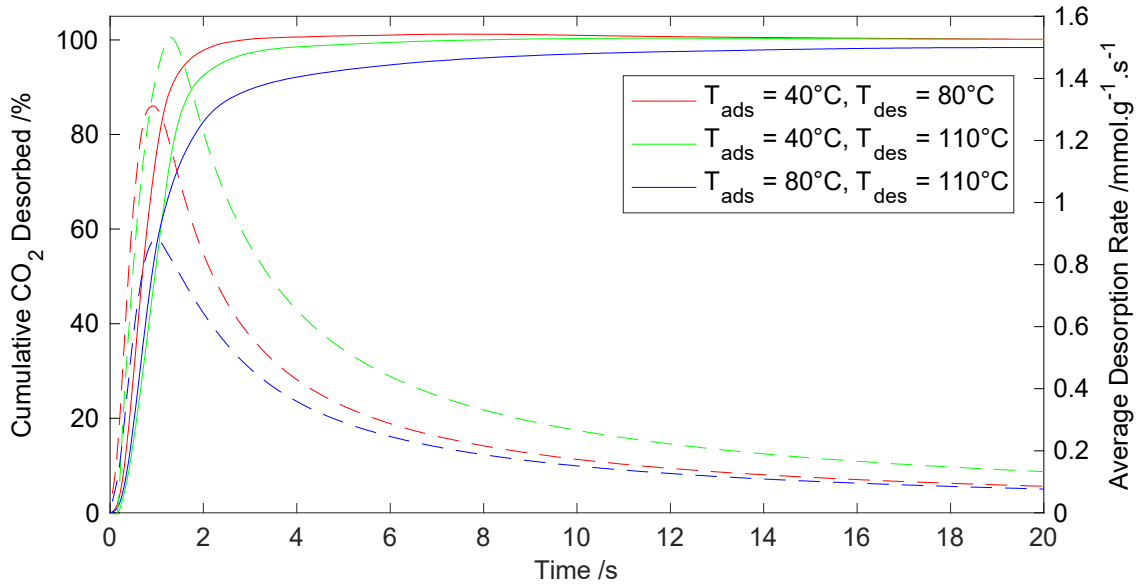


*Figure 6.4 Cumulative percentage of CO2 desorbed and $CO_2$ desorption rates over time as a function of temperature (gas flow rate = 25 L/min, $CO_2$ concentration = 20 vol%); solid lines represent desorption%, dashed lines represent desorption rate*

The maximum desorption rate observed in Figure 6.4 was ~1.48 mmol.g$^{-1}$.s$^{-1}$ (equivalent to 3907.2 mg.g$^{-1}$.min$^{-1}$), with a corresponding desorption efficiency of 84.9%. Table 6.3 compares this desorption rate to different rates observed in the literature using TSA and variations of. The desorption rate observed in the TORBED is one order of magnitude larger than the fluidised bed study, and 2-3 orders of magnitude larger than those observed in packed beds. Since the BPEI material is similar to the adsorbents used in these other studies, it can be concluded that the improvement most likely stems from the intensification of the gas-solid contact in the form of higher stripping velocities [7,8]. *I.e.*, the TORBED enables higher gas velocities to be used without removing material from the bed, which eliminates external mass transfer resistances. The adsorption and desorption processes probably operate at the kinetic limit (as mentioned in 6.2.1, It has not been observed evidence for internal diffusion limitations for adsorption).

*Table 6.3 Comparison of average desorption rates with reported data in the literature*

| Process Type | Reactor Type | Adsorbent | Desorption rate [a] ($mg.g^{-1}.min^{-1}$) | Reference |
|---|---|---|---|---|
| **TCSD[b]** | Packed Bed | Amine loaded silica | 3.67 | [13] |
| **TCSD** | Packed Bed | Amine loaded MOF | 7.39 | [14] |
| **Steam Stripping** | Packed Bed | Amine loaded silica | 12.80 | [17] |
| **Steam Stripping** | Packed Bed | Amine loaded silica | 10.16 | [9] |
| **TCSD** | Packed Bed | Amine loaded carbon | 4.32 | [10] |
| **Rotating bed TVSA** | Rotating Packed Bed | Amine-containing nano-gel particles | 10.37 | [18] |
| **TSA** | Fluidised Bed | 20 wt% $Fe_3O_4$ (13X-IO20) | 461.4 | [8] |
| **TSA** | TORBED | BPEI | 3907.2 | Present study |

(a) Average desorption rate defined as desorbed capacity divided by desorption time ($q_{des}/t_{95}$)

(b) TCSD: Temperature concentration swing desorption

The desorption kinetics can also be analysed in terms of the desorption time. Figure 6.5a plots the breakthrough time and desorption time for the $T_{ads} = T_{des}$ configuration, while Figure 6.5b plots the desorption time for the $T_{des} > T_{ads}$ configuration. Both sets of experiments used the same gas flow rate (25 L/min) and same $CO_2$ concentration during adsorption (20 vol%). Figure 6.5a shows that both the breakthrough time and desorption time decrease as the temperature increases. The decreased desorption time is expected because desorption is thermodynamically more favourable at higher temperatures compared to adsorption. In Figure 6.5b, the desorption time was generally faster when the desorption temperature was 110 °C compared to a desorption temperature of 80 °C. Here, the desorption time was fastest when adsorbing at 80 °C and desorbing at 110 °C, which can be attributed to a smaller pre-heating time (discussed in more detail in 3.7.4).

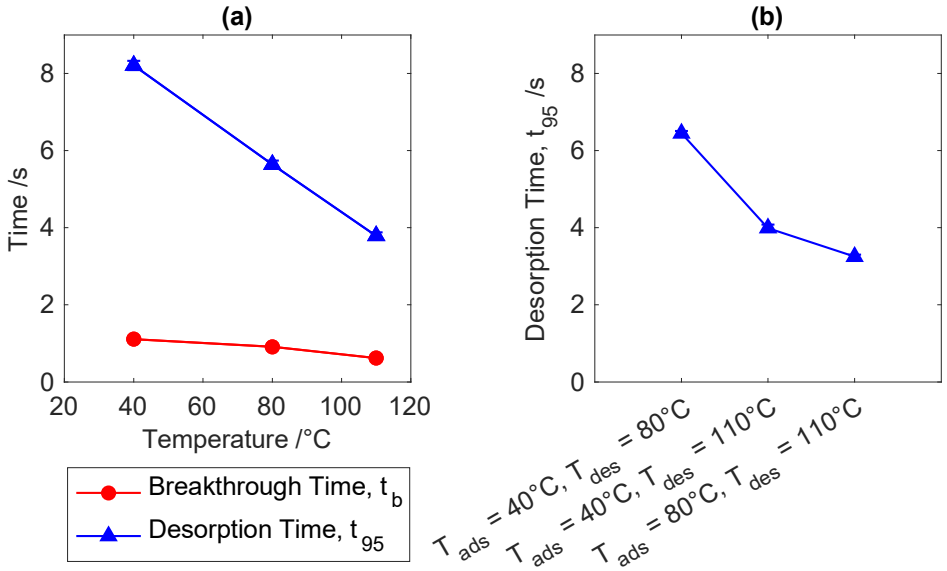


*Figure 6.5(a) Effect of temperature on the breakthrough time (tb) and desorption time (t95) for the $T_{ads}$=$T_{des}$ configuration; and (b) Desorption time (t95) for the $T_{des}$>$T_{ads}$ configuration gas flow rate = 25 L/min, $CO_2$ concentration = 20 vol%*

Overall, it is crucial to determine the appropriate temperature range for both adsorption and desorption to achieve the 'optimal' performance of a $CO_2$ adsorbent. Given the above results, recommendation would be tailoring the temperature to suit the specific requirements of adsorption and desorption, i.e. The $T_{des} > T_{ads}$ configuration for materials screening and development is recommended by our study.

### 6.2.3 Effect of Pre-Heating Rate on Desorption process

The $T_{des} > T_{ads}$ approach requires rapid heating of the bed to optimally screen the desorption kinetics [39-41]. The pre-heating time depends on several factors, including the properties of the adsorbent and adsorbate (*e.g.* heat capacities), operating temperature range, and desired processing conditions (*e.g.* gas flow rate). A pre-heating rate was defined as the difference in adsorption and desorption temperatures divided by the heating time to quantify the differences in the different adsorption/desorption temperatures (see Table 6.2). In the TORBED, the heating rate across all configurations was fairly consistent, averaging around 1.8 °C/s for most of the experiments (see Table 6.2 for a full summary). *E.g.*, this equates to 23 s to heat from 40 °C to 80 °C, 17 s to heat from 80 °C to 110 °C, and 40 s to heat from 40 °C to 110 °C.

Figure 6.6 shows the average desorption rate and desorption efficiency plotted as a function of the pre-heating rate. The desorption rate and efficiency both increase as the pre-heating rate

increases. Both configurations with the 110 °C desorption temperature produce the same desorption rate and efficiency. Longer pre-heating time may result in increased heat loss to the surroundings during an experiment, which can reduce the overall temperature inside the bed which then influences the desorption rate.

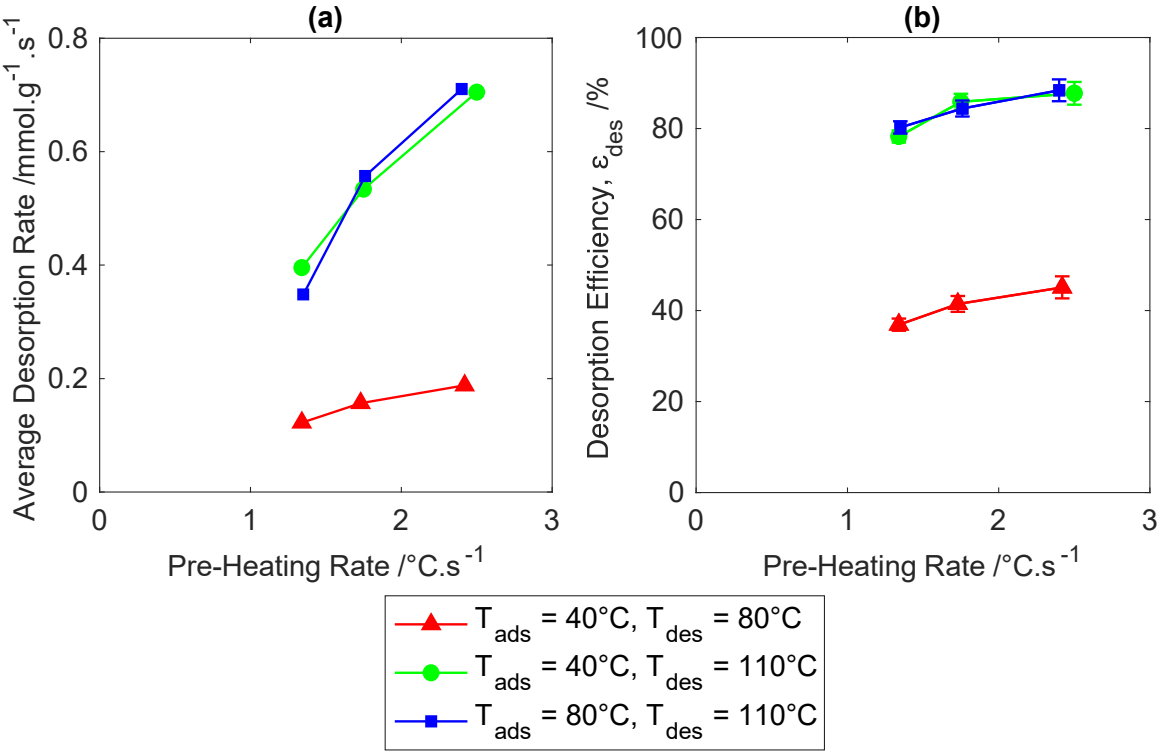


*Figure 6.6 Effect of pre-heating rate on the (a) average desorption rate, and (b) desorption efficiency*

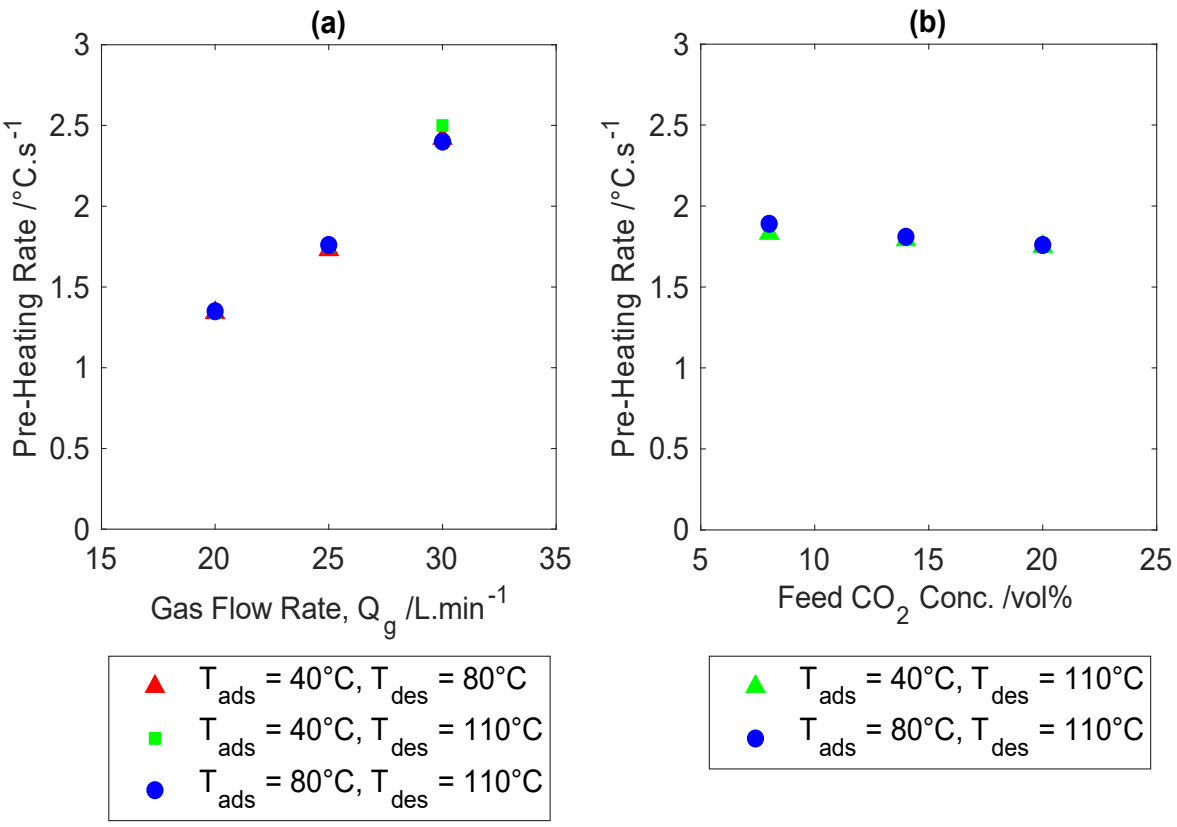


*Figure 6.7Pre-Heating Rate as a function of (a) gas flow rate, and (b) feed $CO_2$ concentration used during adsorption*

Strictly speaking, the pre-heating rate is only an inferred controlled variable. As shown in Figure 6.7, both the gas flow rate and $CO_2$ concentration were found to influence the pre-heating rate and are therefore 'more fundamental' in terms of influencing the desorption kinetics. Generally, it has been observed that higher gas flow rates produced a faster preheating rate (Figure 6.7a), and subsequently, higher desorption rate and efficiency (Figure 6.6). This is because higher gas flow rates increase the swirling intensity and mixing in the bed, which improves the convective heat transfer characteristics from the gas to the particles. Additionally, the higher gas flow rate will have a higher thermal mass (higher $mc_p$ value), resulting in a greater amount of thermal power being delivered to the bed.

The inlet $CO_2$ concentration also influenced the pre-heating rate, and therefore, the desorption rate and efficiency. As a reminder, the pre-heating step was done with $N_2$ and $CO_2$ to attempt to maintain saturation of the adsorbent. Since the specific heat capacity of $CO_2$ is slightly smaller than nitrogen, increasing the $CO_2$ concentration decreases the average heat capacity of the inlet gas mixture. Therefore, the thermal mass ($mc_p$ value) of the inlet gas will decrease as the $CO_2$ concentration increases, which then decreases the energy being delivered to the particles causing a marginally lower pre-heating rate (Figure 6.7b). Additionally, with more $CO_2$ attached to the surface at higher concentrations, more heat will be absorbed by the bed since the desorption process is endothermic, which will also delay the heating rate.

However, interestingly the desorption efficiency actually increased as the $CO_2$ concentration increased (see Figure 6.8). This decoupling (decreased heating rate but increased efficiency) could be a consequence of the increased adsorption capacities at the higher $CO_2$ concentration. Therefore., higher concentrations may increase the driving force for $CO_2$ expulsion from the pores of the sorbent during the desorption process. The higher efficiency for the 80/110 °C configuration can be explained by the marginally higher pre-heating rate as shown in Figure 6.7b.

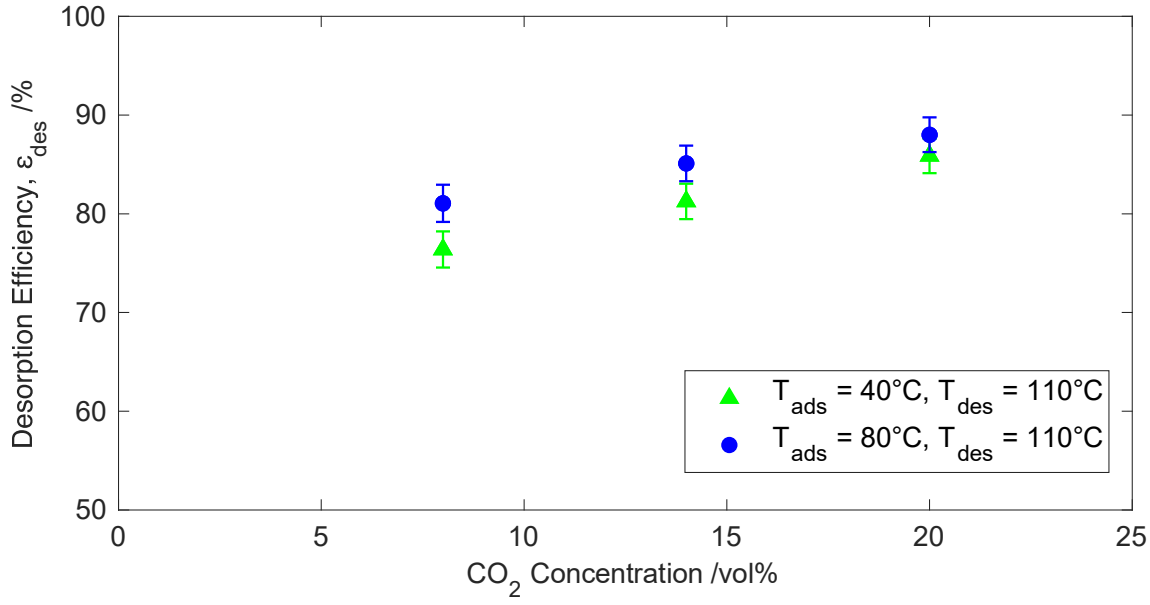


*Figure 6.8 Effect of $CO_2$ concentration used during adsorption and pre-heating on the desorption efficiency.*

### 6.2.4 Effect of $CO_2$ Concentration on Adsorption and Desorption

During desorption, the $CO_2$ concentration reaches 5% of the initial starting value in just 3–9 seconds depending on the conditions (examples are shown in Figure 6.1). This rapid desorption indicates that most of the attached $CO_2$ is likely weakly physisorbed (*e.g.* via Van der Waals interactions). The next phase of desorption where the $CO_2$ concentration approaches 0 vol% produces a long tail, suggesting that a small portion of $CO_2$ is strongly chemisorbed to the surface via bonding with amine groups [35].

For adsorption, increasing the $CO_2$ concentration generally increases the adsorption capacity as reported in adsorption chapter [16]. This can be seen in Figure 6.9a, and is simply a consequence of Henry's Law, which states that the adsorption capacity of $CO_2$ is directly proportional to its partial pressure in the gas phase [6]. There is also likely to be an improvement in mass transfer due to the increased driving force between $CO_2$ in the bulk carrier gas and $CO_2$ diffused inside the pores of the adsorbent. Further increases of $CO_2$ concentration lead to diminishing returns. This can be explained by the Langmuir Isotherm model, which defines the upper limit of the adsorption capacity as when a monolayer completely covers the surface [8]. Thus, as the $CO_2$ concentration increases, more $CO_2$ molecules occupy the available adsorption sites until the monolayer capacity is reached. The maximum adsorption capacity of the BPEI material measured in the present study was 2.55 ± 0.03 mmol/g at 20 vol% $CO_2$ concentration. Wangs *et al.* [52] report comparable adsorption capacities of 2.50 mmol/g for 5% $CO_2$ and 2.70 mmol/g for 50% $CO_2$.

Figure 6.9a expectedly shows that the measured amount of desorbed $CO_2$ is correlated with the starting adsorbed amount (more $CO_2$ can be desorbed if more was adsorbed initially). Figure 6.9a also shows that the adsorption temperature and $CO_2$ concentration used during adsorption and pre-heating have indirect effects on the amount desorbed. Higher $CO_2$ concentrations increase the adsorption capacity as discussed above. The optimal adsorption temperature for this BPEI material is 40 °C; therefore, adsorbing at 40 °C produces a higher adsorption capacity and higher desorbed amount compared to an 80 °C adsorption temperature.

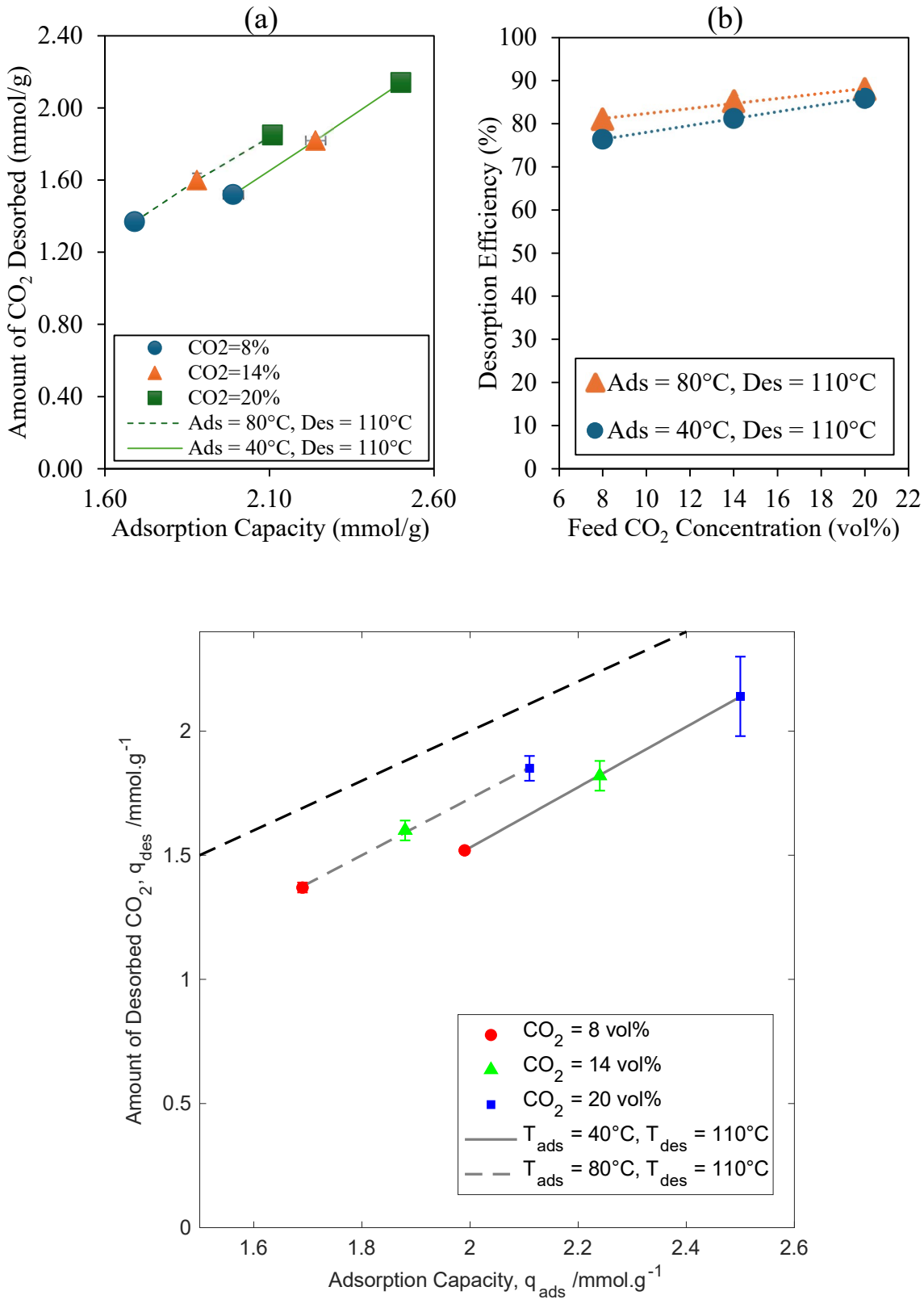


*Figure 6.9 Desorption capacity as a function of adsorption capacity categorised by $CO_2$ concentration and adsorption temperature; the black dotted line indicates complete desorption ($q_{des} = q_{ads}$)*

### 6.2.5 Effect of Gas Flow Rate on Adsorption and Desorption

There are several trade-offs when considering the gas flow rate for the adsorption step. Insufficient gas flow leads to a collapsed or maldistributed bed, which causes poor mixing and gas bypassing. While higher flow rates improve the heat and mass transfer rates, these also reduce the contact time between the $CO_2$ and adsorbent which can lead to premature $CO_2$ breakthrough. As reported in previous chapter 5, the highest apparent adsorption capacities when operating the TORBED in the desirable uniformly swirled flow regime, corresponding to flow rates of 20–30 L/min for 2 g of the BPEI material [7]. This range was subsequently used in the present desorption study.

Figure 6.10a shows the amount of desorbed $CO_2$ as a function of adsorption capacity categorised by gas flow rate and adsorption/desorption temperatures. For all three combinations of $T_{ads}$ and $T_{des}$, increasing the gas flow rate increased the adsorption capacity and the amount of desorbed $CO_2$. Figure 6.10b shows that the desorption efficiency also increases as a function of gas flow rate for all $T_{ads}/T_{des}$ configurations. Clearly the desorption temperature has a stronger influence overall (*e.g.* the $T_{des}$ = 110 °C configuration achieves over double the efficiency of the $T_{des}$ = 80 °C configuration). As already discussed, lower temperatures shift the equilibrium to higher adsorbed concentrations and *vice versa*. Thus, the role of the gas flow rate is to improve the heat transfer characteristics.

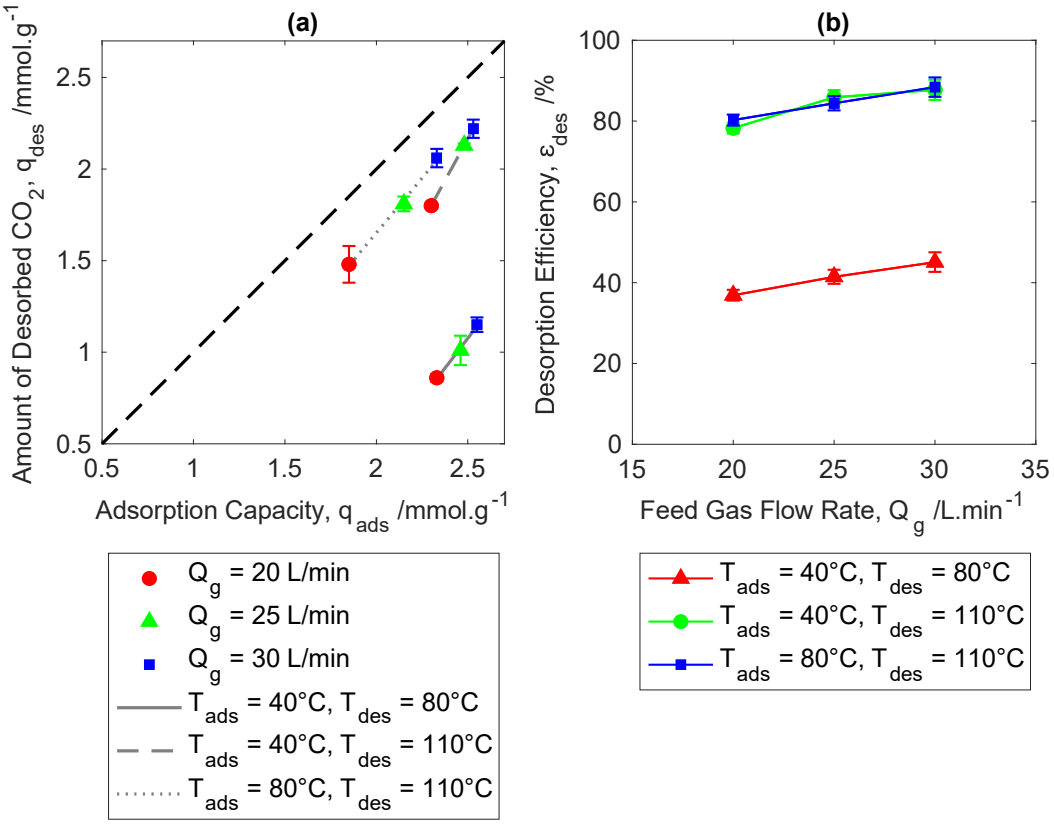


*Figure 6.10 (a) Desorption capacity as a function of adsorption capacity categorised by gas flow rate, and (b) desorption efficiency as a function of gas flow rate at fixed $CO_2$ concentration of 20 vol%*

Adsorption requires that the bed is operated in the uniformly swirled regime to eliminate gas bypassing. This needs to be considered during desorption. However, like the adsorption process, there are still trade-offs. Principally, higher gas flow rates outside of the uniformly swirled regime will continue to promote heat transfer, which is beneficial for the desorption process. But higher gas flow rates will also dilute the 'captured' $CO_2$, reducing the effectiveness of the overall carbon capture process. Thus, selection of a desorbing gas with high heat capacity is recommended to maximise the thermal mass, or use of a condensable desorbing gas such as steam, to promote higher recovered $CO_2$ concentrations.

## 6.3 Cyclic Measurements

Periodic cycling between low and high temperatures often leads to a degradation in performance and efficiency over time due to the accumulation of thermally induced expansions and contractions. Therefore, cyclability of an adsorbent material is an important parameter to consider when evaluating potential carbon capture materials. The ideal sorbent material should have a high adsorption capacity and 'good' stability over many cycles of use [26, 33-36].

To evaluate the recyclability of the BPEI adsorbent in the present study, 50 consecutive adsorption-desorption cycles were performed. For this cyclic testing, adsorption was conducted at 40 °C with 20 vol% $CO_2$ in $N_2$ at a total flow rate of 25 L/min, while desorption was conducted at 110 °C with pure $N_2$ at 25 L/min as a carrier gas. Similar experimental approaches are reported in the wider literature [1-5, 26-32]. Figure 6.11 shows the adsorption and regeneration indices, AI% and RI%, measured across 50 adsorption-desorption cycles in the TORBED reactor.

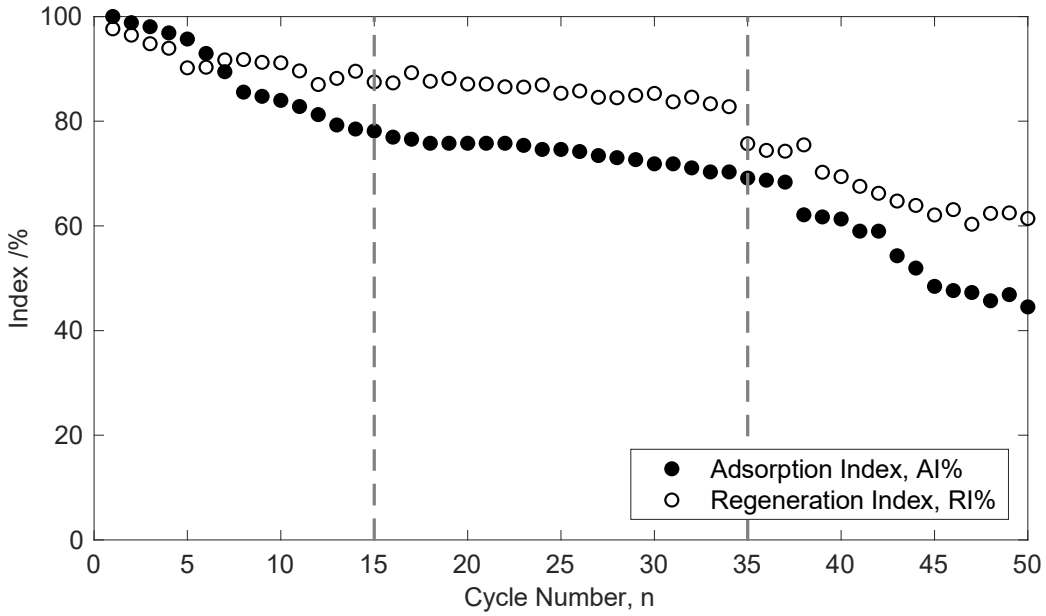


*Figure 6.11 Adsorption index (AI%) and regeneration index (RI%) as a function of cycle number; AI% is based on an adsorption capacity of 2.56 mmol/g for n = 1; RI% is based on a desorbed amount of 2.13 mmol/g for n = 1*

Generally, both AI% and RI% decreased over time as expected; both decline from $n$ = 1 to 15, somewhat stabilise between $n$ = 15 to 35, and rapidly decline from $n$ = 35 to 50. Thus, this BPEI material can be considered to be acceptable for around 35 cycles in the mini-TORBED, where the adsorption capacity and desorbed amount decline to around 70% and 75% of the starting values respectively. For comparison, Su *et al.* evaluated the stability of a CNT-APTS adsorbent during 100 adsorption-desorption cycles and measured AI% values of 92% and 88% after 50 and 100 cycles respectively [35].

The rapid decline in performance after $n$ = 35 indicates that the BPEI must undergo some form of degradation process. In the present study, a combination of chemical, thermal, and mechanical effects are the leading hypotheses. Some researchers have reported on the

formation of urea linkages when PEI/silica adsorbents were exposed to pure $CO_2$ at temperatures higher than 135 °C under dry conditions that can influence the chemical properties (*e.g.* surface groups). Additionally, continual thermal expansion and contraction between the adsorption and desorption processes can induce defects in the material while also changing the dimensions and shapes of the internal pores, which influences internal diffusion. Finally, the intense mixing in the TORBED due to swirling may cause attrition through particle-wall collisions, often observed in fluidised bed reactors.

## 6.4 Desorption Kinetic Modelling

Desorption kinetic models can be used to predict the behaviour of desorption systems (such as gas separation, catalysis, and carbon capture), infer mechanisms of desorption for materials development insight, and for optimisation and design. Numerous kinetic models for adsorption and desorption are reported in the wider literature, including the Langmuir model, pseudo-first order and pseudo-second order models, fractional-order model, Langmuir-Freundlich model and Avrami's model (41, 42, 108). There isn't a one-size-fits-all model that can be universally considered as the best for all desorption processes. Therefore, most studies fit multiple models to the experimental data to find the one with the best fit. This is then often followed by *ad hoc* interpretation of the resulting kinetic rate constants.

The pseudo 1$^{st}$ order, pseudo 2$^{nd}$ order and fractional order kinetics models were considered for the adsorption process for the BPEI adsorbent. The fractional-order model provided the best fit to the experimental data because it could replicate the S-shaped cumulative adsorption curve, which results from changes in relative importance of mass transfer and diffusion during the adsorption process. Table 6.4 summarises the differential and integrated forms of these three models (54, 107).

Here, $t$ represents the time elapsed, $q_t$ represents the amount of $CO_2$ adsorbed at a given point in time (mmol/g), and $q_e$ represents the equilibrium amount adsorbed (mmol/g). The fitted parameters include the pseudo 1$^{st}$ order rate constant $k_f$ ($s^{-1}$), pseudo 2$^{nd}$ order rate constant $k_s$ ($g.mmol^{-1}.s^{-1}$), fractional-order rate constant $k_n$ and fractional-order coefficients $n$ and $m$. This data can be used to understand the underlying mechanism of the desorption process and to optimise the conditions for a particular application.

*Table 6.4 Models for describing the desorption kinetics*

| Model | Differential Form | Integrated form |
|---|---|---|
| Pseudo 1st Order | $\frac{dq_t}{dt} = k_f(q_e - q_t)$ | $q_t = q_e[1 - e^{-k_f t}]$ |
| Pseudo 2nd Order | $\frac{dq_t}{dt} = k_s(q_e - q_t)^2$ | $q_t = \frac{k_s q_e^2 t}{1 + q_e k_s}$ |
| Fractional Order | $\frac{dq_t}{dt} = k_n t^{m-1}(q_e - q_t)^n$ | $q_t = q_e - \frac{1}{\left[\frac{(n-1)k_n t^m}{m} + \frac{1}{q_e^{n-1}}\right]^{\frac{1}{n-1}}}$ |

Figure 6.12 compares the pseudo 1st order, pseudo 2nd order, and fractional order kinetic models against the cumulative desorption curves for different combinations of $T_{ads}/T_{des}$. Table 6.5 summarises the corresponding fitted parameters and $R^2$ values. For all conditions, the fractional-order model produced the closest fit to the experimental data, followed by the pseudo 1st order model, followed by the pseudo 2nd order model.

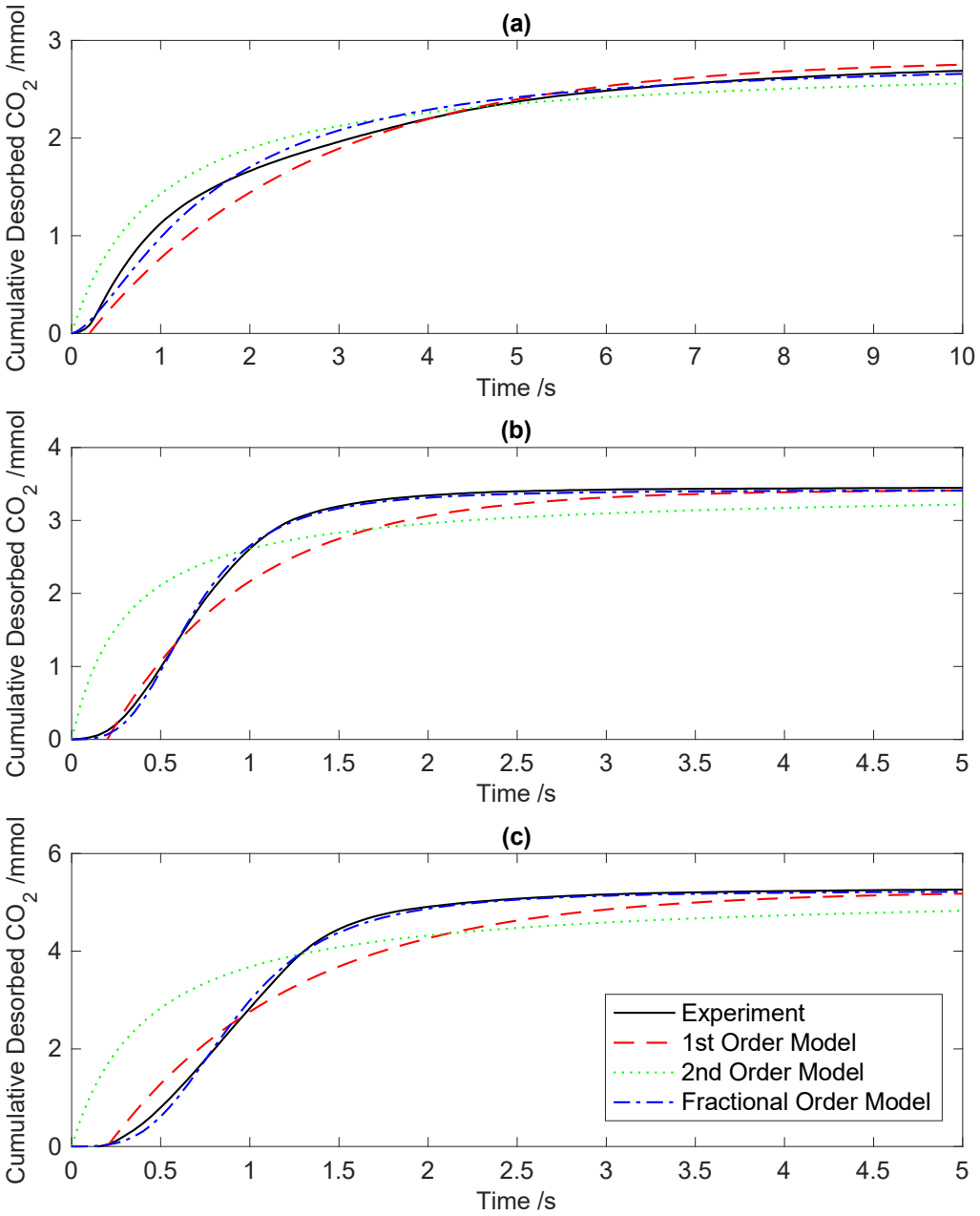


*Figure 6.12 Comparison of kinetic models against experimental cumulative desorption curves, (a) $T_{ads}$ = 40 °C & $T_{des}$ = 80 °C, (b) $T_{ads}$ = 80 °C & $T_{des}$ = 100 °C, (c) (a) $T_{ads}$ = 40 °C & $T_{des}$ = 110 °C*

*Table 6.5 Kinetic parameters fitted from desorption experiments*

| ID | 1st Order Model | | 2nd Order Model | | Fractional Order Model | | | |
|---|---|---|---|---|---|---|---|---|
| | $k_f$ ($s^{-1}$) | $R^2$ (%) | $k_s$ ($g.mmol^{-1}.s^{-1}$) | $R^2$ (%) | $k_n$ ($s^{-1}$) | $n$ (-) | $m$ (-) | $R^2$ (%) |
| **1** | 0.23 ± 0.10 | 93 | 0.21 ± 0.07 | 63 | 0.30 ± 0.05 | 3.11 ± 0.55 | 7.15 ± 0.22 | 98 |
| **2** | 0.70 ± 0.08 | 97 | 0.66 ± 0.06 | 69 | 0.65 ± 0.09 | 1.95 ± 0.15 | 4.5 ± 0.14 | 98 |
| **3** | 0.90 ± 0.03 | 99 | 0.94 ± 0.08 | 71 | 1.10 ± 0.02 | 1.35 ± 0.14 | 2.10 ± 0.17 | 99 |
| **4** | 0.52 ± 0.03 | 92 | 0.46 ± 0.10 | 62 | 0.48 ± 0.15 | 1.33 ± 0.95 | 1.41 ± 0.16 | 98 |
| **5** | 0.65 ± 0.08 | 95 | 0.50 ± 0.05 | 63 | 0.63 ± 0.02 | 2.24 ± 0.15 | 8.98 ± 0.50 | 99 |
| **6** | 0.70 ± 0.03 | 96 | 0.71 ± 0.12 | 83 | 0.75 ± 0.16 | 1.72 ± 0.24 | 1.26 ± 0.25 | 99 |
| **7** | 0.91 ± 0.09 | 97 | 0.93 ± 0.10 | 75 | 0.95 ± 0.05 | 2.07 ± 0.53 | 2.60 ± 0.52 | 99 |
| **8** | 1.01 ± 0.25 | 95 | 1.05 ± 0.10 | 71 | 1.16 ± 0.36 | 2.66 ± 0.64 | 2.53 ± 0.57 | 99 |
| **9** | 1.20 ± 0.08 | 90 | 1.15 ± 0.05 | 79 | 1.20 ± 0.09 | 1.94 ± 0.45 | 3.79 ± 0.95 | 99 |
| **10** | 1.12 ± 0.05 | 95 | 1.04 ± 0.05 | 70 | 1.08 ± 0.10 | 1.97 ± 0.15 | 1.96 ± 0.14 | 99 |
| **11** | 0.78 ± 0.09 | 94 | 0.79 ± 0.08 | 76 | 1.07 ± 0.12 | 1.72 ± 0.13 | 1.97 ± 0.12 | 98 |
| **12** | 1.15 ± 0.09 | 96 | 1.19 ± 0.07 | 76 | 1.32 ± 0.08 | 2.15 ± 0.10 | 3.92 ± 0.15 | 99 |
| **13** | 0.86 ± 0.08 | 91 | 0.86 ± 0.04 | 71 | 0.81 ± 0.01 | 1.40 ± 0.25 | 1.97 ± 0.45 | 99 |
| **14** | 0.85 ± 0.05 | 95 | 0.91 ± 0.05 | 80 | 0.97 ± 0.04 | 1.65 ± 0.18 | 1.87 ± 0.25 | 99 |
| **15** | 1.15 ± 0.05 | 99 | 1.21 ± 0.08 | 82 | 1.18 ± 0.01 | 1.31 ± 0.22 | 3.98 ± 0.56 | 97 |
| **16** | 0.94 ± 0.04 | 92 | 0.92 ± 0.09 | 74 | 0.96 ± 0.05 | 1.69 ± 0.52 | 2.10 ± 0.55 | 99 |
| **17** | 1.14 ± 0.04 | 98 | 1.15 ± 0.10 | 79 | 1.25 ± 0.05 | 1.55 ± 0.56 | 1.79 ± 0.65 | 99 |
| **18** | 1.26 ± 0.25 | 99 | 1.01 ± 0.11 | 64 | 1.16 ± 0.18 | 2.21 ± 0.45 | 3.22 ± 0.58 | 99 |

The pseudo 1st order model assumes that the desorption rate is directly proportional to the amount of adsorbed species remaining on the surface of the adsorbent. This model is relatively simple and has been successfully applied in cases where the desorption process follows an exponential decay pattern. This model is often used when desorption is primarily controlled by the strength of binding at the adsorption sites. Here, a single fitted parameter, $k_f$, provides a measure of the rate at which the adsorbed species is adsorbed or desorbed from the material. Specifically, it represents the proportionality constant between the concentration (or amount) of the adsorbed species and the rate of adsorption or desorption. This rate constant is influenced by various factors such as the affinity between adsorbate and adsorbent, temperature, pressure, and the properties of the adsorbent material. A higher value of $k_f$ generally indicates a faster desorption rate. For the BPEI material in this study, the first-order model produced a closer fit to the experimental data at higher $CO_2$ concentrations (*e.g.* ID13: $R^2$ = 91% at 8 vol% $CO_2$ for ID13, and ID15: $R^2$ = 99% at 20 vol% $CO_2$). Generally, this model does not account for factors such as surface coverage or interactions with other species.

The second-order kinetics model assumes that the rate of desorption is proportional to the square of the amount of adsorbed species remaining on the adsorbent. It is based on the assumption that desorption occurs through the interactions between two adsorbed species and is therefore used when desorption involves complex interactions between adsorbed molecules. These interactions can result in cooperative effects, where the presence of one adsorbed molecule facilitates the desorption of another. This model also uses a single rate constant to describe the desorption rate, denoted as $k_s$. This second-order rate constant is also a measure of the rate at which the adsorbed species is desorbed. For the BPEI material, the pseudo 2$^{nd}$ order model could not simultaneously describe both the final equilibrium desorption ($q_e$) and desorption rate. This can be seen in Figure 6.12 where the second order model initially overestimates the cumulative desorption curve followed by underestimating the curve as equilibrium is reached. Thus, the 2$^{nd}$ order model does not accurately capture the behaviour of the desorption process for the BPEI material. Generally, factors such as surface heterogeneity, competitive adsorption, mass transfer limitations at low concentrations (which inhibits internal diffusion) and environmental conditions are not described by the 2$^{nd}$ order model.

The fractional-order kinetics model assumes that the desorption rate is proportional to some fractional power of the concentration of the adsorbed species. This model was proposed by Hedari-Gorji & Sayari [2011] [113] for $CO_2$ capture on PEI-impregnated silica (adsorption) and accounts for multiple adsorption sites or interactions between adsorbed molecules during the adsorption process. In the context of desorption, the coefficient $n$ describes the 'pseudo order' of the reaction, in that it approximates multiple simultaneous interactions and reactions using a single parameter. The parameter $m$ was not formally defined by Hedari-Gorji & Sayari [29]. However, the inclusion of this parameter was based on the structure of Avrami's model, and here, $m$ has also been referred to as the observed reaction order based on multiple pathways [36]. Generally, larger values of $m$ describe more pronounced tailing behaviour, which for desorption, indicates that desorption continually slows as the adsorbate leaves the material (9, 41). For all conditions, the fractional order model produced the best fit to the experimental data, indicating that the BPEI exhibits fractional order behaviour. Generally, there was no clear relationship between the conditions and the constants $n$ and $m$, which can potentially be interpreted as the mechanism for adsorption (whose macroscopic behaviour is an amalgam of various molecule interactions, physisorption, chemisorption, *etc.*) remaining unchanged across all experiments.

Interestingly, it has been observed that the desorption rate was a reasonably strong function of the amount of $CO_2$ desorbed but not the amount of $CO_2$ initially adsorbed (see Figure 6.13).

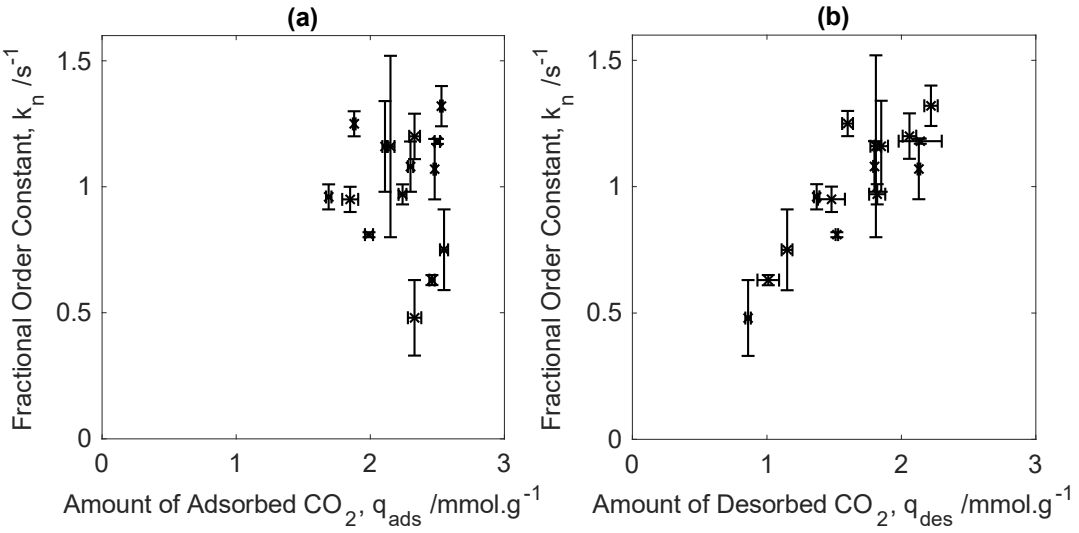


*Figure 6.13 Fractional order rate constant plotted as a function of (a) amount of adsorbed $CO_2$ (no correlation), and (b) amount of desorbed $CO_2$ (positive correlation)*

## 6.5 Conclusion

In this chapter, the desorption characteristics of a commercial $CO_2$ adsorbent (BPEI) using a small-scale TORBED reactor was investigated as a function of adsorption and desorption temperature, $CO_2$ concentration, and gas flow rate. It was found that the implementation of temperature swing adsorption plays a crucial role in the efficiency of the desorption process. When desorption is performed at the same temperature as adsorption ($T_{des} = T_{ads}$), which is easy to implement experimentally, significantly lower desorption efficiencies were observed. This is because thermodynamically, higher temperatures favour desorption while lower temperatures favour adsorption. Thus, the $T_{des} > T_{ads}$ configuration would be recommended for materials screening and development, with the caveat that this introduces a short delay due to the heating time. Faster heating rates increase the amount of desorbed $CO_2$ and increase the desorption efficiency, and these can be achieved by increasing the gas flow rate (which increases the heat transfer rate and heating power) and decreasing the concentration of $CO_2$ (which increases the thermal mass of the gas since it has a lower heat capacity than nitrogen).

Additionally, the study demonstrated that the $CO_2$ concentration used during adsorption and preheating has an indirect effect on the desorption process. Higher concentrations increase the

adsorption capacity, which in turn, influences the amount of $CO_2$ that needs to be desorbed during the desorption stage. Here, higher concentrations produce a positive effect by improving the desorption efficiency and desorption rate.

The effects of flow rate on the desorption process can be complex due to the competing effects on the mixing characteristics and heat transfer characteristics. Within the operating window for swirling fluidisation, increasing the gas flow rate increases the thermal power being delivered to the bed, which increases the preheating rate. However, operating the gas flow rate outside of the optimal window negatively impacts the adsorption capacity, which then indirectly influences the desorption characteristics. Further, operating with high gas flow rates also produces a dilute stream of 'captured $CO_2$', reducing the overall effectiveness of the potential TORBED carbon capture process.

In terms of kinetics, the fractional order kinetic model provided a better fit to our experimental data than the pseudo $1^{st}$ order and pseudo $2^{nd}$ order models. The key benefit of the fractional order model is it can capture the additive effects of molecule-molecule interactions and various binding reactions/processes whereas the pseudo $1^{st}$ and $2^{nd}$ order models can only capture simpler single and double molecular interactions. Ultimately, the success of any carbon capture technology depends on a combination of the technology and materials. The findings reported here contribute to the development of efficient and sustainable $CO_2$ capture technologies, facilitating the design of cost-effective carbon capture systems for mitigating greenhouse gas emissions by providing a platform for small-scale screening experiments.

# 7. Conclusions and Recommendations

In this study, a small-scale screening platform was developed for testing $CO_2$ adsorbents using a mini-TORBED reactor to intensify the heat and mass transfer rates. This platform was tested using a commercial adsorbent (BPEI), which involved first characterising the hydrodynamic behaviour, then performing a series of adsorption and desorption breakthrough experiments at different $CO_2$ concentrations, bed loadings, gas flow rates, and operating temperatures. The comprehensive analysis conducted in this study underscores the potential of mini-TORBED technology for carbon capture adsorbent screening.

## 7.1 Summary of Hydrodynamic Findings

Understanding fluidized beds' hydrodynamic principles is crucial for analysing adsorption kinetics in experiments. This initial exploration helps choose the best operating conditions and identify adsorbents that are suitable for use in the mini-TORBED's adsorption/desorption processes. The complex dynamics of fluidization greatly affect mass transfer and adsorption within the bed, directly impacting the adsorption system's efficiency.

Fluidization dynamics are key in adsorption, where effective interactions between adsorbent and adsorbate depend on the bed's dynamic behaviour. This chapter focused on thoroughly understanding hydrodynamic behaviour through visual experiments and pressure drop measurements. These experiments were conducted at various flow rates and bed loadings, with inert nitrogen ($N_2$) as the fluidizing gas, under ambient temperature and 1 bar.g pressure.

Key observations:

- The optimal pressure drop across the bed and achievement of desirable flow regime characterized by uniform swirling motion were observed with the commercial BPEI particles, indicating their superior performance compared to commercial Hydrotalcite (Geldart C)and Casale particles (Geldart D).
- BPEI consistently demonstrated the desired flow regime within an acceptable range of pressure drop and flow rate, making it the preferred sorbent for further testing in TORBED technology for both adsorption and desorption processes.

## 7.2 Summary of Adsorption Findings

The efficacy of a commercially available sorbent, based on branched polyethyleneimine (BPEI), was rigorously evaluated for its ability to capture $CO_2$ from artificial flue gas streams composed of varying $N_2/CO_2$ ratios. Breakthrough curves were generated across a spectrum of $CO_2$ volume fractions (2–20 vol%), BPEI bed loads (1–2.5 g), gas flow rates (20–35 L/min), and temperatures (40–70 °C) using the TORBED system.

Key Observations:

- Optimized $CO_2$ Capacity: Under optimal operational conditions characterized by uniformly swirled flow regimes, the TORBED measured a maximum $CO_2$ capacity of $2.64 \pm 0.06$ mmol/g, matching the supplier's in-house measurement. This was observed within specific ranges of bed loadings (1.5–2 g) and gas flow rates (25–30 L/min), corresponding to uniform swirling of the sorbent, whose conditions were tailored based on the hydrodynamics experiments. Deviations such as bed maldistribution or entrainment led to diminished capacities, primarily attributed to gas bypassing outside of these conditions.
- Flow Regime Dominance: Within the TORBED, the $CO_2$ adsorption capacity of BPEI demonstrated a significant correlation with prevailing flow regimes, overshadowing the influence exerted by variations in gas flow rates alone (*e.g.* due to residence time changes alone). This observation emphasizes the TORBED's unique capability in modulating flow dynamics, thereby optimizing adsorption performance.
- Temperature Sensitivity: Operating temperature fluctuations caused discernible impacts on adsorption capacities. Elevated temperatures induced reduced capacities due to the inherently exothermic nature of the carbon capture reaction, while lower temperatures favoured thermodynamically favourable adsorption. The TORBED exhibited adept temperature regulation capabilities, evidenced by minimal temperature escalations of merely 2 °C across all operational conditions during adsorption. The TORBED's high gas flow rates enable rapid heat dissipation to preserve desirable adsorbent kinetics and capacity.
- Kinetic Modelling Insights: Kinetic modelling revealed that the fractional-order model provides the closest approximation to experimental data, effectively encapsulating the characteristic 'S'-shaped uptake curve. This observation suggests the coexistence of

physisorption and chemisorption mechanisms within the BPEI adsorbent under the study's conditions.

### 7.3 Summary of Desorption Findings

In this chapter, the desorption characteristics of the same commercial BPEI material was studied using the small-scale TORBED reactor using the temperature swing approach. Here, the effects of pre-heating configuration, $CO_2$ volume fractions (2–20 vol%), gas flow rate (20–35 L/min), and temperatures (40–110 °C) were investigated. Understanding desorption dynamics is crucial for optimizing the efficiency of carbon capture processes. Notably, the implementation of temperature swing adsorption emerges as a pivotal factor in enhancing desorption efficiency. By exploring the interplay between temperature and gas flow dynamics, insights into effective desorption strategies for materials screening and development can be ascertained.

Key observations:

- Temperature Swing Desorption: Desorption performed at temperatures higher than adsorption ($T_{des} > T_{ads}$) yielded significantly higher desorption efficiencies compared to when both processes occur at the same temperature. This is attributed to the thermodynamic favourability of desorption at higher temperatures. Despite introducing a short delay due to heating time, faster heating rates enhance desorption efficiency, achieved by increasing gas flow rates to elevate heat transfer rates.
- Effect of $CO_2$ Concentration: Higher $CO_2$ concentrations during adsorption and preheating positively influence the desorption process by increasing the adsorption capacity, thereby enhancing desorption efficiency and rate due to mass transfer effects.
- Impact of Gas Flow Rate: The effects of gas flow rate on desorption are complex, with optimal operating windows for swirling fluidization needing to be considered. Increasing gas flow rates within this window enhances thermal power delivery to the bed, thereby increasing preheating rates. However, operating outside this window negatively impacts adsorption capacity, indirectly affecting desorption characteristics. Moreover, high gas flow rates produce a dilute stream of 'captured $CO_2$,' reducing the overall effectiveness of the TORBED carbon capture process.
- Kinetic Modelling Insights: The fractional-order kinetic model outperforms pseudo-1$^{st}$ and pseudo-2$^{nd}$ order models in fitting experimental data, capturing the additive effects of molecule-molecule interactions and various binding reactions/processes. This

nuanced understanding of kinetics is crucial for designing efficient carbon capture systems.

## 7.4 Recommendations for Future Work

Based on the research conducted in this study, it is recommended to continue exploring in various areas:

1- Small-scale TORBED screening platform

- Continued Exploration of Sorbent Screening: It is recommended to persist in exploring sorbent screening for carbon capture applications utilizing mini-TORBED reactors. The potential demonstrated in this study highlights the importance of further investigation in refining screening methodologies to unlock new opportunities for carbon capture. Expanding the repertoire of sorbent materials beyond the commercial adsorbent (BPEI) employed in this study is crucial. Exploring a diverse range of sorbent materials, including novel formulations or modifications to existing ones, holds the key to advancing carbon capture technology. While BPEI was one of the sorbents tested, it's essential to acknowledge that other materials were also evaluated. Notably, during the hydrodynamic stage, both smaller and larger particle sizes were tested, yielding suboptimal results for continuation in the adsorption stage due to issues with flow regimes. In future investigations, there is potential to enhance the structure of the TORBED reactor to accommodate uniform swirling motion with finer and cohesive particles or even larger particle sizes, such as Geldart D. This expansion in particle size range could significantly broaden the scope of sorbent screening and provide insights into the performance of diverse materials under varying conditions.
- Cyclic Testing: Continuous adsorption and desorption testing allows for a better estimate of working capacity and performance over prolonged operations, providing valuable information for scaling up and optimizing industrial carbon capture processes. Continuous operation mimics real-world conditions more accurately, offering insights into long-term performance, stability, and maintenance requirements of the carbon capture system. Incorporating continuous testing methodologies alongside semi-batch breakthrough testing enhances the robustness of the findings and facilitates the development of practical and effective carbon capture solutions for industrial-scale implementation.

- Optimization of Operating Parameters: Conduct experiments to optimize operating parameters such as $CO_2$ concentrations, bed loadings, gas flow rates, and operating temperatures to enhance the efficiency of the carbon capture process.
- Scale-Up Studies: Conduct studies to identify scaling rules for the mini-TORBED to assess its feasibility and effectiveness at larger scales. This can involve evaluating the scalability of the reactor design and its performance with increased throughput.
- Long-Term Stability Assessment: Investigate the long-term stability and durability of sorbent materials under continuous operation conditions to understand their performance over extended periods. This could be achieved by comparing particle size distributions before and after processing in the TORBED to study degradation mechanisms.
- Comparative Studies: Perform comparative studies between different sorbent materials and screening platforms to identify the most effective and economically viable options for carbon capture applications.

2- Multi-stage TORBED

- Investigation of Multi-Stage Configurations: Explore the implementation of a multi-stage TORBED reactor, where an additional bed stage could be added on top of the existing bed. This configuration has the potential to increase efficiency by allowing for enhanced contact between the sorbent material and the gas stream.
- Comparative Studies: Conduct comparative studies between single-stage and multi-stage TORBED reactor configurations to assess the performance improvements achieved with the addition of the extra bed stage. This can involve evaluating factors such as $CO_2$ adsorption capacity, breakthrough behaviour, and desorption efficiency.
- Optimization of Multi-Stage Operation: Experiment with different operating parameters and configurations of the multi-stage TORBED reactor to optimize its performance. This can include variations in bed loadings, gas flow rates, operating temperatures, and the placement of the additional bed stage.
- Long-Term Stability Assessment: Investigate the long-term stability and durability of the multi-stage TORBED reactor under continuous operation conditions to ensure its reliability over extended periods.

3- Computational Fluid Dynamics (CFD) studies

- CFD Study for Design Optimization: Use CFD simulations to analyse the flow patterns, velocity distributions, and pressure drop within the TORBED reactor. Focus on modifying the design parameters of the distributor and bed geometry to achieve improved flow characteristics and minimize pressure drop.
- Evaluation of Various Designs: Explore different configurations of the distributor and bed geometry through CFD simulations to identify the most efficient design options. This can involve variations in the shape, size, and arrangement of components within the reactor.
- Optimization for Uniform Flow Regime: Investigate methods to achieve a more uniform flow regime throughout the reactor by optimizing the design of the distributor and bed geometry. This can help mitigate issues such as channelling and uneven distribution of gases, leading to improved performance and sorbent utilization.
- Validation through Experimental Testing: Validate the findings from CFD simulations through experimental testing using the modified reactor designs. Compare the performance of the optimized configurations with the original design to assess the effectiveness of the proposed modifications.
- Integration with Multi-Stage Configuration: Consider incorporating the insights gained from the CFD studies into the design of the multi-stage TORBED reactor, as previously recommended. This integration can further enhance the efficiency and effectiveness of the reactor system.

## References


1. Osman AI, Hefny M, Abdel Maksoud M, Elgarahy AM, Rooney DW. Recent advances in carbon capture storage and utilisation technologies: a review. Environmental Chemistry Letters. 2021;19[2]:797-849.
2. Sartor O, Spencer T, Julia P-E, Bart I, Gawlikowska-Fyk A, Neuhoff K, et al. The EU's 2030 climate and energy framework and energy security. 2014.
3. Dubey A, Arora A. Advancements in carbon capture technologies: A review. Journal of Cleaner Production. 2022:133932.
4. Gibbins J, Chalmers H. Carbon capture and storage. Energy policy. 2008;36[12]:4317-22.
5. Wilberforce T, Olabi A, Sayed ET, Elsaid K, Abdelkareem MA. Progress in carbon capture technologies. Science of The Total Environment. 2021;761:143203.
6. Wang M, Oko E. Special issue on carbon capture in the context of carbon capture, utilisation and storage (CCUS). Springer; 2017. p. 1-4.
7. Kumar VV, Batcha M, Raghavan VR. Study of the fluid dynamic performance of distributor type in TORBED type reactors. Engineering E-Transaction. 2011;6[1]:70-5.
8. Groszek M, Laughlin B. TORBED Process reactor technology description: TORBE D Compact Bed Reactor ('CBR'). Torftech Ltd (White Paper). 2015.
9. Drage TC, Snape CE, Stevens LA, Wood J, Wang J, Cooper AI, et al. Materials challenges for the development of solid sorbents for post-combustion carbon capture. Journal of Materials Chemistry. 2012;22[7]:2815-23.
10. Ebner AD, Gray M, Chisholm N, Black Q, Mumford D, Nicholson MA, et al. Suitability of a solid amine sorbent for $CO_2$ capture by pressure swing adsorption. Industrial & engineering chemistry research. 2011;50[9]:5634-41.
11. Girimonte R, Formisani B, Testa F. Adsorption of $CO_2$ on a confined fluidized bed of pelletized 13X zeolite. Powder Technology. 2017;311:9-17.
12. Yi C, Jo S, Seo Y, Park S, Moon K, Yoo J, et al., editors. Feasibility test for $CO_2$ capture by dry sorbents in two fluidized bed reactors. Proceedings of the 4th Annual Conference on Carbon Capture and Sequestration; 2005.
13. Arromdee P, Kuprianov VI, Kaewklum R, Sirisomboon K. Experimental study on combustion of sunflower shells in a pilot swirling fluidized-bed combustor. Energy & fuels. 2010;24[7]:3850-9.
14. Aworinde SM, Holland DJ, Davidson JF. Investigation of a swirling flow nozzle for a fluidised bed gas distributor. Chemical Engineering Science. 2015;132:22-31.
15. Hafiz M, Batcha MFM, Asmuin N, editors. Effect of plenum chamber depth in a swirling fluidized bed. IOP Conference Series: Materials Science and Engineering; 2013: IOP Publishing.
16. Jamei R, McDonough J, Reay D, Zivkovic V. Rapid and intensified screening of a carbon capture adsorbent using a 3D-printed swirling fluidised bed. Chemical Engineering Journal. 2023;451:138405.
17. Kaewklum R, Kuprianov VI. Experimental studies on a novel swirling fluidized-bed combustor using an annular spiral air distributor. Fuel. 2010;89[1]:43-52.
18. Shukrullah S, Naz MY, Ghaffar A, Khan Y, Al-Arainy AA, Meer R. Experimental and statistical validation of data on mesh-coupled annular distributor design for swirling fluidized beds. Processes. 2020;8[5]:632.
19. Yudin ASM, Anuar S, Oumer AN. Improvement on particulate mixing through inclined slotted swirling distributor in a fluidized bed: An experimental study. Advanced Powder Technology. 2016;27[5]:2102-11.

20. Jassim MS, Rochelle G, Eimer D, Ramshaw C. Carbon dioxide absorption and desorption in aqueous monoethanolamine solutions in a rotating packed bed. Industrial & engineering chemistry research. 2007;46[9]:2823-33.
21. Ghiat I, Al-Ansari T. A review of carbon capture and utilisation as a CO2 abatement opportunity within the EWF nexus. Journal of CO2 Utilization. 2021;45:101432.
22. McDonough JR, Law R, Reay DA, Zivkovic V. Intensified carbon capture using adsorption: Heat transfer challenges and potential solutions. Thermal Science and engineering progress. 2018;8:17-30.
23. D'Alessandro DM, Smit B, Long JR. Carbon dioxide capture: prospects for new materials. Angewandte Chemie International Edition. 2010;49[35]:6058-82.
24. Singh J, Dhar DW. Overview of carbon capture technology: microalgal biorefinery concept and state-of-the-art. Frontiers in Marine Science. 2019;6:29.
25. Rubin ES, Mantripragada H, Marks A, Versteeg P, Kitchin J. The outlook for improved carbon capture technology. Progress in energy and combustion science. 2012;38[5]:630-71.
26. Lai JY, Ngu LH, Hashim SS. A review of CO2 adsorbents performance for different carbon capture technology processes conditions. Greenhouse Gases: Science and Technology. 2021;11[5]:1076-117.
27. Al-Ghurabi EH, Ajbar A, Asif M. Enhancement of CO2 removal efficacy of fluidized bed using particle mixing. Applied Sciences. 2018;8[9]:1467.
28. Moreno H, Pontiga F, Valverde JM. Low concentration CO2 capture in fluidized beds of Ca (OH) 2 as affected by storage humidity. Chemical Engineering Journal. 2021;407:127179.
29. Theo WL, Lim JS, Hashim H, Mustaffa AA, Ho WS. Review of pre-combustion capture and ionic liquid in carbon capture and storage. Applied energy. 2016;183:1633-63.
30. Stanger R, Wall T, Spörl R, Paneru M, Grathwohl S, Weidmann M, et al. Oxyfuel combustion for CO2 capture in power plants. International journal of greenhouse gas control. 2015;40:55-125.
31. Diaz-Herrera PR, Ascanio G, Romero-Martinez A, Alcaraz-Calderon AM, Gonzalez-Diaz A. Theoretical comparison between post-combustion carbon capture technology and the use of blue and green H2 in existing natural gas combined cycles as CO2 mitigation strategies: A study under the context of mexican clean energy regulation. International Journal of Hydrogen Energy. 2021;46[2]:2729-54.
32. Wang M, Lawal A, Stephenson P, Sidders J, Ramshaw C. Post-combustion CO2 capture with chemical absorption: A state-of-the-art review. Chemical engineering research and design. 2011;89[9]:1609-24.
33. Kothandaraman A. Carbon dioxide capture by chemical absorption: a solvent comparison study: Citeseer; 2010.
34. Commission AU. Investing in renewable energies for Southern Africa's sustainable development. 2023.
35. Hart A, Gnanendran N. Cryogenic CO2 capture in natural gas. Energy Procedia. 2009;1[1]:697-706.
36. Seo Y, Jo S-H, Ryu CK, Yi C-K. Effects of water vapor pretreatment time and reaction temperature on CO2 capture characteristics of a sodium-based solid sorbent in a bubbling fluidized-bed reactor. Chemosphere. 2007;69[5]:712-8.
37. Lee C-H, Park S-W, Kim S-S. Breakthrough analysis of carbon dioxide adsorption on zeolite synthesized from fly ash. Korean Journal of Chemical Engineering. 2014;31:179-87.
38. Raganati F, Ammendola P. Sound-assisted fluidization for temperature swing adsorption and calcium looping: A review. Materials. 2021;14[3]:672.
39. Edubilli S, Gumma S. A systematic evaluation of UiO-66 metal organic framework for CO2/N2 separation. Separation and Purification Technology. 2019;224:85-94.

40. Varghese AM, Karanikolos GN. CO2 capture adsorbents functionalized by amine–bearing polymers: A review. International Journal of Greenhouse Gas Control. 2020;96:103005.
41. Teng Y, Liu Z, Xu G, Zhang K. Desorption kinetics and mechanisms of CO2 on amine-based mesoporous silica materials. Energies. 2017;10[1]:115.
42. Wang H, Jahandar Lashaki M, Fayaz M, Hashisho Z, Philips JH, Anderson JE, et al. Adsorption and desorption of mixtures of organic vapors on beaded activated carbon. Environmental science & technology. 2012;46[15]:8341-50.
43. Xu X, Song C, Andresen JM, Miller BG, Scaroni AW. Novel polyethylenimine-modified mesoporous molecular sieve of MCM-41 type as high-capacity adsorbent for CO2 capture. Energy & Fuels. 2002;16[6]:1463-9.
44. Geldart D. Mixing in fluidized beds. Mixing in the process industries. 1992:62-78.
45. Siriwardane RV, Shen M-S, Fisher EP, Poston JA. Adsorption of CO2 on molecular sieves and activated carbon. Energy & Fuels. 2001;15[2]:279-84.
46. Tsuda T, Fujiwara T. Polyethyleneimine and macrocyclic polyamine silica gels acting as carbon dioxide absorbents. Journal of the Chemical Society, Chemical Communications. 1992[22]:1659-61.
47. Chen C, Yang S-T, Ahn W-S, Ryoo R. Amine-impregnated silica monolith with a hierarchical pore structure: enhancement of CO 2 capture capacity. Chemical Communications. 2009[24]:3627-9.
48. Dillon EP, Crouse CA, Barron AR. Synthesis, characterization, and carbon dioxide adsorption of covalently attached polyethyleneimine-functionalized single-wall carbon nanotubes. Acs Nano. 2008;2[1]:156-64.
49. AL-SAEDI RW. A review on modified MOFs as CO2 adsorbents using mixed metals and functionalized linkers. Samarra Journal of Pure and Applied Science. 2023;5[1]:1-18.
50. Li FS, Qiu W, Lively RP, Lee JS, Rownaghi AA, Koros WJ. Polyethyleneimine-functionalized polyamide imide (Torlon) hollow-fiber sorbents for post-combustion CO2 capture. ChemSusChem. 2013;6[7]:1216-23.
51. Li X, Cheng Y, Zhang H, Wang S, Jiang Z, Guo R, et al. Efficient CO2 capture by functionalized graphene oxide nanosheets as fillers to fabricate multi-permselective mixed matrix membranes. ACS applied materials & interfaces. 2015;7[9]:5528-37.
52. Wang M, Yao L, Wang J, Zhang Z, Qiao W, Long D, et al. Adsorption and regeneration study of polyethylenimine-impregnated millimeter-sized mesoporous carbon spheres for post-combustion CO2 capture. Applied Energy. 2016;168:282-90.
53. Liu F, Chen S, Gao Y. Synthesis of porous polymer based solid amine adsorbent: effect of pore size and amine loading on CO2 adsorption. Journal of colloid and interface science. 2017;506:236-44.
54. Siriwardane R, Shen M, Fisher E, Poston J, Shamsi A. Adsorption and desorption of CO2 on solid sorbents. National Energy Technology Laboratory, and Morgantown, WV (United States); 2001.
55. Tejavath V, Kasarabada V, Gonuguntla S, Perupoga V, Nandury SV, Bojja S, et al. Technoeconomic investigation of amine-grafted zeolites and their kinetics for CO2 capture. ACS omega. 2021;6[9]:6153-62.
56. Florin NH, Mac Dowell N, Fennell PS, Maitland GC. Carbon capture: materials and process engineering. Materials for a Sustainable Future: The Royal Society of Chemistry; 2012. p. 385-429.
57. Shu J, Lakshmanan V, Dodson C. Hydrodynamic study of a toroidal fluidized bed reactor. Chemical Engineering and Processing: Process Intensification. 2000;39[6]:499-506.
58. Sandu V-C, Cormos A-M, Dumbrava I-D, Imre-Lucaci A, Cormos C-C, de Boer R, et al. Assessment of CO2 capture efficiency in packed bed versus 3D-printed monolith reactors

for SEWGS using CFD modeling. International Journal of Greenhouse Gas Control. 2021;111:103447.
59. Shirzad M, Karimi M, Silva JA, Rodrigues AE. Moving bed reactors: challenges and progress of experimental and theoretical studies in a century of research. Industrial & Engineering Chemistry Research. 2019;58[22]:9179-98.
60. Serna-Guerrero R, Sayari A. Modeling adsorption of CO2 on amine-functionalized mesoporous silica. 2: Kinetics and breakthrough curves. Chemical Engineering Journal. 2010;161(1-2):182-90.
61. Salazar Duarte G, Schürer B, Voss C, Bathen D. Adsorptive separation of CO2 from flue gas by temperature swing adsorption processes. ChemBioEng Reviews. 2017;4[5]:277-88.
62. Javed MA, Shukrullah S, Naz MY, Sarfraz RA. Image velocimetry and statistical analysis of a mesh-coupled axial blade distributor for mass transfer in a swirling bed. Journal of Theoretical and Applied Mechanics. 2020;58.
63. Thanh BT. Determination on Fluidization Velocity Types of the Continuous Refined Salt Fluidized Bed Drying. Current Drying Processes: IntechOpen; 2020.
64. Sobrino C, Almendros-Ibáñez JA, Santana D, De Vega M. Fluidization of Group B particles with a rotating distributor. Powder Technology. 2008;181[3]:273-80.
65. Alamri A, McDonough J, Zivkovic V. Fluidisation behaviour and wall effects of cohesive hydrotalcite powder in a micro-fluidised bed. Powder Technology. 2023;415:118192.
66. Xie P, Lu X, Yang X, Ingham D, Ma L, Pourkashanian M. Characteristics of liquid flow in a rotating packed bed for CO2 capture: A CFD analysis. Chemical Engineering Science. 2017;172:216-29.
67. Reay D. The role of process intensification in cutting greenhouse gas emissions. Applied Thermal Engineering. 2008;28[16]:2011-9.
68. McDonough J, Law R, Reay D, Groszek D, Zivkovic V. Miniaturisation of the toroidal fluidisation concept using 3D printing. Chemical Engineering Research and Design. 2020;160:129-40.
69. Wang H, Mustaffar A, Phan AN, Zivkovic V, Reay D, Law R, et al. A review of process intensification applied to solids handling. Chemical Engineering and Processing: Process Intensification. 2017;118:78-107.
70. Liu X, Xu G, Gao S. Micro fluidized beds: Wall effect and operability. Chemical Engineering Journal. 2008;137[2]:302-7.
71. Fan L, Chang C, Yu Y, Takahashi T, Tanaka Z. Incipient fluidization condition for a centrifugal fluidized bed. AIChE journal. 1985;31[6]:999-1009.
72. Basu P, Fraser SA. Circulating fluidized bed boilers: Springer; 1991.
73. Kunii D, Levenspiel O. Circulating fluidized-bed reactors. Chemical Engineering Science. 1997;52[15]:2471-82.
74. Shukla P. Biomass energy in India: Transition from traditional to modern. The social engineer. 1997;6[2]:1-21.
75. Lin C, Teng J, Chyang C. Evaluation of the combustion efficiency and emission of pollutants by coal particles in a vortexing fluidized bed. Combustion and Flame. 1997;110(1-2):163-72.
76. Chyang C-S, Wan H-P, Su L-C. Effect of interaction of operation parameters on elutriation behavior in a vortexing fluidized bed. Korean Journal of Chemical Engineering. 2007;24:1106-12.
77. Ma H-J, Chen Y-S. Evaluation of effectiveness of highly concentrated alkanolamine solutions for capturing CO2 in a rotating packed bed. International Journal of Greenhouse Gas Control. 2016;55:55-9.

78. Xie P, Lu X, Ding H, Yang X, Ingham D, Ma L, et al. A mesoscale 3D CFD analysis of the liquid flow in a rotating packed bed. Chemical Engineering Science. 2019;199:528-45.
79. Yu C-H, Wu T-W, Tan C-S. CO2 capture by piperazine mixed with non-aqueous solvent diethylene glycol in a rotating packed bed. International Journal of Greenhouse Gas Control. 2013;19:503-9.
80. Yi C-K, Jo S-H, Seo Y, Lee J-B, Ryu C-K. Continuous operation of the potassium-based dry sorbent CO2 capture process with two fluidized-bed reactors. International Journal of Greenhouse Gas Control. 2007;1[1]:31-6.
81. Javed MA, Shukrullah S, Naz MY, Sarfraz RA. IMAGE VELOCIMETRY AND STATISTICAL ANALYSIS OF A MESH-COUPLED AXIAL BLADE DISTRIBUTOR FOR MASS TRANSFER IN A SWIRLING BED. JOURNAL OF THEORETICAL AND APPLIED MECHANICS. 2020;58[3]:779-90.
82. Eslami Afrooz I, Chuan Ching DL, editors. Effect of novel swirl distributor plate on gasification efficiency of bubbling fluidized bed gasifier. Advances in Manufacturing Engineering: Selected articles from ICMMPE 2019; 2020: Springer.
83. Mohideen MIH, Xiao B, Wheatley PS, McKinlay AC, Li Y, Slawin AM, et al. Protecting group and switchable pore-discriminating adsorption properties of a hydrophilic–hydrophobic metal–organic framework. Nature chemistry. 2011;3[4]:304-10.
84. Latif MLA, Nawi M, Hazwan M, Amin MR, Ibrahim KMYK, Hussein H, editors. Characteristics on air flow distribution via spiral blade distributor in a swirling fluidized bed. AIP Conference Proceedings; 2020: AIP Publishing.
85. Dodson CE. Apparatus for processing matter in a turbulent mass of particulate material. Google Patents; 1984.
86. Ouyang F, Levenspiel O. Spiral distributor for fluidized beds. Industrial & Engineering Chemistry Process Design and Development. 1986;25[2]:504-7.
87. Tawfik MHM, Diab MR, Abdelmotalib HM. Heat transfer and bed dynamics study on a swirling fluidized bed under various inlet configurations. International Journal of Thermal Sciences. 2020;158:106523.
88. McDonough J, Law R, Reay D, Zivkovic V. Fluidization in small-scale gas-solid 3D-printed fluidized beds. Chemical Engineering Science. 2019;200:294-309.
89. Rees AC, Davidson JF, Dennis JS, Fennell PS, Gladden LF, Hayhurst A, et al. The nature of the flow just above the perforated plate distributor of a gas-fluidised bed, as imaged using magnetic resonance. Chemical Engineering Science. 2006;61[18]:6002-15.
90. Bakhurji A. Hydrodynamics and solids mixing behaviour of fluidized beds with inclined-hole distributor: University of British Columbia; 2017.
91. Bakhurji A, Bi X, Grace JR. Hydrodynamics and solids mixing in fluidized beds with inclined-hole distributors. Particuology. 2019;43:19-28.
92. De Wilde J, de Broqueville A. Experimental investigation of a rotating fluidized bed in a static geometry. Powder Technology. 2008;183[3]:426-35.
93. Latif MLA, Nawi M, Hazwan M, Amin MR, Ibrahim KMYK, Hussein H, editors. Characteristics on air flow distribution via spiral blade distributor in a swirling fluidized bed. AIP Conference Proceedings; 2020: AIP Publishing LLC.
94. McDonough J, Law R, Reay D, Groszek D, Zivkovic V. Miniaturisation of the toroidal fluidization concept using 3D printing. Chemical Engineering Research and Design. 2020.
95. Faizal M, Vinod K, Raghavan V, editors. Experimental Studies on a Swirling Fluidized Bed with Annular Distributor. Int Conference on Plant, Equipment and Reliability; 2010.
96. Halim LA, Basrawi M, Yudin ASM, Faizal SN, editors. Fluidized bed drying of stingless bee pot-pollen: Performance of swirling distributor. IOP Conference Series: Materials Science and Engineering; 2020: IOP Publishing.

97. Kumar VV, Batcha M, Raghavan VR. Study of the fluid dynamic performance of distributor type in TORBED type reactors. Engineering e-Transaction (ISSN 1823-6379). 2011;6[1]:70-5.
98. Odeleye AOO, Chui C-Y, Nguyen L, Castrejon-Pita AA, Ye H, Cui Z. On the use of 3D-printed flow distributors to control particle movement in a fluidized bed. Chemical Engineering Research and Design. 2018;140:194-204.
99. MacDowell N, Florin N, Buchard A, Hallett J, Galindo A, Jackson G, et al. An overview of CO 2 capture technologies. Energy & Environmental Science. 2010;3[11]:1645-69.
100. Zhu S, Lee S. Co-combustion performance of poultry wastes and natural gas in the advanced Swirling Fluidized Bed Combustor (SFBC). Waste management. 2005;25[5]:511-8.
101. McQueen M. Heat recovery from molten blast furnace slag in a fluidized bed: National Library of Canada= Bibliothèque nationale du Canada, Ottawa; 2001.
102. Sundaram P, Sudhakar P. Experimental performance investigation of swirling flow enhancement on fluidized bed dryer. ARPN journal of engineering and applied sciences. 2016;11:12529-33.
103. Khurana M. Integrated adsorbent and process design for carbon capture from power plant flue gas: National University of Singapore (Singapore); 2016.
104. Folorunso O. Microwave processing of vermiculite: University of Nottingham; 2015.
105. Liu S. Microwave-assisted catalytic thermochemical conversion of organic solid wastes for biofuels production: University of Minnesota; 2019.
106. McGurk SJ, Martín CF, Brandani S, Sweatman MB, Fan X. Microwave swing regeneration of aqueous monoethanolamine for post-combustion CO2 capture. Applied energy. 2017;192:126-33.
107. Liu Q, Shi J, Zheng S, Tao M, He Y, Shi Y. Kinetics studies of CO2 adsorption/desorption on amine-functionalized multiwalled carbon nanotubes. Industrial & Engineering Chemistry Research. 2014;53[29]:11677-83.
108. Sun Z, Fan M, Argyle M. Desorption kinetics of the monoethanolamine/macroporous TiO2-based CO2 separation process. Energy & fuels. 2011;25[7]:2988-96.
109. Webley PA, Zhang J. Microwave assisted vacuum regeneration for CO 2 capture from wet flue gas. Adsorption. 2014;20:201-10.
110. Otero AR, Munoz RC. Fluidized bed gas distributors of bubble cap type. Powder Technology. 1974;9(5-6):279-86.
111. Monazam ER, Spenik J, Shadle LJ. Fluid bed adsorption of carbon dioxide on immobilized polyethylenimine (PEI): Kinetic analysis and breakthrough behavior. Chemical Engineering Journal. 2013;223:795-805.
112. Xu X, Pejcic B, Heath C, Wood CD. Carbon capture with polyethylenimine hydrogel beads (PEI HBs). Journal of Materials Chemistry A. 2018;6[43]:21468-74.
113. Heydari-Gorji A, Belmabkhout Y, Sayari A. Polyethylenimine-impregnated mesoporous silica: effect of amine loading and surface alkyl chains on CO2 adsorption. Langmuir. 2011;27[20]:12411-6.